

Vibration damping of lightweight sandwich structures

Submitted by Pierre Aumjaud to the University of Exeter as a thesis for the degree of Doctor of Philosophy in engineering in November 2015.

This thesis is available for Library use on the understanding that it is copyright material and that no quotation from the thesis may be published without proper acknowledgement.

I certify that all material in this thesis which is not my own work has been identified and that no material has previously been submitted and approved for the award of a degree by this or any other University.

Signature:



College of Engineering, Mathematics and Physical Sciences

Acknowledgements

Foremost, I would like to thank Prof Chris Smith and Prof Ken Evans for their guidance and continuous support throughout this fascinating project. They gave me the opportunity to engage with the various aspects of academic research, helping me to acquire excellent technical knowledge.

I am also deeply grateful for the help and technical advice provided by Dr Jonathan Fieldsend and Prof Paul Reynolds on evolutionary optimisation and modal testing, respectively. Special thanks to Dominique Lefranc for his help with the manufacture of the samples.

I wish to acknowledge INTERREG IV-A for funding this research project and Heathcote Industrial Plastics Ltd. for supplying the constrained layer damper samples at no charge.

I have been honoured to have Dr Jack Hale and Dr Prakash Kripakaran as examiners of my thesis and Prof Aleksandar Pavic as independent chair, thank you.

I sincerely would like to thank all the friends whom I met during my PhD studies for their stimulating conversations, cheerfulness, wisdom and fun.

Last but not least, my warmest gratitude goes to my parents, these two benevolent and loving beings who supported me in each and every single of my endeavours in life.

Abstract

Honeycomb-cored sandwich structures are widely used in transport for their high strength-to-mass ratio. Their inherent high stiffness and lightweight properties make them prone to high vibration cycles which can incur deleterious damage to transport vehicles. This PhD thesis investigates the performance of a novel passive damping treatment for honeycomb-cored sandwich structures, namely the Double Shear Lap-Joint (DSLJ) damper. It consists of a passive damping construct which constrains a viscoelastic polymer in shear, thus dissipating vibrational energy. A finite element model of such DSLJ damper inserted in the void of a hexagonal honeycomb cell is proposed and compared against a simplified analytical model. The damping efficiency of the DSLJ damper in sandwich beams and plates is benchmarked against that of the Constrained Layer Damper (CLD), a commonly used passive damping treatment. The DSLJ damper is capable of achieving a higher damping for a smaller additional mass in the host structure compared to the optimised CLD solutions found in the literature. The location and orientation of DSLJ inserts in honeycomb sandwich plates are then optimised with the objective of damping the first two modes using a simple parametric approach. This method is simple and quick but is not robust enough to account for mode veering occurring during the optimisation process. A more complex and computationally demanding evolutionary algorithm is subsequently adopted to identify optimal configurations of DSLJ in honeycomb sandwich plates. Some alterations to the original algorithm are successfully implemented for this optimisation problem in an effort to increase the convergence rate of the optimisation process. The optimised designs identified are manufactured and the modal tests carried out show an acceptable correlation in the trends identified by the numerical simulations, both in terms of damping per added mass and natural frequencies.

Contents

1	Introduction	1
1.1	Context and motivation	1
1.2	Thesis objectives and outline	2
2	Background of the study	5
2.1	Introduction	5
2.2	Sandwich structure	5
2.3	Finite element vibration Analysis	8
2.3.1	Governing equation	10
2.3.2	Modal analysis - Free vibrations	12
2.3.3	Response history	13
2.3.4	Harmonic response analysis - Forced vibration	14
2.4	Vibration damping	16
2.4.1	Viscoelastic damping models	19
2.4.2	Measurement of damping	20
2.5	Passive viscoelastic damping in sandwich structures	21
2.5.1	Full viscoelastic core	22
2.5.2	Partial constrained layer damper	24
2.5.3	Optimisation of partial constrained layer dampers	25
2.5.4	Structural damping of sandwich structures with lightweight cellular solid cores	28
2.6	Conclusion	31
3	Modelling methods	33
3.1	Introduction	33
3.2	DSLJ inserted in a single hexagonal cell	33
3.2.1	Analytical model	33
3.2.2	Finite element model	43
3.2.3	DSLJ insert vs CLD	44
3.3	Honeycomb sandwich structures	46
3.3.1	Analytical model	46
3.3.2	Finite element model	48

3.4	Preliminary results	50
3.4.1	DSLJ inserted in a single hexagonal cell	50
3.4.2	DSLJ insert vs CLD	52
3.4.3	Honeycomb sandwich structures	52
3.5	Conclusion	57
4	Viscoelastic damper comparison	59
4.1	Introduction	59
4.2	Methods	59
4.2.1	Positioning of the DSLJ inserts	62
4.2.2	CLD and DSLJ dampers comparison	62
4.3	Results	64
4.3.1	Parametric optimisation of the DSLJ inserts	64
4.3.2	CLD and DSLJ dampers comparison	64
4.4	Discussion	71
4.5	Conclusion	72
5	Parametric optimisation of the DSLJ damping inserts	73
5.1	Introduction	73
5.2	Methods	74
5.3	Results	76
5.3.1	Optimised configurations	76
5.3.2	Mode veering	77
5.4	Discussion	79
5.5	Conclusion	83
6	Evolutionary optimisation of DSLJ damping inserts	85
6.1	Introduction	85
6.2	Methods	86
6.2.1	Evolutionary optimisation	86
6.2.2	Optimisation convergence	92
6.2.3	Parametric vs Adaptive IBEA optimisation	93
6.3	Results	94
6.3.1	Optimisation convergence	94
6.3.2	2-objective optimisation	96
6.3.3	3-objective optimisation	102
6.3.4	Parametric vs Adaptive IBEA optimisation	105
6.4	Discussion	108
6.4.1	Optimisation convergence	108
6.4.2	Adaptive IBEA optimisation	108
6.5	Conclusion	110

7 Experimental modal testing of optimally damped honeycomb sandwich panels	113
7.1 Introduction	113
7.2 Method	114
7.2.1 Manufacturing of the samples	114
7.2.2 Experimental setup	116
7.2.3 Finite element model	122
7.3 Results	122
7.3.1 Repeatability of the tests	123
7.3.2 Repeatability of the samples	124
7.3.3 Amplitude response comparison	124
7.3.4 Damping efficiency comparison	125
7.4 Discussion	127
7.5 Conclusion	129
8 Conclusion	131
8.1 General discussion	131
8.2 Recommendations for future work	133
A Modal Strain Energy method	135
B Finite element model	137
C Parametric optimiser	149
D Evolutionary optimiser	155

List of Figures

1.1 Structure of the wing leading edge of an aircraft. Adapted from [1].	2
2.1 A honeycomb core sandwich panel. Adapted from [2].	6
2.2 The stress distribution in a homogeneous panel (a) and a sandwich panel (b). Adapted from [3].	7
2.3 Closed (left) and open-cell (right) cellular structures. Adapted from [4].	8
2.4 Stochastic (left) and deterministic (right) cell architecture. Adapted from [4].	8
2.5 Honeycomb-cored sandwich structures. Adapted from [5].	9
2.6 Amplitude and phase response of a single d.o.f. system for various values of damping ratio. Adapted from [6].	16
2.7 Stress and strain versus time for a viscoelastic material subjected to a sinusoidal excitation. Adapted from [7].	18
2.8 Half-power bandwidth method. Adapted from [8].	21
2.9 Unconstrained or free layer damper on an undeformed (a) and deformed (b) structure.	22
2.10 Constrained layer damper on an undeformed (a) and deformed (b) structure.	23
2.11 Multiple constrained layer damper on an undeformed (a) and deformed (b) structure.	24
2.12 Stand-off constrained damping treatment on an undeformed (a) and deformed (b) structure.	24
2.13 Cell insert damper. Adapted from [9].	25
2.14 Lightweight passive damping treatment patented by Staley. Adapted from [10].	29
2.15 Polymer particles in a honeycomb-cored sandwich panel. Adapted from [11].	30
2.16 A honeycomb cell embedded with shape memory alloys. Adapted from [12].	31
2.17 A DSLJ damper in a hexagonal honeycomb cell before (a) and after deformation (b). The viscoelastic material is shown in yellow.	31

3.1 (a) A DSLJ insert in a hexagonal honeycomb cell, (b) a single DSLJ damper, (c) and (d) a DSLJ damper deformed as the sandwich panel undergoes flexural vibration. The viscoelastic material is represented in yellow and the constraining material in grey.	34
3.2 A honeycomb unit cell	34
3.3 Three possible orientations of a DSLJ damper in a hexagonal cell.	35
3.4 A honeycomb unit cell with a DSLJ damping insert.	36
3.5 Deformed honeycomb cell with DSLJ insert. The area identified with a red ellipse is shown in Figure 3.6.	38
3.6 Free body diagram of a cell wall.	39
3.7 Loading of the honeycomb cell.	39
3.8 Strain profile in the viscoelastic material of half of a DSLJ insert when the cell is deformed in bending.	41
3.9 Mesh, load and boundary conditions of the finite element model. The load and the constrained nodes are represented by red arrows and yellow crosses, respectively.	44
3.10 Simplified representation of the deformation of the viscoelastic layer in a CLD.	46
3.11 CLD on a deformed host structure.	47
3.12 Honeycomb-cored sandwich beam, with upper skin removed for clarity.	49
3.13 The array of hexagonal cells in the honeycomb core and the lower skin, with upper skin removed for clarity. A single DSLJ insert is sketched in the centre.	49
3.14 Contour plot of the strain energy in a honeycomb cell with a DSLJ damper (a) and in a DSLJ damper (b). The regions of highest and lowest strain energy are indicated in red and white, respectively.	51
3.15 Strain energy density in the viscoelastic material contained either by a CLD or a DSLJ damper when the host structure bends by an angle α . The thickness of the viscoelastic layer is kept constant at $h_i = 1\text{mm}$	53
3.16 Strain energy density in the viscoelastic material contained either by a CLD or a DSLJ damper as the thickness of the viscoelastic layer varies from 0.001 mm to 3 mm. The bending angle of the host structure is kept constant at $\alpha = 10^\circ$	54
3.17 The amplitude response of the SFSF sandwich plate when the structure is excited in one corner and the response is measured at the opposite corner, showing the first five modes.	57

4.1	Loss efficiency Ef_η vs the additional mass as a percentage of the total mass of the undamped structure, as rows of cells are filled sequentially with DSLJ inserts on all structures (a) or as the thickness of the viscoelastic element is increased from 0.25 to 2.33 mm (b).	65
4.2	(a) The amplitude of the cantilever beams excited at their first modes. The vibration amplitude (X) of each structure is normalised to that of the undamped structure(X_0). (b) Detail of the distribution of the vibration amplitude about each resonant frequency.	66
4.3	(a) and (b) as per Figure 4.2a and 4.2b but for the simply supported beam.	66
4.4	(a) and (b) as per Figure 4.2a and 4.2b but for the cantilever plate.	67
4.5	(a) and (b) as per Figure 4.2a and 4.2b but for the simply supported plate.	67
4.6	Comparison of the loss efficiency Ef_η vs added mass for the cantilever (a) and simply supported (b) beam solutions.	69
4.7	Comparison of the loss efficiency Ef_η vs added mass for the cantilever (a) and simply supported (b) plate solutions.	69
5.1	Four possible DSLJ damper configuration within a hexagonal honeycomb cell – absent or one of the three orientations.	76
5.2	A deformed (green) and undeformed (black) honeycomb cell.	76
5.3	Optimised distributions of DSLJ dampers on the cantilever sandwich plate under mode 1 (flapping mode).	77
5.4	Optimised distributions of DSLJ dampers on the cantilever sandwich plate under mode 2 (torsion mode).	77
5.5	Optimised distributions of DSLJ dampers on the free sandwich plate under mode 1 (bending mode).	78
5.6	Optimised distributions of DSLJ dampers on the free sandwich plate under mode 2 (torsion mode).	78
5.7	Damping efficiency versus the number of DSLJ inserts for the cantilever plate. The numbers correspond to the configuration numbers shown in Figures 5.3 and 5.4 for mode 1 and 2, respectively. The optimal number of DSLJ is identified by an arrow for each mode.	80
5.8	Damping efficiency versus the number of DSLJ inserts for the free plate. The numbers correspond to the configuration numbers shown in Figures 5.5 and 5.6 for mode 1 and 2, respectively. The second mode shape of configurations 13, 14 and 18 is indicated.	81

5.9	First and second eigenfrequency versus the the number of DSLJ inserts for the cantilever plate. The numbers correspond to the configuration shown in Figures 5.3 and 5.4 for mode 1 and 2, respectively.	82
5.10	First and second eigenfrequency versus the the number of DSLJ inserts for the free plate. The numbers correspond to the configuration shown in Figures 5.5 and 5.6 for mode 1 and 2, respectively. The presence of mode veering is identified by green circles.	82
5.11	Second mode shape corresponding to the configurations shown in Figure 5.6 (Free plate optimised for its second torsion mode).	83
6.1	Flowchart of the Adaptive IBEA algorithm. The main sections are identified in orange and the ANSYS cost function (green) is detailed in Figure 6.2.	89
6.2	ANSYS cost function used in the Adaptive IBEA optimiser (see flowchart 6.1).	90
6.3	Graphical representation of the hypervolume for a 2-objective set of non-dominated solutions. The absolute reference point was chosen as the worst design possible with respect to each objective.	94
6.4	Hypervolume median of 20 optimisation runs when initialising the search population with either 20 random individuals or the 20 individuals identified by the parametric optimisation. The error bars represent the minimum and maximum hypervolume value of each group.	95
6.5	Hypervolume median of 20 optimisation runs when symmetry reflections occur with a probability of 0, 0.3, 0.6 and 0.9. The error bars represent the minimum and maximum hypervolume value of each group.	96
6.6	Cantilever sandwich plate - the initial population, the non-dominated solutions and all the evaluated configurations are represented by the negative of their first modal loss factor and their percentage of additional mass.	98
6.7	Cantilever sandwich plate - the initial population, the non-dominated solutions and all the evaluated configurations are represented by the negative of their second modal loss factor and their percentage of additional mass.	98
6.8	Free sandwich plate - the initial population, the non-dominated solutions and all the evaluated configurations are represented by the negative of their first modal loss factor and their percentage of additional mass. The initial population features two different mode shapes, represented by either a circle or a diamond.	99

6.9 Free sandwich plate - the initial population, the non-dominated solutions and all the evaluated configurations are represented by the negative of their second modal loss factor and their percentage of additional mass. The initial population features two different mode shapes, represented by either a circle or a diamond.	99
6.10 Optimal designs identified by Adaptive IBEA for the cantilever sandwich plate when targeting the first mode (flapping). The configuration in the red box is identified by a green point in Figure 6.6.	100
6.11 Optimal designs identified by Adaptive IBEA for the cantilever sandwich plate when targeting the second mode (torsion). The configuration in the red box is identified by a green point in Figure 6.7.	100
6.12 Optimal designs identified by Adaptive IBEA for the free sandwich plate when targeting the first mode (bending). The configuration in the red box is identified by a green point in Figure 6.8.	101
6.13 Optimal designs identified by Adaptive IBEA for the free sandwich plate when targeting the second mode (torsion). The configuration in the red box is identified by a green point in Figure 6.9.	101
6.14 The non-dominated solutions identified by the 3-objective (red points) and 2-objective optimisations targeting the first mode (yellow crosses) or second mode (blue crosses) are shown for the cantilever sandwich plate.	102
6.15 The non-dominated solutions identified by the 3-objective (red points) and 2-objective optimisations targeting the first mode (yellow crosses) or second mode (blue crosses) are shown for the sandwich plate in free boundary conditions.	103
6.16 Optimal designs identified by Adaptive IBEA for the cantilever sandwich plate when targeting the first and second mode simultaneously. The configuration in the red box is identified by a green point in Figure 6.14.	103
6.17 Optimal designs identified by Adaptive IBEA for the free sandwich plate when targeting the first and second mode simultaneously. The configuration in the red box is identified by a green point in Figure 6.15.	104
6.18 Amplitude of the frequency response function of the selected configurations optimised for the cantilever plate with the parametric approach, Adaptive IBEA when targeting mode 1, mode 2 and mode 1 and 2 simultaneously. The amplitude response of the undamped plate is also shown.	106

6.19 Amplitude of the frequency response function of the selected configurations optimised for the free plate with the parametric approach, Adaptive IBEA when targeting mode 1, mode 2 and mode 1 and 2 simultaneously. The amplitude response of the undamped plate is also shown.	107
7.1 Undamped samples without upper skin shown in top (a) and isometric views (b).	115
7.2 Honeycomb sandwich panel with a CLD damper (a). A close-up view of the bonding of the CLD onto the sandwich skin is shown in (b).	115
7.3 Sketch of a DSLJ damping insert for hexagonal honeycomb cells.	116
7.4 A sketch of an optimised DSLJ configuration (a) and photographs of manufactured samples (b-d) including detail of DSLJ in place (c).	117
7.5 All of six of the sandwich panel samples used in testing.	118
7.6 Sketch of the modal testing setup. The sample is excited with a random waveform excitation and the FRF is computed from the input force and output acceleration signals.	119
7.7 Modal testing setup of a honeycomb sandwich panel.	120
7.8 Sample free supports using elastic cords and transducers attachments. The load cell is connected to the exciter via a nylon stinger and attached to the sample with a mounting stud (a). The accelerometer is stuck onto the sandwich skin with beeswax (b).	120
7.9 First mode shape (at 1346 Hz) of the undamped sandwich plate with honeycomb core under free boundary conditions predicted by the finite element model. The colours indicate the displacement, with blue being the lowest and red the highest.	121
7.10 Amplitude, phase and coherence function of a modal test.	123
7.11 Average and standard deviation of the amplitude response obtained after 20 successive modal tests.	123
7.12 Amplitude response of the four undamped samples.	124
7.13 Amplitude response of the four CLD samples.	124
7.14 Amplitude response of the four DSLJ samples.	124
7.15 Amplitude response of the samples with CLD (blue), DSLJ (red) and undamped (black) treatments measured experimentally (a) and predicted numerically by finite element analysis (b).	125

List of Tables

2.1	Relative weight, bending stiffness and bending strength of sandwich panels compared to a homogeneous solid material [3].	6
2.2	Optmisation studies seeking to optimise the location and dimensions of passive CLD treatments giving the maximum damping for the least additional mass.	28
3.1	Material properties of the honeycomb cell and the DSLJ damper. The honeycomb cell is made of aluminium and the viscoelastic material is a silicone rubber whose material properties were adapted from references [8] and [13], respectively. Subscripts <i>a</i> and <i>v</i> stand for ‘aluminium’ and ‘viscoelastic’, respectively.	35
3.2	Dimensions and loading values of the honeycomb cell and the DSLJ damper. Subscripts <i>c</i> , <i>f</i> and <i>i</i> stand for ‘core’, ‘face’ and ‘insert’, respectively.	36
3.3	Comparison of the mass, loss factor and strain energy stored in a honeycomb cell with a DSLJ insert either computed analytically or via the finite element method.	52
3.4	First five mode shapes of the honeycomb-core sandwich structures considered in this thesis.	56
3.5	First five natural frequencies (in Hertz) of the structures considered in this thesis.	56
4.1	Benchmarked optimised damper configurations for beam and plate structures. The sandwich skins are shown removed for clarity. The presence of a damper is given by solid colouring (CLD) or inserts in cells (DSLJ). Boundary conditions are indicated by solid triangles (encastred) and open circles (pinned) for the cantilever and simply supported cases, respectively.	62

4.2	Relative amplitude reduction A , additional mass m_a , amplitude reduction efficiency Ef_a and strain energy density in the viscoelastic material u_{vem} at peak amplitude for all configurations. The amplitude reduction and amplitude reduction efficiency are relative to the undamped structure. The strain energy density in the viscoelastic material is relative to that of the DSLJ structure.	68
4.3	Modal loss factor η_1 and additional mass relative to the undamped structure m_a at peak loss efficiency Ef_η for all configurations. The modal loss factor was estimated by means of both the Modal Strain Energy (MSE) and the Half-Power Bandwidth (HPB) methods.	70
5.1	First and second mode shapes of the sandwich plate under cantilever and free boundary conditions, along with their corresponding natural frequency. The colours of the mode shapes indicate the nodal displacements, with red being maximal and blue minimal. The encastered boundary condition is represented by black lines on the left of the cantilevered structures.	75
6.1	Generation number after which the differences between groups become significant according to the Mann-Whitney U test with a confidence level of 0.05.	96
6.2	Performance comparison between the parametric and Adaptive IBEA optimisation for the cantilever and free boundary condition cases. The configurations compared are identified by a magenta and a green point in Figures 6.6 to 6.15 for the parametric and the Adaptive IBEA optimisation, respectively. The mass, the first η_1 and second η_2 loss factors are presented as a ratio of the empty structure value. The damping efficiencies are also indicated.	106
7.1	Dimensions of the samples shown in Figure 7.5. The dimensions of the finite element model is also indicated.	116
7.2	Mass, natural frequencies, modal loss factors and damping efficiencies of the samples.	126
7.3	The mass, natural frequencies, modal loss factors and damping efficiencies of the samples measured experimentally and averaged are compared to the values predicted by finite element analysis.	126
7.4	The average values of the mass, natural frequencies, modal loss factors and damping efficiencies of the samples are shown normalised to that of the undamped configuration.	127

Nomenclature

Acronyms

APDL	ANSYS Parametric Design Language
CF	Cantilevered beam
CFFF	Cantilevered plate
CLD	Constrained Layer Damper
d.o.f.	Degree Of Freedom
DSLJ	Double Shear Lap-Joint
FFFF	Plate with free boundary conditions
FRF	Frequency Response Function
HPB	Half Power Bandwidth
MSE	Modal Strain Energy
RMS	Root Mean Square
SFSF	Plate simply supported on the short edge and free on the long edge
SS	Simply supported beam
SSSS	Plate simply supported on all edges

Greek symbols

α	Bending angle of the host structure
$\delta(z)$	Deflection of the honeycomb cell wall
$\delta_i(z)$	Deflection of the DSLJ damper's rigid element
δ_l	Logarithmic decrement
η_a	Material loss factor of the aluminium

η_v	Material loss factor of the viscoelastic material
Γ^2	Coherence function
γ_c	Shear strain in the CLD's viscoelastic material
$\gamma_i(z)$	Shear strain in the DSLJ damper's viscoelastic material
κ	Scaling fitness coefficient
λ_i^*	Complex eigenvalue corresponding to mode i
λ_i	Eigenvalue of mode i
ν_a	Poisson's ratio of the aluminium
ν_v	Poisson's ratio of the viscoelastic material
Ω	External excitation's circular frequency
ω_i	Circular modal frequency of mode i
ϕ_i	Phase angle of the FRF of mode i
ρ	Mass density
ρ_a	Density of the aluminium
ρ_v	Density of the viscoelastic material
τ_c	Shear stress in the CLD's viscoelastic material
$\tau_i(z)$	Shear stress in the DSLJ damper's viscoelastic material
θ	Angle between the honeycomb cell wall and the vertical axis
θ_i	Angle of twist of the DSLJ damper
ξ_i	Modal damping ratio of mode i
$\{\Phi_k^*\}$	Complex eigenvector corresponding to mode i
$\{\Phi_i\}$	Eigenvector of mode i

Latin symbols

$[C]$	Global damping matrix
$[c]$	Element damping matrix
$[K]$	Global stiffness matrix

$[k]$	Element stiffness matrix
$[K^*]$	Complex stiffness matrix
$[K_{i,k}]$	Global stiffness matrix of material i in mode k
$[M]$	Global mass matrix
$[m]$	Element mass matrix
$[N]$	Element shape function matrix
\mathbf{x}	DSLJ design (described by a binary string)
\mathcal{P}	Pareto set of designs
$\{\delta u\}$	Virtual displacement vector
$\{D\}$	Global nodal displacement vector
$\{d\}$	Element nodal d.o.f. vector
$\{F^{ext}\}$	Vector of external forces applied to the global system
$\{f^{ext}\}$	Element force vector
$\{p^{ext}\}$	Vector of external forces applied to the element of volume
$\{u\}$	Displacement vector
$A(\cdot)$	Frequency response function (acceleration)
$A_i(\cdot)$	Frequency response function of mode i (acceleration)
b_i	Depth of the DSLJ insert (y axis)
c	Viscous damping coefficient
c_I	Maximum absolute indicator value of all members in the search population
E_a	Young's modulus of the aluminium
E_v	Young's modulus of the viscoelastic material
Ef_η	Loss efficiency
Ef_a	Amplitude reduction efficiency
$F(\mathbf{x})$	Fitness of a design \mathbf{x}

f_i	Modal frequency of mode i
$F_i(z)$	Reaction force of the DSLJ damper on the cell wall
G_a	Shear modulus of the aluminium
G_v	Shear modulus of the viscoelastic material
$h = l$	Length of the honeycomb cell wall
H	Hypervolume
$H(\cdot)$	Frequency response function (receptance)
h_i	Width of the DSLJ insert (z axis)
$H_i(\cdot)$	Frequency response function of mode i (receptance)
I	Second moment of area of the cell wall
$I_{\epsilon+}(A, B)$	Additive epsilon indicator function of two Pareto sets A and B
k	Stiffness constant
K_i	Geometric parameter relating to the DSLJ insert
k_i	Stiffness of the DSLJ damper
l_i	Length of the DSLJ insert (x axis)
n	Number of degrees of freedom in the finite element model
$R(\cdot, \cdot)$	Reference point in 2-objective space
$R_{ff}(\tau)$	Autocorrelation function of signals $f(t)$ and $x(t)$
$R_{xf}(\tau)$	Cross correlation function of signals $f(t)$ and $x(t)$
$S_{ff}(\omega)$	Power spectral density of signals $f(t)$ and $x(t)$
$S_{xf}(\omega)$	Cross spectral density of signals $f(t)$ and $x(t)$
T	Period of the oscillations
t_c	Depth of the honeycomb cell
t_f	Stiffness of the sandwich skin
T_i	Torque applied to the DSLJ damper
t_w	Thickness of the honeycomb walls

U_a	Strain energy in the aluminium
U_v	Strain energy in the DSLJ's viscoelastic material
$U_{1/2}$	Strain energy in half of the DSLJ insert
U_{cld}	Strain energy CLD's viscoelastic material
u_{cld}	Strain energy density in the CLD's viscoelastic material
$U_{i,k}$	Strain energy of material i in mode k
u_i	Strain energy density in half of the DSLJ insert
U_{tot}	Total strain energy in the damped system
u_{vem}	Strain energy density in the viscoelastic material
V_c	Volume of the honeycomb cell
V_i	Volume of the DSLJ insert's viscoelastic material
V_s	Volume of the DSLJ's rigid elements
$W(z)$	Compression force applied to the honeycomb cell
X	Search population
Z_i	Complex amplitude of the generalised coordinate of mode i
z_i	Modal or generalised coordinates

Mathematical notation

$[X]$	Matrix
$\{\dot{x}\}$	Time differentiation
$\{x\}$	Vector
$\{x\}^T$	Vector or matrix transpose
$\{x\}^{-1}$	Vector or matrix inverse
$j = \sqrt{-1}$	Complex number
x	scalar

Dissemination

During the course of this PhD, two papers have been published in a peer-reviewed journal and three conference presentations have been delivered.

Published papers

P. Aumjaud, J.E. Fieldsend, M.A. Boucher, K.E. Evans, C.W. Smith, *Multi-objective optimisation of viscoelastic damping inserts in honeycomb sandwich structures*, Composite Structures, 132 (2015), 451-463.

P. Aumjaud, C.W. Smith, K.E. Evans, *A novel viscoelastic damping treatment for honeycomb sandwich structures*, Composite Structures, 119 (2015), 322-332.

Conference presentations

P. Aumjaud, D. Lefranc, J.E. Fieldsend, K.E. Evans, C.W. Smith, *Damping performance of novel viscoelastic double shear lap joint dampers in lightweight honeycomb sandwich panels - simulation and experimental measurement*, 10th International Conference on Advances in Experimental Mechanics, Edinburgh, UK, Sept 2015.

P. Aumjaud, C.W. Smith, J.E. Fieldsend, K.E. Evans., *Optimised location and orientation of passive viscoelastic dampers for lightweight sandwich structures*, International Conference of Experimental Mechanics 16 (ICEM16), Cambridge, UK, Jul 2014.

P. Aumjaud, C.W. Smith, K.E. Evans, *Effective use of viscoelastic dampers in lightweight stiff honeycomb core sandwich panels*, 17th International Conference of Composite Structures (ICCS17), Porto, Portugal, Jun 2013.

Articles in preparation

P. Aumjaud, C.W. Smith, K.E. Evans, Experimental modal analysis of DSLJ dampers deployed in honeycomb sandwich panels.

P. Aumjaud, C.W. Smith, K.E. Evans, Quantification of mode veering for optimally damped lightweight structures.

P. Aumjaud, C.W. Smith, K.E. Evans, Passive vibration damping in lightweight sandwich structures - a review.

Chapter 1

Introduction

1.1 Context and motivation

The globalisation of our world has led to an increasing demand for transport technologies, requiring faster and safer vehicles able to carry heavier freight over a longer distance. In a report published in June 2015, the International Air Transport Association announced a 60% and 42% increase in the number of passengers and freight mass respectively between 2004 and 2014 [14]. Such an important increase requires the need for higher energy consumption combined with more efficient engines to convert this energy into motion. However, the vast majority of expenditure in commercial transport lies in fuel consumption. The global airline industry's fuel expenses are estimated to total \$226 billion in 2014 (against \$44 billion in 2003). An increase in fuel consumption also comes at the expense of adverse effects on the environment. Air transport accounts for 2% of global man-made CO₂ emissions [14]. Reducing the mass of an aircraft by 100 kg prevents releasing about four tons of CO₂ into the atmosphere each year [14]. Therefore, much effort has been spent in reducing the mass of structural components of transport vehicles without compromising their structural integrity. In many cases, sandwich panels have been found to be a very good compromise between high stiffness and low weight, and they have been extensively used as structural elements in the aerospace, marine and automotive sectors [15]. For instance, components of the nacelle of a jet engine or the wing leading edge of an aircraft are often made as a sandwich construction, see Figure 1.1. Because of their application in transport, these structures tend to experience high levels of dynamic loading. If a system is excited with a forcing frequency corresponding to one of its modal frequencies, it may enter into resonance, which may lead to high vibration amplitudes and instability in the system. Slender and lightweight structures – driven by economic pressures – are also more easily excited than heavier and sturdier designs. Vibrations are usually undesirable in a structure because they tend to (i) increase stresses in components reducing their service

life, (ii) induce wear and high cycle fatigue leading to more frequent service intervals and maintenance, (iii) cause energy losses affecting the efficiency of the system, (iv) create passenger discomfort. Much effort has been made to mitigate the deleterious effects of vibrations in order to improve reliability, safety and passenger comfort in transport. Numerous techniques and methods to damp vibration in a system have been developed over the years, including the commonly used Constrained Layer Damper (CLD). The work described in this thesis concerns efforts to damp vibration by passive means in lightweight honeycomb sandwich structures.

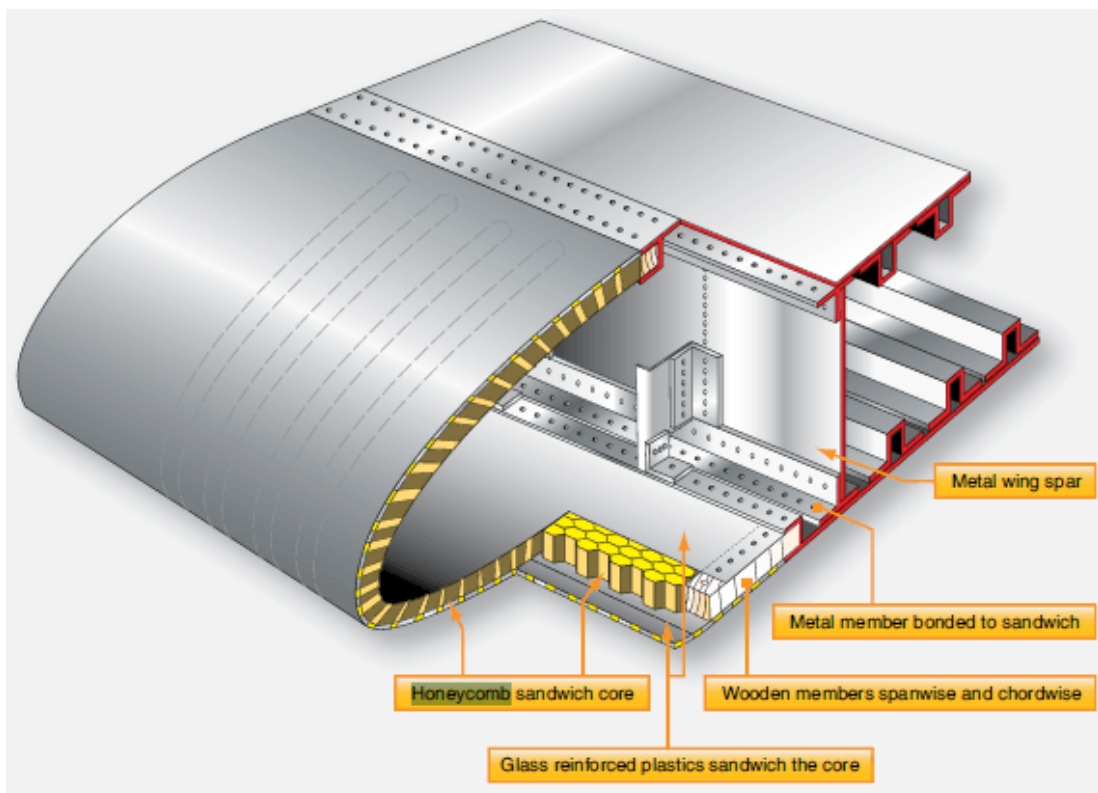


Figure 1.1: Structure of the wing leading edge of an aircraft. Adapted from [1].

1.2 Thesis objectives and outline

The purpose of this thesis is to investigate the application of passive damping to honeycomb-cored sandwich constructions with a minimal increase in the structure's mass. It focuses on the Double Shear Lap-Joint (DSLJ) damper technology discovered and patented by Boucher et al. in 2013 [16]. It is a lightweight damping device characterised by a novel passive damping mechanism. Attention is focused on the performance of the DSLJ damper in terms of damping produced per unit of added mass to the system. This thesis is structured as follows.

The second chapter provides the reader with the necessary technical background for understanding the work in this thesis. The literature to date on passive vibration damping in lightweight sandwich structures will be reviewed. This chapter also introduces the key concepts of passive vibration damping analysed with the finite element method. It includes the derivation of the governing equations of a damped system and their solution for free and forced vibration.

Chapter 3 introduces the numerical models used in the subsequent chapters of this thesis. An analytical model of a DSLJ in a hexagonal honeycomb cell is derived and compared to its equivalent finite element model. The mode shapes and natural frequencies of the sandwich beam and plate geometries considered later in the thesis are also computed.

In Chapter 4, the damping performance of the DSLJ damper is compared to that of the traditional CLD, both in terms of modal loss factors and added mass. The damping efficiency (i.e. modal loss factor per unit mass) of optimised CLD solutions is benchmarked against that of the DSLJ damper placed at a strategic location on a sandwich structure.

In Chapter 5, the optimal location and orientation of DSLJ dampers are determined for a honeycomb sandwich plate under various boundary conditions. A parametric approach based on the modal strain distribution in the system is used to identify lightweight designs that maximise damping in the first or second mode.

A more complex and robust method – able to account for the effects of mode veering occurring during the optimisation process – is implemented in Chapter 6. The evolutionary algorithm implemented determined superior configurations to those identified by the earlier parametric approach.

The vibration testing of honeycomb-cored sandwich panels treated with optimised DSLJ and CLD configurations is conducted in Chapter 7. Trends in the evolution of modal loss factors and modal frequencies between the damped and undamped system are similar to those predicted numerically.

Finally, Chapter 8 discusses the findings of the study, concludes the thesis and provides the reader with some recommendations for further research.

CHAPTER 1. INTRODUCTION

Chapter 2

Background of the study

2.1 Introduction

Vibration damping in sandwich structures is a vast field of research dating back to the early fifties. This chapter provides the reader with a review of the literature to date, focusing on passive damping techniques for lightweight sandwich structures. It also introduces the main physical concepts involved in studying this phenomenon, including finite element vibration analysis.

2.2 Sandwich structure

A sandwich structure is composed of two stiff skins bonded by an adhesive onto a lightweight core, typically a cellular solid [17] as illustrated in Figure 2.1. These structures exhibit excellent density specific properties combined with a high bending stiffness and strength and high resistance to impact compared to a homogeneous structure. Because of the separation of the two sheets by the core, the moment of inertia of the panel is increased. Thus, the structure can efficiently resist bending and buckling loads, with little increase in weight [17]. The relative weight and flexural stiffness and strength of a sandwich structure can be found in Table 2.1. In a sandwich panel, the bending moments are carried mostly by the skins in the form of tensile and compressive stress whereas the transverse forces are mainly carried by the core, see Figure 2.2. Such mechanical properties are greatly appreciated in the transport industry, and as a result, sandwich constructions have increasingly been used in aerospace for more than fifty years [15]. Sandwich structures are also widely found in nature, for example in the human skull or the wing of a bird. Since the core and the skins carry different types of loading, they are usually designed with different architectures and constitutive materials. Cellular solids are widely used as sandwich core materials in transport and other industries, even though they are

CHAPTER 2. BACKGROUND OF THE STUDY

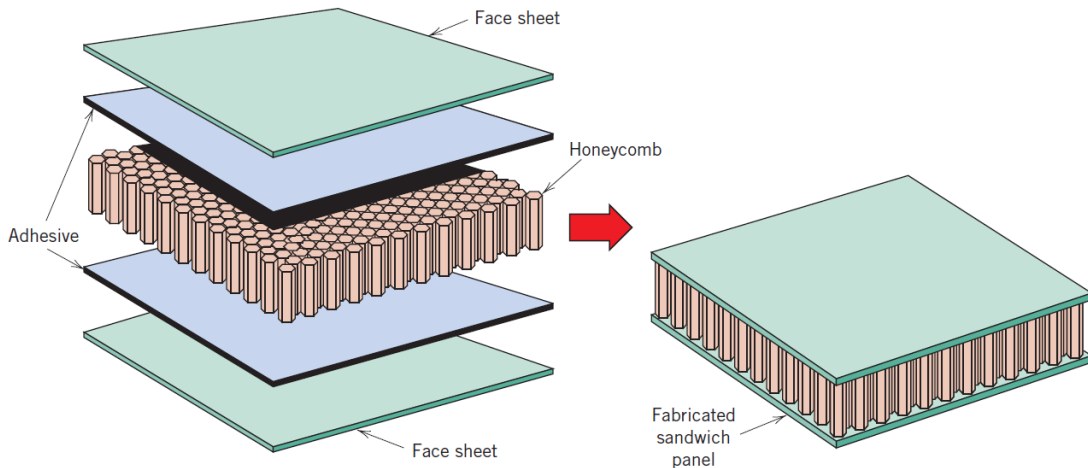


Figure 2.1: A honeycomb core sandwich panel. Adapted from [2].

	Relative weight	Relative bending stiffness	Relative bending strength
	1	1	1
	1.03	7.0	3.5
	1.06	37.0	9.2

Table 2.1: Relative weight, bending stiffness and bending strength of sandwich panels compared to a homogeneous solid material [3].

more expensive to manufacture than traditional materials [18]. Cellular solids are a class of materials made of solid struts or plates which form a network of interconnected cells [17] and have a low relative density compared to that of their constituent material. Cellular solids can be classified by their pore type. If the cell's faces are solid so that fluid communication is not allowed between the cells, the cellular solid is said to be *closed-cell*. If only the cell edges are solid, i.e. fluids can flow between cells, a cellular solid is said to be *open-cell*.

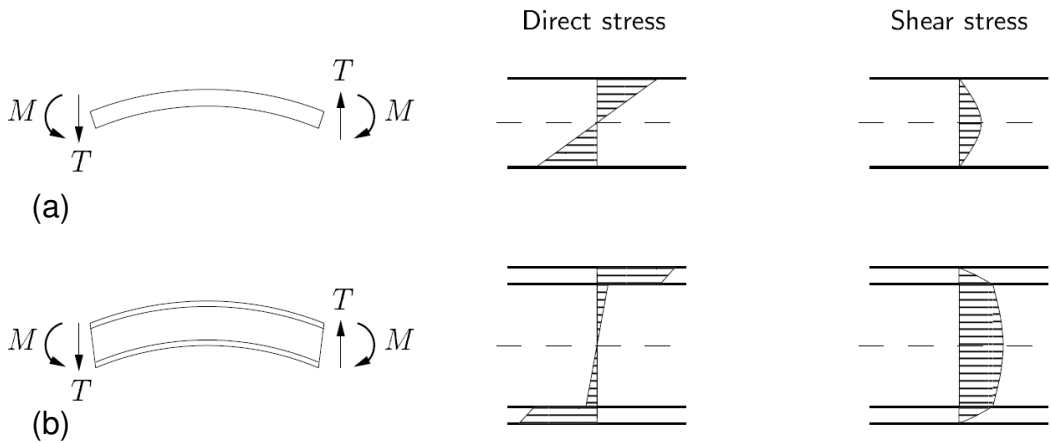


Figure 2.2: The stress distribution in a homogeneous panel (a) and a sandwich panel (b). Adapted from [3].

Cellular solids can also be classified according to their variability in cell size. *Stochastic cellular solids* are characterised by a disordered distribution of cell sizes, rib lengths and angles, and node coordination (connectivity between neighbouring ribs). The most common type of stochastic cellular solids are foams, which are three-dimensional cellular solids usually formed via a surface energy minimisation process, leaving either open cells or closed pores depending how much minimisation is allowed to occur. *Deterministic cellular solids* possess periodically ordered architectures, formed by a systematic process in which each cell is shaped. Examples include honeycombs, prismatic corrugated architecture or lattice truss materials [17]. An illustration of the different classifications of cells can be found in Figures 2.3 and 2.4. Stochastic foams have different mechanical properties from deterministic cellular solids and thus have different applications. They are better suited for acoustic attenuation and impact energy absorption than deterministic cellular solids. However, honeycombs are preferred over foams as core materials for sandwich panels for load-bearing application. Indeed, they exhibit a superior strength and stiffness, but they are also more expensive to manufacture [18]. Moreover, it is possible to optimise the mechanical performance of periodic architectures by placing reinforcing materials at strategic locations, which is not possible with foams [18]. In this thesis, attention will be focused on honeycomb-cored sandwich structures. A honeycomb can be defined as a two-dimensional array of prismatic cells [19]. It is generally periodic and regular although the cell size distribution can be very broad such as in the random Voronoi honeycomb. Typically, a honeycomb is composed of hexagonal cells such as the bee's honeycomb, but it can also be made up of square or triangular or rhombic cells, as illustrated in Figure 2.5 [17].

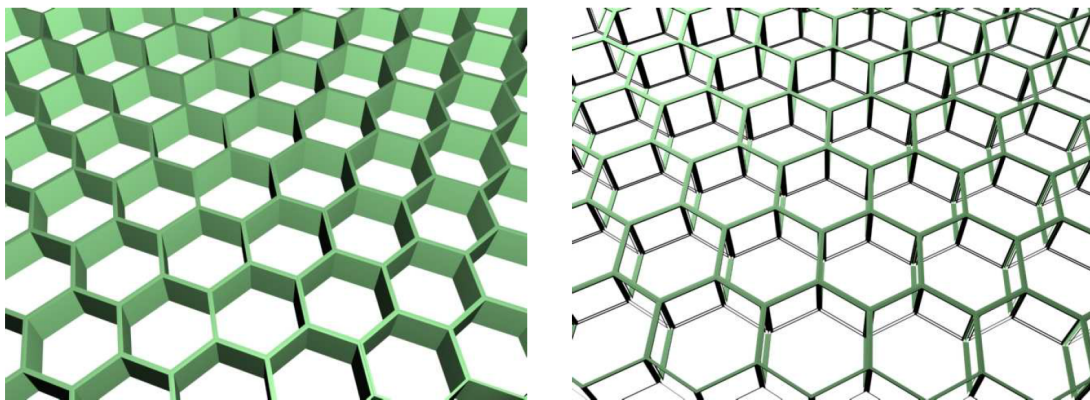


Figure 2.3: Closed (left) and open-cell (right) cellular structures. Adapted from [4].

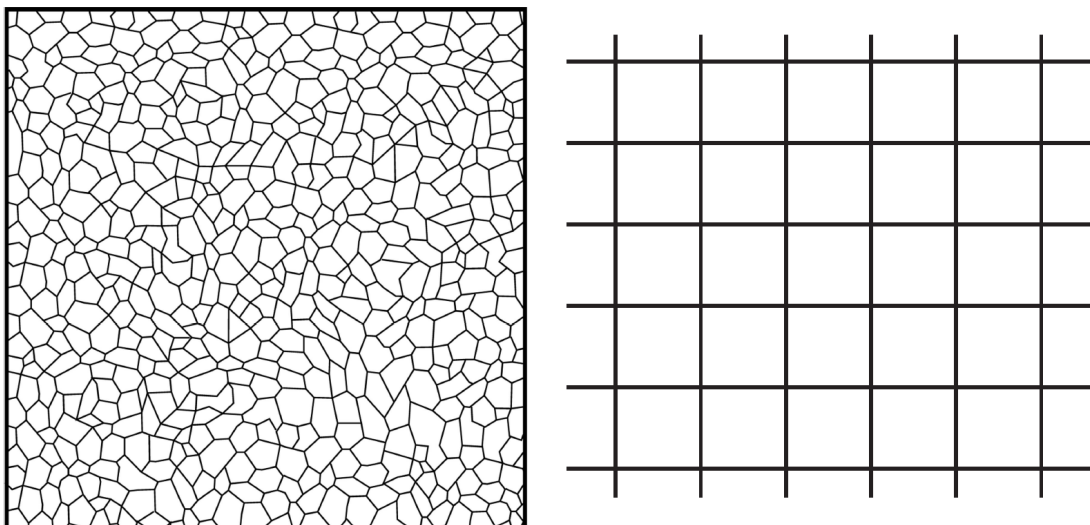


Figure 2.4: Stochastic (left) and deterministic (right) cell architecture. Adapted from [4].

2.3 Finite element vibration Analysis

This section aims at providing the reader with an introduction to the finite element analysis of vibrating systems necessary to the understanding of the subsequent finite element model used in this thesis.

Vibration is a mechanical phenomenon in which a “system subjected to restoring forces oscillates about an equilibrium point” [20]. Vibration is present in any system with a mass and elasticity and thus most structures are subjected to vibration to some extent [21]. Vibration is very often undesirable since it represents a loss of energy, causes unwanted noise and increases damage and fatigue in a mechanical device in operation by friction. It has therefore been the subject of many analytical and numerical models in order to predict the dynamic behaviour of a system. The *degrees of freedom* (d.o.f.) are the number of independent coordinates required to describe the motion of a system. Depending on its complexity, a system can be described with a finite or an

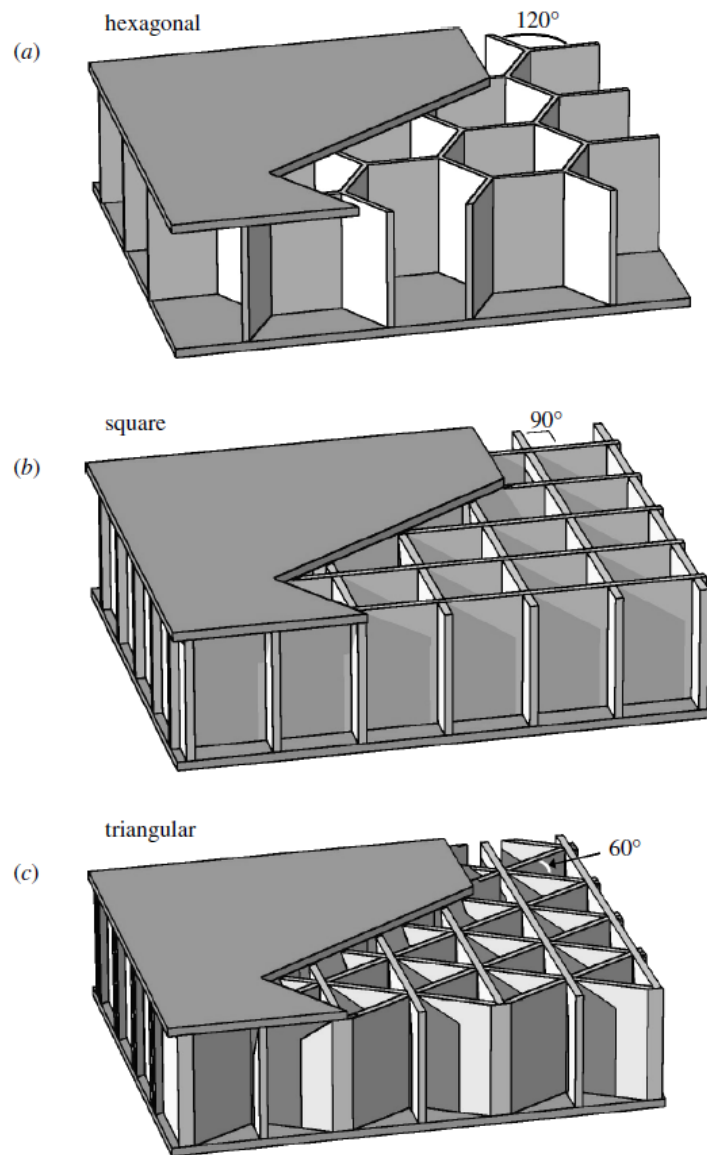


Figure 2.5: Honeycomb-cored sandwich structures. Adapted from [5].

infinite number of degrees of freedom, i.e. a *discrete or continuous system*, respectively. However, the analytical modelling of complex continuous systems can very quickly become complicated. Therefore, numerical methods are used for approximating the solution of many complex structural vibration problems. The finite element method is a computationally effective numerical method for modelling and evaluating the dynamic characteristics of a vibrating system. Vibration can be classified into two groups: *free vibration*, when the system oscillates without any external excitation other than an initial disturbance, or *forced vibration* if the system is excited by an external force. If the value of the external excitation acting on a system is known at any time and repeats periodically, the excitation is said to be *deterministic* or *periodic*. Otherwise the excitation is *random*. A deterministic excitation that varies sinusoidally with time is said to be *harmonic*. If the system's response is proportional to the external excitations, the system is said to be *linear*. In this case, the motion of

the system is harmonic and the principle of superposition can be used to solve the governing equation. Vibrating systems become nonlinear as the amplitude of oscillation increases [8]. The systems in this thesis will be considered linear and subjected to harmonic excitations.

2.3.1 Governing equation

The governing equation of motion of a vibrating system is derived using the principle of virtual displacements [6]. This principle states that “if a system in equilibrium under the action of a set of forces is subjected to a virtual displacement, the work done by externally applied loads (i.e. body forces, surface traction and concentrated loads) must balance the work absorbed by the inertial, dissipative and internal elastic forces.” [22]. A *virtual displacement* is a small physically possible motion i.e. a displacement that satisfies compatibility with the system’s boundary conditions. Note that the Hamilton’s principle or the Lagrange equation can also be used to derive the equation of motion. In the case of a linear elastic material, the principle of virtual displacements applied to an element of volume V , mass density ρ , viscous damping coefficient c and stiffness constant k gives:

$$\int_V (\{\delta u\}^T \rho \{\ddot{u}\} + \{\delta u\}^T c \{\dot{u}\} + \{\delta u\}^T k \{u\}) dV = \int_V \{\delta u\}^T \{p^{ext}\} dV \quad (2.1)$$

where $\{u\}$ is the displacement vector, $\{\delta u\}$ is the virtual displacement vector and $\{p^{ext}\}$ is the vector of external forces applied to the element of volume. The finite element discretisation gives:

$$\begin{aligned} \{u\} &= [\mathbf{N}] \{d\} \\ \{\dot{u}\} &= [\mathbf{N}] \{\dot{d}\} \\ \{\ddot{u}\} &= [\mathbf{N}] \{\ddot{d}\} \\ \{\delta u\}^T &= \{\delta d\}^T [\mathbf{N}]^T \end{aligned} \quad (2.2)$$

where $\{d\}$ is the element nodal d.o.f. vector and $[\mathbf{N}]$ is the element shape function matrix. Substituting Equation 2.2 into Equation 2.1 yields:

$$\begin{aligned} \{\delta d\}^T \int_V \left(\rho [\mathbf{N}]^T [\mathbf{N}] \{\ddot{d}\} + c [\mathbf{N}]^T [\mathbf{N}] \{\dot{d}\} + k [\mathbf{N}]^T [\mathbf{N}] \{d\} \right) dV \\ = \{\delta d\}^T \int_V [\mathbf{N}]^T \{p^{ext}\} dV \end{aligned} \quad (2.3)$$

2.3. FINITE ELEMENT VIBRATION ANALYSIS

The element mass $[m]$, damping $[c]$ and stiffness $[k]$ matrices and element force vector $\{f^{ext}\}$ are defined as follows:

$$\begin{aligned} [\mathbf{m}] &= \int_V \rho[\mathbf{N}]^T[\mathbf{N}]dV \\ [\mathbf{c}] &= \int_V c[\mathbf{N}]^T[\mathbf{N}]dV \\ [\mathbf{k}] &= \int_V k[\mathbf{N}]^T[\mathbf{N}]dV \\ \{f^{ext}\} &= \int_V [\mathbf{N}]^T\{p^{ext}\}dV \end{aligned} \quad (2.4)$$

Equation 2.3 then becomes:

$$[\mathbf{m}]\{\ddot{d}\} + [\mathbf{c}]\{\dot{d}\} + [\mathbf{k}]\{d\} = \{f^{ext}\} \quad (2.5)$$

The premise of the finite element method is that the response of the global system can be approximated by combining the contribution of each individual element to the global response using the connectivity between elements, in a process called assembly [23]. This assembly process can be illustrated by considering a system of three 2-noded bar elements with one degree-of-freedom per node. Let the element matrices be as follows,

$$[\mathbf{m}_i] = \begin{bmatrix} m_{i,11} & m_{i,12} \\ m_{i,21} & m_{i,22} \end{bmatrix} \quad [\mathbf{c}_i] = \begin{bmatrix} c_{i,11} & c_{i,12} \\ c_{i,21} & c_{i,22} \end{bmatrix} \quad [\mathbf{k}_i] = \begin{bmatrix} k_{i,11} & k_{i,12} \\ k_{i,21} & k_{i,22} \end{bmatrix} \quad (2.6)$$

where i is the element number. If the three bar elements 1, 2 and 3 are connected in line, the global equation of motion would be assembled as follows,

$$\begin{bmatrix} m_{1,11} & m_{1,12} & 0 & 0 \\ m_{1,21} & m_{1,22} + m_{2,11} & m_{2,12} & 0 \\ 0 & m_{2,21} & m_{2,22} + m_{3,11} & m_{3,12} \\ 0 & 0 & m_{3,21} & m_{3,22} \end{bmatrix} \begin{Bmatrix} \ddot{d}_1 \\ \ddot{d}_2 \\ \ddot{d}_3 \\ \ddot{d}_4 \end{Bmatrix} + \begin{bmatrix} c_{1,11} & c_{1,12} & 0 & 0 \\ c_{1,21} & c_{1,22} + c_{2,11} & c_{2,12} & 0 \\ 0 & c_{2,21} & c_{2,22} + c_{3,11} & c_{3,12} \\ 0 & 0 & c_{3,21} & c_{3,22} \end{bmatrix} \begin{Bmatrix} \dot{d}_1 \\ \dot{d}_2 \\ \dot{d}_3 \\ \dot{d}_4 \end{Bmatrix} + \begin{bmatrix} k_{1,11} & k_{1,12} & 0 & 0 \\ k_{1,21} & k_{1,22} + k_{2,11} & k_{2,12} & 0 \\ 0 & k_{2,21} & k_{2,22} + k_{3,11} & k_{3,12} \\ 0 & 0 & k_{3,21} & k_{3,22} \end{bmatrix} \begin{Bmatrix} d_1 \\ d_2 \\ d_3 \\ d_4 \end{Bmatrix} = \begin{Bmatrix} f_1 \\ f_2 \\ f_3 \\ f_4 \end{Bmatrix} \quad (2.7)$$

This assembly process is applied here to the local equations of motion (Equation 2.5) in order to build the global equation of motion:

$$[\mathbf{M}]\{\ddot{\mathbf{D}}\} + [\mathbf{C}]\{\dot{\mathbf{D}}\} + [\mathbf{K}]\{\mathbf{D}\} = \{F^{ext}\} \quad (2.8)$$

where $[\mathbf{M}]$, $[\mathbf{C}]$, $[\mathbf{K}]$ are the global mass, damping and stiffness matrices respectively, $\{\mathbf{D}\}$ is the global nodal displacement vector and $\{F^{ext}\}$ is the vector of external forces applied to the global system. Physically, this equation means that the external forces applied to the system are in equilibrium with the inertia, damping and elastic forces. It is analogous to Newton's second law, $\sum F = ma$. The global matrices can be regarded as a discrete representation of a continuous mass, damping and stiffness distribution. They are symmetric and positive definite but not diagonal, which makes Equation 2.8 a system of coupled, second order ordinary differential equations. This system cannot be solved easily under its present form and needs to be uncoupled as will be explained later.

2.3.2 Modal analysis - Free vibrations

The modal analysis of a continuous system consists in determining its natural frequencies and mode shapes. The undamped system is considered in free vibration, i.e. $[\mathbf{C}] = 0$ and $\{F^{ext}\} = 0$. Equation 2.8 becomes:

$$[\mathbf{M}]\{\ddot{\mathbf{D}}\} + [\mathbf{K}]\{\mathbf{D}\} = 0 \quad (2.9)$$

When the system is linear, vibratory motions are harmonic i.e. the nodal displacements follow a sinusoidal motion varying with time at a frequency ω and amplitude $\{\Phi\}$. The solution of Equation 2.9 can thus be assumed to be of the following form:

$$\{\mathbf{D}_i\} = \{\Phi_i\} e^{j\omega_i t} \quad (2.10)$$

Substituting Equation 2.10 into 2.9 yields the generalised eigenproblem:

$$([\mathbf{K}] - \omega_i^2 [\mathbf{M}])\{\Phi_i\} = \{0\} \quad (2.11)$$

where $\lambda_i = \omega_i^2$ is the i^{th} eigenvalue, ω_i is the natural frequency of mode i and $\{\Phi_i\}$ is the i^{th} eigenvector or mode shape. Equation 2.11 can be written as $[\mathbf{K}]\{\Phi_i\} = \omega_i^2 [\mathbf{M}]\{\Phi_i\}$. Physically, it means that a vibration mode can be considered as a system where elastic and inertia loads are in equilibrium. There are a large number of numerical methods for solving the eigenproblem and extracting the eigenpairs. Here, the iterative preconditioned conjugate gradient Lanczos eigensolver will be used to extract the eigenmodes and

eigenfrequencies [6]. Pre-multiplying the eigenproblem 2.11 by $\{\Phi_i\}^T$, the Rayleigh quotient can be defined as follows,

$$\omega_i^2 = \frac{\{\Phi_i\}^T [\mathbf{K}] \{\Phi_i\}}{\{\Phi_i\}^T [\mathbf{M}] \{\Phi_i\}} \quad (2.12)$$

2.3.3 Response history

In order to determine the response history of the system (i.e. the nodal displacement vector $\{D\}$), Equation of motion 2.8 is solved for a given loading $\{F^{ext}\}$. Since the mass, damping and stiffness matrices are symmetric and positive definite, this equation constitutes a system of coupled differential equations. The mode superposition method is used to uncouple the system which can then be solved easily. The nodal displacement vector can be defined as a linear combination of eigenvectors:

$$\{D\} = \sum_{i=1}^n z_i \{\Phi_i\} \quad (2.13)$$

where z_i are the modal (or generalised) coordinates and n is the number of degrees of freedom in the finite element model. In practice and for reasons of computational efficiency, a reduced number of modes $m \ll n$ is used such that:

$$\{D\} \approx \sum_{i=1}^m z_i \{\Phi_i\} \quad (2.14)$$

By substituting Equation 2.14 into Equation 2.8 and pre-multiplying by a typical mode shape $\{\Phi_k\}^T$, we obtain the following system of equations:

$$\sum_{i=1}^m \{\Phi_k\}^T [\mathbf{M}] \{\Phi_i\} \ddot{z}_i + \sum_{i=1}^m \{\Phi_k\}^T [\mathbf{C}] \{\Phi_i\} \dot{z}_i + \sum_{i=1}^m \{\Phi_k\}^T [\mathbf{K}] \{\Phi_i\} z_i = \{\Phi_k\}^T \{F^{ext}\} \quad (2.15)$$

It can be shown that the eigenvectors are orthogonal with respect to the stiffness and the mass matrices,

$$\begin{aligned} \forall i \neq k \quad & \{\Phi_k\}^T [\mathbf{K}] \{\Phi_i\} = 0 \\ & \{\Phi_k\}^T [\mathbf{M}] \{\Phi_i\} = 0 \end{aligned} \quad (2.16)$$

The governing equation can only be uncoupled and therefore solved if the non-diagonal terms of the system are equal to zero. Therefore,

$$\forall i \neq k \quad \{\Phi_k\}^T [\mathbf{C}] \{\Phi_i\} = 0 \quad (2.17)$$

Substituting Equations 2.16 and 2.17 into Equation 2.15, one can obtain:

$$\{\Phi_k\}^T [\mathbf{M}] \{\Phi_k\} \ddot{z}_k + \{\Phi_k\}^T [\mathbf{C}] \{\Phi_k\} \dot{z}_k + \{\Phi_k\}^T [\mathbf{K}] \{\Phi_k\} z_k = \{\Phi_k\}^T \{F^{ext}\} \quad (2.18)$$

If the mode shapes are normalised to the mass matrix, we have:

$$\{\Phi_k\}^T [\mathbf{M}] \{\Phi_k\} = 1 \quad (2.19)$$

Substituting this equation in the Rayleigh quotient (Equation 2.12) gives,

$$\{\Phi_k\}^T [\mathbf{K}] \{\Phi_k\} = \omega_k^2 \quad (2.20)$$

If the viscous damping model is adopted, each mode can be considered as single d.o.f. system for which we have:

$$\{\Phi_k\}^T [\mathbf{C}] \{\Phi_k\} = 2\xi_k \omega_k \quad (2.21)$$

where ξ_k is the modal damping ratio of mode k . The calculation of ξ_k will be detailed later in this chapter. Finally, we note,

$$p_k = \{\Phi_k\}^T \{F^{ext}\} \quad (2.22)$$

Combining Equations 2.18, 2.19, 2.20, 2.21 and 2.22 yields:

$$\ddot{z}_k + 2\xi_k \omega_k \dot{z}_k + \omega_k^2 z_k = p_k \quad (2.23)$$

This equation is analogous to the governing equation of a single d.o.f. system. The global response of the system is thus described by a system of m uncoupled equations that can be solved individually by direct integration when the initial conditions are known.

2.3.4 Harmonic response analysis - Forced vibration

The harmonic response analysis of a system consists in determining its amplitude and phase response when the system is subjected to a harmonic loading i.e. a loading that varies sinusoidally with time at a known frequency. The solution of the nonhomogeneous differential equation 2.23 is the sum of its associated homogeneous solution and a particular solution of the nonhomogeneous equation. The homogeneous solution, which is the solution of the system under free vibration, dies out because of damping after a few oscillations and it is called the *transient response*. The particular solution is known as the *steady-state response* or, in the case of harmonic loading, as the *harmonic response*. In steady-state response, the system oscillates with a constant amplitude at

the frequency of the forcing excitation. This equation is usually solved in the frequency domain by considering each mode k as a single d.o.f. system excited under a load p_k of circular frequency Ω and amplitude P_k :

$$p_k = P_k e^{j\Omega t} \quad (2.24)$$

Equation 2.23 must be satisfied at all times; therefore the solution must have a similar form to the loading,

$$z_k = Z_k e^{j\Omega t} \quad (2.25)$$

where Z_k is the complex amplitude of the generalised coordinates. Substituting Equations 2.24 and 2.25 in Equation 2.23 yields:

$$-\Omega^2 Z_k e^{j\Omega t} + 2j\xi_k \omega_k \Omega Z_k e^{j\Omega t} + \omega_k^2 Z_k e^{j\Omega t} = P_k e^{j\Omega t} \quad (2.26)$$

After simplification of the expression, we obtain:

$$H_k(j\Omega) = \frac{Z_k}{P_k} = \frac{1}{\omega_k^2 - \Omega^2 + 2j\xi_k \omega_k \Omega} \quad (2.27)$$

where $H_k(j\Omega)$ is called the *Frequency Response Function* (FRF) and characterises the mode's intrinsic dynamic behaviour. The FRF is a complex number that can be expressed in terms of its modulus and argument:

$$H_k(j\Omega) = |H_k| e^{j\phi_k} \quad (2.28)$$

The amplitude response and the phase angle are given by the modulus and the argument of the FRF, respectively. It is often convenient to represent these values in terms of $\beta_k = \Omega/\omega_k$:

$$\begin{aligned} |H_k| &= \frac{1/\omega_k}{\sqrt{(1 - \beta_k^2)^2 + (2\xi_k \beta_k)^2}} \\ \phi_k &= \arctan \left(\frac{2\xi_k \beta_k}{(1 - \beta_k^2)^2} \right) \end{aligned} \quad (2.29)$$

A typical plot of the amplitude response and phase angle is shown in Figure 2.6. When the system is excited at the frequency of a mode k , i.e. when $\beta_k = \Omega/\omega_k = 1$, the amplitude reaches a peak and the system enters into *resonance*. The amplitude peak decreases as the modal damping ratio ξ_j increases. A FRF whose output parameter is a displacement is called a *receptance*. The FRF can also be measured experimentally using input force measurements and input acceleration readings. The acceleration is obtained by differentiation of the displacement with respect to time, such as $\ddot{z}_k = -\Omega^2 Z_k e^{j\Omega t}$. The FRF can then

be expressed under another form called *accelerance* [24]:

$$A_k(j\Omega) = -\Omega^2 H_k(j\Omega) \quad (2.30)$$

Using Equations 2.27 and 2.25, the generalised displacements can be obtained as follows,

$$z_k = |H_k| e^{j\phi_k} P_k e^{j\Omega t} \quad (2.31)$$

where P_k is known from Equation 2.24. Finally, the nodal displacements can be calculated from Equation 2.13.

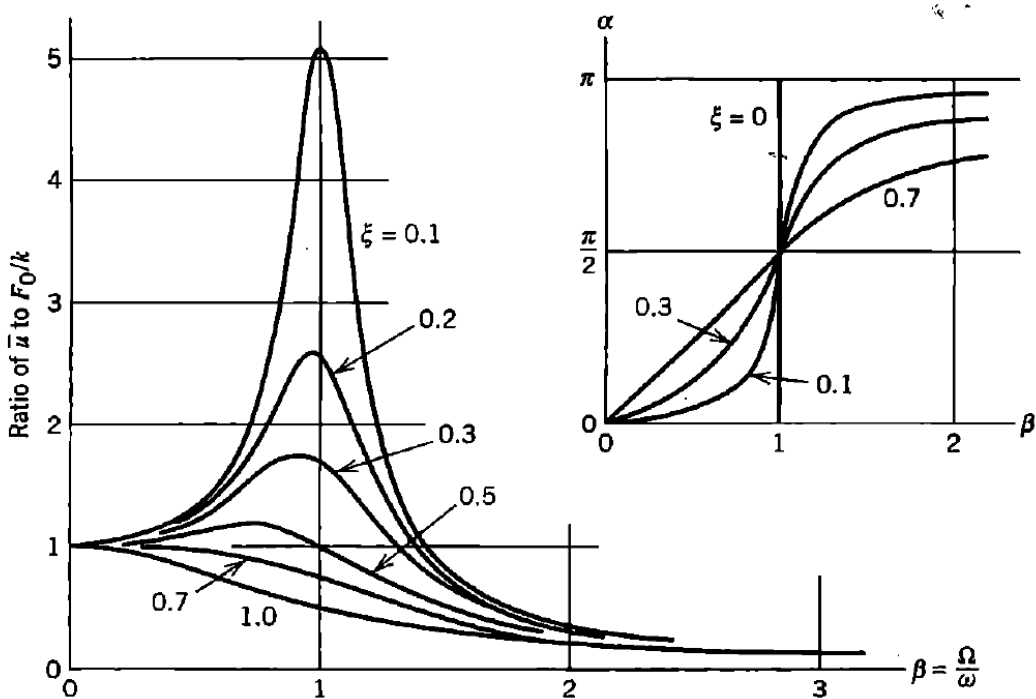


Figure 2.6: Amplitude and phase response of a single d.o.f. system for various values of damping ratio. Adapted from [6].

2.4 Vibration damping

As seen in the introduction, it is generally desirable to reduce the vibratory level of a system excited by harmonic forces. If the exciting force can be modified, the amplitude of vibration can be diminished by,

1. Moving the excitation frequency away from the resonance frequency of the system,
2. Reducing the amplitude of the excitation,
3. Changing the location where the excitation is applied to the system in order to make the excitation signal orthogonal to the resonant mode.

If the exciting force has a constant frequency over time and cannot be altered, the vibratory level can be reduced by,

1. Altering the mass and/or the stiffness of the system in order to push the resonant frequency away from the excitation frequency,
2. Adding a dynamic vibration absorber (tuned mass damper) to the system.
This consists in storing vibrating energy in a device mounted on the vibrating system which is tuned to cancel out the applied excitation. The tuned mass damper's mass and spring constants are tuned to bring its resonance frequency as close as possible to the excitation's frequency, in order to create an anti-resonance.

If the forcing excitation cannot be modified and its frequency is not constant, attenuating vibration level may be achieved by increasing the damping in the system. This solution is one of the most commonly used in industrial applications and this thesis will focus on it. Mechanical damping refers to the dissipation of vibrational energy of an oscillating system [25]. As a result, the system's peak response amplitude and the duration of its oscillations are reduced. Vibration damping can be broken down into three main categories: active, passive and semi-active (or hybrid). Active damping involves measuring the system's vibration response and applying automatically out-of-phase forces, cancelling out the measured vibration [26]. Pairs of piezoelectric sensors and actuators are typically used for active damping. Passive damping consists in energy dissipation by incorporating isolating materials into the vibrating structure. Vibrations of the host structure induce strains in such damping material, which in turn generate a force that opposes to the system's oscillations. Typically, passive damping can be introduced by viscoelastic materials, impact particles, shape memory alloys or friction. Although passive damping is not as effective for small amplitude and low frequency vibration, it has numerous advantages over active damping. Passive damping devices are generally cheaper to develop and manufacture, simpler to implement in vehicles, they generate less heat and they are maintenance-free. They are therefore more suitable for high volume production and more cost-effective. They also do not require electrical connectors, control algorithms, a power supply, actuators and sensors, which can be a critical design constraint in transport applications, for instance. Therefore, passive damping has found applications in the automotive and aerospace industries since the early sixties in an effort to extend service life and improve reliability and safety while reducing manufacturing costs [26]. Semi-active or hybrid damping consists in using active devices to amplify the strains in a lossy material, which enhance the damping. Typically, it consists of the combination of a viscoelastic material with piezoelectric ceramics, electro- or magneto-rheological fluids or

magnetostrictive materials. The hybrid constrained layer damper combines the ability of both passive viscoelastic materials to dissipate vibrational energy at high frequencies and active piezoelectric materials to cancel out low frequency excitations [27]. The work in this thesis will focus on the use of passive viscoelastic damping. A viscoelastic material exhibits both viscous and elastic behaviour when undergoing deformation: it stores mechanical energy elastically during loading and dissipates the rest in the form of heat [7]. A viscoelastic material is typically a polymer (such as a silicone rubber) composed of long molecular chains cross-linked together. The damping effect is produced by the relaxation of the polymer network to its original shape after being deformed, but it deforms more slowly than an elastic material. The strain in the viscoelastic material lags behind the deformation produced by the excitation and opposes the next cycle of vibration. The phase shift between strain and stress in a viscoelastic material is illustrated in Figure 2.7. Since the relaxation rate depends on the strength of the bonds between the molecular chain varies with the temperature, the dynamic properties of viscoelastic materials are frequency- and temperature-dependant.

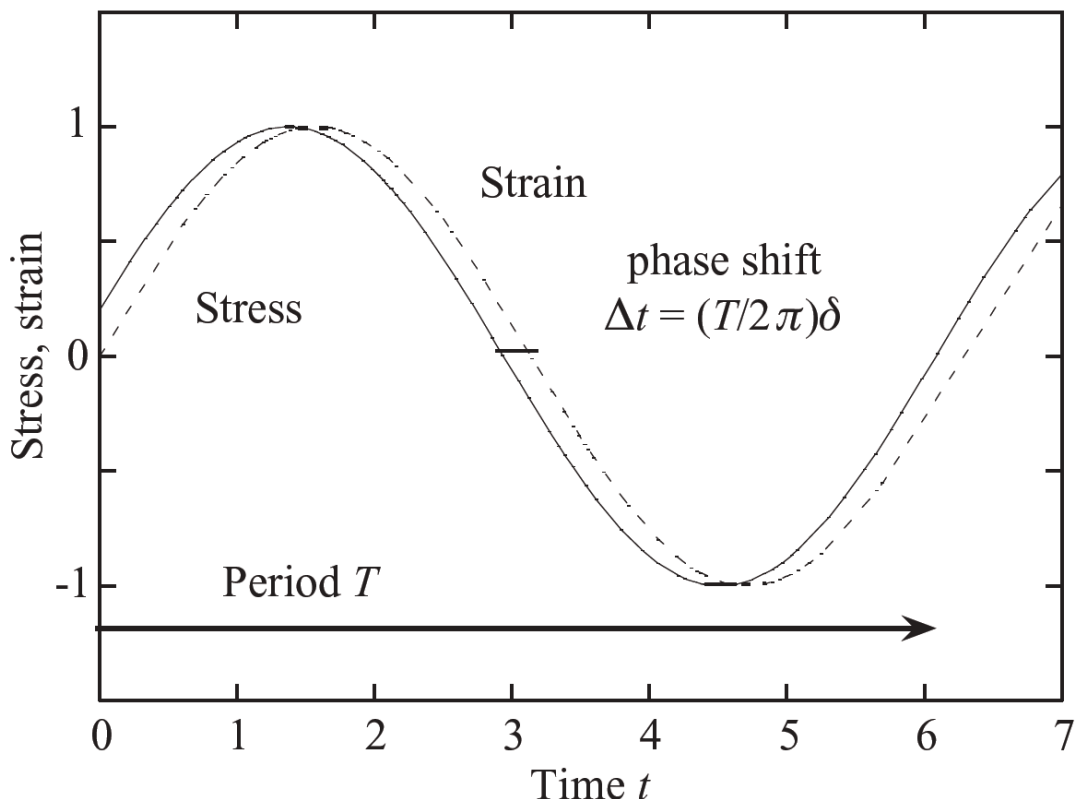


Figure 2.7: Stress and strain versus time for a viscoelastic material subjected to a sinusoidal excitation. Adapted from [7].

2.4.1 Viscoelastic damping models

Three main types of damping models can be identified: viscous damping, Coulomb damping and structural or hysteresis damping. *Viscous damping* refers to energy dissipation due to the vibration of a structure in a fluid medium. It is the most common form of damping and the simplest to implement in mathematical models. *Coulomb damping* is caused by dry friction between rubbing surfaces. *Structural damping* results from internal deformation within the structure causing energy dissipation. Although a viscoelastic material would be naturally described by the structural damping model, this form of damping cannot be easily represented in mathematical models and viscous damping is often considered as an alternative. As a rule of thumb, this assumption is valid when the damping forces $[C]\{\dot{D}\}$ are less than about 10% of the inertia and stiffness forces $[M]\{\ddot{D}\}$ and $[K]\{D\}$, see Equation 2.8 [6]. The viscous damping model allows the damping matrix to be diagonalised which is necessary in order to uncouple the system of equations of motion, see Equation 2.15. The damping matrix can either be described by a linear combination of the mass and stiffness matrices (Rayleigh or proportional damping) or defined as in Equation 2.21 (modal damping). The modal loss factor is this equation may be estimated by the Modal Strain Energy (MSE) method derived by Johnson and Kienholtz [28], which is detailed in Appendix A. In a system composed of m damping materials, the MSE method gives the following estimation of the modal loss factor of mode k :

$$\eta_k = \frac{\sum_{i=1}^m \eta_{i,k} U_{i,k}}{U_{tot}} \quad (2.32)$$

where η_i is the material loss factor of material i , $U_{i,k}$ is the strain energy in the material i under mode k and U_{tot} is the total strain energy in the system. The modal loss factor is related to the modal damping ratio by the following relations,

$$\eta_k = \frac{2\xi_k}{\sqrt{1 - \xi_k^2}} \simeq 2\xi_k \quad (2.33)$$

The MSE method can estimate the modal loss factors of a viscoelastically damped composite structure based on strain energy considerations from the undamped structure. This method is relatively easy to implement with the finite element method but it is only applicable to systems under harmonic loading with a constant frequency and in steady-state vibration. Although it is known that the MSE method may give an inaccurate evaluation of the modal loss factor and can tend to overestimate it – especially for highly damped systems [29, 30], it can efficiently provide a relative comparison of damping between different structures. Since the MSE method was applied consistently across this thesis, the results are at least comparable internally. Modified versions of the MSE method have been formulated in order to provide a more accurate description of

the modal loss factor [30–35] but they would add complexity without necessarily aiding comparison between the different damping devices presented here. A similar approach was adopted by Chia et al. [13]. An accurate mathematical model accounting for the frequency and temperature dependence of viscoelastic materials is complicated to formulate and the solution of the governing equation difficult to obtain. Thus, it is common practice to assume isothermal conditions and to only take into account the frequency dependence of viscoelastic materials [29]. Some damping models accounting for the frequency dependence of viscoelastic materials have been derived and implemented in finite element formulations, such as the Golla-Hughes-McTavish [36,37] model or the Anelastic Displacement Fields [38] methods, among others. Douglas and Yang [39] formulated the frequency-dependant complex shear modulus of the viscoelastic core of a constrained layer damper as $G_v^*(\omega) = 0.142 \left(\frac{\omega}{2\pi}\right)^{0.494} (1 + 1.46j)$ MPa. For the range of frequency considered in this study (100 to 560 Hz), the storage and loss moduli of the viscoelastic material considered would vary by 1.7 MPa and 2.5 MPa, respectively. Hence the frequency dependence of the viscoelastic material will be neglected in this study.

2.4.2 Measurement of damping

In simple structures such as single d.o.f systems, viscous damping can be measured experimentally using the logarithmic decrement δ_l . The system is subjected to an initial impact load and the decay of the free oscillations is recorded. The peak amplitudes at times t and $t + nT$, where T is the period of the oscillations and n is the number of pseudo-periods considered, are related to the logarithmic decrement by the following equation [40],

$$\delta_l = \frac{1}{n} \ln \left(\frac{A(t)}{A(t + nT)} \right) \quad (2.34)$$

where $A(t)$ is the amplitude of the damped oscillations. The viscous damping ratio can then be calculated with,

$$\xi = \frac{\delta_l}{\sqrt{(2\pi)^2 + \delta_l^2}} \quad (2.35)$$

When a system is subjected to harmonic excitation, the damping ratio can be measured using the Half-Power Bandwidth method (HPB). The response amplitude must be calculated first in the frequency domain and the resonant amplitude Q is recorded at the natural frequency ω_n . The frequencies at $Q/\sqrt{2}$ or -3dB from the peak are then measured (see Figure 2.8) and the modal loss

factor can be calculated using the following equation [24],

$$\eta_n = \frac{\omega_2 - \omega_1}{\omega_n} \quad (2.36)$$

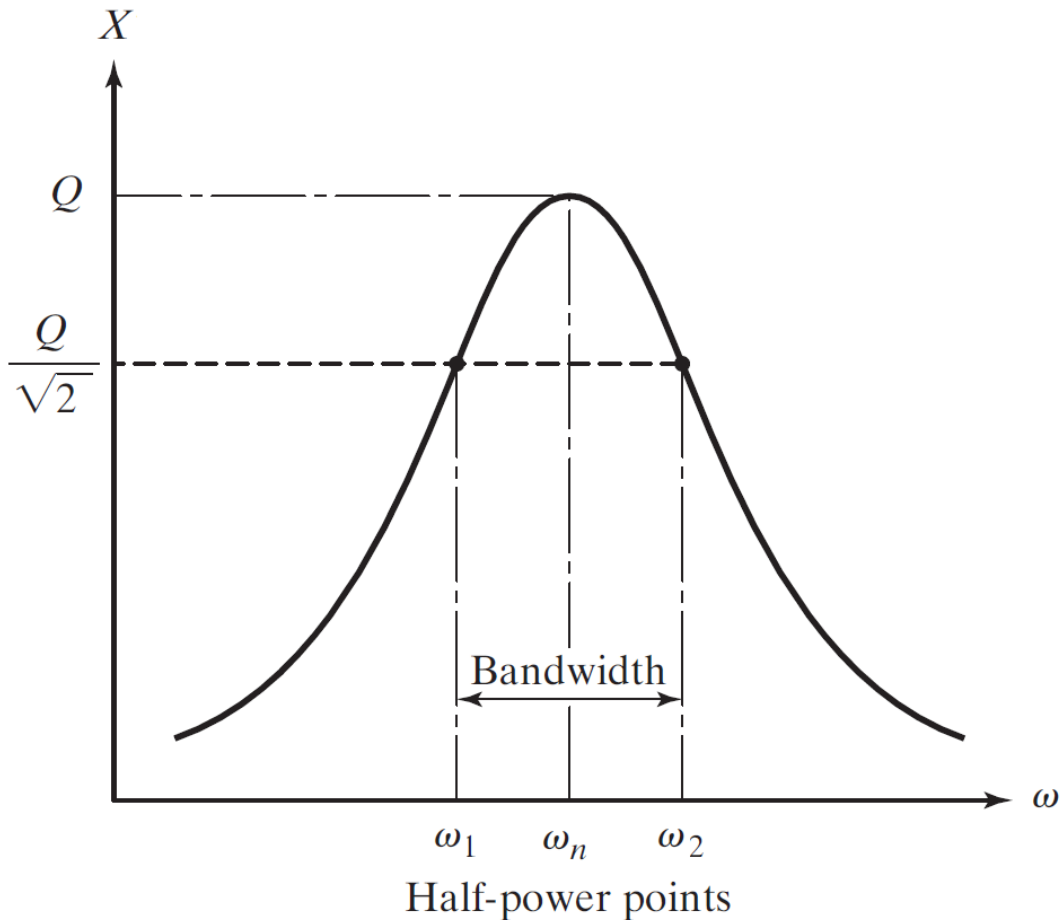


Figure 2.8: Half-power bandwidth method. Adapted from [8].

2.5 Passive viscoelastic damping in sandwich structures

Sandwich structures are widely used in the aerospace and other transport sectors for their low density and excellent mechanical properties [15]. They exhibit high stiffness-to-mass and strength-to-mass ratios which make them ideal candidates for load-bearing applications where mass is a critical issue. However, structures used in transport are often deployed in vibration-rich environments which leads to high cycle fatigue (and thus more frequent service intervals) and passenger discomfort. The natural frequency of a sandwich panel varies with the inverse of the relative density of the core ($\omega \sim \rho^{-1/2}$). Thus, it is sometimes

possible to increase the natural frequency beyond resonances by reducing the core panel density [18]. However, in many applications, the constitutive properties of the sandwich panel cannot be modified and additive damping solutions must be applied to the vibrating structure. The various passive viscoelastic damping solutions for sandwich structures will be reviewed herein, excluding research regarding acoustic isolation, wave propagation attenuation, active and semi-active damping and nonlinear vibration since these topics lie outside the scope of this thesis. An extensive review of the literature on vibration damping in sandwich structure was conducted by Li and Crocker in 2005 [41].

2.5.1 Full viscoelastic core

The initial stage of passive damping in sandwich structures consists in applying a single layer of damping material on the vibrating host structure [40]. The damping material, typically a viscoelastic material, is deformed as the host structure vibrates, subjecting the viscoelastic material to tension-compression deformation and thus inducing energy dissipation. This type of damping treatment is called an unconstrained or free layer damper and it is illustrated in Figure 2.9. However, this extensional damping treatment achieves lower damping at a given weight than shear damping treatments [40]. One of the most common examples of shear damping treatment is the Constrained Layer Damper (CLD), in which a thin viscoelastic layer is sandwiched between the host vibrating structure and a stiff constraining layer [40], see Figure 2.10. This device constrains the viscoelastic material to deform in shear and at relatively high strain thereby efficiently dissipating vibration energy in the form of heat [25]. Ross, Ungar and Kerwin [42–45] derived an analytical model for estimating the loss factor of such extensional and shear damping treatments applied to beam and plate structures. Later, DiTaranto [46, 47] derived the governing equation of motion

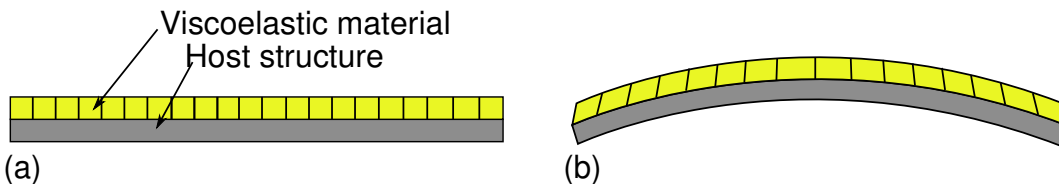


Figure 2.9: Unconstrained or free layer damper on an undeformed (a) and deformed (b) structure.

of a sandwich beam with a viscoelastic core in free vibration and computed its loss factor and natural frequency. Mead [48–51] extended DiTaranto's work to include the study of the forced vibration of viscoelastic damped sandwich beams under a variety of boundary conditions. The damping behaviour of cantilever sandwich beams with a viscoelastic core under forced harmonic excitation was

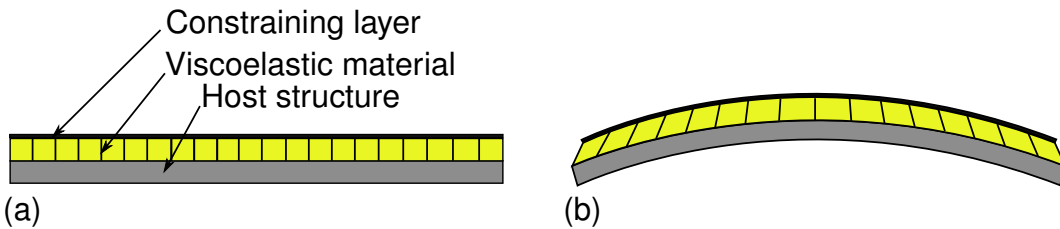


Figure 2.10: Constrained layer damper on an undeformed (a) and deformed (b) structure.

studied both theoretically and experimentally [52–55]. Yan and Dowell [56] derived a simplified governing equation of motion that describes the free vibration of sandwich beams and plates with a viscoelastic core. A large number of research projects then used these models to compute the loss factor in sandwich beams [39, 57–70]. Sylwan [71] developed a formulation for sandwich beam which combines the shear and compressional damping effects of the CLD and tuned mass damper, respectively. The first analytical model of simply supported sandwich plates and cylindrical shells with a viscoelastic core was proposed by Yu [72, 73]. Contrary to the Ross-Ungar-Kerwin model, he calculated the damping in the system by solving the equation of motion directly, taking into account the inertia effects due to transverse, longitudinal and rotary motions. Other models of sandwich plate [74–77] and cylindrical shell [78] with a viscoelastic core followed. The nonlinear response of viscoelastically damped sandwich beams [79–83] and plates [84, 85] to forced excitation has been investigated analytically, experimentally and numerically. The damping properties of CLDs were also measured experimentally [86, 87]. Many techniques that further enhance this shear damping mechanism have been investigated. For instance, the multiple constrained layer damping treatment, in which multiple alternate layers of damping material and constraining layers [88] are used to increase the shear strain in the viscoelastic material significantly, see Figure 2.11. Such treatments have been studied on sandwich beams [88–94], plates [95, 96] and cylindrical shells [97]. Other research focused on enhancing load bearing structures by inserting viscoelastic material in constructs that use a similar shear damping mechanism to the CLD. Ruzicka [9, 98] proposed the so-called cell insert beam in which a stiff rod covered with a damping polymer is inserted in a vibrating beam. The relative displacement between the beam and the rod constrains the viscoelastic material in shear, which dissipates vibrational energy. This concept is illustrated in Figure 2.13. A similar damping construct involving shear tubes was proposed by Marsh [99, 100]. A spacer layer (see Figure 2.12) can be placed between the damping material and the constraining layer of a traditional CLD, increasing the distance between the neutral axis of the host structure and the constraining layer, thus magnifying the shear in the viscoelastic material

and the structural damping of the structure. Both the bending rigidity and the mass of the damper can be reduced by inserting slots in the spacer [26]. The use of composite laminates such as fibre-reinforced polymer or carbon fibre in the constraining layer allows a further weight reduction in the damped structure while enhancing its load bearing properties. Such enhancements to the CLD have been studied analytically in sandwich beams [101], plates [102–104] and cylindrical shells [105, 106]. The development of numerical methods such as

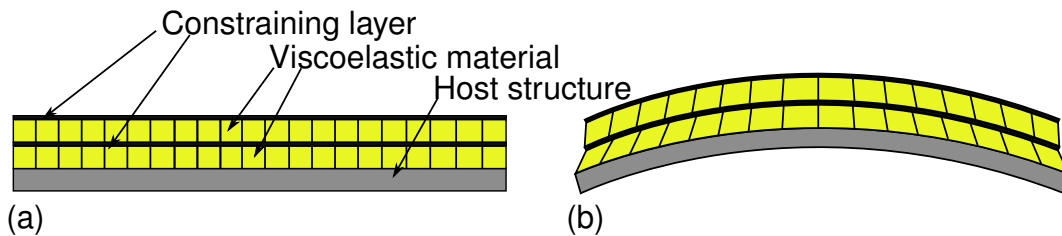


Figure 2.11: Multiple constrained layer damper on an undeformed (a) and deformed (b) structure.

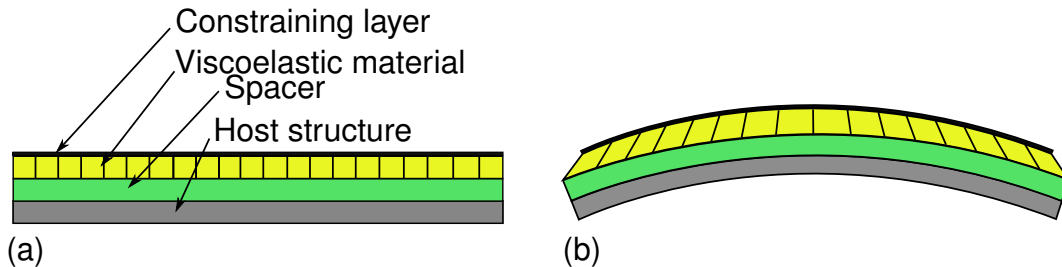


Figure 2.12: Stand-off constrained damping treatment on an undeformed (a) and deformed (b) structure.

the Rayleigh-Ritz, Galerkin and finite element methods allowed the modelling of more complex structures. They have been applied to viscoelastically damped sandwich beams [107–115], plates [116–121], cylindrical shells [122–124] and rings [125]. The finite element method was also used to model the free vibration of sandwich beams [126–136], plates [137–143] and cylindrical shells [144] with fibre composite skins and soft damping cores. Finite element analysis was also successfully applied to the modelling of forced vibration of damped sandwich beams [145–148] and plates [149–153].

2.5.2 Partial constrained layer damper

Continuous layer CLDs are effective in damping vibrations but may add significant extra mass to lightweight structures, which is a critical design constraint for the transport industry. Discrete CLD patches were designed in an effort to improve the weight efficiency of the CLD. It consists in partially covering the host structure with dampers and this was proven to be more mass efficient than a

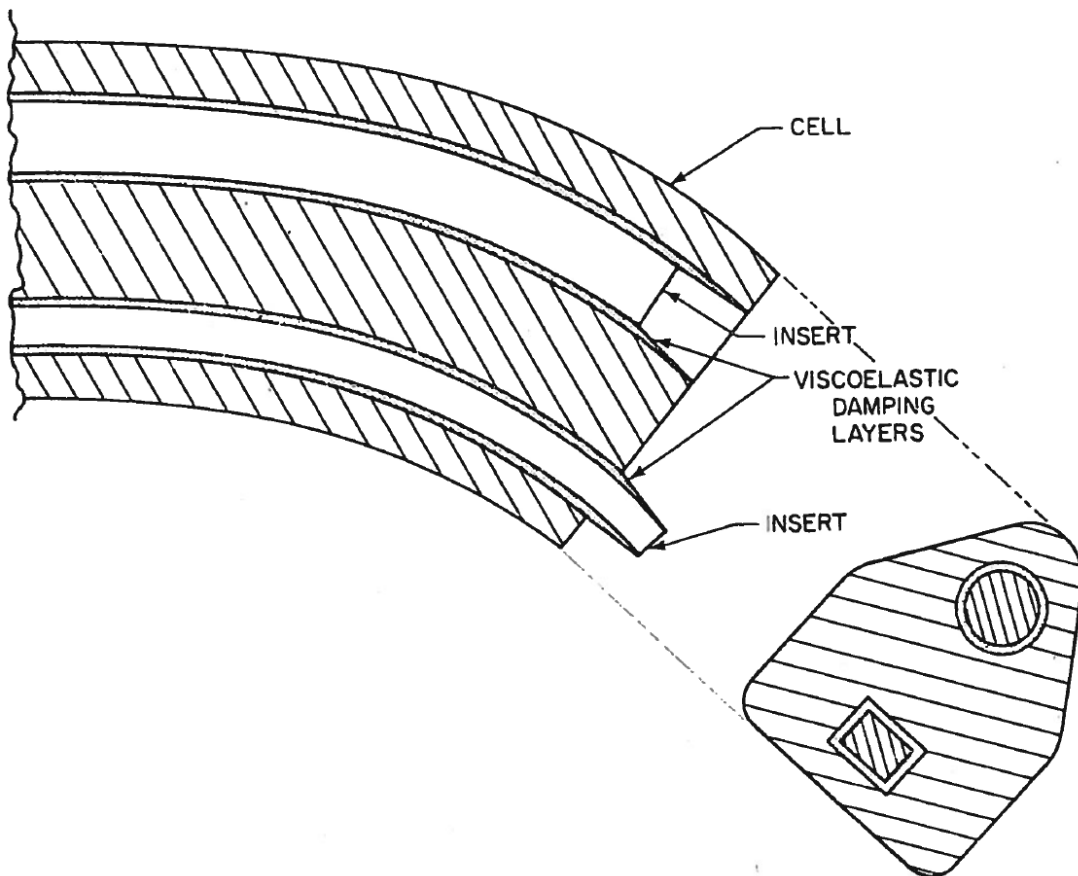


Figure 2.13: Cell insert damper. Adapted from [9].

complete coverage. Nokes and Nelson [154] were among the first to investigate partial coverage with CLDs and showed both theoretically and experimentally that more efficient damping is possible for partially covered beams. The partial coverage of beams [155–160], plates [161–167] and cylindrical shells [168, 169] with a single CLD patch and under a wider range of boundary conditions was studied extensively. Granger [170] studied the transient response after impact of a cantilever beam treated with a CLD. Levy et al. [171–173] proposed a partial double CLD on a beam. Multiple CLD patches have also been placed at strategic locations in order to maximise the damping efficiency of the treatment [174–176]. Torvik [177] investigated the performance of a plate damped with multiple CLDs whose constraining layer was segmented and showed that significant damping can be achieved. Spalding [178] measured the vibration response of CLD patches on a plate with a laser vibrometer.

2.5.3 Optimisation of partial constrained layer dampers

Minimising additional mass and maximising damping in a structure would normally be competing objectives. Further efforts to combine lightweight and high damping properties naturally led to the use of optimisation techniques. Early optimisation attempts consisted in varying a design parameter iteratively in

order to determine the optimal damping configuration [89]. These parametric optimisation studies sought to find the optimal damping and constraining layer thicknesses, material properties and location of CLD dampers for various types of structures [179–182] Subsequently, the development of heuristic algorithms contributed to identify optimal damping configurations more efficiently, especially for problems characterised by a large number of potential solutions. These techniques determine the optimal configuration of a problem by a process of trial and error. Heuristic search methods include evolutionary algorithms whose optimisation mechanism is based on the principle of survival of the fittest or the natural selection [183]. Evolutionary algorithms were applied to optimised CLD parameters such as the length of the damper [184], the thickness of the viscoelastic and constraining layers [185–190], the viscoelastic material's shear modulus [191], the distribution of ablations in the CLD [192–194], the composite skin fibre orientation [195–199] or the design of a periodic pattern in the damping layer [200]. However, most authors focused their efforts on determining the location and dimensions of CLD patches that were intended to maximise the damping whilst minimising the additional mass. These studies employed a wide range of evolutionary optimisation algorithms and considered different geometries of host structures. They are listed in Table 2.2.

Author	Year	Geometry	Optimisation algorithm
Lunden [201]	1979	Cantilever beam	Sequential unconstrained minimization technique
Lunden [202]	1980	Plane frame	Sequential unconstrained minimization technique
Hajela and Lin [203]	1991	Cantilever beam	Genetic algorithm
Marcelin et al. [204]	1992	Cantilever beam	Method of the moving asymptotes
Marcelin et al. [205]	1994	Clamped clamped plate	Genetic algorithm
Marcelin et al. [206, 207]	1995	Free-free beam	Genetic algorithm
Marcelin et al. [206]	1995	Free-free beam	Genetic algorithm
Chen and Huang [208]	2002	Simply supported plate	Topographical method
Al-Ajmi [209]	2004	Cantilever beam and plate	Topology optimisation
Zheng et al. [210, 211]	2004	Simply supported beam	Genetic algorithm
Zheng et al. [212]	2005	Cylindrical shell	Genetic algorithm
Pau et al. [213]	2006	Cantilever beam	Sequential quadratic programming
Alvelid [214]	2008	Clamped plate	Gradient-based optimisation
Chia et al. [13, 215]	2009	Free plate	Cellular automata
Hou et al. [216]	2011	Simply supported beam	Genetic algorithm
Le Maout et al. [217]	2011	Free plate	Linear-search algorithm
Kim [218]	2011	Cantilever plate	Genetic algorithm
Ling et al. [219]	2011	Cantilever and simply supported plate	Method of the moving asymptotes
Hou et al. [220]	2012	Simply supported plate	Genetic algorithm
Li et al. [221]	2012	Free plate	Cellular automata
Kang [222]	2012	Cantilever and simply supported plate	Solid isotropic material with penalization
Ansari et al. [223]	2013	Cantilever plate	Level-set method
Grewal et al. [224]	2013	Cantilever and clamped beam	Genetic algorithm

Montemurro et al. [225]	2013	Cantilever and simply supported plate	Two-level optimisation strategy
Kim et al. [226]	2013	Cylindrical shell	Topology optimisation
Zheng et al. [227]	2013	Simply supported plate	Method of the moving asymptotes
Zoghaib and Mattei [228]	2014	Cantilever beam	Conjugate gradient algorithm
Fang and Zheng [229]	2014	Cantilever plate	Level-set method
Fang and Zheng [230]	2015	Cantilever and clamped plate	Evolutionary Structural Optimisation
Xu et al. [231]	2015	Cantilever beam and simply supported plate	Genetic algorithm (NSGA-II)

Table 2.2: Optimisation studies seeking to optimise the location and dimensions of passive CLD treatments giving the maximum damping for the least additional mass.

2.5.4 Structural damping of sandwich structures with lightweight cellular solid cores

Replacing the soft viscoelastic polymer by a lightweight cellular solid core can considerably enhance the load-bearing properties of sandwich constructions [15]. Many recent research projects have investigated the damping behaviour of sandwich structures with lightweight cellular solid cores, including PVC [232–236] or expanded polystyrene [237] foam core. The combination of foam core with carbon fibre [238–241] or fibre-reinforced polymer [135, 242] skins allowed further weight saving while still providing the structure with significant damping. Other researchers investigated the damping properties of alternative types of core materials such as cork [243, 244], sand [245–247], nanocomposites [248] or perforated viscoelastic cores [249]. Vibration damping in honeycomb-core sandwich structures is also an important field of research [250–253]. Maher and Adams [254–259] estimated the damping in such structures both experimentally and numerically using the finite element method. Staley [10] patented a damping treatment using a honeycomb sandwich structure as constraining layer, see Figure 2.14. Renji [260] and Nagasankar [261] explored the damping properties of honeycomb sandwich structures with fibre-reinforced polymer skins. In an attempt to further maximise the damping-to-weight ratio in vibrating structures,

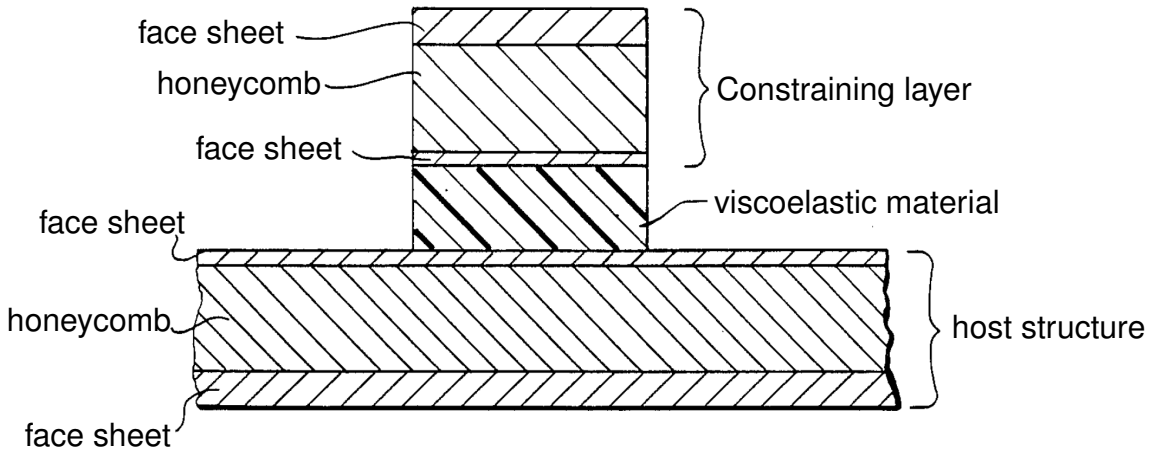


Figure 2.14: Lightweight passive damping treatment patented by Staley. Adapted from [10].

some authors have sought to integrate damping materials in the lightweight cellular solid core of sandwich structures. One advantage is that it prevents the bonding of damping treatments on the external surface of the host structure, which may be an issue for devices designed to control a fluid flow such as an aircraft wing or a gas turbine blade. Various damping techniques can be combined with honeycomb structures in order to increase the structural damping. For instance, appreciable damping can be achieved across a large frequency range by filling the cells of a honeycomb sandwich structure with fine particles or granular material, see Figure 2.15. It was shown that repeated particle collisions on the face sheets of the honeycomb cell leads to a significant attenuation of the amplitude of vibration [262, 263]. This comes at the expense of a minimal increase in the structure's mass and a moderate change in the structure's stiffness. A wide range of materials can be used for such particles, including solder balls [264], polyimide [11], perlite [265], sand [266], metal rubber [267], aluminium, steel or tungsten carbide [268]. Michon et al. [262, 263] filled the cell of a honeycomb-cored sandwich beam with hollow metallic and glass sphere particles in order to further improve the damping-to-mass ratio of the structure. Honeycomb structures can also be filled with energy absorbing foam in order to damp vibrations [269–274]. Romberg et al. [275, 276] have studied the performance of a passive friction ledge damping device which can be inserted into a flat honeycomb-core sandwich panel. Shape memory alloys and polymers can also be used as vibration damping materials in sandwich panels [277, 278]. Boucher et al. [12] designed a honeycomb structure embedded with shape memory alloys in order to enhance its damping capabilities, see Figure 2.16. Finally, a recent development of this concept was to combine viscoelastic materials with cellular solids in sandwich cores in order to provide significant energy dissipation while retaining a good mechanical integrity. The insertion

Particles

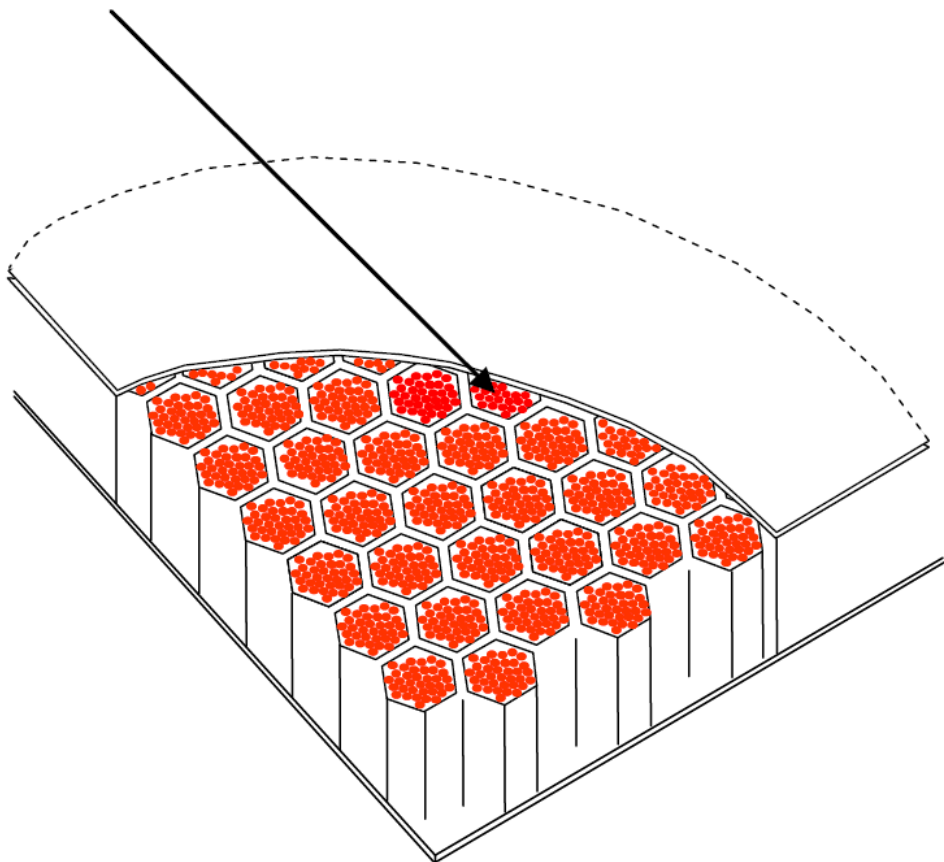


Figure 2.15: Polymer particles in a honeycomb-cored sandwich panel. Adapted from [11].

of silicon rubber into the void of a honeycomb cell was proven an efficient way of damping vibration [279]. Murray et al. [280–282] proposed to fill the cells of a metallic honeycomb structure with a lossy polymer which significantly increased the structural loss factor. Jung and Aref [283] have investigated experimentally the stiffness and damping properties of a hybrid honeycomb viscoelastic system. It was shown that embedded viscoelastic layers in the carbon-fibre skins of a honeycomb or truss core sandwich structure can provide substantial damping [284–286]. Guo and Jiang [287] designed a cylindrical damper acting as a member of a Kagome truss lattice. It consists of a stiff sleeve threaded into a rod and with a viscoelastic material in between. The relative displacement of the sleeve and the rod due to the deflection of the sandwich structures causes shear in the damping polymer and dissipates energy. Boucher et al. [288] showed that a partial filling of the honeycomb cell void can produce significant damping, and importantly with only a minimal increase in mass. Subsequently, they patented the design of elastomer fillets which can be inserted at the acute vertices of an auxetic honeycomb cell [289]. Recently, the authors also developed a new concept – the Double Shear Lap

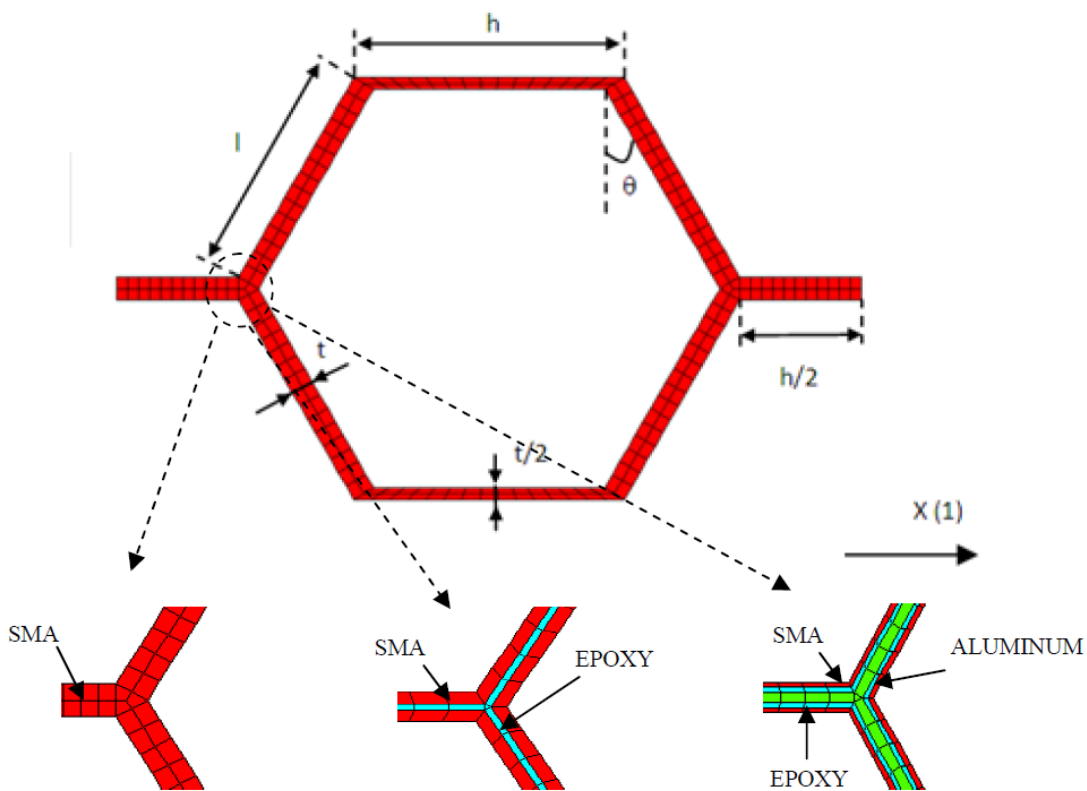


Figure 2.16: A honeycomb cell embedded with shape memory alloys. Adapted from [12].

Joint (DSLJ) damper – a weight-efficiency viscoelastic damper that can be inserted into the hexagonal cell of a honeycomb lattice [16]. It consists of a double shear lap-joint construct (see Figure 2.17) located internally in a structure so that flexure of the host structure results in rotation of the arms of the lap joint and thus, magnifying shear in the viscoelastic material and leading to significant energy dissipation.

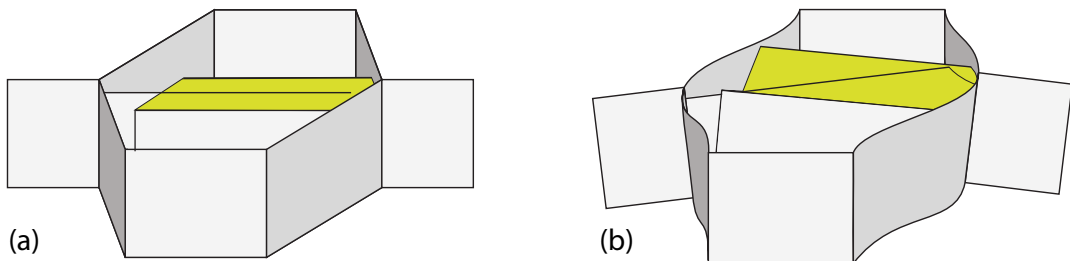


Figure 2.17: A DSLJ damper in a hexagonal honeycomb cell before (a) and after deformation (b). The viscoelastic material is shown in yellow.

2.6 Conclusion

This chapter presented a review of the literature on passive vibration damping for lightweight sandwich structures. It also introduced the derivation of the

CHAPTER 2. BACKGROUND OF THE STUDY

governing equation of motion of a vibrating system using the finite element method. The solution of this equation was given for both the free and forced vibration responses of a vibrating system as will be used subsequently in this thesis.

Chapter 3

Modelling methods

3.1 Introduction

In this chapter, the damping mechanism of the DSLJ damper will be described, both at the scale of a single hexagonal cell and an entire honeycomb sandwich structure. An analytical model will be derived in order to evaluate the reliability of the numerical finite element model used subsequently in this thesis. The mode shapes, natural frequencies, modal loss factors and amplitude responses of a variety of honeycomb-core sandwich structures will be given as preliminary results.

3.2 DSLJ inserted in a single hexagonal cell

3.2.1 Analytical model

The DSLJ damper [16] is composed of three rectangular metallic sheets arranged in a double lap-joint layout with viscoelastic material filled in between, as illustrated in Figure 3.1. It can be inserted between two opposite corners of a hexagonal honeycomb cell. Honeycomb structures are very often used as a core material for sandwich structures, which are slender structures prone to out-of-plane flexural vibration. Under such conditions, the honeycomb cell sees alternately its bottom and top deformed in tension and in compression, and its core deformed in shear, as illustrated in Figure 3.2. Consequently, a honeycomb cell with a DSLJ insert in a sandwich panel in bending is deformed as shown in Figures 3.1 (c - d). The viscoelastic material undergoes shear deformation from the relative rotation of the three constraining rigid elements, which dissipates vibrational energy. The DSLJ damper can be inserted along three different orientations in a hexagonal honeycomb cell, see Figure 3.3.

The structure considered here is a DSLJ damper inserted in a hexagonal cell which has two opposite edges deformed statically by a tension-compression

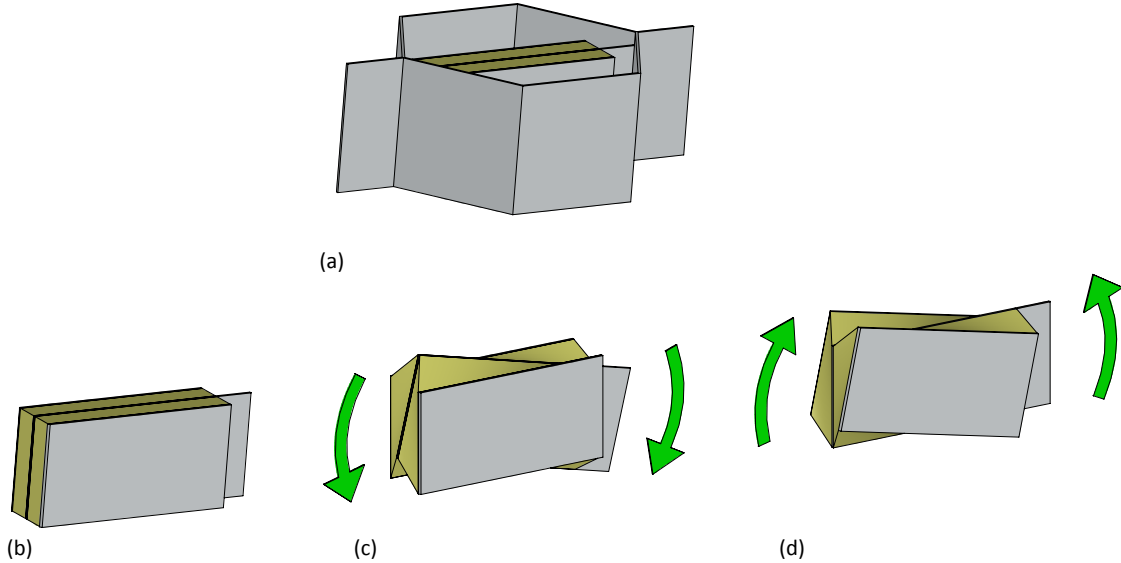


Figure 3.1: (a) A DSLJ insert in a hexagonal honeycomb cell, (b) a single DSLJ damper, (c) and (d) a DSLJ damper deformed as the sandwich panel undergoes flexural vibration. The viscoelastic material is represented in yellow and the constraining material in grey.

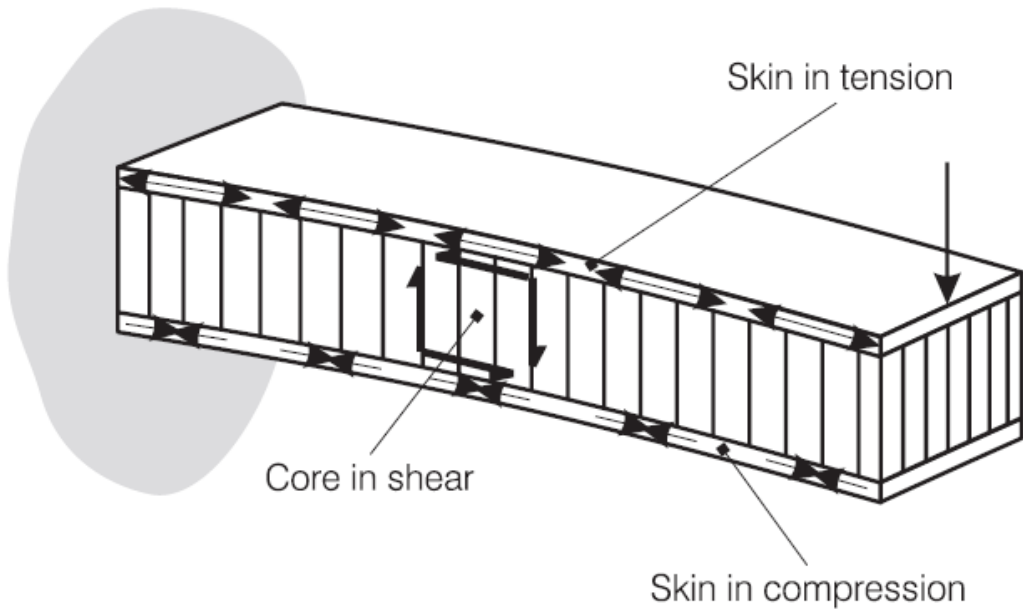


Figure 3.2: A honeycomb unit cell

loading of maximum amplitude $W = 10N$. The dimensions of the structure are shown in Figure 3.4. The cell is a regular hexagon of side $l = h = 10mm$, angle $\theta = 30^\circ$ and height $t_c = 10mm$, being fairly typical of honeycombs used in the aerospace sector. The DSLJ damper is $l_i = 16.5mm$ long, $h_i = 1mm$ wide and is offset by 1 mm from the bottom and top of the cell such that its height is $b_i = 8mm$, thus preventing the DSLJ's rigid elements from coming into

3.2. DSLJ INSERTED IN A SINGLE HEXAGONAL CELL

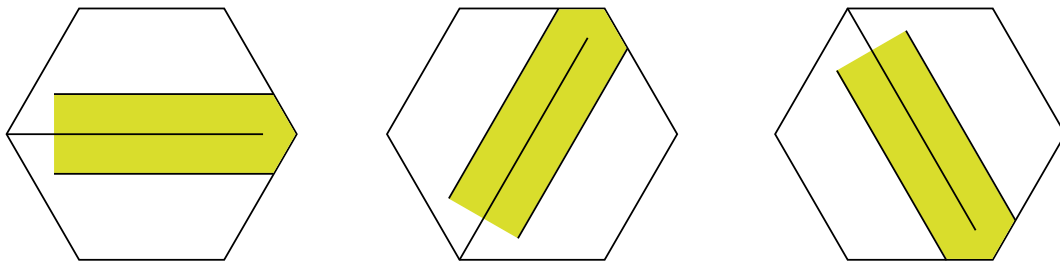


Figure 3.3: Three possible orientations of a DSLJ damper in a hexagonal cell.

contact with the sandwich face sheets during flexure of the sandwich panel. An initial static test showed that the tip displacement of a 270mm-long cantilever sandwich beam required for the DSLJ's arms to come into contact with the upper or lower skin was approximately 80 mm. Such a large deflection is unlikely to occur for the small vibration amplitude considered so such contact was not considered any further. The honeycomb cell walls, the DSLJ's rigid elements and the sandwich skins are made of a $t_w = 0.2\text{mm}$ thick aluminium sheet. The dimensions of the structure are referenced in Table 3.2. The damping material is a viscoelastic silicone rubber whose density is less than half that of the aluminium's density, its modulus about 8,000 times lower than aluminium, and its material loss factor is 3,000 times higher than aluminium. These values are similar to that of Chia et al. [13] and are typical of a silicone rubber at constant room temperature. The properties of the materials used here can be found in Table 3.1.

	Aluminium	Viscoelastic material (silicone rubber)
Young's modulus (MPa)	$E_a = 70,000$	$E_v = 8.7$
Poisson's ratio	$\nu_a = 0.3$	$\nu_v = 0.45$
Shear modulus (MPa)	$G_a = E_a/(2(1 + \nu_a)) = 26.9$	$G_v = E_v/(2(1 + \nu_v)) = 3$
Material loss factor	$\eta_a = 0.0001$	$\eta_v = 0.3$
Density (kg/m^3)	$\rho_a = 2,700$	$\rho_v = 1,100$

Table 3.1: Material properties of the honeycomb cell and the DSLJ damper. The honeycomb cell is made of aluminium and the viscoelastic material is a silicone rubber whose material properties were adapted from references [8] and [13], respectively. Subscripts a and v stand for 'aluminium' and 'viscoelastic', respectively.

As seen in Chapter 2, the MSE method is widely used for estimating the loss factor of structures composed of two or more materials. It is generalised

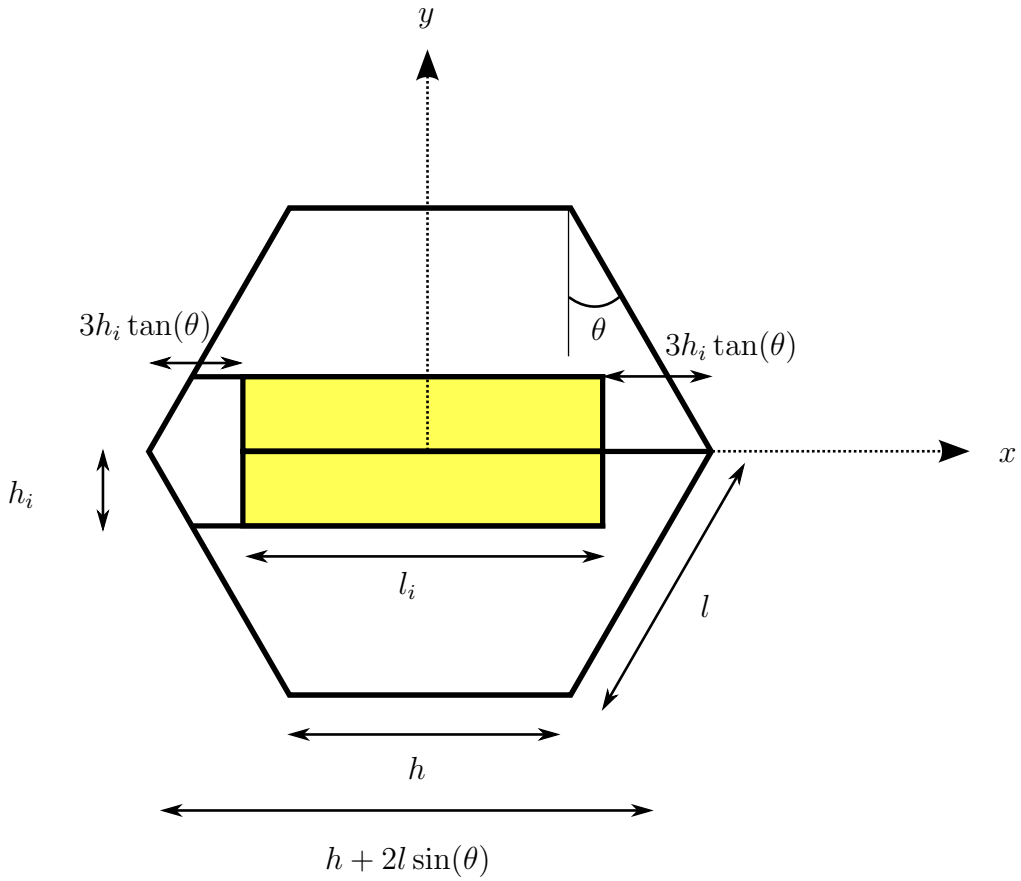


Figure 3.4: A honeycomb unit cell with a DSLJ damping insert.

	honeycomb cell	DSLJ insert
length (mm)	$h = l = 10$	$l_i = 16.5$
cell thickness (mm)	$t_c = 10$	$b_i = 8$
width (mm)		$h_i = 1$
wall thickness (mm)	$t_w = 0.2$	$t_i = 0.2$
skin thickness (mm)	$t_f = 0.2$	
cell angle ($^\circ$)	$\theta = 30$	

 Table 3.2: Dimensions and loading values of the honeycomb cell and the DSLJ damper. Subscripts c , f and i stand for ‘core’, ‘face’ and ‘insert’, respectively.

here to a structure under static loading,

$$\eta = \frac{\eta_v U_v + \eta_a U_h}{U_{tot}} \quad (3.1)$$

where η_v and η_a are the material loss factors of the viscoelastic material and the constitutive material of the honeycomb cell (aluminium), respectively. U_v , U_h and $U_{tot} = U_v + U_h$ are the elastic strain energies stored in the viscoelastic material, in the honeycomb constitutive material and in the global structure,

respectively [40]. The strain energy in the rigid elements of the DSLJ damper is neglected here. Viscoelastic materials dissipate part of the work applied by external forces in the form of heat [7]. If this heat is not dissipated quickly, the consequent temperature increase may change the material's damping properties. The MSE method adopted here estimates the loss factor of a structure as the ratio of elastic strain energy stored in the viscoelastic material (in the MSE method this is assumed to be equivalent to the external work done on the viscoelastic) multiplied by a material loss factor, to the total elastic strain energy stored in the structure, see Equation 3.1. It considers the mode shapes of the undamped structure with the viscoelastic material treated as if it was purely elastic with a real modulus [28]. The main drawback of this method is that it does not account for the temperature- and frequency-dependence of viscoelastic materials and can thus be inaccurate if they change markedly; see for example [29]. More refined and complex damping models such as the Golla-Hugues-McTavish method or the anelastic displacement fields method would give more realistic results but it would not necessarily aid comparison between the analytical and finite element models in this chapter or different DSLJ configurations as in subsequent chapters.

Forces applied to the structure

Gibson and Ashby [17, 290] have proposed an analytical model for the elastic deformation of honeycomb cells under uniaxial in-plane loading. The cell wall can be modelled as a cantilever beam fixed at one end and guided at the other, see Figures 3.5 and 3.6. For slender cell walls (i.e. small t_w/l ratio) and for internal angles θ not approaching 0° , the axial and shear deformations in the cell wall are small compared to the bending deflection and can therefore be neglected [291]. As mentioned previously, the honeycomb cell is part of a sandwich panel under flexural vibration whose core is deformed in tension at the top and in compression at the bottom. It is assumed here that such loading varies linearly across the depth of the cell, being equal to W at $z = t_c/2$, $-W$ at $z = -t_c/2$ and zero at the transverse mid-plane $z = 0$, such as illustrated in Figure 3.7,

$$W(z) = W \frac{z}{t_c/2} \quad \forall z \in \left[\frac{-t_c}{2}; \frac{t_c}{2} \right] \quad (3.2)$$

The honeycomb cell wall is loaded in bending under the action of this external force $W(z)$ but is also subjected to the reacting force of the insert $F_i(z)$ acting in the opposite direction, see the free-body diagram of the cell wall in Figure 3.6. Thus, the total force $R(z)$ bending the cell wall is,

$$R(z) = W(z) - F_i(z) \quad (3.3)$$

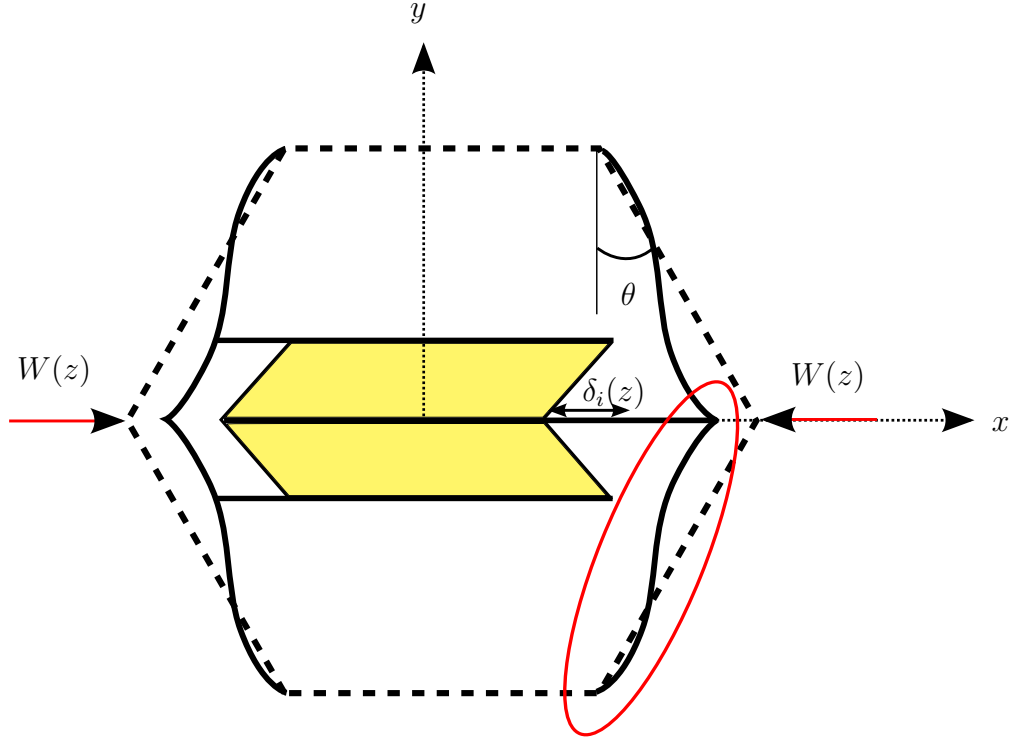


Figure 3.5: Deformed honeycomb cell with DSLJ insert. The area identified with a red ellipse is shown in Figure 3.6.

The bending moment moment applied on the cell wall is,

$$M(z) = R(z)l \cos \theta \quad (3.4)$$

According to the classical beam theory [292], the bending deflection $\delta(z)$ of the cell wall is,

$$\delta(z) = \frac{M(z)l^2}{12E_aI} \quad (3.5)$$

where $I = t_c t_w^3 / 12$ is the second moment of area of the cell wall. Assuming small linear elastic deformations, the insert is considered as a spring of constant k_i . The reaction force $F_i(z)$ of the DSLJ damper on the cell wall can be expressed as,

$$F_i(z) = k_i \delta_i(z) \quad \forall z \in \left[\frac{-b_i}{2}; \frac{b_i}{2} \right] \quad (3.6)$$

where $\delta_i(z)$ is the deflection of the DSLJ's rigid element in the x -direction, see Figure 3.5. The DSLJ damper constrains two rectangular cuboids made of viscoelastic material in torsion. First considering only half of the DSLJ damper (i.e. a single lap-joint damper), the viscoelastic solid may be seen as a bar of rectangular cross section of dimensions $b_i \times l_i \times h_i$ subjected to an in-plane force $F_{1/2}(z) = F_i(z)/2$ such as illustrated in Figure 3.8. Using the linear elastic constitutive equations in shear $\tau_i(z) = F_{1/2}(z)/b_i l_i$, $\gamma_i(z) = \delta_i(z)/h_i$,

3.2. DSLJ INSERTED IN A SINGLE HEXAGONAL CELL

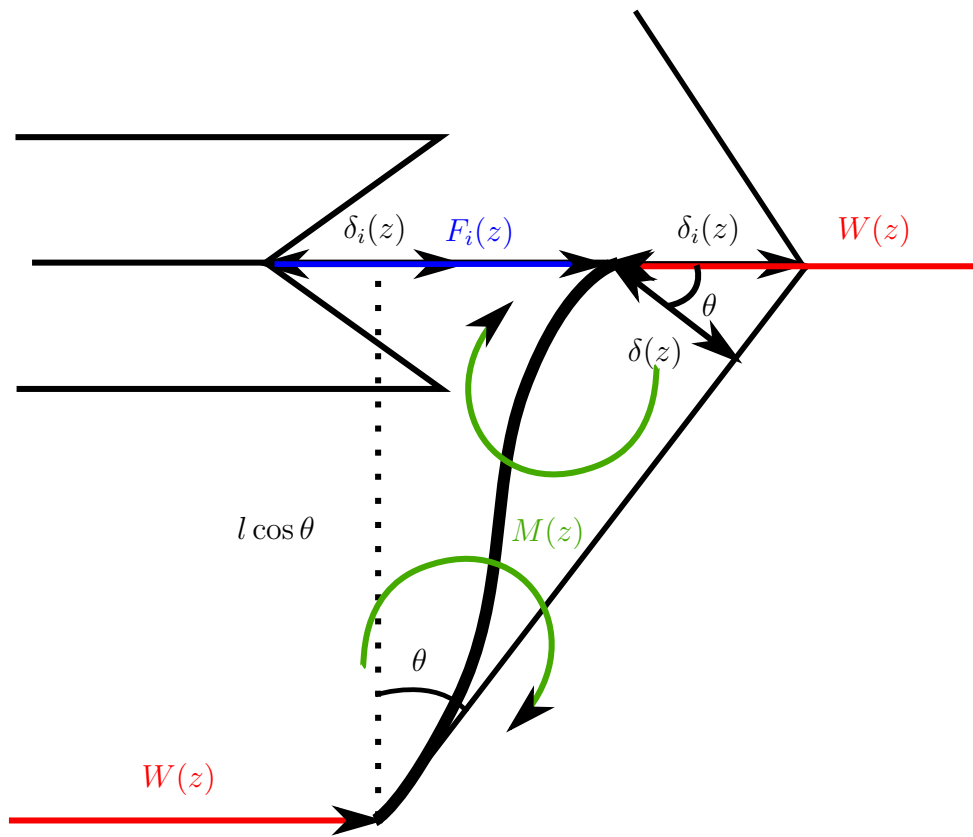


Figure 3.6: Free body diagram of a cell wall.

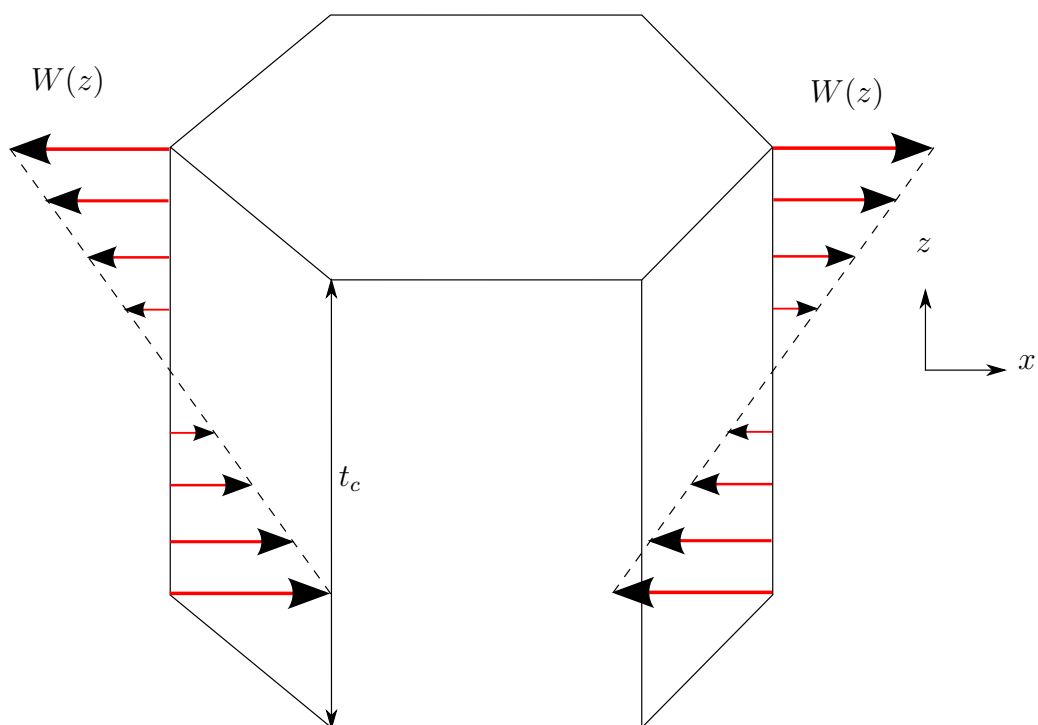


Figure 3.7: Loading of the honeycomb cell.

$\tau_i(z) = G_v \gamma_i(z)$ and Equation 3.6, one can obtain the stiffness of the insert:

$$k_i = \frac{2G_v b_i l_i}{h_i} \quad (3.7)$$

where b_i , l_i and h_i are the height, length and width of the single lap-joint damper defined in Figure 3.4. Simple geometry yields $l_i = (h + 2l \sin \theta) - 6h_i \tan \theta$. From geometrical considerations (see Figure 3.6) we have,

$$\delta_i(z) = \frac{\delta(z)}{\cos \theta} \quad \forall \theta \neq \pi \quad (3.8)$$

Using Equations 3.4, 3.5, 3.6 and 3.8, the force acting on the DSLJ damper can be expressed as follows,

$$F_i(z) = \frac{k_i l^3 R(z)}{12E_a I} \quad (3.9)$$

Defining the adimensional constant $A = \frac{k_i l^3}{12E_a I}$ and substituting from Equation 3.3, we have,

$$F_i(z) = \frac{W(z)}{1 + 1/A} \quad (3.10)$$

$$R(z) = \frac{W(z)}{1 + A} \quad (3.11)$$

Using Equation 3.2, the force applied on the cell wall and the force exerted by half of the DSLJ insert can be expressed in terms of z :

$$F_{1/2}(z) = \frac{W}{(1 + 1/A)t_c} z \quad (3.12)$$

$$R(z) = \frac{W}{(1 + A)t_c/2} z \quad (3.13)$$

Elastic strain energy stored in the honeycomb cell

From Gibson and Ashby [17], the strain and stress in the cell wall can be expressed as,

$$\begin{aligned} \varepsilon_x(z) &= \frac{\delta(z) \cos \theta}{h + l \sin \theta} \\ \sigma_x(z) &= \frac{R(z)}{lt_c \cos \theta} \end{aligned} \quad (3.14)$$

The strain energy in a cell wall in the x -direction is defined as,

$$U_w = \frac{1}{2} \int_V \sigma_x(z) \varepsilon_x(z) dV \quad (3.15)$$

Substituting from Equations 3.14, 3.5 and 3.2, one can obtain,

$$U_w = \iiint_V \frac{R(z)^2 l^2 \cos \theta}{24E_a I(h + l \sin \theta)t_c} dx dy dz \quad (3.16)$$

3.2. DSLJ INSERTED IN A SINGLE HEXAGONAL CELL

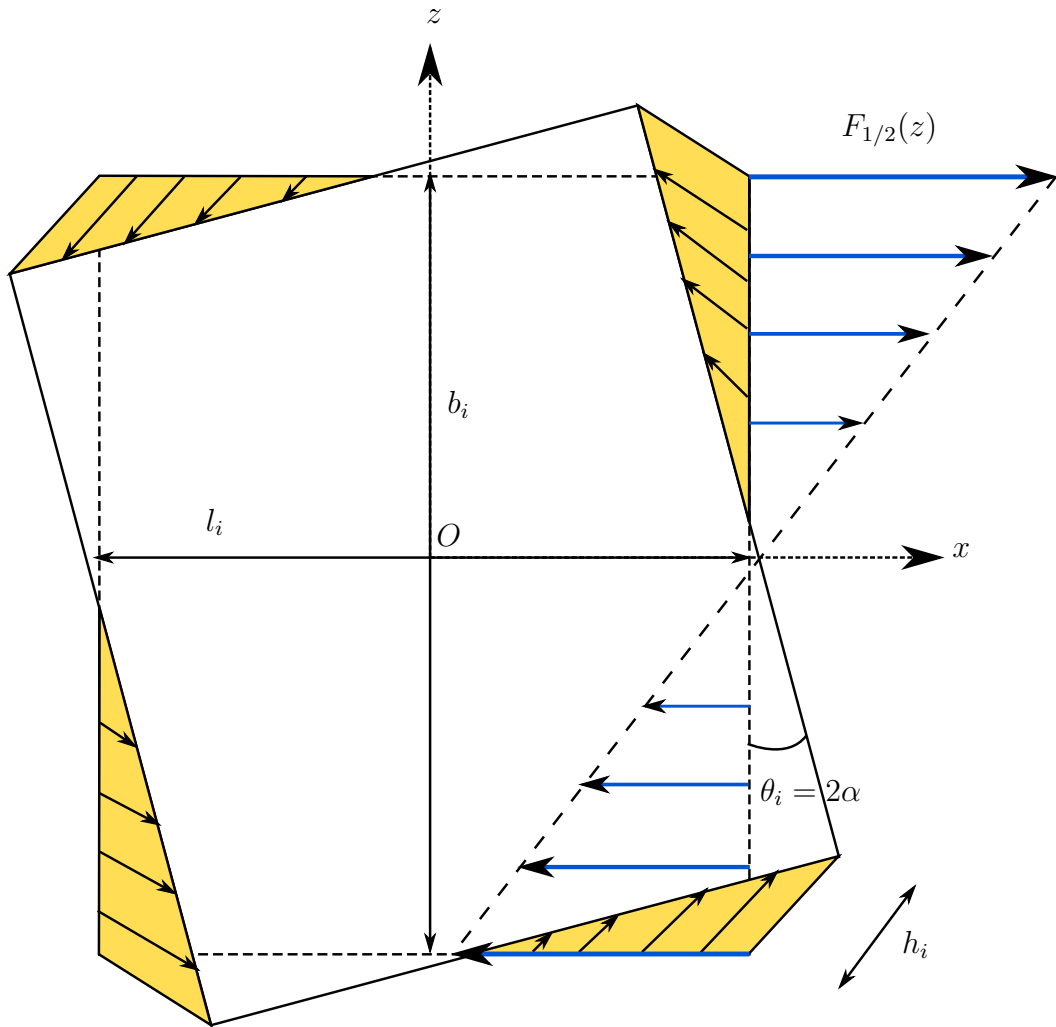


Figure 3.8: Strain profile in the viscoelastic material of half of a DSLJ insert when the cell is deformed in bending.

This equation can be expressed as,

$$U_w = \frac{W^2 l^2 \cos \theta}{6E_a I t_c^3 (h + l \sin \theta)(A + 1)^2} \iint_A dx dy \int_{-t_c/2}^{t_c/2} z^2 dz \quad (3.17)$$

Assuming that the cross-section of the cell remains undeformed for a given altitude z , simple geometry gives $\iint_A dx dy = t_w l$. After integration, one can obtain,

$$U_w = \frac{W^2 l^3 t_w \cos \theta}{72 E_a I (h + l \sin \theta)(A + 1)^2} \quad (3.18)$$

Assuming that the strain energy in two cell walls parallel to the loading is small compared to that in the four other walls (see Figure 3.5), the strain energy in the honeycomb cell is approximately four times U_w .

$$U_h \simeq 4U_w \quad (3.19)$$

Elastic strain energy stored in the viscoelastic material

The principle of conservation of energy states that the strain energy in an elastic material is equal to the work done by the external forces:

$$U_{1/2} = \int_0^{\theta_i} T_i d\theta_i \quad (3.20)$$

where T_i is the torque applied to the single and θ_i is the angle of twist. Assuming that the material is homogeneous, isotropic, linear elastic and is undergoing pure torsion, the shear strain energy can be expressed as:

$$U_{1/2} = \frac{T_i \theta_i}{2} \quad (3.21)$$

From the elastic torsion theory [292], the angle of twist in a bar of rectangular cross section is:

$$\theta_i = \frac{T_i h_i}{K_i G_v} \quad (3.22)$$

where K_i is a geometric parameter defined as follows,

$$K_i = ab^3 \left[\frac{16}{3} - 3.36 \frac{b}{a} \left(1 - \frac{b^4}{12a^4} \right) \right] \quad (3.23)$$

where $a = l_i/2$, $b = b_i/2$ and l_i is the length of the DSLJ insert. Following Figure 3.8, the applied torque T_i can be expressed as:

$$T_i = \int_{-b_i/2}^{b_i/2} \overrightarrow{F_{1/2}(z)} dz \quad (3.24)$$

Using the sign convention in Figure 3.8, we have,

$$T_i = \int_0^{b_i/2} F_{1/2}(z) dz + \int_{-b_i/2}^0 -F_{1/2}(z) dz \quad (3.25)$$

Using Equation 3.12, the torque can be expressed as,

$$T_i = \frac{W}{(1 + 1/A)t_c} \int_0^{b_i/2} zdz + \int_{-b_i/2}^0 -zdz \quad (3.26)$$

After integration, one can obtain:

$$T_i = \frac{W b_i^4}{4(1 + 1/A)t_c} \quad (3.27)$$

Finally, the total shear strain energy stored in the DSLJ's viscoelastic material is the double of $U_{1/2}$:

$$U_v = 2U_{1/2} \quad (3.28)$$

Mass of the structure

The total mass of the structure is,

$$m = \rho_a V_h + \rho_a V_s + \rho_v V_i \quad (3.29)$$

where V_h , V_s and V_i are the volumes of the honeycomb cell, the DSLJ's stiff elements and the viscoelastic polymer, respectively. Simple geometry yields,

$$\begin{aligned} V_h &= 2t_w t_c(h + 2l) \\ V_s &\simeq 3t_w b_i(h + 2l \sin \theta - 3h_i \tan \theta) \\ V_i &= 2l_i h_i b_i \end{aligned} \quad (3.30)$$

3.2.2 Finite element model

The DSLJ damper in a honeycomb cell was modelled with the commercial finite element software ANSYS 14.0 [293] using the dimensions and material properties described in Tables 3.2 and 3.1. Four-noded structural shell elements with six degrees of freedom per node (SHELL181 in ANSYS) were used to mesh the honeycomb cell wall and the DSLJ's rigid elements. The viscoelastic material in the DSLJ was meshed with an eight-noded brick element with three degrees of freedom per node (SOLID185 in ANSYS). A total of approximately 20,000 elements were used to mesh the structure. The contact interaction between the solid and shell elements required to overlap the contact surfaces in order to ensure that the nodes were coincident at the interface. The degrees of freedom of these nodes were then coupled in order to enforce compatibility at the interface between shell and solid elements, in a similar way to the approach adopted by Chia et al. [13]. The enhanced strain formulation was used to prevent shear locking of the brick elements. The MSE method was adopted to evaluate the loss factor. Similarly to the analytical model, flexural loading was applied to the cell via static in-plane forces to the nodes on the opposing edges of the cell. These forces were parallel to the x axis, and applied in opposite directions on each contralateral edge. Their magnitude was varied linearly in the z -direction, being maximal (i.e. $W = 10N$) at the top and bottom and zero at the cell's transverse mid-plane. Two nodes located on the mid plane and at the centre of the opposing parallel walls of the cell (shown in Figure 3.9) were 'pinned'. Specifically these nodes were constrained in all their degrees of freedom except the rotation along the y axis in order to allow relative motion between the DSLJ's rigid elements. The mesh, boundary conditions and applied loading are represented in Figure 3.9.

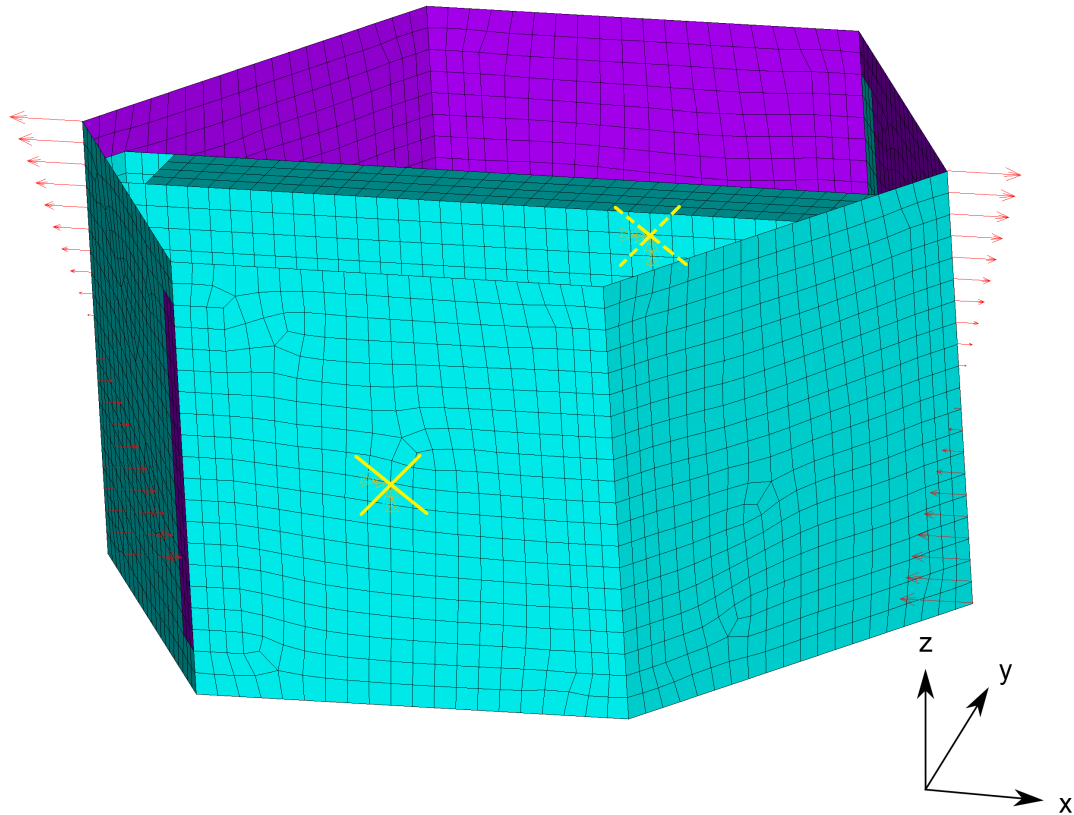


Figure 3.9: Mesh, load and boundary conditions of the finite element model. The load and the constrained nodes are represented by red arrows and yellow crosses, respectively.

3.2.3 DSLJ insert vs CLD

The DSLJ insert utilises a similar damping mechanism to the commonly used Constrained Layer Damper (CLD), i.e. it converts the global deformation in the host structure into relative internal displacement, which generates shear strain in a lossy polymer. However, the innovation in the DSLJ damper is that it induces relative rotation of the stiff elements, as opposed to relative translations in the case of the CLD. Since the damping is mainly driven by the strain energy seen by the viscoelastic polymer, the strain energy density (i.e. strain energy per unit volume) in the viscoelastic layer is a measure of the efficiency of a damping mechanism using viscoelastic materials. It is proposed here to compare the damping efficiency of the CLD and a single shear lap joint damper by comparing the strain energy densities seen by the viscoelastic polymer when the host structure is bent under the same deflection angle α .

Strain energy density in the DSLJ's viscoelastic material

In the case of a single shear lap joint damper, using equations 3.21 and 3.22, it can be shown that the strain energy seen by the viscoelastic polymer is:

$$U_{1/2} = \frac{K_i G_v \theta_i^2}{2h_i} \quad (3.31)$$

When the host sandwich panel bends by an angle α , the single lap-joint's rigid element also rotate relatively from each other by an angle α . Therefore, the angle of twist in the insert's viscoelastic layer is $\theta_i = 2\alpha$. The volume of a single lap-joint insert is $V_{1/2} = h_i l_i b_i$. Therefore, the strain energy density in the DSLJ's viscoelastic material is:

$$u_i = \frac{2K_i G_v \alpha^2}{h_i^2 b_i l_i} \quad (3.32)$$

Strain energy density in the CLD's viscoelastic layer

The viscoelastic material in a CLD can be modelled as a rectangular cuboid whose top surface is translated by a distance δ_c , see Figure 3.10. The dimensions of the CLD's viscoelastic layer are chosen identical to that of the single lap-joint damper previously considered, i.e. length l_i , width b_i and thickness h_i . The shear strain energy is defined as,

$$U_{cld} = \frac{1}{2} \int_V \tau_c \gamma_c dV \quad (3.33)$$

Assuming that the material is homogeneous, isotropic and linear elastic, Hooke's law in shear ($\tau_c = G_v \gamma_c$) yields,

$$U_{cld} = \frac{1}{2} \int_V G_v \gamma_c^2 dV \quad (3.34)$$

The strain is $\gamma_c \simeq \tan \gamma_c = \frac{\delta_c}{h_i}$, see Figure 3.10. The shear strain energy density in the CLD's damping layer thus becomes,

$$u_{cld} = \frac{G_v \delta_c^2}{2h_i^2} \quad (3.35)$$

From geometrical considerations (see Figure 3.11), the deformation δ_c corresponding to a deflection of the host structure by an angle α can be expressed as:

$$\delta_c = \alpha R - \beta d \quad (3.36)$$

where R , d and β are defined in Figure 3.11. For better performance, the viscoelastic layer is usually designed very thin, therefore we can assume that

$\beta \simeq \alpha$:

$$\delta_c \simeq \alpha(R - d) \quad (3.37)$$

d can be expressed from geometrical reasoning as $d = R - c + h_1 + h_i$ where $c = \delta_c / \sin \alpha$. In order to obtain a consistent comparison between the CLD and the DSLJ damper, the thickness of the CLD's host structure is chosen equal to the honeycomb cell thickness $h_1 = t_c = 10\text{mm}$. Thus δ_c can be expressed as,

$$\delta_c = \frac{h_1 + h_i}{1/\sin \alpha - 1/\alpha} \quad (3.38)$$

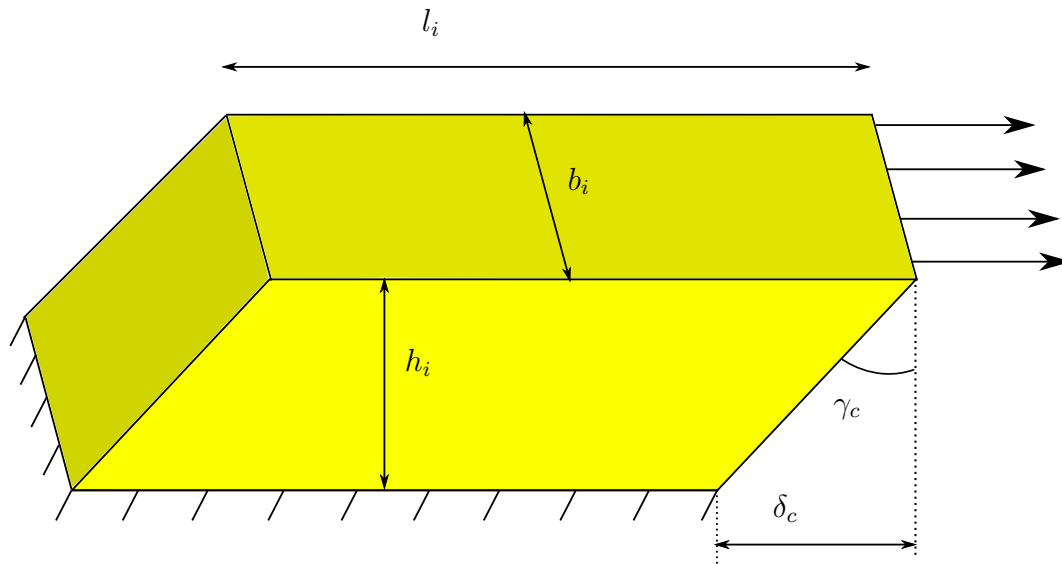


Figure 3.10: Simplified representation of the deformation of the viscoelastic layer in a CLD.

3.3 Honeycomb sandwich structures

The finite element model of the honeycomb-core sandwich structures studied subsequently in this thesis will be described here in the case of free and forced vibration. The results will be compared with those of an analytical model from the literature.

3.3.1 Analytical model

As seen in the literature review, there are numerous analytical models of honeycomb sandwich structures in free vibration. Raville and Ueng [294] derived an analytical model of a sandwich plate with an orthotropic core simply supported along all edges. Their model does not include the effects of the rotatory inertia

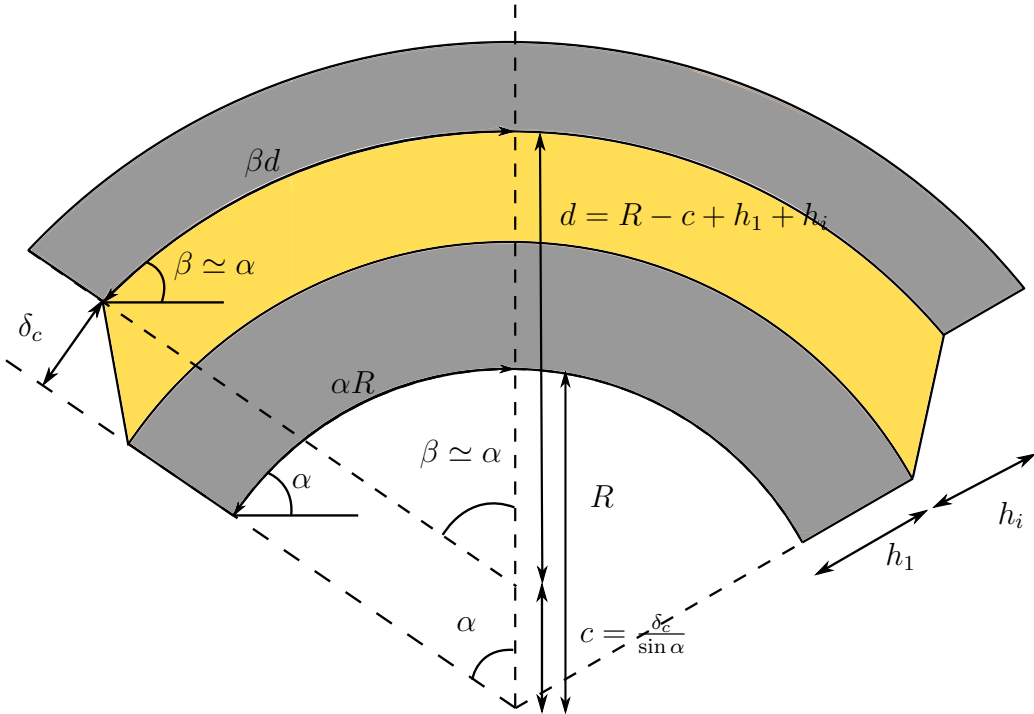


Figure 3.11: CLD on a deformed host structure.

and transverse shear of the facings. The eigenfrequencies $f_{mn} = \omega_{mn}/2\pi$ of a $a = 300\text{mm}$ long and $b = 173\text{mm}$ wide rectangular and simply supported honeycomb sandwich plate are given as,

$$\omega_{mn}^2 = \frac{E_a(\xi^2 + \eta^2)^2}{\rho_{area}(1 - \nu_a^2)t_c^4} \left(I_f + \frac{I_t}{1 + S_{mn}} \right) \quad (3.39)$$

where,

$$\begin{aligned} \xi &= m\pi t_c/a \\ \eta &= n\pi t_c/b \\ I_f &= 2t_f/12 \\ I_t &= t_f(t_c + t_f)^2/2 \\ r &= G_{xz}/G_{yz} \\ \beta &= a/b \end{aligned} \quad (3.40)$$

$$\Lambda_{mn} = m^2 + (n\beta)^2/r$$

$$W = \frac{t_c t_f \pi^2 E_a}{2b^2 G_{xz} (1 - \nu_a^2)}$$

$$S_{mn} = \frac{W}{\Lambda_{mn}} \left(\frac{(m^2 + (n\beta)^2)^2}{\beta^2} + \frac{m^2 n^2 r (1 - 1/r)^2}{1 + \Lambda_{mn} W r (1 - \nu_a)/(2\beta^2)} \right)$$

m and n are integers corresponding to the mode numbers along the length

and the width, respectively. The shear moduli of the honeycomb core in the zx and yz plane are given by Gibson and Ashby [17] as,

$$\begin{aligned} G_{xz} &= \left(\frac{t_w}{l}\right)^3 \frac{G_a \cos \theta}{h/l + \sin \theta} \\ G_{yz} &= \left(\frac{t_w}{l}\right)^3 \frac{G_a(h/l + 2 \sin^2 \theta)}{2 \cos \theta(h/l + \sin \theta)} \end{aligned} \quad (3.41)$$

Note that for regular hexagonal cells (i.e. $h = l$ and $\theta = \pi/6$), we have $G_{xz} = G_{yz}$. The mass density of the plate per unit area ρ_{area} can be computed by calculating the mass and area of a single honeycomb cell with skins. The area and volume of the cell can be calculated using simple geometry,

$$\begin{aligned} A_{cell} &= 4(h + l \sin \theta)(l \cos \theta) \\ V_{cell} &= 2t_c t_w(h + 2l) + h t_c t_w + 2t A_{cell} \end{aligned} \quad (3.42)$$

The mass density per unit area can then be computed as follows,

$$\rho_{area} = \frac{\rho_a V_{cell}}{A_{cell}} \quad (3.43)$$

The mode shapes of a simply supported sandwich plate follow the classical Navier's solutions,

$$w_{mn}(x, y) = A_{mn} \sin \frac{m\pi x}{a} \sin \frac{n\pi y}{b} \quad (3.44)$$

where A_{mn} is a coefficient that can be normalised to unity.

3.3.2 Finite element model

The sandwich structures considered in this thesis are modelled in three dimensions using the commercial finite element software ANSYS 14.0 [293]. A computationally efficient approach would consist in modelling the sandwich structure with laminated shell elements. However, it was necessary here to model the geometric details of the core (i.e. the hexagonal cells) because of the particular damping mechanism of the DSLJ damper which is based on the internal deformation of the honeycomb cells. The honeycomb-cored sandwich beam and plate considered here are illustrated in Figures 3.12 and 3.13, respectively. The plate's honeycomb core is composed of 181 hexagonal cells, with 10 complete cells along its length and 10 complete cells across its width, plus 9×9 interleaving cells. The beam's honeycomb core is made of 9×2 complete cells and 8×1 interleaving cells, making a total of 26 cells. The beam's length, width and thickness are 270 mm, 34.6 mm and 10 mm, respectively. The plate is 300 mm long, 173 mm wide and 10 mm thick. This gives a length-to-depth aspect ratio of 27:1 for the beam and 30:1 for the plate. The panel skins are

3.3. HONEYCOMB SANDWICH STRUCTURES

considered to be thin (2% of the panel's depth), and made of the same material as the honeycomb cells (aluminium in this case).

The six structures considered here are a cantilever beam (*CF beam*), a simply supported beam (*SS beam*), a cantilever plate (*CFFF plate*), a plate with free boundary conditions (*FFFF plate*), a plate with simply supported and free boundary conditions on the short and long edges, respectively (*SFSF plate*) and a plate with simply supported boundary conditions along all edges (*SSSS plate*). The cantilever boundary condition consists in fixing the degrees of freedom of all the nodes on the edge (i.e. $u_x = u_y = u_z = r_{xy} = r_{xz} = r_{yz} = 0$). Simply supported boundary conditions involve constraining the nodes on the bottom surface of the structure's edge with no translational freedom but retaining rotational freedom, i.e. $u_x = u_y = u_z = 0$, following Srinivas [295]. The free boundary condition imposes no constraint on any nodes. The two sandwich skins are perfectly bonded to the core by merging the coincident nodes at the core-skin interface. The type of element used and the finite element model of the honeycomb cell were described earlier in this chapter.

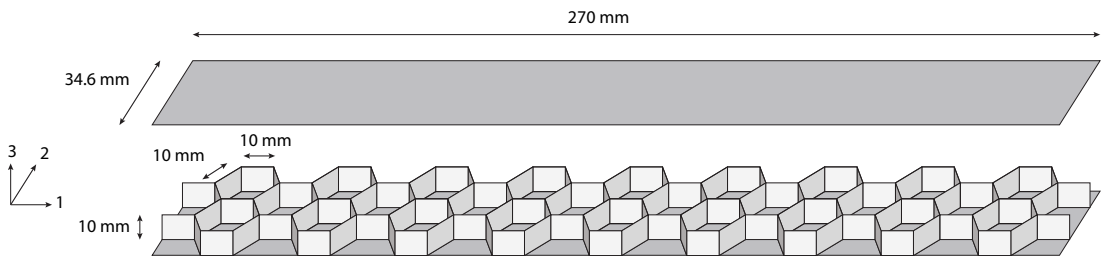


Figure 3.12: Honeycomb-cored sandwich beam, with upper skin removed for clarity.

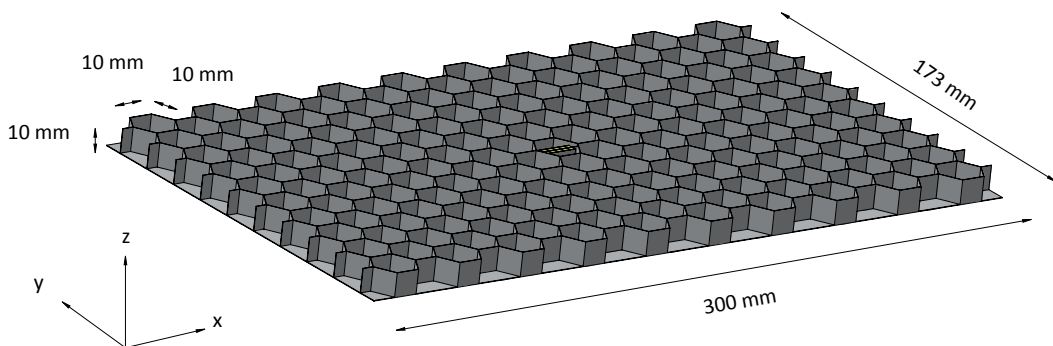


Figure 3.13: The array of hexagonal cells in the honeycomb core and the lower skin, with upper skin removed for clarity. A single DSLJ insert is sketched in the centre.

The first five mode shapes and eigenfrequencies are extracted by modal analysis as described in Chapter 2. In the case of the free boundary conditions, the rigid body modes are ignored. The FRF of the sandwich structures is computed in single input single output configuration by mode superposition

harmonic analysis. Ten thousand substeps are used across a frequency range of 2,700 Hz and the forcing excitation has an amplitude of 10 N. The finite element model implemented using ANSYS Parametric Design Language (APDL) is presented in Appendix B.

3.4 Preliminary results

3.4.1 DSLJ inserted in a single hexagonal cell

The contour plot of the strain energy in the honeycomb cell with a DSLJ damper is shown in Figure 3.14. The vast majority of the strain energy is seen by the viscoelastic polymer, suggesting that the DSLJ's damping mechanism is effective. A comparison of the loss factor and mass of the honeycomb cell computed analytically and via the finite element method can be found in Table 3.3. The value of the mass is comparable between the finite element and analytical models, however the loss factor of the analytical model is higher than the one computed via the finite element method. This is likely due to the following assumptions and in this order of importance:

- The analytical model cannot adequately capture the pattern of strain in the cell walls, particularly the angled cell walls, and so the damping loss factor (which is a ratio of viscoelastic loss to total strain energy) is underestimated. In the model for honeycomb cells developed by Gibson and Ashby and others since, the in-plane and shear deformations in the flexural cell wall are assumed to be near zero under in-plane loading and are ignored [17]. This is known to be correct for slender cell walls loaded in-plane and angles θ not approaching 0° [291]. However, these deformations appear not to be insignificant for the loading mode adopted here, i.e. a tension-compression force simulating flexure. In this case, there is significant in-plane deformation of the angled cell walls, captured by the finite element model but not the analytical, which gives rise to a near hundredfold difference in strain energy in the aluminium component of the cell, see Table 3.3.
- The viscoelastic material is undergoing pure torsion in the analytical model. In the finite element model this is the case in much of the material in the middle but ceases to be so towards the edges of the DSLJ, and this is where the material sees higher strain energy. These boundary effects are captured by the finite element model, see Figure 3.14, but not the analytical. Indeed, the strain energy stored in the viscoelastic material is slightly higher in the finite element model, see Table 3.3.

Other assumptions in either the analytical model alone or both models which are unlikely to account for the difference in loss factor are:

- The strain energy in two cell walls parallel to the loading and thus under axial stress is small compared to that in the four other walls which are under flexural stress. This assumption is acceptable for the uniaxial in-plane loading adopted here. The same assumption was made in the honeycomb cell model by Gibson and Ashby [17]. The strain energy in those wall computed in the finite element model is small compared to the strain energy in the bending wall, see Table 3.3.

The assumptions that are common to both the analytical and finite element model are:

- The bending of the sandwich panel imposes a tension-compression loading that varies linearly across the depth of the cell. This assumption may not be exact at the interface between the sandwich skins and the cell but is valid in the sandwich core. This assumption is commonly used in sandwich construction; see for example [3].
- The viscoelastic material is treated as if it were linear elastic. Though this is incorrect the magnitude of the strains under consideration for this vibration problem are small, and thus differences between linear elasticity and rubber elasticity will be small [296].

Based on the above assumptions, the finite element model is likely to produce more accurate results.

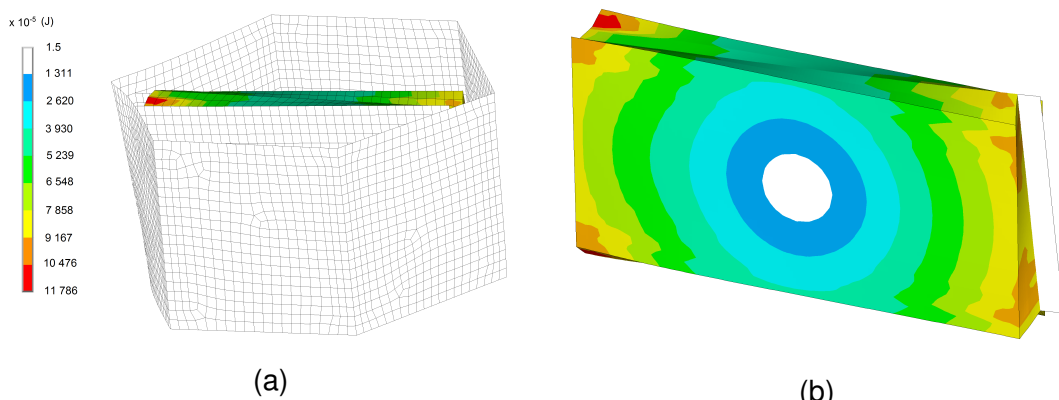


Figure 3.14: Contour plot of the strain energy in a honeycomb cell with a DSLJ damper (a) and in a DSLJ damper (b). The regions of highest and lowest strain energy are indicated in red and white, respectively.

	Analytical model	Finite element model
mass (g)	0.852	0.847
loss factor	0.293	0.143
strain energy stored in the viscoelastic material (J)	2.96×10^{-3}	3.41×10^{-3}
strain energy stored in the aluminium (J)	6.75×10^{-5}	3.76×10^{-3}
strain energy stored in the angled wall (J)	1.69×10^{-5}	7.22×10^{-4}
strain energy stored in the parallel wall (J)	0	7.84×10^{-6}
bending strain in the angled wall	4.46×10^{-4}	1.62×10^{-4}
in-plane strain in the angled wall	0	4.03×10^{-4}
shear strain in the angled wall	0	4.68×10^{-14}

Table 3.3: Comparison of the mass, loss factor and strain energy stored in a honeycomb cell with a DSLJ insert either computed analytically or via the finite element method.

3.4.2 DSLJ insert vs CLD

The strain energy density seen by a soft polymer constrained by two parallel and rigid plates which displace relatively from each other either in rotation (DSLJ damper) or in translation (CLD) can be found in Figures 3.15 and 3.16. The DSLJ insert's damping mechanism generates a higher strain energy per unit volume in the viscoelastic material than that of the CLD, which implies that more energy is dissipated. As expected, both damping mechanisms lose efficiency as the thickness of the viscoelastic layer increases, see Figure 3.16. As the bending angle of the host structure increases, more strain energy is seen by the viscoelastic material, which is also expected. For small bending angles, the DSLJ damper and the CLD show a similar damping efficiency. However as this angle increases, the DSLJ damper becomes much more efficient than the CLD, see Figure 3.16.

3.4.3 Honeycomb sandwich structures

The five first mode shapes and natural frequencies of the six structures considered in this thesis are given in Tables 3.4 and 3.5, respectively. The mode shapes of the sandwich structures resemble those of a homogeneous plate with the same boundary conditions. In the case of the SSSS plate, the mode shapes and natural frequencies found analytically and via the finite element method

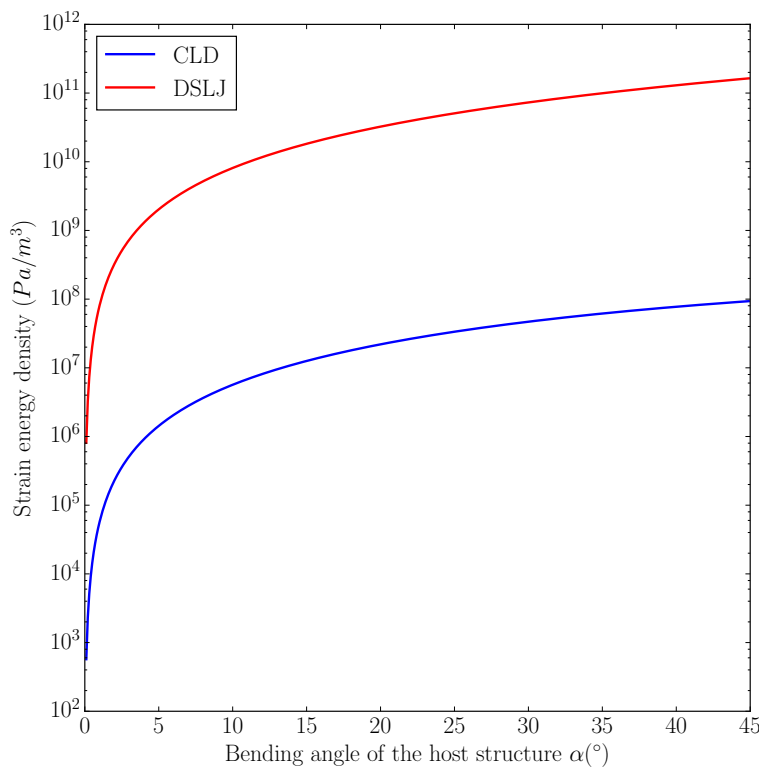


Figure 3.15: Strain energy density in the viscoelastic material constrained either by a CLD or a DSLJ damper when the host structure bends by an angle α . The thickness of the viscoelastic layer is kept constant at $h_i = 1\text{mm}$.

are similar, which suggests that the finite element models are correct. The amplitude response of the SFSF plate is shown in Figure 3.17. As expected, a peak in amplitude corresponds to each modal frequency, suggesting that the FRF is computed correctly.

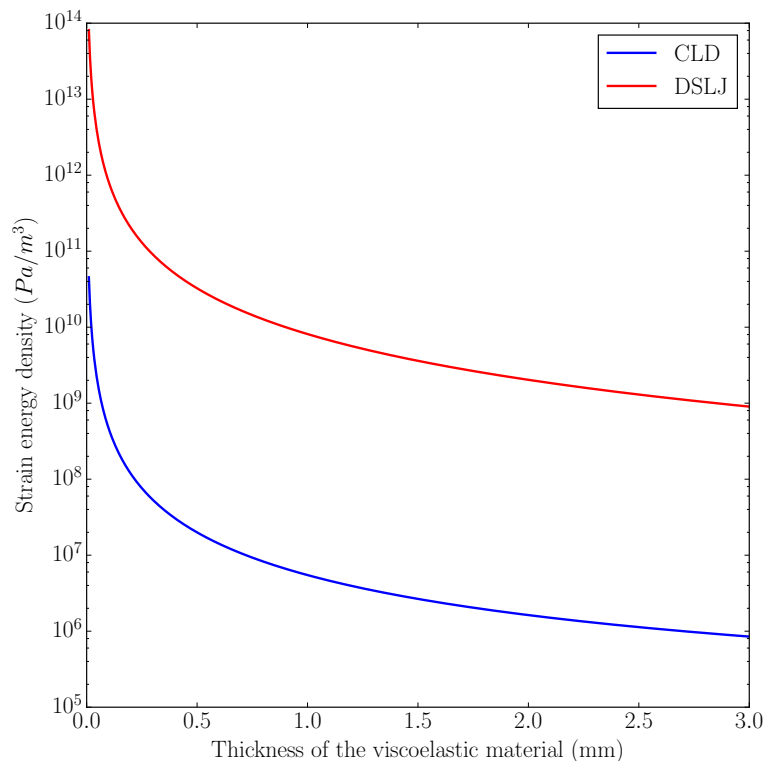
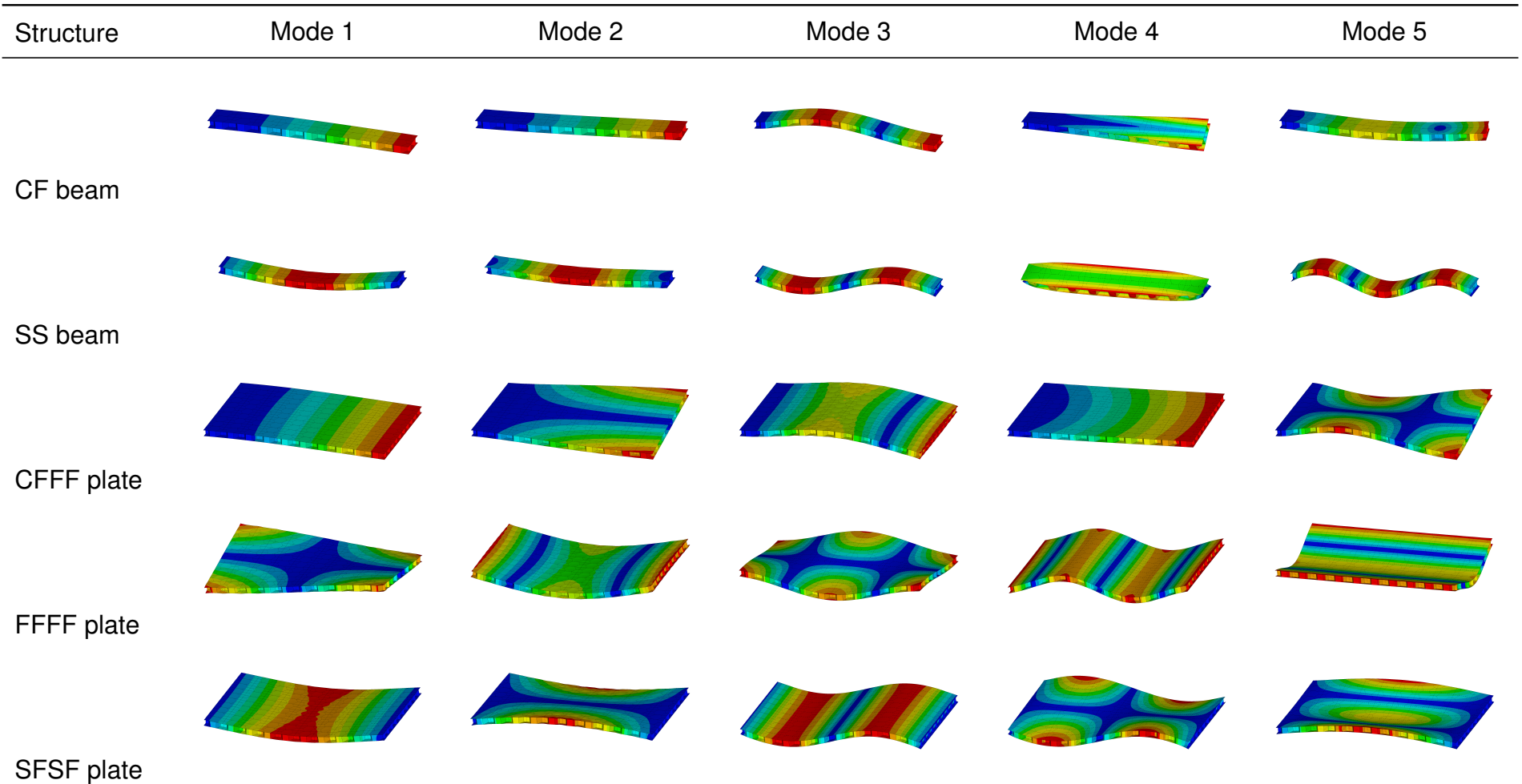


Figure 3.16: Strain energy density in the viscoelastic material contained either by a CLD or a DSLJ damper as the thickness of the viscoelastic layer varies from 0.001 mm to 3 mm. The bending angle of the host structure is kept constant at $\alpha = 10^\circ$.



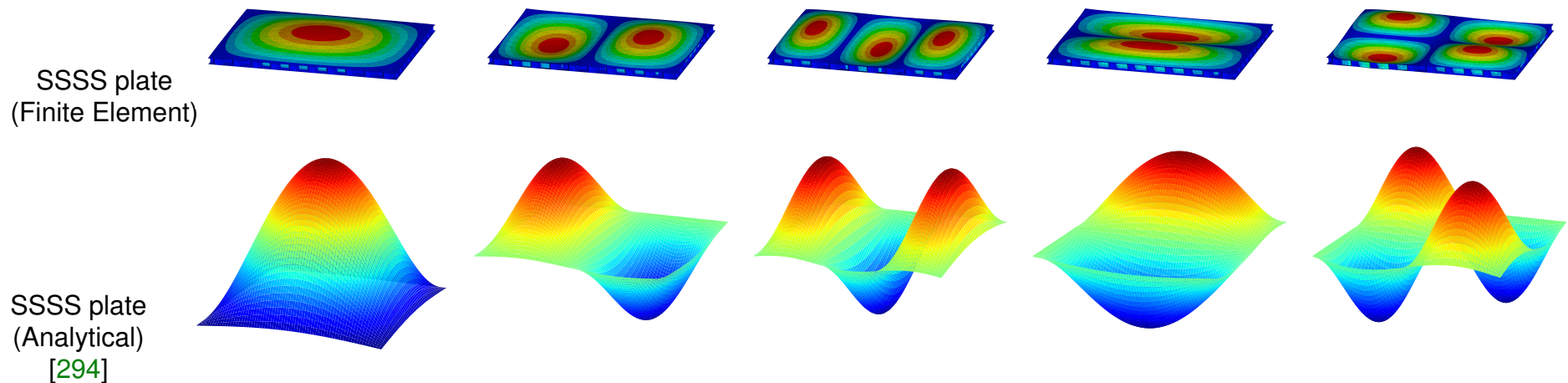


Table 3.4: First five mode shapes of the honeycomb-core sandwich structures considered in this thesis.

Mode	CF beam	SS beam	CFFF plate	FFFF plate	SFSF plate	SSSS plate (FE)	SSSS plate (Analytical) [294]
1	155	1611	130	787	457	1611	1398
2	310	2359	446	789	820	2359	2059
3	918	3524	766	1693	1336	3524	3830
4	1391	3630	1048	2026	1891	3630	4113
5	1809	3983	1417	2245	2617	4190	4915

Table 3.5: First five natural frequencies (in Hertz) of the structures considered in this thesis.

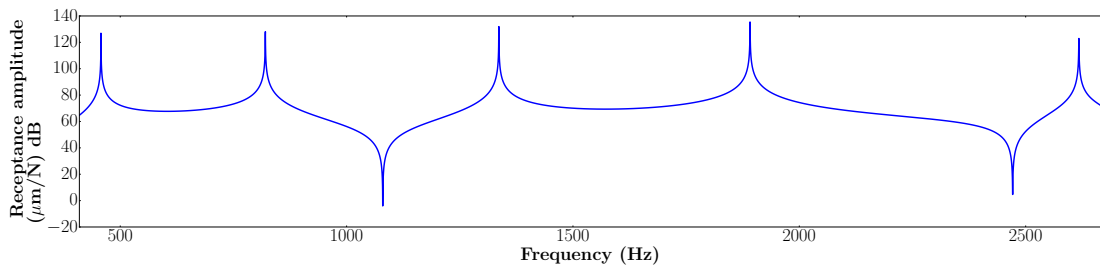


Figure 3.17: The amplitude response of the SFSF sandwich plate when the structure is excited in one corner and the response is measured at the opposite corner, showing the first five modes.

3.5 Conclusion

An analytical model of the DSLJ damper within a regular honeycomb cell was derived and compared with its equivalent finite element model. The aim was twofold: (i) to describe how the DSLJ damper deforms the viscoelastic material in shear caused by the rotation of the three rigid elements relatively from each other, thus dissipating energy. A block of polymer constrained by this shearing mechanism sees a higher strain energy density than one constrained by a CLD, which exploits relative translations instead of rotations between constraining elements. This suggest that the DSLJ damper may be more efficient than the CLD in terms of damping generated per unit mass added in the host structure. The performance of both the DSLJ and the CLD will be compared in the next chapter. (ii) to ensure that the finite element model derived gives a reliable description of the damping mechanism occurring in a DSLJ when the sandwich structure undergoes out-of-plane flexural vibrations.

The various sandwich geometries examined later in this thesis, namely the CF beam, SS beam, CFFF plate, FFFF plate and SFSF plate, were modelled using the finite element method and their first five natural frequencies and mode shapes were given for future reference. The amplitude response of the SFSF sandwich plate was also provided. The analytical and finite element solutions of the SSSS sandwich plate gave comparable eigenmodes and eigenfrequencies, thereby suggesting that the finite element model is sufficiently accurate and reliable.

CHAPTER 3. MODELLING METHODS

Chapter 4

Viscoelastic damper comparison

4.1 Introduction

The review of the literature showed that extensive research has been carried out on passive damping of structures using CLDs, including optimisation of their location and extent. In this chapter, a simple parametric approach based on the strain energy distribution of a particular mode shape will be used to determine the optimal distribution of DSLJ dampers on honeycomb-core sandwich beams and plates under simply supported and cantilever boundary conditions. The performance of the DSLJ configuration will then be compared to some optimised CLD configurations for beams and plates, albeit adapted for the present structures. The objective is to identify the most mass efficient CLD and DSLJ configurations for these structures via numerical simulation using the finite element method. The work presented in this chapter is also described in the article entitled “A novel viscoelastic damping treatment for honeycomb sandwich structures” [297] published in Composite Structures in 2015.

4.2 Methods

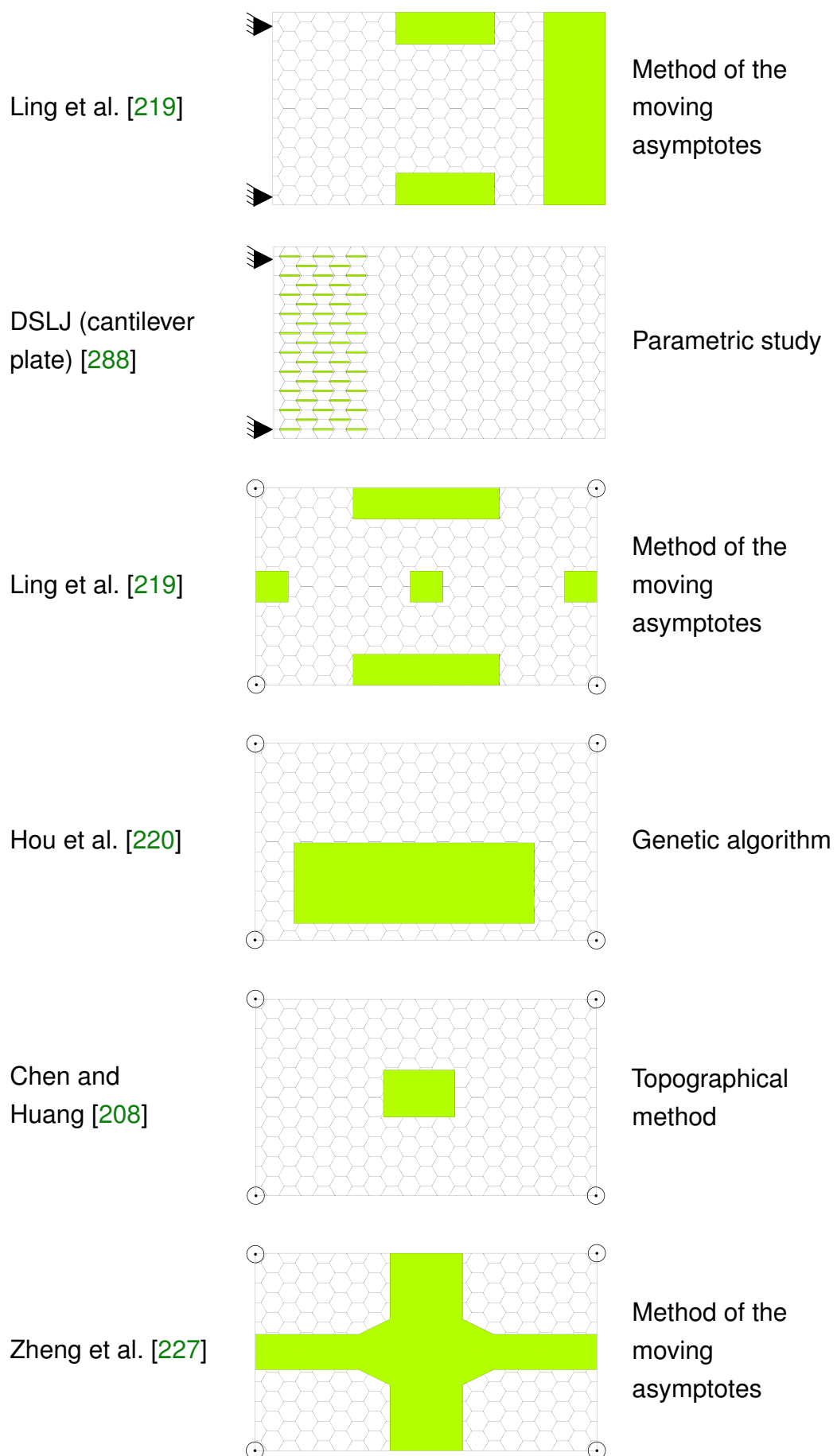
The structures considered here are the cantilever and simply supported honeycomb-core sandwich beam and plate described in the previous chapter. The CLD patches were modelled using a 8-noded brick element with 3 degrees of freedom per node (SOLID185 in ANSYS) for both the viscoelastic and constraining layers. The viscoelastic material is the same as the one used to model the DSLJ damper and the material properties are as those given in Chapter 3. Preliminary results indicated that for both beams and plates in both the cantilevered and simply supported modes, the first mode accounts for the largest fraction of the modal participation factor when the 10 first modes are considered. Similar results can be found in reference [298]. Hence only the first mode was consid-

CHAPTER 4. VISCOELASTIC DAMPER COMPARISON

ered further herein, though the same method could be applied to any modes of interest.

Adapted from	Damper location and geometry	Optimisation technique
Hajela and Lin [203]		Genetic algorithm
Marcelin et al. [204]		Method of the moving asymptotes
Hau and Fung [299] ¹		Multi-objective genetic algorithm
DSLJ (cantilever beam) [288]		Parametric study
Pau et al. [213]		Sequential quadratic programming
Zheng et al. [210]		Genetic algorithm
Hou et al. [216]		Genetic algorithm
DSLJ (simply supported beam) [288]		Parametric study
Kim [218]		Genetic algorithm

¹These solutions are for hybrid dampers.



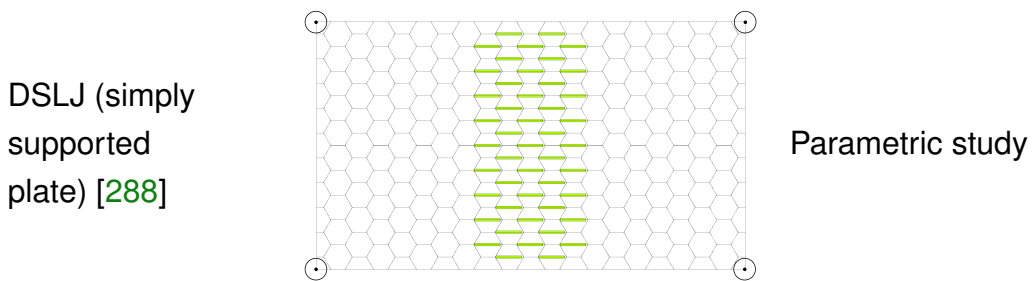


Table 4.1: Benchmarked optimised damper configurations for beam and plate structures. The sandwich skins are shown removed for clarity. The presence of a damper is given by solid colouring (CLD) or inserts in cells (DSLJ). Boundary conditions are indicated by solid triangles (encastred) and open circles (pinned) for the cantilever and simply supported cases, respectively.

4.2.1 Positioning of the DSLJ inserts

A simple and effective method for identification of the optimal position of a damper on a vibrating structure is to locate the area of maximal strain energy via the MSE method, as for example by Marcellin et al. [204]. Therefore, DSLJ dampers might be rationally placed at locations of high modal curvature where strains are maximal [40] i.e. near the clamped edge for a cantilever structure and at the middle for a simply supported structure. A parametric optimisation based on this approach, similar to that of Sher and Moreira [182], was adopted to identify the most efficient number of DSLJ inserts on the cantilever and simply supported beam and plate structures. Rows of honeycomb cells were sequentially filled with DSLJ inserts, starting at the clamped end for the cantilever geometries and from the middle for the simply supported geometries. The evolution of the modal loss factor with the increase in mass was recorded and an optimal number of DSLJ inserts was identified for each configuration based on the loss efficiency Ef_η (defined in Equation 4.2). A further parametric study was used to determine the optimal thickness of the viscoelastic element in the DSLJ dampers. In this case, the thickness of the DSLJ insert was varied from 0.25 to 2.33 mm and its optimal value was identified by the highest modal loss factor produced.

4.2.2 CLD and DSLJ dampers comparison

The present analysis is essentially a comparison of two damping structures, CLDs and DSLJ, the former in configurations identified in the literature, using the finite element method. Specifically, the amplitude, frequency and modal loss factor are calculated both before and after the addition of the dampers to the honeycomb-cored sandwich structures. Configuration of CLDs identified for

hybrid dampers were also included, i.e. those utilising active elements such as piezoelectric ceramics, however a passive-only viscoelastic material replaced the piezoceramic element. The literature hybrid CLD damper configurations had been through optimisation processes, albeit in their active modes.

The CLD optimisation studies from the literature [203, 204, 208, 210, 213, 216, 218–220, 227, 299] presented their optimal CLD configurations in slightly different formats. They were adapted to conform to either a beam or plate structure and in a consistent format for ease of comparison. The dimensions and locations of CLDs were taken from the original studies and implemented pro rata on the beam and plate used herein, as illustrated in Table 4.1. For example, Hou et al. [216] identified a CLD which stretched from 40% to 52% of the total length of their simply supported beam, and this was reconfigured to be the same proportion of the beam used in this study. Some of the literature studies did not optimise parameters such as the thickness of the viscoelastic layer (for example Zheng [210]), but will be explored and optimised in this study. An identical core configuration was used across all beam and plate cases. The vibration amplitude and frequency of the first mode was first computed and the change in amplitude and frequency was compared across the literature CLD and DLSJ configurations. Mass-efficient configurations were identified for each structure and set of boundary conditions. The amplitude reduction efficiency Ef_a was defined as follows:

$$Ef_a = \frac{A}{m_a} \quad (4.1)$$

where A is the amplitude reduction relative to the undamped structure and m_a is the additional mass of the dampers as a proportion of the native structure's mass.

A second comparison was made in which the thickness of the viscoelastic material in both dampers was varied and the modal loss factors calculated using both the Modal Strain Energy (MSE) approach [28] and the Half-Power Bandwidth (HPB) method [24] as described in Chapter 2. The thickness of the viscoelastic layer was increased from 0.2 to 2.7 mm for the CLDs and from 0.25 to 2.33 mm for the DLSJ inserts. These values allow to explore a wide range of thicknesses while keeping the design feasible under manufacturing constraints. The loss efficiency Ef_η was defined similarly as:

$$Ef_\eta = \frac{\eta_1}{m_a} \quad (4.2)$$

where η_1 is the modal loss factor of the first mode and m_a is the additional mass of the dampers as a proportion of the native structure's mass.

4.3 Results

The present finite element model was benchmarked against the work by Chia et al. [13], in which they predicted a loss factor ratio per unit mass of 1.35 (see Table 2 in [13]) for one CLD configuration (see Figure 7 in [13]). The same configuration modelled in this study predicted a loss factor ratio per unit mass of 1.34. This close match validates the method used here for adapting the literature configuration and demonstrates the present model's suitability for simulating the damping mechanism of the CLD and by extension the DSLJ. In this section, the modal loss factor will be calculated using the MSE method here and it is shown in Table 4.3 that very similar values can be obtained using the HPB method.

4.3.1 Parametric optimisation of the DSLJ inserts

Figure 4.1a shows the loss efficiency Ef_η vs the added mass in percent as the honeycomb cells were filled row by row with DSLJ inserts for all structures. For all structures the peak loss efficiency was identified when only one row was filled with DSLJ inserts. It then decreased rapidly as more rows of cells were filled. A compromise solution was selected arbitrarily between maximal loss efficiency and maximal added mass, specifically was 5 rows filled with inserts (out of 17) for the beams and 6 rows filled (out of 19) for the plates. These configurations were used in further comparisons.

The effect of viscoelastic thickness on the loss efficiency Ef_η in the DSLJ is shown in Figure 4.1b. There is an inverse relationship between the thickness of the viscoelastic element and the loss efficiency in the DSLJ. The thickness of the DSLJ damper affects rapidly its performance, and whilst the optimal thickness within this study was 0.5 mm, it seems likely that even thinner solutions would have higher damping efficiencies. The configurations with the thinnest viscoelastic layer were selected for later comparison. These selected configurations on cantilever beam, simply supported beam, cantilever plate and simply supported plate exhibited a peak modal loss factor of 1.52×10^{-3} , 1.34×10^{-3} , 1.66×10^{-3} and 1.50×10^{-3} , respectively.

4.3.2 CLD and DSLJ dampers comparison

Amplitude and frequency comparison

The amplitude response of the first mode is shown in Figures 4.2a - 4.5a for both the CLD and DSLJ configurations, with the undamped beam or plate for comparison. In the Figures 4.2a - 4.5a the amplitude is shown vs frequency

4.3. RESULTS

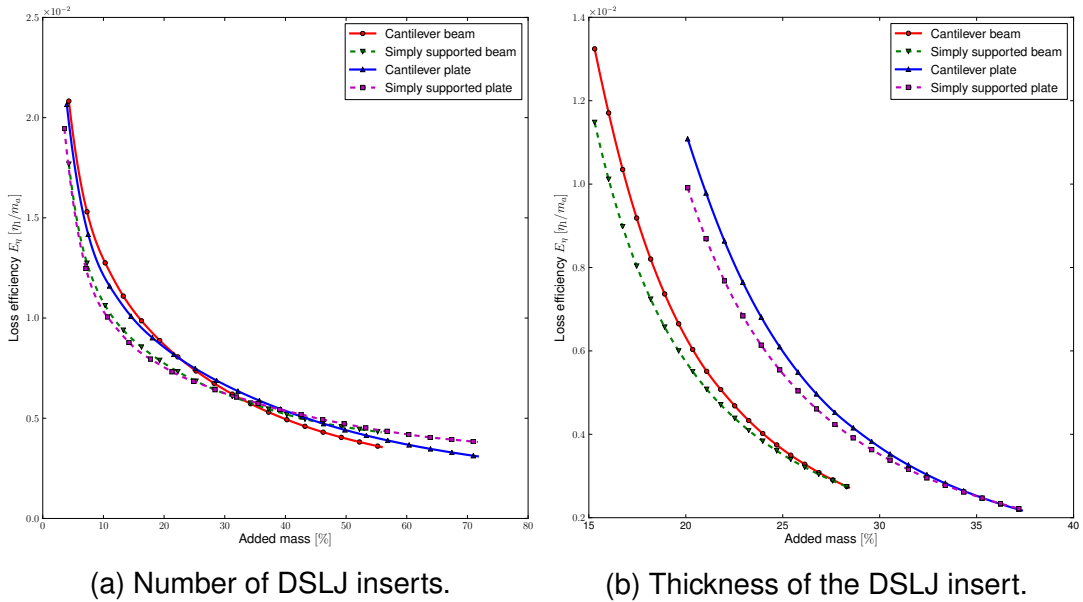


Figure 4.1: Loss efficiency Ef_η vs the additional mass as a percentage of the total mass of the undamped structure, as rows of cells are filled sequentially with DSLJ inserts on all structures (a) or as the thickness of the viscoelastic element is increased from 0.25 to 2.33 mm (b).

in absolute units, whereas in Figures 4.2b - 4.5b it is shown vs frequency normalised to the natural frequency of each case, in order to show more clearly the individual differences in amplitude response. In most cases the dampers reduced the amplitude response vs the undamped structures, as would be expected. The DSLJ damper was competitive in all case and even showed the largest amplitude reduction in the simply supported beam and cantilever plate configuration, see Figures 4.3a and 4.3b. It exhibits an amplitude reduction of 64% (cantilever beam), 53% (simply supported beam), 67% (cantilever plate) and 54% (simply supported plate) from the undamped configuration. The amplitude reduction efficiency Ef_a of the DSLJ damper is 18, 24, 3 and 4 times higher than the best CLD configuration on the cantilever beam, simply supported beam, cantilever plate and simply supported plate, respectively, see Table 4.2. It can be seen that the high amplitude reduction efficiency noted for the DSLJ configuration correlates with a high strain energy density in the viscoelastic material.

In most cases the dampers also produced a decrease in natural frequency, with some cases showing large reductions, e.g. the CLD configuration by Ling [219] reduced the natural frequency by almost 44%, see Figure 4.4a. In almost all cases, the DSLJ damper produced the least change in natural frequency, except for the simply supported case where the natural frequency was reduced by 14%. In three cases the frequency was increased by the damper, and the ratio of modal stiffness to modal mass for these cases was larger vs the undamped versions; the DSLJ cantilevered beam (Figure 4.1b),

CHAPTER 4. VISCOELASTIC DAMPER COMPARISON

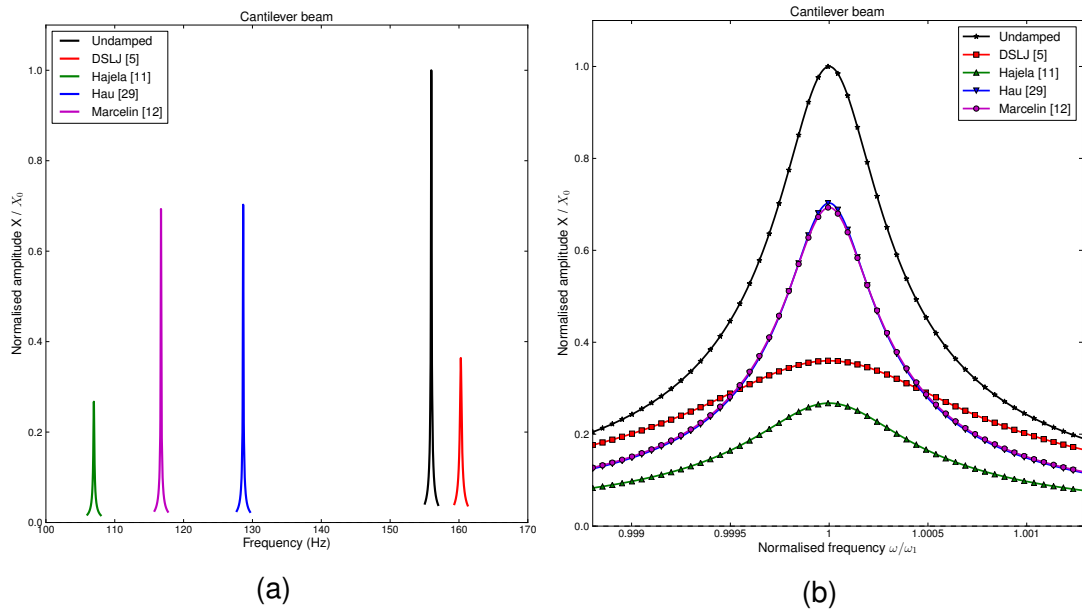


Figure 4.2: (a) The amplitude of the cantilever beams excited at their first modes. The vibration amplitude (X) of each structure is normalised to that of the undamped structure(X_0). (b) Detail of the distribution of the vibration amplitude about each resonant frequency.

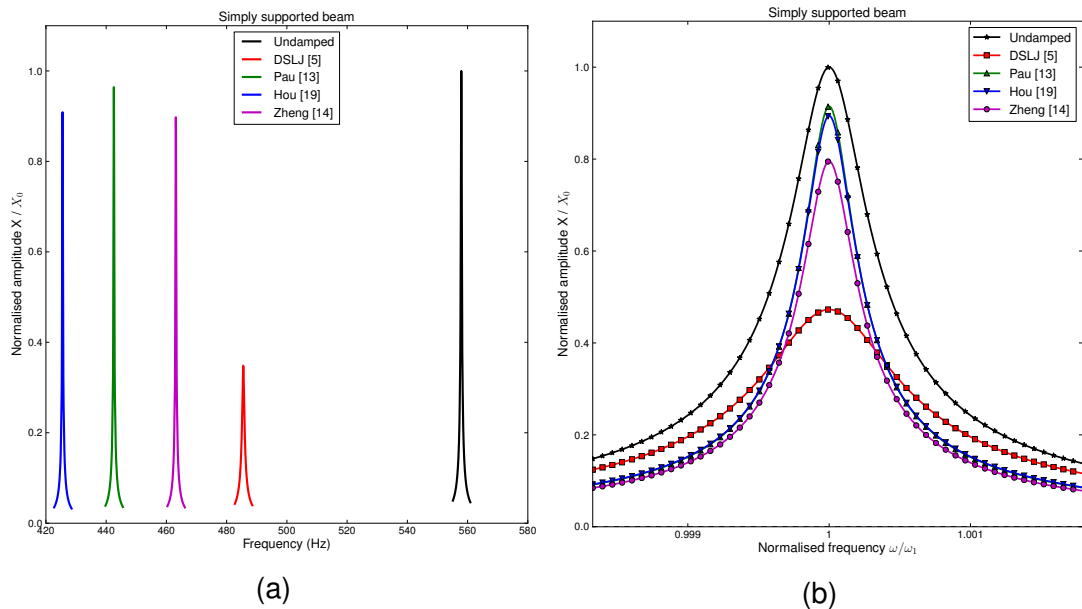


Figure 4.3: (a) and (b) as per Figure 4.2a and 4.2b but for the simply supported beam.

the Kim CLD [218] and DSLJ cantilevered plate (Figure 4.3a).

Loss efficiency comparison

The loss efficiencies Ef_η for the CLD and DSLJ damper in all of the structures along with their added masses as a percentage of the total mass of the undamped structure are shown in Figures 4.6a - 4.7b. In all cases and for all types of dampers, the loss efficiency Ef_η decreased as the thickness of the

4.3. RESULTS

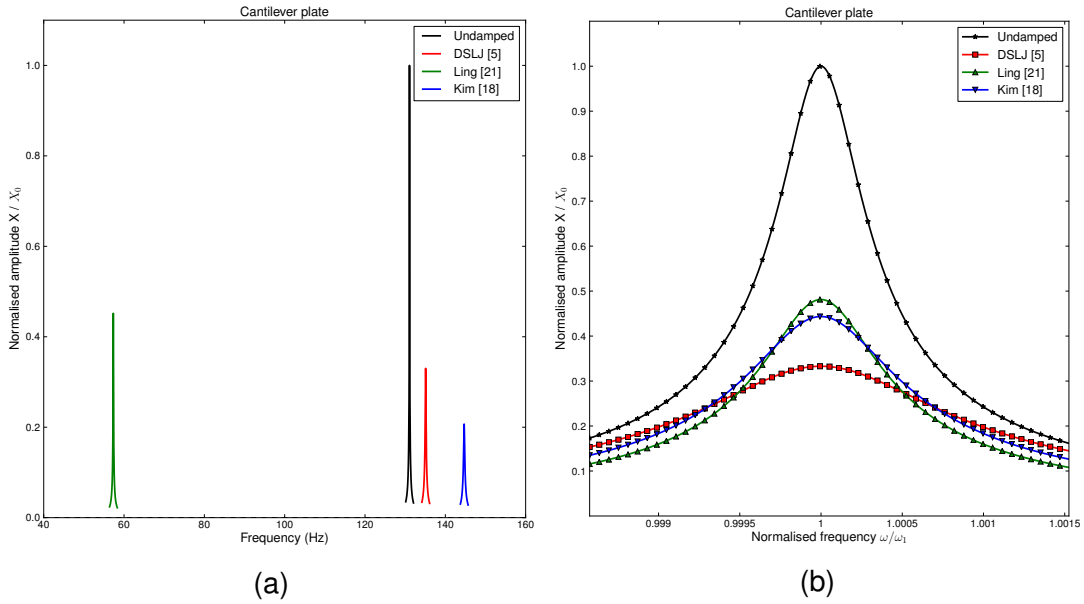


Figure 4.4: (a) and (b) as per Figure 4.2a and 4.2b but for the cantilever plate.

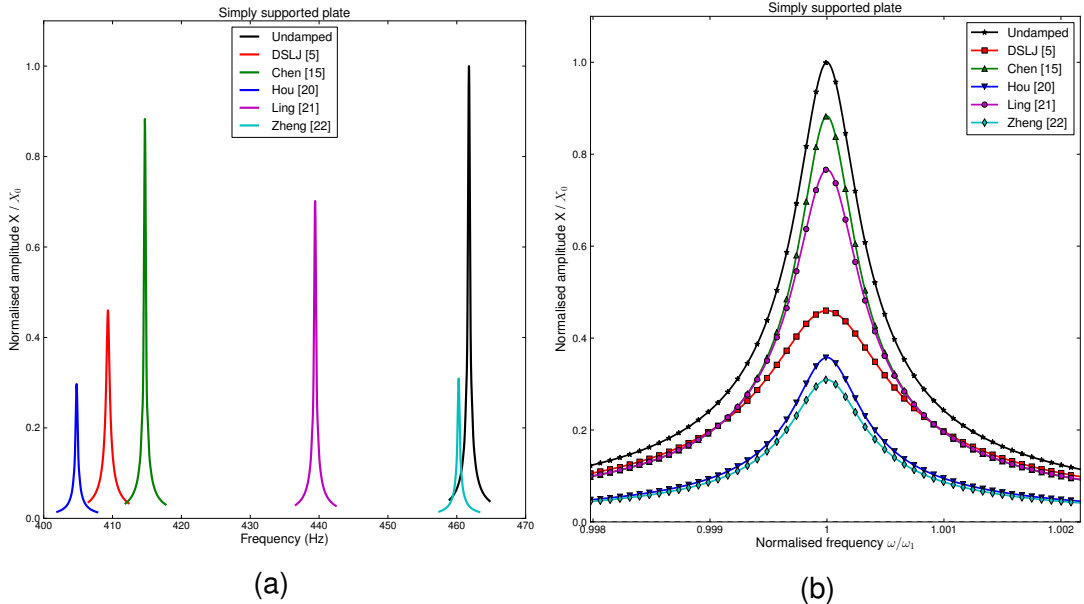


Figure 4.5: (a) and (b) as per Figure 4.2a and 4.2b but for the simply supported plate.

viscoelastic layer was increased. DSLJ configurations were generally lighter and more efficient at low added mass than CLD configurations, except for the simply supported plate case where the CLD configuration proposed by Chen and Huang [208] achieved comparable loss efficiency at lower added mass. For example the DSLJ damper was more than 5 times more efficient than the best CLD damper for the cantilevered beam, see Figure 4.6a. The stars on Figures 4.6a - 4.7b indicate the added mass of the CLD configuration as proposed in the original study where those authors considered the thickness of the viscoelastic layer as an optimisation parameter. In these cases there are CLD configurations identified here which were more efficient than those originally identified by the

	A (%)	m_a (%)	$E f_a$	u_{vem} (%)
<i>Cantilever beam</i>				
Hajela and Lin [203]	73	287	0.25	1.61
Marcelin et al. [204]	31	151	0.12	9.68
Hau [299] ²	31	128	0.24	13.09
DSLJ [288]	64	14	4.57	100
<i>Simply supported beam</i>				
Pau et al. [213]	9	117	0.08	19.17
Zheng et al. [210]	21	179	0.12	46.99
Hou et al. [216]	11	70	0.16	207.21
DSLJ [288]	53	12	3.79	100
<i>Cantilever plate</i>				
Kim [218]	56	67	0.84	31.05
Ling et al. [219]	52	196	0.26	6.65
DSLJ [288]	67	19	3.53	100
<i>Simply supported plate</i>				
Ling et al. [219]	23	27	0.85	45.11
Hou et al. [220]	64	123	0.52	7.57
Chen and Huang [208]	12	19	0.63	63.11
Zheng et al. [227]	69	652	0.11	18.24
DSLJ [288]	54	19	6.84	100

Table 4.2: Relative amplitude reduction A , additional mass m_a , amplitude reduction efficiency $E f_a$ and strain energy density in the viscoelastic material u_{vem} at peak amplitude for all configurations. The amplitude reduction and amplitude reduction efficiency are relative to the undamped structure. The strain energy density in the viscoelastic material is relative to that of the DSLJ structure.

authors, for example the CLD configuration as proposed by Hou [220] was more efficient with a thinner viscoelastic layer, see Figure 4.7b. Table 4.3 gives the values for peak modal loss factor, relative added mass and loss efficiency at peak amplitude for all configurations. The two techniques used to calculate the modal loss factor, i.e. the MSE and the HPB methods, demonstrated very similar results.

4.3. RESULTS

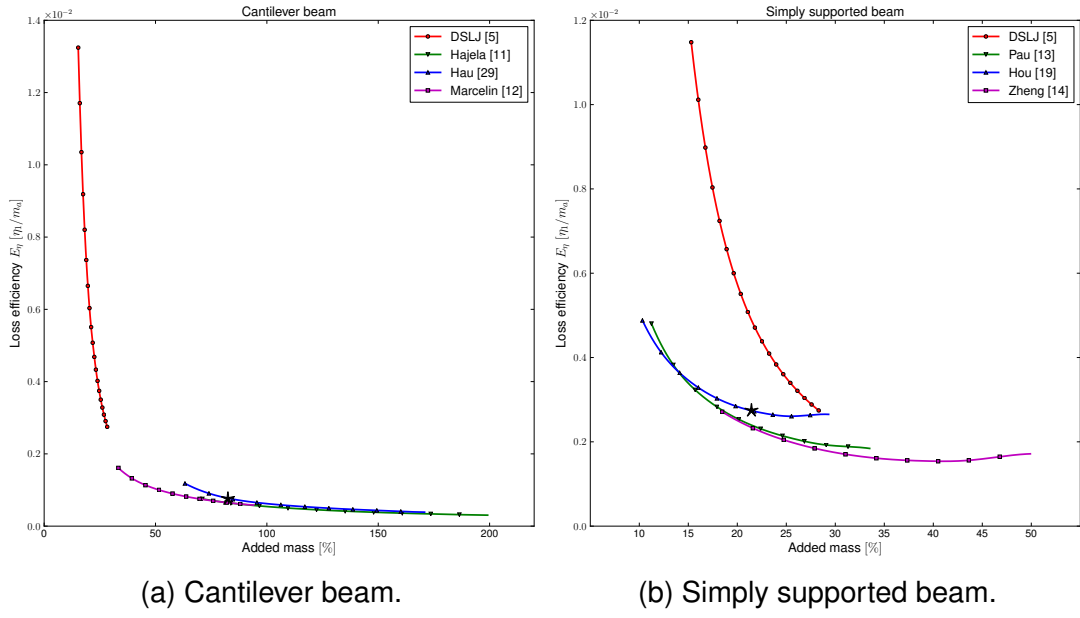


Figure 4.6: Comparison of the loss efficiency Ef_n vs added mass for the cantilever (a) and simply supported (b) beam solutions.

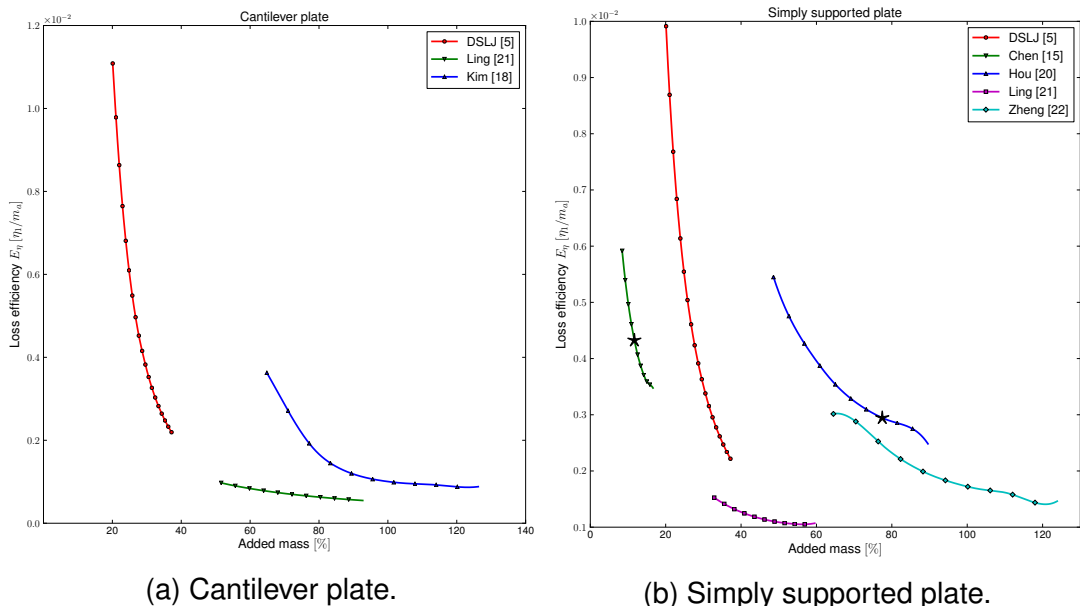


Figure 4.7: Comparison of the loss efficiency Ef_n vs added mass for the cantilever (a) and simply supported (b) plate solutions.

	$\eta_1 (\times 10^{-4})$ MSE	$\eta_1 (\times 10^{-4})$ HPB	m_a (%)	$Ef_\eta (\times 10^{-6})$
<i>Cantilever beam</i>				
Hajela and Lin [203]	5.19	5.65	71	7.31
Marcelin et al. [204]	5.25	5.62	33	15.8
Hau [299] ³	6.10	7.33	11	47.1
DSLJ [288]	15.2	13.33	18	85.0
<i>Simply supported beam</i>				
Pau et al. [213]	5.29	5.45	11	47.1
Zheng et al. [210]	5.00	5.08	18	27.1
Hou et al. [216]	5.03	5.11	10	48.7
DSLJ [288]	13.4	9.98	18	75.3
<i>Cantilever plate</i>				
Kim [218]	17.1	23.78	65	26.4
Ling et al. [219]	5.02	7.10	52	9.73
DSLJ [288]	16.6	14.33	23	70.8
<i>Simply supported plate</i>				
Ling et al. [219]	5.01	5.17	32	15.8
Hou et al. [220]	30.0	27.59	49	61.8
Chen and Huang [208]	5.00	5.15	8	59.2
Zheng et al. [227]	21.8	19.52	64	33.7
DSLJ [288]	15.0	10.63	23	64.0

Table 4.3: Modal loss factor η_1 and additional mass relative to the undamped structure m_a at peak loss efficiency Ef_η for all configurations. The modal loss factor was estimated by means of both the Modal Strain Energy (MSE) and the Half-Power Bandwidth (HPB) methods.

4.4 Discussion

The parametric optimisation of the DSLJ damper revealed that a single row of inserts is the most efficient for both cantilevered and simply supported structures, and a small number of inserts (5 or 6 rows in these cases) is a good compromise between peak loss efficiency Ef_η , large modal loss factor and added mass, see Figure 4.1a. The DSLJ damper was most effective when the viscoelastic layer was thin, see Figure 4.1b. For a given global deformation the strain energy density in the viscoelastic layer was higher when the layer was thinner. There will likely be some practical manufacturing limits on the thickness of the viscoelastic layer, as well as other possible limits arising from the ultimate shear strain and adhesive strength of the viscoelastic material.

The DSLJ configurations were best for amplitude reduction for most configurations though not all, and were competitive with all the CLD configurations, in both absolute and mass efficient reduction. This is due to the fact that the strain energy in the viscoelastic material was usually higher in the DSLJ damper than in a CLD for a given global strain (see Table 4.2). The DLSJ damper therefore appeared to be a more effective way of configuring viscoelastic material in order to reach a higher loss factor. The exceptions were Hajela and Lin [203] and Zheng [227] in the cantilevered beam and simply supported plate cases, both of which showed the highest amplitude reduction. However this was at the cost of high added mass and coverage of most of the surface. Indeed, the amplitude reduction efficiency Ef_a was always the highest for all configurations. The hybrid CLD proposed by Hau [299], which was never designed to operate purely passively, did not perform well in comparison to other configurations.

In most cases the dampers reduced the natural frequency as might be expected. In some notable cases however the dampers raised the ratio of modal stiffness to modal mass and therefore the resonance frequency (see Figures 4.2a and 4.4a). With weight efficient dampers it should be possible in many cases to conserve initial model frequencies when adding dampers.

There was an inverse relationship between the loss efficiencies Ef_η for both the CLD and DSLJ configurations and the viscoelastic layer thickness, see Figs. 4.6a - 4.7b. The thickness of the viscoelastic layer was the primary determinant of the strain and strain energy density in the viscoelastic layer, and thus efficiency of the dampers in this study using both the MSE and HPB methods. The loss efficiency is very sensitive to the DSLJ thickness. As with amplitude reduction the data for loss efficiency indicate that DSLJ tend to be more efficient because the viscoelastic layer sees higher strains for given global deformations. For example, the DSLJ configuration had a loss factor of almost twice of that of the Hou CLD configuration (1.14×10^{-3} and 5.62×10^{-4} for the DSLJ and CLD configurations, respectively), see Figure 4.6b. The exception

was in the simply supported plate with the configuration of Chen [208], i.e. a small patch in the centre of the plate, which was more mass efficient than the DSLJ, see Figure 4.7b and Table 4.3.

It was shown analytically in Chapter 3 that the DSLJ's damping mechanism exploits the damping material more effectively than that of the CLD, i.e. more strain energy is generated in the viscoelastic material per unit volume. Indeed, the DSLJ is sensitive to both internal shear and flexure of the base structure whereas the CLD's shearing mechanism is only due to flexure. In this chapter, the numerical predictions confirmed that the viscoelastic material sees higher shear strain energy per unit volume in a DSLJ damper than in the CLD configuration explored here, see Table 4.2. Hence for applications where the lightweight properties are critical, the DSLJ damper can be an efficient alternative to the CLD.

4.5 Conclusion

This chapter presents the performance of a new kind of viscoelastic damper for honeycomb sandwich structures and compares its efficiency to benchmarked optimal configurations of CLDs on beam and plate structures. It provides a parametrically optimised configuration for DSLJ dampers for beams and plates structures under both cantilever and simply supported boundary conditions. This simple parametric method works well in most of the cases considered here. A more sophisticated optimisation approach will be adopted in the next chapters.

The new DSLJ inserts exhibit an excellent ability to damp vibrations for small increases in mass, in terms of both amplitude reduction and modal loss factor. They also generally produce a smaller shift in natural frequency from the undamped structure which may be an important asset for many transport applications. Therefore, DSLJ inserts represent a competitive alternative to CLDs. Since they are internal to the honeycomb cell, they can be implemented in applications where adding dampers externally is difficult. This may be the case for gas turbine blades with large internal void spaces convenient for DSLJ deployment, but which cannot have external dampers interfering with air flow. If deployed in honeycombs, the orientation of the DSLJ damper can be altered, raising the possibility for tuning of orientation according to global vibration modes.

Chapter 5

Parametric optimisation of the DSLJ damping inserts

5.1 Introduction

As discussed in the introduction chapter, fuel efficiency in transport is currently of considerable interest, mainly because fuel consumption is the principal source of expenditure in commercial transport. One of the most effective ways of improving fuel efficiency is to manufacture lighter vehicle structures. However, slender and lighter structures are also prone to higher vibration levels, leading to higher fatigue cycles and more severe damage in the structural components. There is therefore a desire to combine lightweight structures with vibration damping in transport vehicles. However, light and stiff materials are not usually inherently lossy, meaning that increasing vibration damping in a structure generally leads to increasing its mass and vice-versa. It is often necessary to seek a compromise between these two contradictory properties in order to determine which damper configuration yields the optimal performance.

This compromise can be effectively identified using a so-called parametric study, such as the one adopted by Kung and Singh [175, 176], whereby a design parameter is altered iteratively in order to determine its optimal value. As we have seen in Chapters 2 and 4, such problems can also be successfully tackled using heuristic optimisation algorithms. However, this approach can be computationally expensive and difficult to implement. The question arises whether such evolutionary methods are necessary or whether simpler parametric approaches can yield a similar quality of results. In this chapter, attention is focused on implementing a parametric method to determine the optimal location and orientation of DSLJ dampers in a honeycomb-cored sandwich plate, with the objective of simultaneously minimising the total mass and maximising the damping in the structure. This relatively quick and simple parametric approach is based on the strain distribution of the mode shape of each structure considered.

In Chapter 6, the performance of this parametric approach will be compared to that of an evolutionary optimisation algorithm. The methods, results and discussion presented in this chapter are partly described in the article “Multi-objective optimisation of viscoelastic damping inserts in honeycomb sandwich structures” [300] published in Composite Structures in 2015.

5.2 Methods

The approach taken here consisted in determining the distribution (i.e. locations and orientations) of DSLJ dampers that achieves the highest damping for the least additional mass onto the structure. The structure chosen was a rectangular sandwich panel with a honeycomb core with 10×10 hexagonal cells plus 9×9 interleaving cells, making a total of 181 cells. The plate was considered in both cantilevered and free boundary conditions. The first and second mode shapes of such structures, along with their respective natural frequencies, are illustrated in Table 5.1 for both types of boundary conditions. The finite element model was presented in Chapter 3, along with the materials properties. The size of the panel was chosen so as to provide the subsequent optimisation with a large enough search space, while keeping the computational cost within reason. For this particular problem, there are four possible damper configurations within the hexagonal cell – absent or one of three orientations, as illustrated in Figure 5.1. This makes a total of 4^{181} combinations or potential damper configurations; too large a solution space to evaluate every solution.

The parametric optimisation method was based upon deformation data taken from the mode shape of a sandwich panel without any inserts, i.e. the empty panel. For each hexagonal cell in the empty panel core, the distance between two opposite vertices was calculated in the undeformed and deformed cases. Using the notation defined in Figure 5.2, the intracellular strain was calculated as follows,

$$\begin{aligned}\varepsilon_{AB} &= \frac{\|\overrightarrow{AB}\| - \|\overrightarrow{A'B'}\|}{\|\overrightarrow{AB}\|} \\ \varepsilon_{CD} &= \frac{\|\overrightarrow{CD}\| - \|\overrightarrow{C'D'}\|}{\|\overrightarrow{CD}\|} \\ \varepsilon_{EF} &= \frac{\|\overrightarrow{EF}\| - \|\overrightarrow{E'F'}\|}{\|\overrightarrow{EF}\|}\end{aligned}\tag{5.1}$$

where $\|\cdot\|$ is the Euclidean norm. The algorithm used to extract these vertex-to-vertex strain data was implemented in ANSYS Parametric Design Language (APDL) and it is shown in Appendix C. The absolute values of these strains

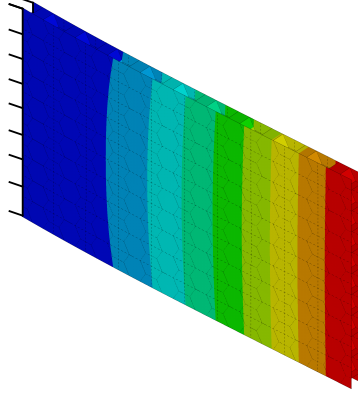
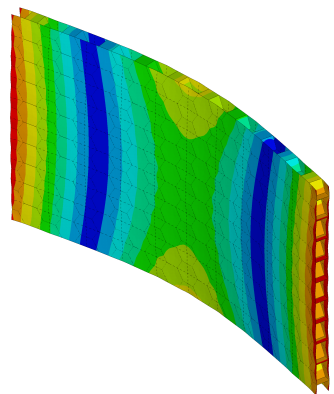
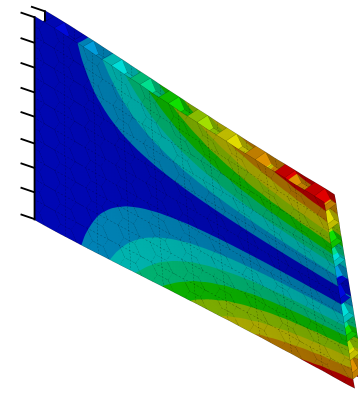
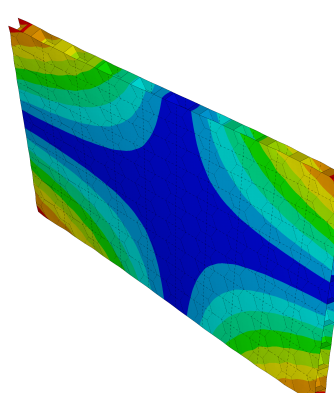
Mode number	Cantilever boundary conditions	Free boundary conditions
Mode 1		
	129 Hz	785 Hz
Mode 2		
	443 Hz	788 Hz

Table 5.1: First and second mode shapes of the sandwich plate under cantilever and free boundary conditions, along with their corresponding natural frequency. The colours of the mode shapes indicate the nodal displacements, with red being maximal and blue minimal. The encastered boundary condition is represented by black lines on the left of the cantilevered structures.

were then ranked in descending order and the DSLJ dampers were oriented and placed successively between the corresponding opposite vertices. This process assumes that larger deformation in the DSLJ damper would result in higher strain energy in the viscoelastic material, thus yielding a higher modal loss factor. This process was repeated iteratively, adding further DSLJ dampers until all cells were occupied. Sets of weight- and damping- efficient configurations could thus be identified for each of the four cases considered here. The damping efficiency is an indicator of the performance of the DSLJ inserts in terms of damping and weight reduction. It is defined as the ratio of the modal loss factor η to the total mass of the structure m :

$$Ef = \frac{\eta}{m} \quad (5.2)$$

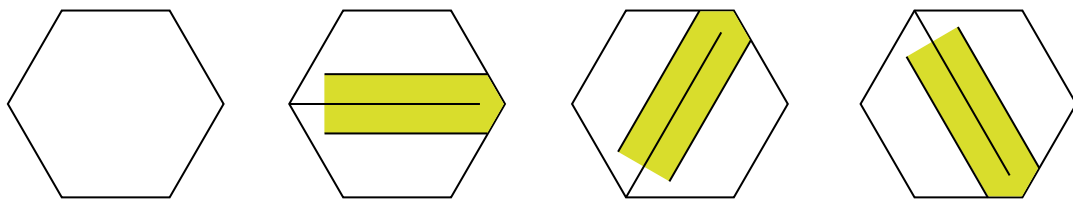


Figure 5.1: Four possible DSLJ damper configuration within a hexagonal honeycomb cell – absent or one of the three orientations.

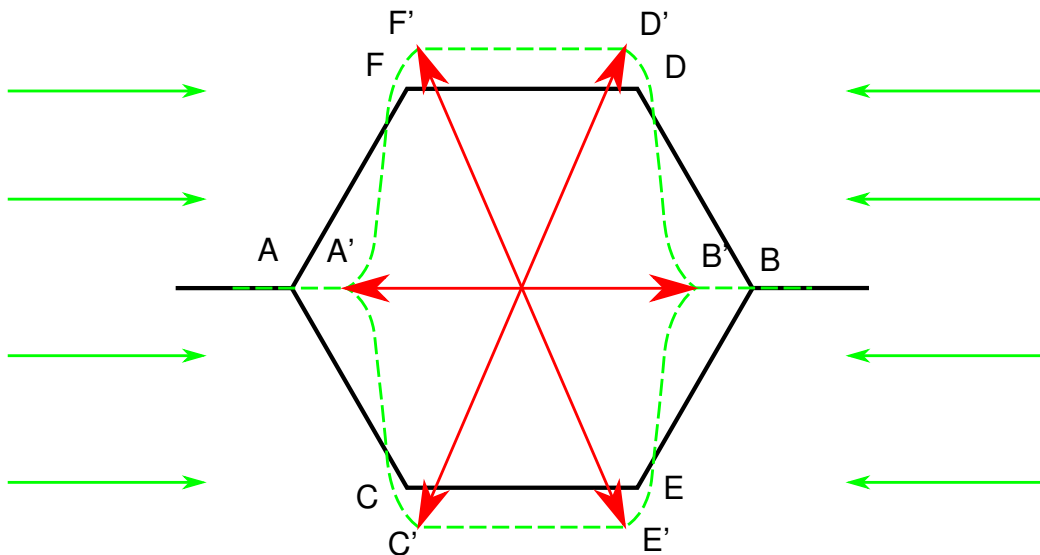


Figure 5.2: A deformed (green) and undeformed (black) honeycomb cell.

5.3 Results

5.3.1 Optimised configurations

The optimised distributions of DSLJ dampers on the cantilever and free sandwich plates are presented in Figures 5.3 to 5.6. For clarity purposes, only 20 out of the 181 configurations obtained were represented. For the cantilever plate under its first mode (flapping), the optimal orientation of the DSLJ dampers in parallel to the long dimension of the plate, see Figure 5.3. Under the second mode (torsional), the optimised orientations for damping inserts are angled at either $\pm 60^\circ$ to the long axis of the plate, as illustrated in Figure 5.4. For the sandwich plate under free boundary conditions, the optimal locations tend to be near the centre of the plate. In the first mode (bending) the damping inserts are optimal when oriented axially (see Figure 5.5), as opposed to the second mode (torsion) where the best orientation tends to be radially outwards (see Figure 5.6).

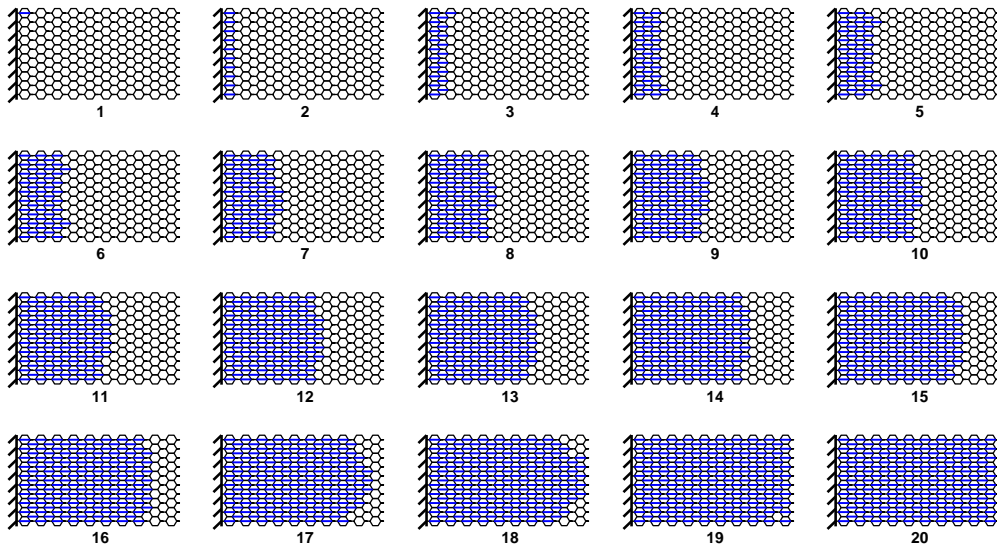


Figure 5.3: Optimised distributions of DSLJ dampers on the cantilever sandwich plate under mode 1 (flapping mode).

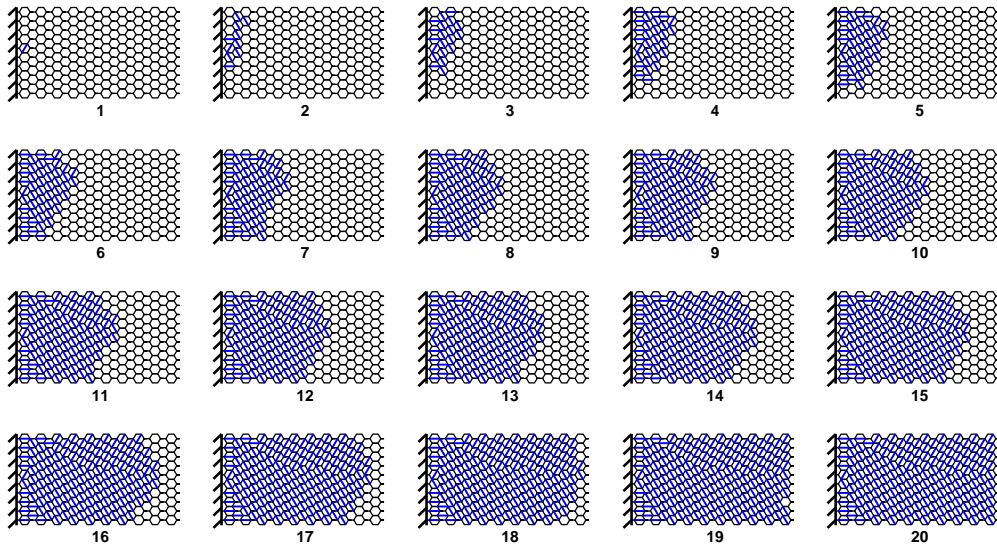


Figure 5.4: Optimised distributions of DSLJ dampers on the cantilever sandwich plate under mode 2 (torsion mode).

5.3.2 Mode veering

The evolution of the damping efficiency with the number of DSLJ inserts added is shown in Figures 5.7 and 5.8. In the cantilever case, the number of DSLJ dampers corresponding to the maximum damping efficiency can be identified i.e. 87 and 117 inserts when the first and second modes are targeted, respectively (see Figure 5.7). After this point, the rate at which the sandwich plate gets heavier is higher than the rate at which the modal loss factor increases. The optimal number of insert corresponds to the point where the derivative of the damping efficiency becomes zero.

In the case of the sandwich panel under free boundary conditions, an

CHAPTER 5. PARAMETRIC OPTIMISATION OF THE DSLJ DAMPING INSERTS

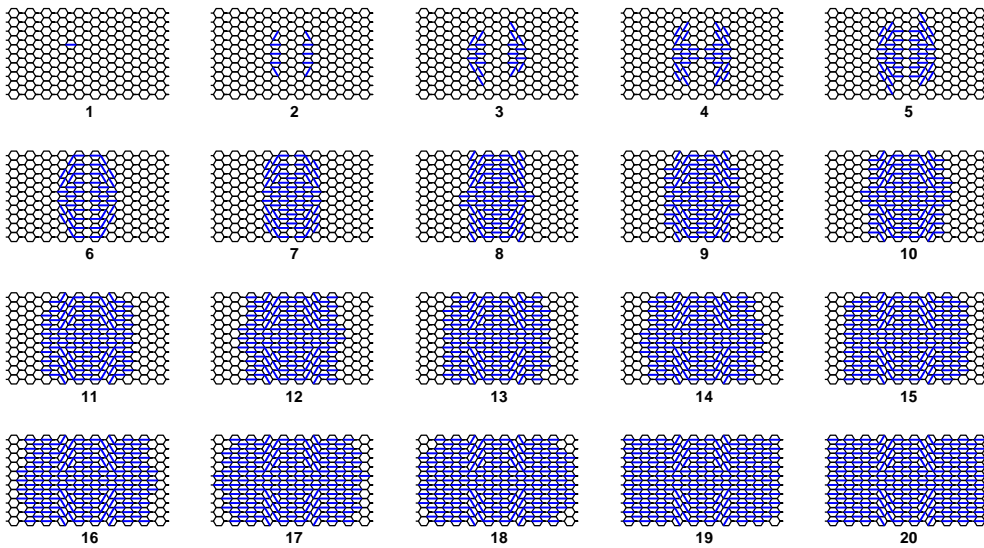


Figure 5.5: Optimised distributions of DSLJ dampers on the free sandwich plate under mode 1 (bending mode).

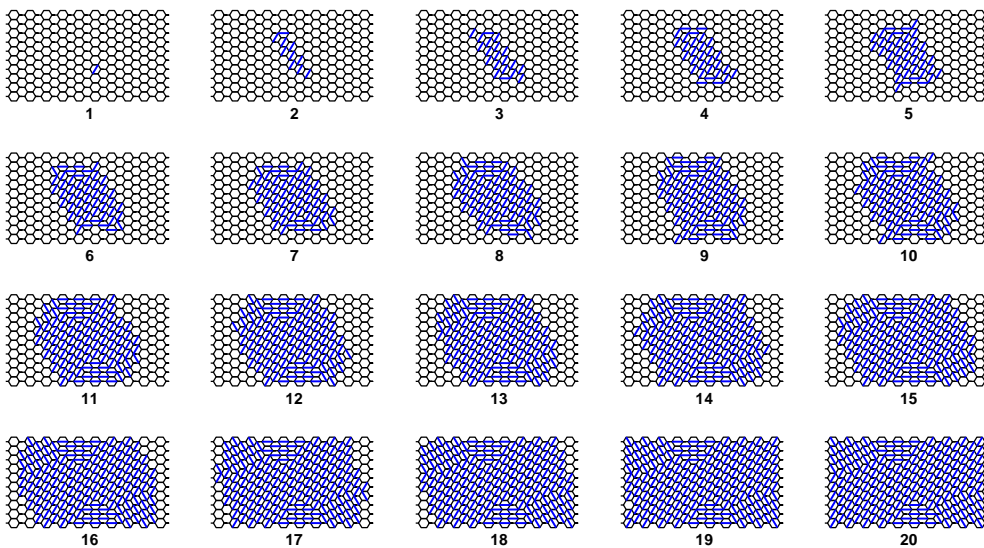


Figure 5.6: Optimised distributions of DSLJ dampers on the free sandwich plate under mode 2 (torsion mode).

interesting phenomenon has occurred: the addition of a few damping inserts induced a swap in the order of the natural frequencies, known as *mode veering*. Specifically, the erstwhile second mode (a torsion mode originally at 788 Hz) had its frequency decline below the frequency of the erstwhile first mode (a bending mode originally at 785 Hz). This phenomenon can be highlighted by studying the evolution of the natural frequencies as the number of dampers increases. In the cantilever case, the first two natural frequencies are separated enough not to interact with each other, see Figure 5.9. However in the case of the free plate, the first two modal frequencies are originally close and the alteration of the structure causes them to collapse towards each other and

then ‘veer away’, see Figure 5.10b. Mode veering is clearly evident between configurations 13 and 14, 17 and 18, and 18 and 19. The second mode shapes of the 20 optimised configurations that supposedly attempted to target the second mode (torsion) of the free plate are shown in Figure 5.11 and mode veering is also manifest between the same configurations. The optimiser was designed to damp the mode shapes corresponding to those of the undamped structure, assuming the order of the natural frequencies remained the same all along the optimisation process. However, the order in which the finite element eigensolver extracted the first and second eigenvalues swapped as dampers were added to the structure, leading the parametric optimiser to place and orient the dampers inadequately. The damping efficiency in Figure 5.8 rises dramatically when the second mode switches from torsion to bending because by chance the solutions proposed for torsion were much more effective than those originally intended for the bending mode. This shows that the underlying assumption that placing a damper at location of high vertex-to-vertex strain generates high damping is not strictly exact in all cases, especially when veering is present.

5.4 Discussion

A simple and quick parametric approach has been successfully implemented to optimise the location and orientation of DSLJ dampers deployed in a honeycomb-core sandwich plate under cantilever and free boundary conditions. 181 configurations optimised to damp the first and second vibration mode were identified. In both of the cases considered here, the optimiser identified configurations with much higher damping efficiency than the empty native structure, suggesting that it is a suitable approach to tackle this kind of problem (see the dashed line in Figures 5.7 and 5.8). The parametric optimiser placed the DSLJ inserts in priority in regions of high strain energy for each mode shape, as could have been expected. For instance, the highest strains on the cantilevered plate is near the clamped edge for modes 1 and 2 (see Figures 5.3 and 5.4), and at the middle for the free plate (see Figures 5.5 and 5.6). Earlier research also concluded that placing a constrained layer damper in regions of high strain energy is more mass-efficient; see for example [166].

This parametric optimiser does not account for the additional mass and stiffness which is inevitable when dampers are inserted in the structure. This has two consequences, (i) the vertex-to-vertex strain distribution across the structure changes with additional mass and stiffness, ergo the optimal location and orientation of DSLJ inserts changes, (ii) the additional mass and stiffness can cause veering, i.e. a change in the order of natural frequencies of modes,

CHAPTER 5. PARAMETRIC OPTIMISATION OF THE DSLJ DAMPING INSERTS

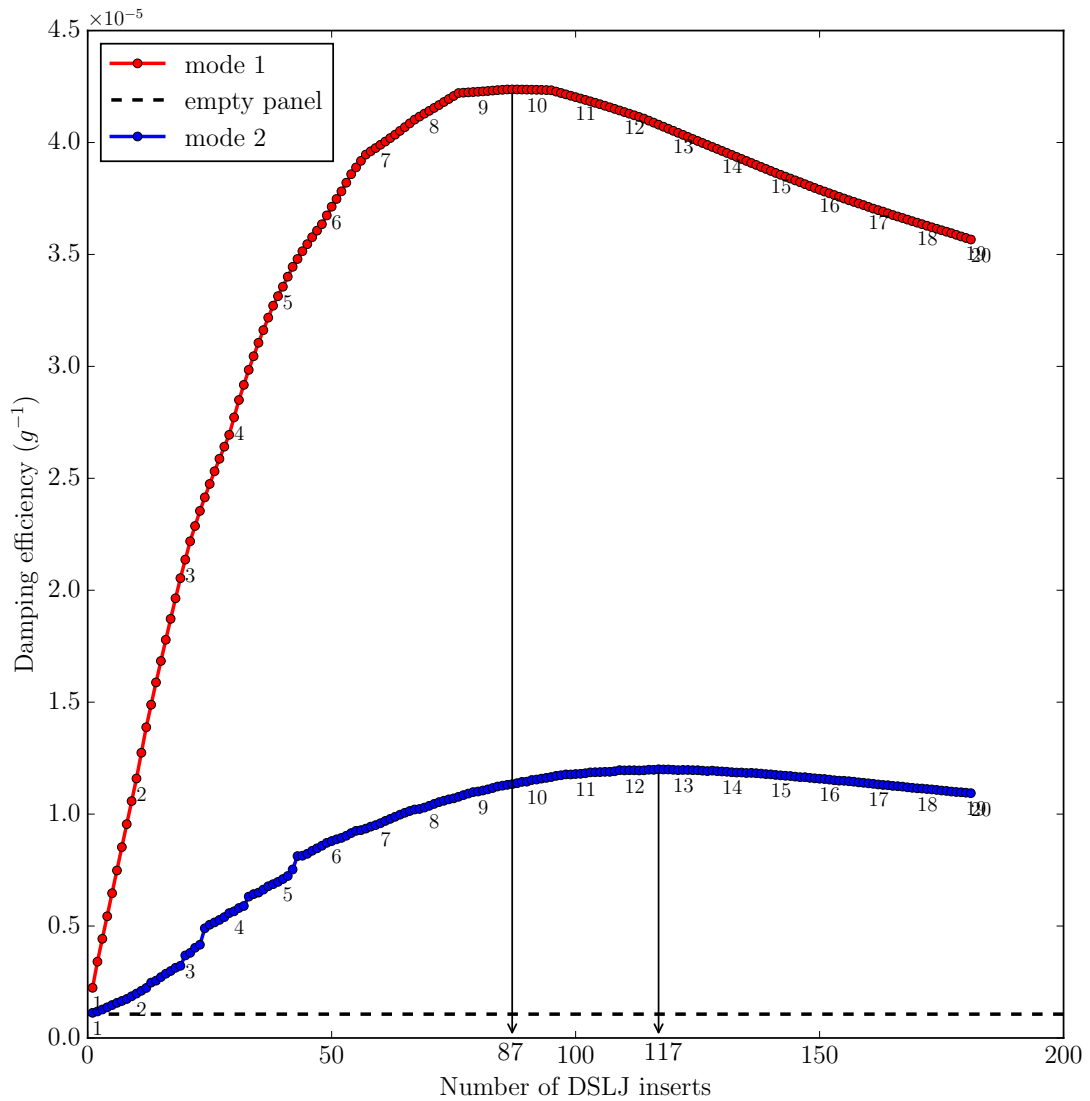


Figure 5.7: Damping efficiency versus the number of DSLJ inserts for the cantilever plate. The numbers correspond to the configuration numbers shown in Figures 5.3 and 5.4 for mode 1 and 2, respectively. The optimal number of DSLJ is identified by an arrow for each mode.

which can radically alter the efficacy of the dampers. For instance, mode veering has occurred when attempting to damp the second (torsion) mode of the free plate (see Figures 5.8, 5.10 and 5.11), leading to an inadequate placement of the damping inserts for the mode targeted initially. The reason for this is that the parametric approach adopted here places and orients the dampers based on the intracellular vertex-to-vertex strain of the mode shapes of the undamped structure. However, it was assumed here that such strain would remain the same during the optimisation process, which is not always the case especially when veering occurs.

Mode veering is a well-known phenomenon which has been identified as early as 1973 by Nair [301] and Leissa [302]. It is more likely to happen when neighbouring modes are close in frequency, which is the case here for the

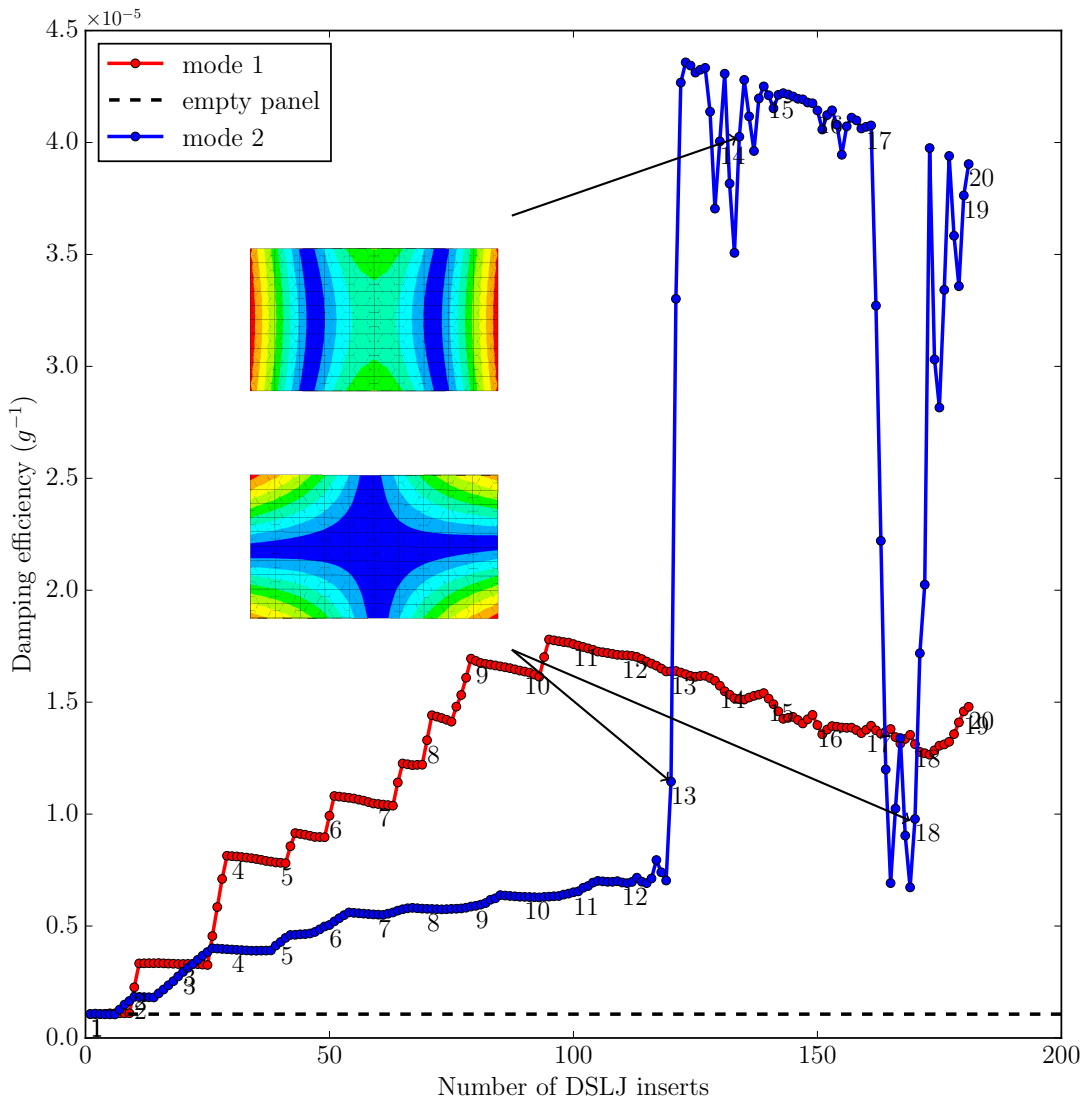
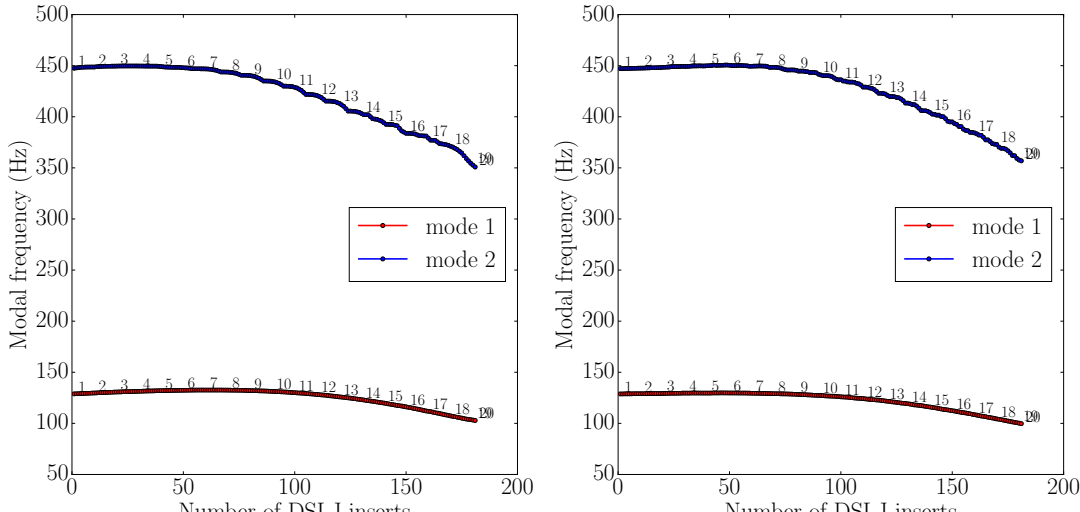


Figure 5.8: Damping efficiency versus the number of DSLJ inserts for the free plate. The numbers correspond to the configuration numbers shown in Figures 5.5 and 5.6 for mode 1 and 2, respectively. The second mode shape of configurations 13, 14 and 18 is indicated.

free sandwich plate (785 Hz and 788 Hz for modes 1 and 2, respectively). It is possible to predict the occurrence of mode veering, for instance using the veering index derived by Dubois et al. [303]. This index, based on the eigenvalue sensitivity of the system, can identify mode veering due to alteration of the mass or the stiffness without any prior knowledge of the structure studied. It should be computed before using any optimiser that does not update its quality measures during optimisation, as it is the case here.

The particular parametric optimisation approach adopted here is quite time-efficient and computationally inexpensive, requiring only one initial finite element evaluation to deduce the optimal configurations. However in this case, it was possible to constrain the problem to a relatively small solution space, generated by the intracellular strain data. If it is not possible to do this, parametric optimisa-

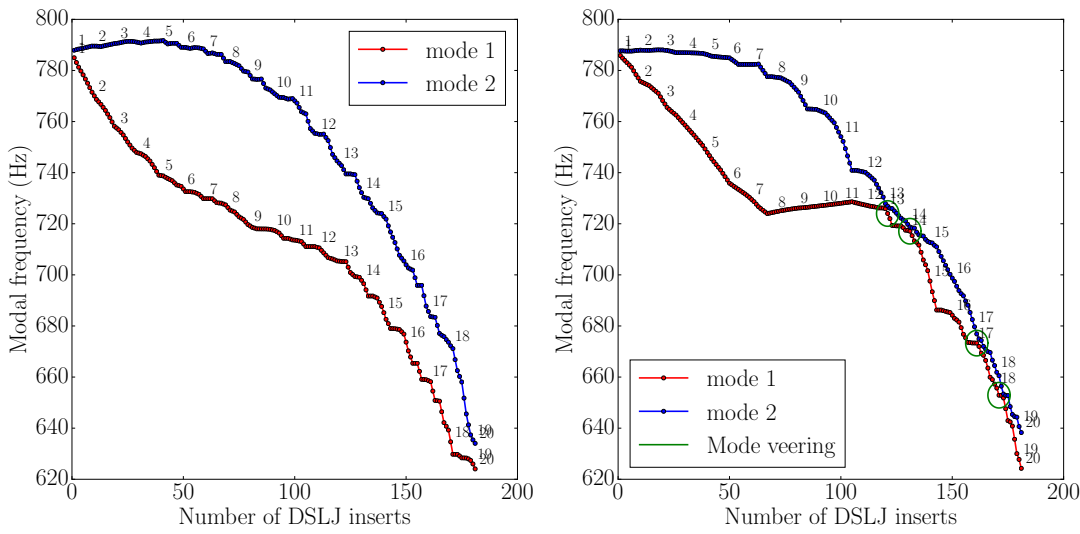
CHAPTER 5. PARAMETRIC OPTIMISATION OF THE DSLJ DAMPING INSERTS



(a) Solutions optimised for mode 1.

(b) Solutions optimised for mode 2.

Figure 5.9: First and second eigenfrequency versus the the number of DSLJ inserts for the cantilever plate. The numbers correspond to the configuration shown in Figures 5.3 and 5.4 for mode 1 and 2, respectively.



(a) Solutions optimised for mode 1.

(b) Solutions optimised for mode 2.

Figure 5.10: First and second eigenfrequency versus the the number of DSLJ inserts for the free plate. The numbers correspond to the configuration shown in Figures 5.5 and 5.6 for mode 1 and 2, respectively. The presence of mode veering is identified by green circles.

tion can require enormous computational power, for instance if we considered all possible combinations of damper orientation and location for many modes. Since it only requires calculating the nodal strains between the honeycomb cell vertices, it is also relatively simple to implement while combined with a finite element model.

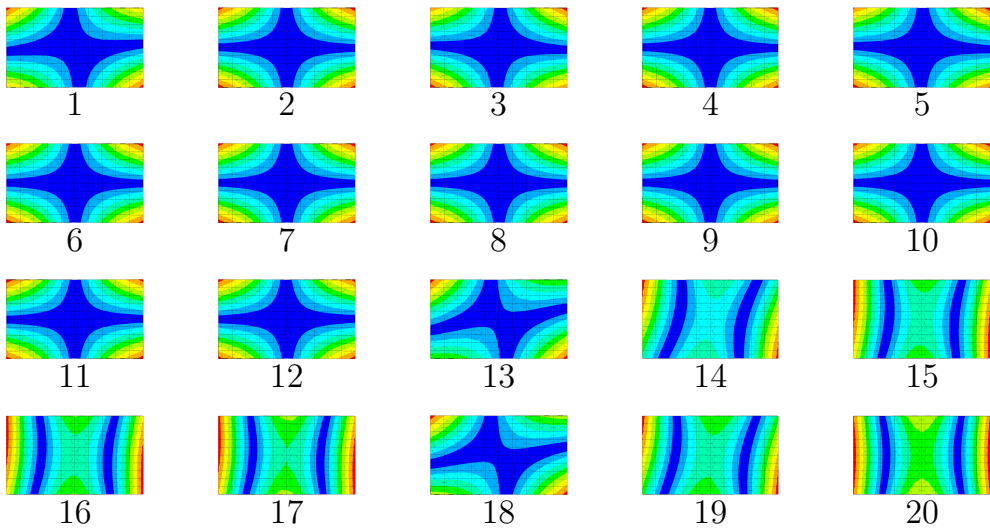


Figure 5.11: Second mode shape corresponding to the configurations shown in Figure 5.6 (Free plate optimised for its second torsion mode).

5.5 Conclusion

In this chapter, the optimal location and orientation of DSLJ dampers in a honeycomb sandwich structure have been determined using a parametric approach. This parametric method is fast, simple to implement, requires low computer power and may be very efficient, especially in some simple cases (see Figure 5.7). However the mass and the stiffness of the structure may be altered during the optimisation process, which may affect the mode shape geometry or even shift the modal frequencies, causing mode veering. In such cases, the parametric approach places and orients the dampers in an inadequate manner which severely detracts from their efficiency. This parametric algorithm is exposed to mode veering because the quality measures of its optimisation mechanism are not dynamically updated during the optimisation process. Therefore, extreme care should be taken when attempting to tackle a problem whose properties and nature may change during optimisation. The veering index of the system [303] should be computed prior to using parametric optimisers applied to vibration problems. If such phenomenon is likely to occur during the process, a more robust and sophisticated optimisation approach should be adopted. It will be shown in the next chapter that evolutionary optimisation techniques can effectively cope with the coupling between objective values and optimised design geometries, and can thus be an effective alternative to parametric studies.

CHAPTER 5. PARAMETRIC OPTIMISATION OF THE DSLJ DAMPING INSERTS

Chapter 6

Evolutionary optimisation of DSLJ damping inserts

6.1 Introduction

The transport industry has long been striving for both lighter and better damped vehicles in an effort to simultaneously reduce fuel consumption, passenger discomfort and fatigue in structural parts. However, weight reduction and increase in damping are usually competing objectives and a compromise must be made between low vibration levels and addition of mass. In the previous chapter, a parametric approach was implemented to optimise the location and orientation of DSLJ dampers deployed in a standard honeycomb sandwich plate. Although this approach was relatively quick and straightforward, it may not yield reliable results, especially in situations where mode veering is present. This problem can be tackled effectively by using a more complex and robust optimisation method such as heuristic optimisation algorithms. In this chapter, the location and orientation of DSLJ dampers on a honeycomb-cored sandwich plate are optimised using a multi-objective evolutionary algorithm, namely the adaptive Indicator-Based Evolutionary Algorithm (IBEA) [304]. The objective is to identify the configurations that generate the maximum damping for the least additional mass. The performance of the parametric and evolutionary optimisation methods are compared in terms of damping efficiency and absolute values of modal loss factors and mass. The methods, results and discussion presented in this chapter are also described in the article entitled “Multi-objective optimisation of viscoelastic damping inserts in honeycomb sandwich structures” [300] published in Composite Structures in 2015.

6.2 Methods

The objective here is to determine the optimal location and orientation of DSLJ dampers in the same honeycomb sandwich plate geometry and sets of boundary conditions considered previously in Chapter 5, but this time using a multi-objective evolutionary optimisation technique rather than a parametric approach. The purpose of an optimisation algorithm is to return the minimum or maximum of one or more objective values which can be expressed as a function of decision vectors for a particular problem [305]. Contrary to brute-force search or even parametric methods, heuristics optimisation techniques are very often better suited for problems with a large number of potential solutions. Since the DSLJ damper can be inserted in four different configurations within the hexagonal cell (absent or one of three orientations), there are 4^{181} combinations possible (or search space cardinality) for this particular problem.

6.2.1 Evolutionary optimisation

The adaptive Indicator-Based Evolutionary Algorithm (IBEA), introduced by Zitzler and Künzli [304], is a modern set-based multi-objective evolutionary algorithm. Although there are successful point-based optimisers for multi-objective design problems (e.g. simulated annealing [306]), using a set-based optimiser has a number of benefits for this type of design problem. The recombination of designs that crossover provides allows the algorithm to make larger movements in the search space, but within regions bounded by already ‘good’ solutions. The small refinements (such as mutations) used in point-based approaches are also exploited here, so this ability is not sacrificed. Furthermore, from a scalability standpoint, population-based optimisers are parallelised relatively easily, with the evaluation of each member fed to a different core, which enables computationally expensive optimisation problems to be tackled. Point-based approaches cannot be transferred as directly into parallel architectures. Set-based optimisers are also less likely to be stuck at a local optimum as may be the case for point-based algorithms such as hill climbing search algorithms for instance.

A multi-objective optimiser aims at identifying a good estimate of the Pareto set of designs for a particular problem. That is, those designs for which it is impossible to improve performance on one objective, by varying its design parameters, without causing a degradation in performance of one or more other objective. In the case of minimisation problems, a legal design \mathbf{x}_1 is said to *dominate* another legal design \mathbf{x}_2 , denoted $\mathbf{x}_1 \succ \mathbf{x}_2$, iff $f_i(\mathbf{x}_1) \leq f_i(\mathbf{x}_2)$ for all objective functions $f_i(\cdot)$ such as $f_i(\mathbf{x}_1) \neq f_i(\mathbf{x}_2)$. The Pareto set of designs is therefore defined as $\mathcal{P} = \{\mathbf{x} \in X \mid \nexists \mathbf{u} \in \mathcal{X}, \mathbf{u} \prec \mathbf{x}\}$, where \mathcal{X} is the set of potential designs.

Adaptive IBEA is one of the first evolutionary algorithms to employ a binary quality indicator in its selection mechanism. A binary quality indicator is a function that compares the quality of two Pareto set approximations by mapping them to a real number [307]. Specifically, a Pareto set approximation is ‘better’ than another one if it is characterised by a higher indicator score. Adaptive IBEA uses a binary indicator by exploiting it in the *fitness* assigned to each member (design) maintained by its search population, X . This fitness quantifies a design’s contribution to the overall quality of the set of designs maintained by the optimiser, and is used to decide which designs to replace with newly evolved solutions as the search progresses. The fitness of a design \mathbf{x} is calculated as:

$$F(\mathbf{x}) = \sum_{\mathbf{u} \in X \setminus \{\mathbf{x}\}} -e^{-I(\{\mathbf{u}\}, \{\mathbf{x}\})/c_I \kappa} \quad (6.1)$$

where c_I is the maximum absolute indicator value calculated across all members of X . κ is a term to scale the assigned fitnesses set to 0.05 as in [304]. The additive epsilon indicator function $I_{\epsilon+}(A, B)$ is used to compute the quality indicator term $I(\{\mathbf{u}\}, \{\mathbf{x}\})$ [308]. This quality indicator gives the minimum distance (in objective space) required for one Pareto set approximation A to dominate another approximation, B . Formally, its calculation is:

$$I_{\epsilon+}(A, B) = \min_{\epsilon} \{ \forall \mathbf{b} \in B \exists \mathbf{a} \in A : f_i(\mathbf{a}) - \epsilon \leq f_i(\mathbf{b}) \quad \text{for } i \in \{1, \dots, n\} \} \quad (6.2)$$

for a n -objective problem. Adaptive IBEA was implemented in the MATLAB numerical computing environment and the code is given in Appendix D. It invoked the finite element model of the sandwich plate presented in Chapter 3, running on the commercial software ANSYS. The sandwich plates were considered under both cantilevered and free boundary conditions. The first two mode shapes and natural frequencies of the empty structures were given in Chapter 5 Table 5.1 for each set of boundary conditions. The objective values to be minimised were the negative of the modal loss factor (computed via the modal strain energy method, see equation 2.32 in Chapter 2) and the percentage of additional mass on the structure. The design parameters were the location and the orientation of the DSLJ damping inserts, which were encoded as a 362-element long binary string. A bit pair represents the different damper orientations (or no damper), with the location in the string of a particular bit pair determining the location in the sandwich plate it encodes. Overall six different cases were optimised. The sandwich plate was optimised for modes 1 and 2 under both cantilever and free boundary conditions, i.e. four cases. Two further cases consisted of optimising over three objectives – the negative of the first two modal loss factors as well as the additional mass in percent – for the sandwich

CHAPTER 6. EVOLUTIONARY OPTIMISATION OF DSLJ DAMPING INSERTS

plate under both free and cantilever boundary conditions. The flowchart of the optimisation process implemented here – including the modifications added to the original Adaptive IBEA algorithm – is shown in Figures 6.1 and 6.2.

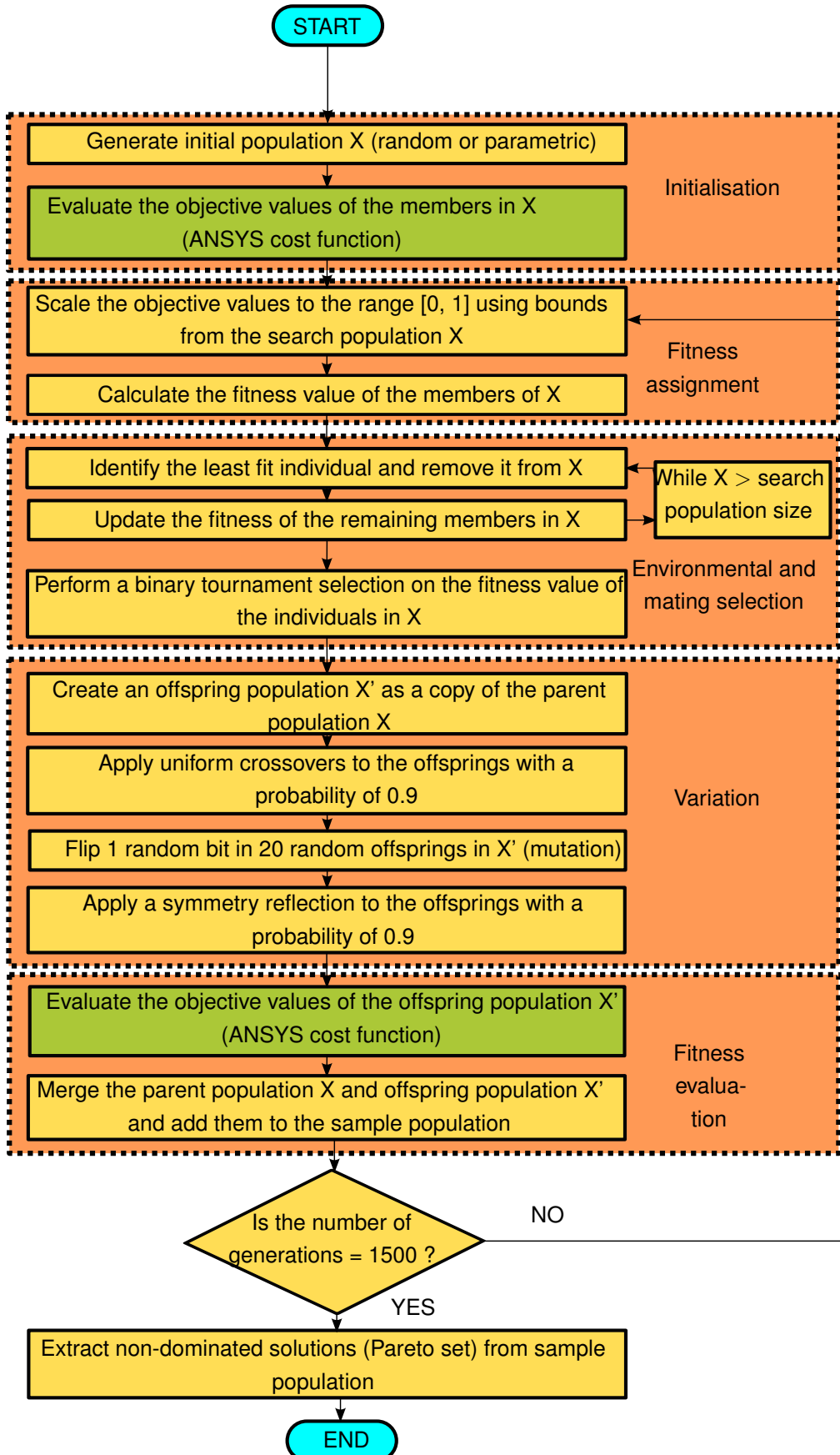


Figure 6.1: Flowchart of the Adaptive IBEA algorithm. The main sections are identified in orange and the ANSYS cost function (green) is detailed in Figure 6.2.

CHAPTER 6. EVOLUTIONARY OPTIMISATION OF DSLJ DAMPING INSERTS

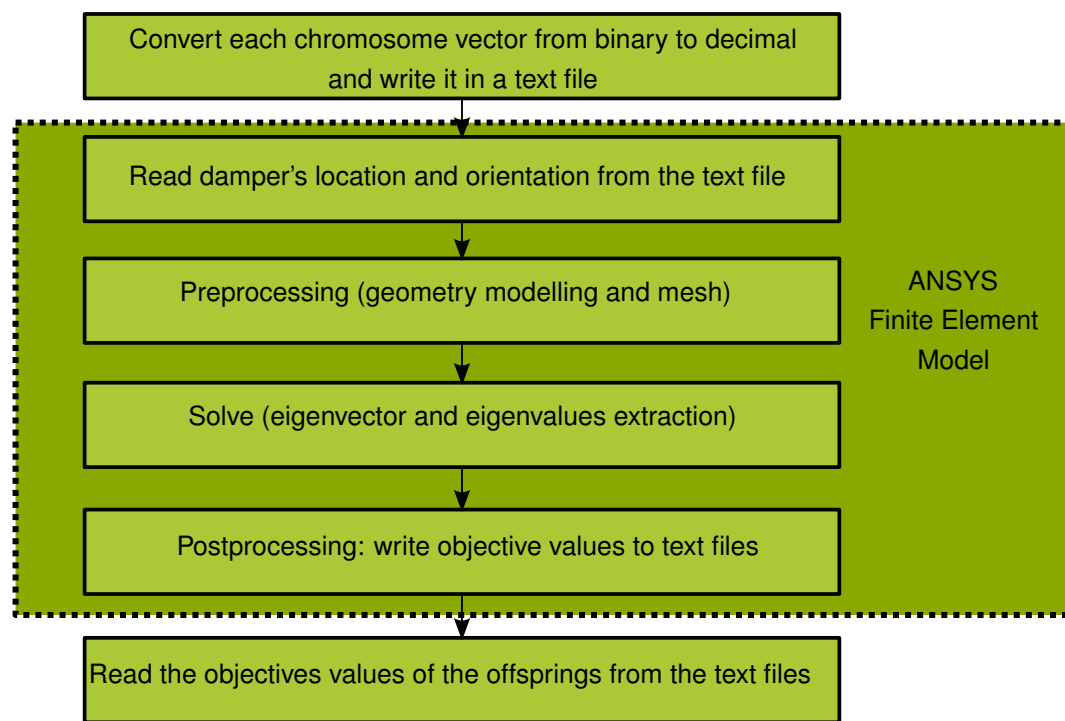


Figure 6.2: ANSYS cost function used in the Adaptive IBEA optimiser (see flowchart 6.1).

For the 2-objective optimisation, the optimiser search population was initialised with the $m = 20$ configurations identified by the parametric optimisation (see Chapter 5), instead of a random set of designs. As will be shown later, this contributed to identify optimal designs faster. In the case of the 3-objective optimisation, the initial population was created as the union of the non-dominated solutions yielded from the two 2-objective optimisation runs targeting modes 1 and 2 individually. In this case, the population size was set to $m = 100$ in order to obtain a better populated estimated Pareto surface. At each algorithm iteration, the objective values were scaled to the interval $[0, 1]$ and these scaled objectives were used to compute the indicator values (see equations 6.1 and 6.2) and the resultant fitness for each member of X .

The ‘environmental selection’ section of Adaptive IBEA then progressively discarded the least fit members of X in turn (recalculating the fitnesses of all remaining members of X each time) until the size of the population reached m . A set of individuals X' (a mating pool) was filled by tournament selection between two randomly chosen individuals from X , with the fitter individual added to the mating pool X' . This was repeated until $|X| = |X'|$.

In the vary subroutine, designs were evolved using uniform crossover with a probability of occurrence of 0.9. Uniform crossover consists in creating new children designs by swapping the binary string representation of two parent designs, cut at a random point on the binary string. These newly created children solutions were then subjected to mutation, which involves flipping a random bit in the chromosome string representation from 0 to 1 or vice-versa. When crossover was not used, a single parent copy was instead subjected to this mutation. A *symmetry reflection* operator was also introduced, which was applied to 90% of designs after the mutation step. The choice for this probability was arbitrary but guided by results which showed that a probability of symmetry reflection of this order yielded faster convergence rates. A probability of symmetry reflection of 100% would enforce symmetry on all configurations and thereby prevent any optimal solutions which happened to be asymmetric. Ergo, it was necessary to allow some offspring members to be created without enforcing symmetry and only undergoing bit flip mutations, thus allowing the optimiser to explore asymmetric regions of the search space. Due to the symmetry of the mode shapes considered (see Figure 5.1), a symmetric damper distribution with respect to the horizontal or vertical medial axis of the sandwich plate is likely to be advantageous. The symmetric reflection operator generated children designs by folding an intermediate design’s left-hand honeycomb cells through the line of vertical symmetry to assign the right-hand cells (or the reverse) or alternatively reflecting horizontally the top half to the bottom half (or vice versa). The cantilevered plates were reflected only horizontally whereas

the free plates were reflected randomly either vertically or horizontally, following the directions of the axis of symmetry of the mode shape. This combination of variation mechanism allows an exhaustive exploration of the search space by testing combinations of already fit patterns (crossover and symmetry reflection), while promoting diversity in the search population via mutation. The optimiser was run for 1500 iterations on a modern desktop machine with eight 16 GB RAM processors running in shared-memory parallel – meaning 30,000 designs were evaluated in an optimiser run. The 3-objective optimisation was only run for 50 iterations since its population size was bigger than the 2-objective case.

6.2.2 Optimisation convergence

Evolutionary optimisers are suited to this type of problem but they may be computationally expensive. Generally, better designs are identified more easily and quickly at the beginning of the optimisation process. As the number of generations increases, the convergence rate reduces until it reaches a plateau value meaning that little further improvement can be achieved. In order to limit the computational cost and optimisation time, it is necessary to determine the number of generations after which the benefit of interrupting the optimisation process exceeds that of finding better solutions. A measure of the convergence rate may be obtained by computing the hypervolume. In the context of multi-objective optimisation, the hypervolume was first defined by Zitzler (which he called *the size of the dominated space*) as a ‘measure of how much of the objective space is weakly dominated by a given non-dominated set’ [309]. In 2-objective optimisation, the hypervolume is defined as the area of the objective space dominated by the Pareto optimal solutions and delimited by an absolute reference point [310]. The coordinates of this reference point correspond to the worst possible design, so that any achievable design would dominate the reference point. The larger the area dominated by the Pareto front, the higher the hypervolume and the better the solutions identified are. In this case, the heaviest design (i.e. the sandwich plate with all its cell filled) is characterised by 73.9% additional mass and the worst modal loss factor (i.e. when no dampers were added) was $\eta = 10^{-4}$. The hypervolume may be approximated as the sum of the areas of the discrete rectangles covering the 2-objective space dominated by the Pareto set, as illustrated in Figure 6.3. Given two objectives a and b , a reference point $R(r_a, r_b)$ and n Pareto optimal designs \mathbf{x}_i ranked in ascending order of objective b , the hypervolume is defined as follows,

$$H = \sum_{i=1}^{n-1} [(r_a - f_a(\mathbf{x}_i))(f_b(\mathbf{x}_{i+1}) - f_b(\mathbf{x}_i))] + (r_a - f_a(\mathbf{x}_n))(r_b - f_b(\mathbf{x}_n)) \quad (6.3)$$

where $f_a(\cdot)$ and $f_b(\cdot)$ are the fitness functions with respect to objectives a and b , respectively. In this equation, the term under the sum sign represents the area of the red rectangles shown in Figure 6.3. In an effort to improve the convergence rate of Adaptive IBEA, two alterations were added to the initial algorithm, specifically the symmetry reflection operator and the initialisation of the search population by a sample of the parametrically optimised configurations. It is necessary to quantify the effect of such alterations on the convergence of the optimiser by studying the evolution of the hypervolume with the number of generations. To this end, 20 consecutive optimisation runs were carried out where the initial search population was either allocated randomly or assigned as the sample of individuals optimised using the parametric approach described in Chapter 5. A similar strategy was adopted to assess the benefit of using symmetry reflections by executing 20 optimisation runs with a probability of symmetry of 0, 0.3, 0.6 and 0.9, respectively.

Since the hypervolume value is restricted to a range between 0 and a fixed upper limit towards which it plateaus, its statistical distribution is not normal. Hence, the median of each group is an appropriate performance indicator for each cases considered. The initial population runs were tested for 20 generations (or approximately 150 minutes) whereas the symmetry runs were tested for 40 generations (or around 400 minutes). The reason for allowing the optimiser to run for longer when studying the effects of symmetry on the convergence is due to the particular nature of the present problem. In such a problem, the benefit of initialising the search population is more evident than that of increasing the probability of symmetry mutation, at least at an early stage of the optimisation process, see Figures 6.4 and 6.5. At the point where the value of the hypervolume reaches a plateau there is little scope for further improvement and it is usual to cease the optimisation process. This point occurred earlier for the initialisation runs than for the symmetry runs.

6.2.3 Parametric vs Adaptive IBEA optimisation

Since this work is concerned with identifying the lightest and most damped structures, the damping efficiency was a relevant indicator of the performance of the different optimisation approaches adopted here. As described in Chapter 4, the damping efficiency of mode i is defined as the modal loss factor of the mode in question η_i divided by the mass of the structure M :

$$E f_i = \frac{\eta_i}{M} \quad (6.4)$$

The performance of the various designs identified by the different optimisation approaches can also be investigated by comparing the frequency response of

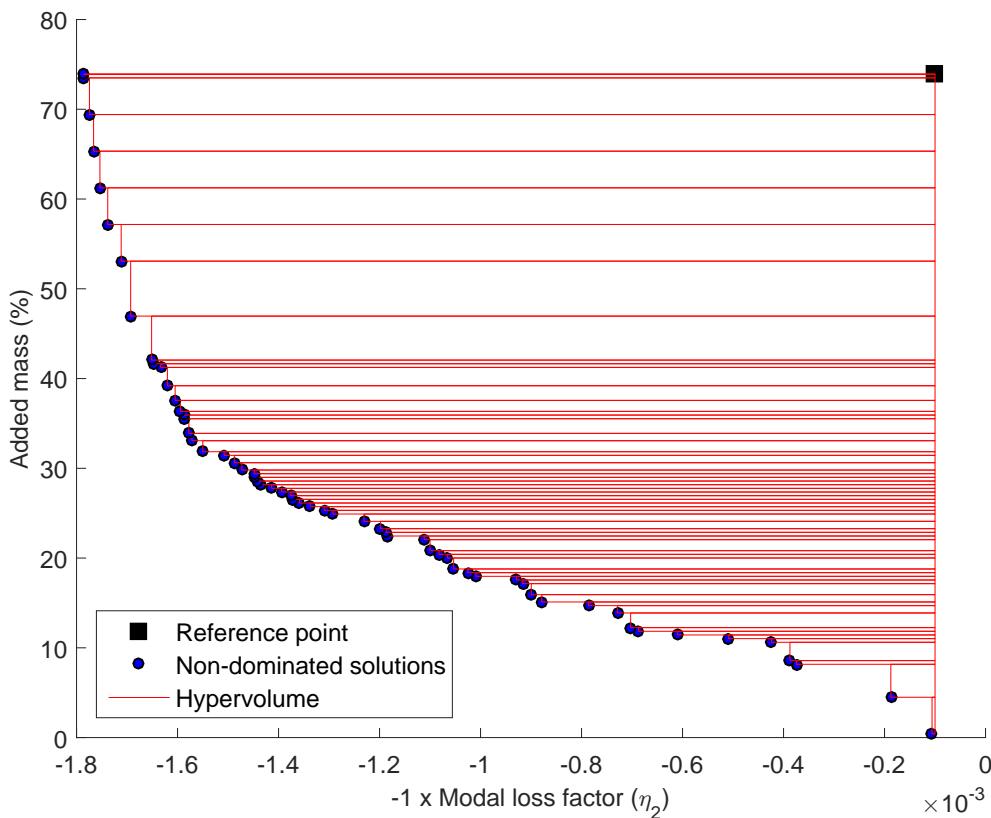


Figure 6.3: Graphical representation of the hypervolume for a 2-objective set of non-dominated solutions. The absolute reference point was chosen as the worst design possible with respect to each objective.

the optimised structures. Here, designs optimised either with the parametric approach or Adaptive IBEA were selected for their similar added mass. Their amplitude response was computed by mode superposition harmonic analysis as described in Chapter 2, using 20,000 substeps and a frequency range of ± 50 Hz before and after the first and second modal frequency, respectively.

6.3 Results

6.3.1 Optimisation convergence

The initial Adaptive IBEA was modified in an attempt to improve its convergence rate. The effects of such modifications on the hypervolume value are presented in this section. It is noteworthy that a higher hypervolume value corresponds to a more advanced Pareto front and therefore to better solution. The evolution of the hypervolume as the number of generations increases when considering different initial search populations and various probabilities of symmetry reflection is shown in Figures 6.4 and 6.5, respectively. It is clear that initialising the search population with the individuals identified by the parametric optimisation rather than with randomly generated designs improves the performance of adaptive

IBEA significantly. Although an increase in probability of symmetry reflection seems to enhance the convergence rate of Adaptive IBEA for this type of problem (see Figure 6.5), the medians of the four groups are overlapping and an immediate conclusion cannot be drawn. It is therefore necessary to employ statistical tests in order to determine whether there are significant differences between each group. Since the hypervolume data is not normally distributed and no assumptions can be made about the distribution of the sample population, nonparametric statistical tests must be used. Since the hypervolume values of four distinct sample groups need to be compared (i.e. groups with a probability of symmetry of 0, 0.3, 0.6 and 0.9, respectively), and each individual run is independent from the other runs in a same group, the Kruskal-Wallis test is used to establish whether at least one group is significantly different from the other groups. This test, applied with a significance level of 0.05, showed that at least one group is significantly different from the other groups after the first generation. In order to test whether one group is notably distinct from another one, the Mann-Whitney U test is applied with a significance level of 0.05 and the results are shown in Table 6.1. The generation number after which there is 95% confidence that all the groups are significantly different from each other is 19. This confidence limit is indicated in Figure 6.5 by a purple dashed line.

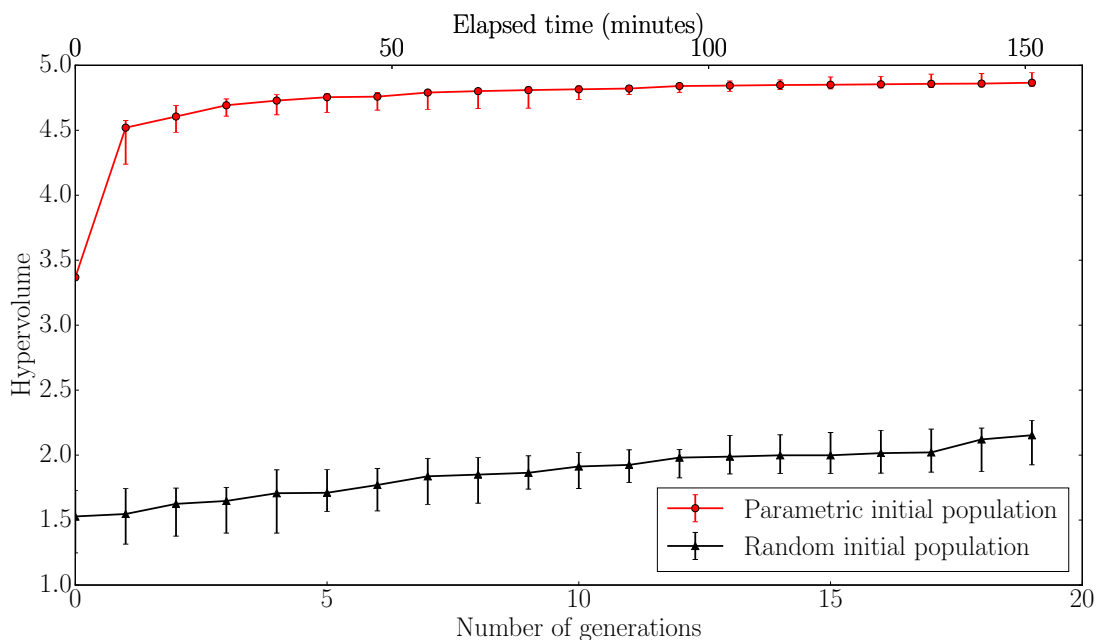


Figure 6.4: Hypervolume median of 20 optimisation runs when initialising the search population with either 20 random individuals or the 20 individuals identified by the parametric optimisation. The error bars represent the minimum and maximum hypervolume value of each group.

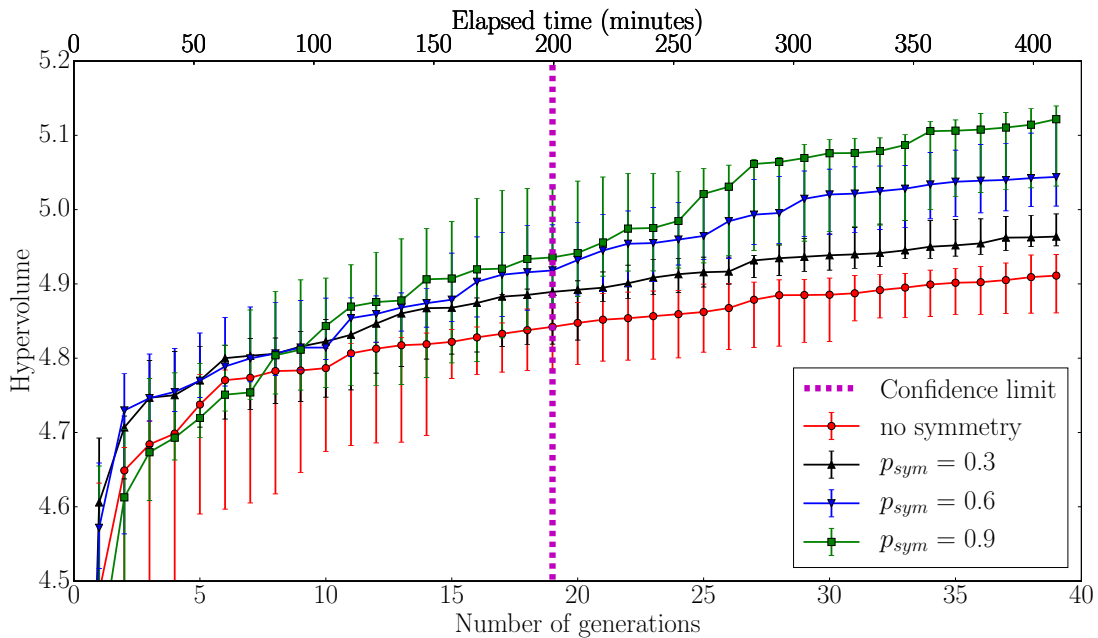


Figure 6.5: Hypervolume median of 20 optimisation runs when symmetry reflections occur with a probability of 0, 0.3, 0.6 and 0.9. The error bars represent the minimum and maximum hypervolume value of each group.

Groups	Generation number after which the differences between groups become significant
$p_{sym} = 0.0 \text{ vs } p_{sym} = 0.3$	3
$p_{sym} = 0.0 \text{ vs } p_{sym} = 0.6$	2
$p_{sym} = 0.0 \text{ vs } p_{sym} = 0.9$	9
$p_{sym} = 0.3 \text{ vs } p_{sym} = 0.6$	19
$p_{sym} = 0.3 \text{ vs } p_{sym} = 0.9$	11
$p_{sym} = 0.6 \text{ vs } p_{sym} = 0.9$	12

Table 6.1: Generation number after which the differences between groups become significant according to the Mann-Whitney U test with a confidence level of 0.05.

6.3.2 2-objective optimisation

The estimated Pareto sets identified by the 2-objective Adaptive IBEA for the cantilever and free plate are shown in Figures 6.6 to 6.9. The generation number in these figures is indicated by colour, with blue being early and red being later. For all cases the parametric initial population and the non-dominated solutions are identified with blue and red markers, respectively. The numbers refer to the configurations identified by a red rectangular box in Figures 5.3 to 5.6 for the parametric initial population and in Figures 6.10 to 6.13 for the non-dominated solutions. It can be noted that most of the cantilever non-dominated configurations are symmetrical with respect to the horizontal mid axis of the

plate (see Figures 6.10 and 6.11), following the symmetry of the mode shape. Similarly, in the case of the free boundary conditions most of the non-dominant configurations are symmetrical both vertically and horizontally, see Figures 6.12 and 6.13.

For the cantilever plate under its first flapping mode, the initial population which was derived from the parametric optimisation and the non-dominated Adaptive IBEA solutions have similar objective values, as shown in Figure 6.6, and the two optimised configurations are also similar, see Figures 6.10 and 5.3. In contrast under the first torsional mode (mode 2), the non-dominated configurations are better than the initial population, see Figure 6.7. Specifically, the non-dominated solutions achieve up to 27% higher modal loss factors than the parametrically optimised configuration with a similar additional mass.

In the case of the free plate (see Figures 6.8 and 6.9), the consequences of mode veering identified in the previous chapter are clear: the parametric optimisation identified configurations that exhibit much poorer performance than those determined by Adaptive IBEA. Since the parametric approach optimise the location and orientation of the DSLJ inserts based on the mode shape geometry of the empty structure, a swap in the order of the natural frequencies led the optimiser to target the wrong mode, thus misplacing the dampers. For instance, the maximum loss factor reached only 2.5×10^{-3} for a significant 70% increase in mass in the case of the free sandwich plate originally optimised for its first mode. These mode swaps – or veering – occurring in the initial population are illustrated in Figure 6.8 and 6.9 by circle and diamond markers. In contrast Adaptive IBEA was able to identify much superior configurations appropriate to the new shape of the first mode, with a modal loss factor of up to 4.2×10^{-3} for only an 15% increase in mass with respect to the empty structure. The Adaptive IBEA optimised configurations appear thoroughly different from the parametrically optimised configurations, see Figure 6.12. A similar situation can be noted in the case of the free boundary condition plate optimised for its second mode, where four mode swaps can be identified as dampers are added to the structure in the parametric optimisation, see the diamond and circle markers in Figure 6.9. It is not surprising that Adaptive IBEA has identified significantly better configurations in this case; beating the parametric method by more than sevenfold in modal loss factor for a similar additional mass, see Table 6.2.

CHAPTER 6. EVOLUTIONARY OPTIMISATION OF DSLJ DAMPING INSERTS

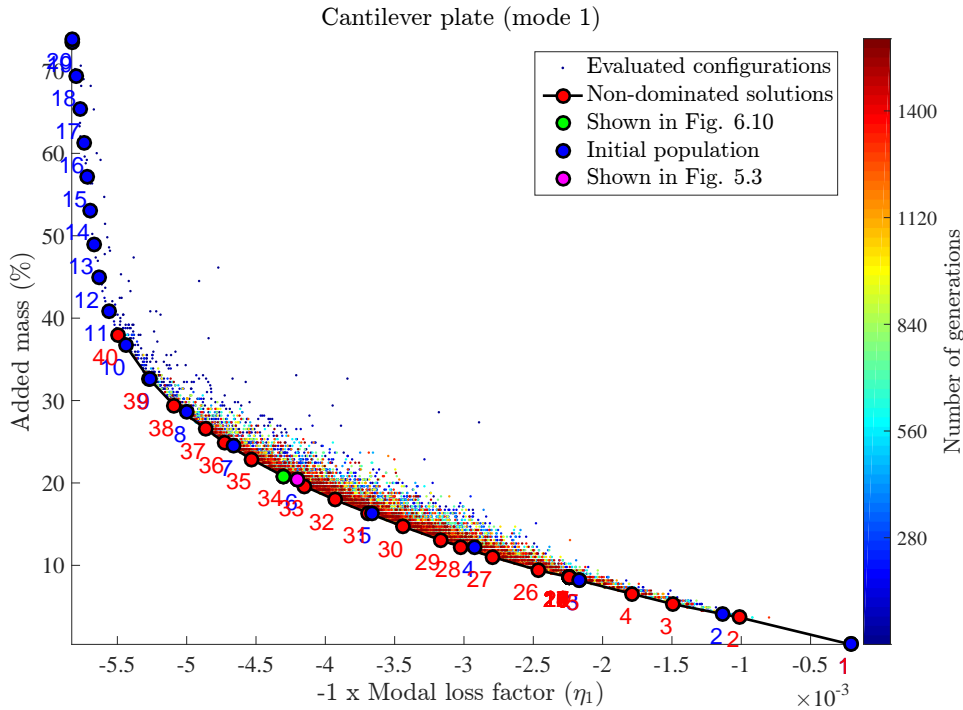


Figure 6.6: Cantilever sandwich plate - the initial population, the non-dominated solutions and all the evaluated configurations are represented by the negative of their first modal loss factor and their percentage of additional mass.

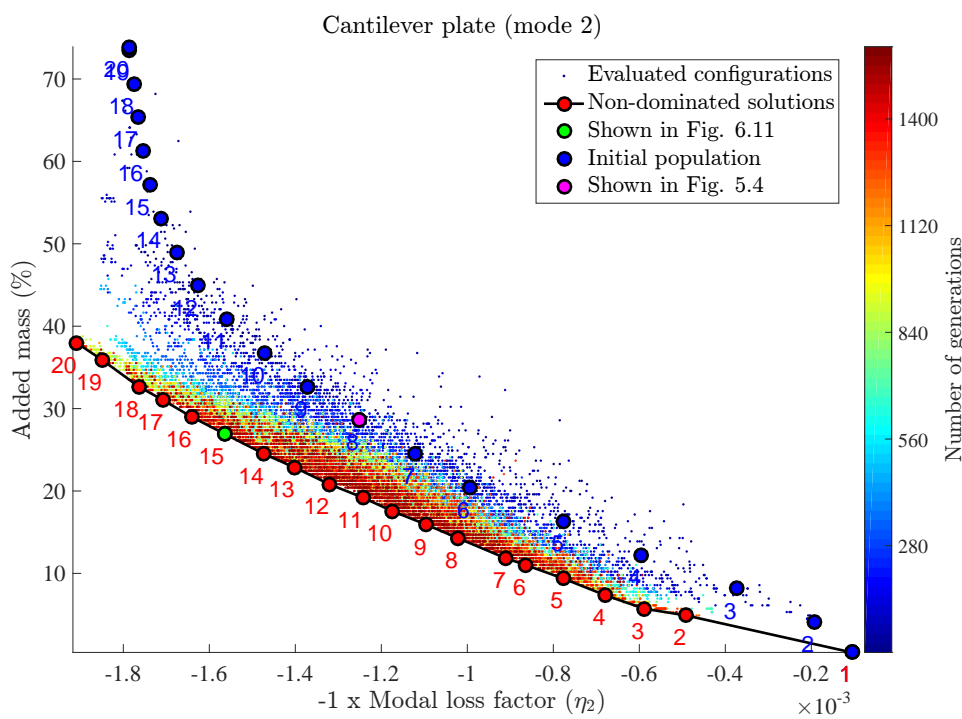


Figure 6.7: Cantilever sandwich plate - the initial population, the non-dominated solutions and all the evaluated configurations are represented by the negative of their second modal loss factor and their percentage of additional mass.

6.3. RESULTS

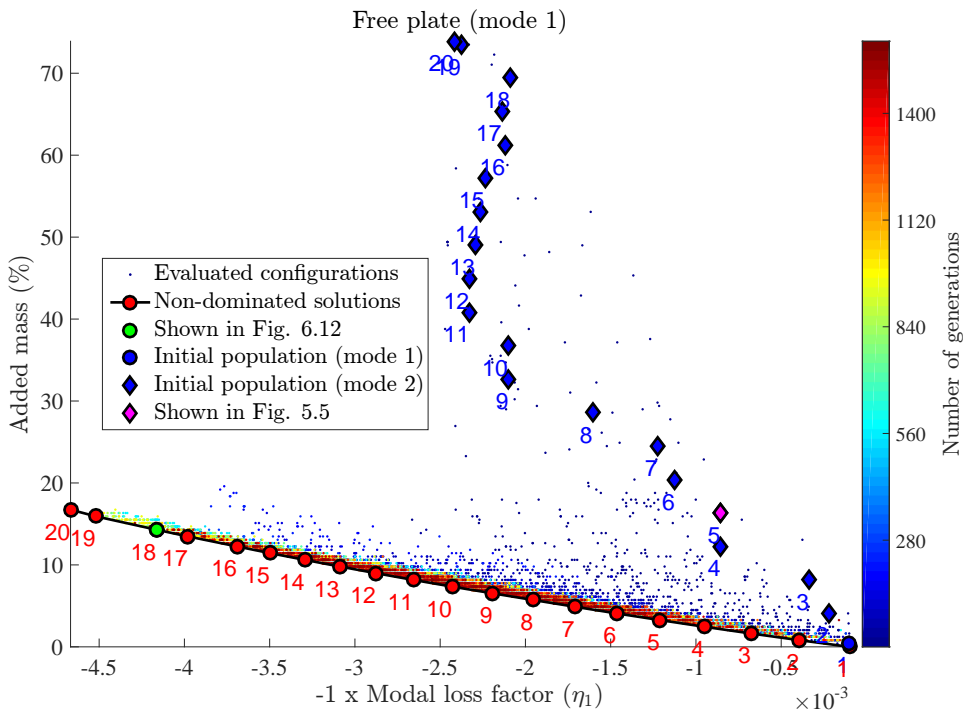


Figure 6.8: Free sandwich plate - the initial population, the non-dominated solutions and all the evaluated configurations are represented by the negative of their first modal loss factor and their percentage of additional mass. The initial population features two different mode shapes, represented by either a circle or a diamond.

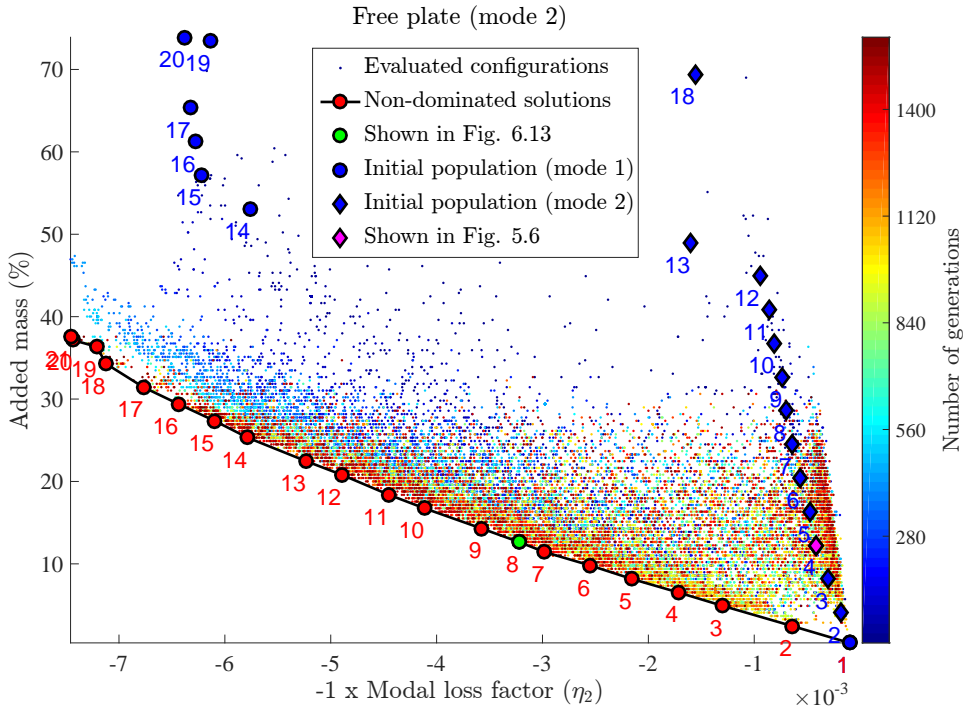


Figure 6.9: Free sandwich plate - the initial population, the non-dominated solutions and all the evaluated configurations are represented by the negative of their second modal loss factor and their percentage of additional mass. The initial population features two different mode shapes, represented by either a circle or a diamond.

CHAPTER 6. EVOLUTIONARY OPTIMISATION OF DSLJ DAMPING INSERTS

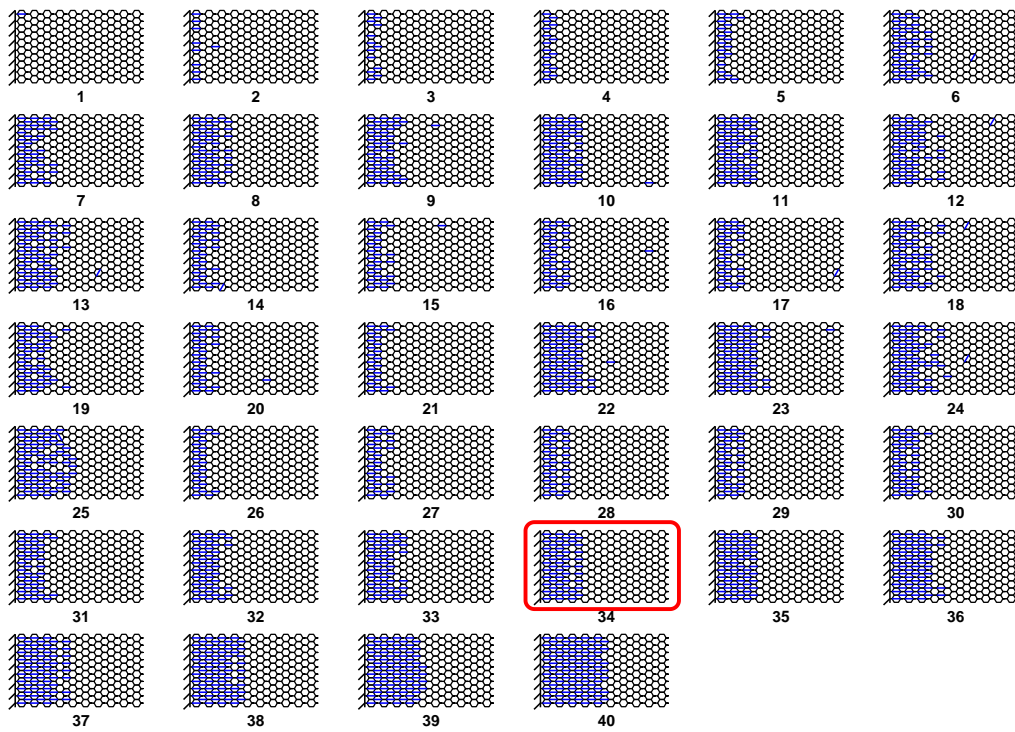


Figure 6.10: Optimal designs identified by Adaptive IBEA for the cantilever sandwich plate when targeting the first mode (flapping). The configuration in the red box is identified by a green point in Figure 6.6.

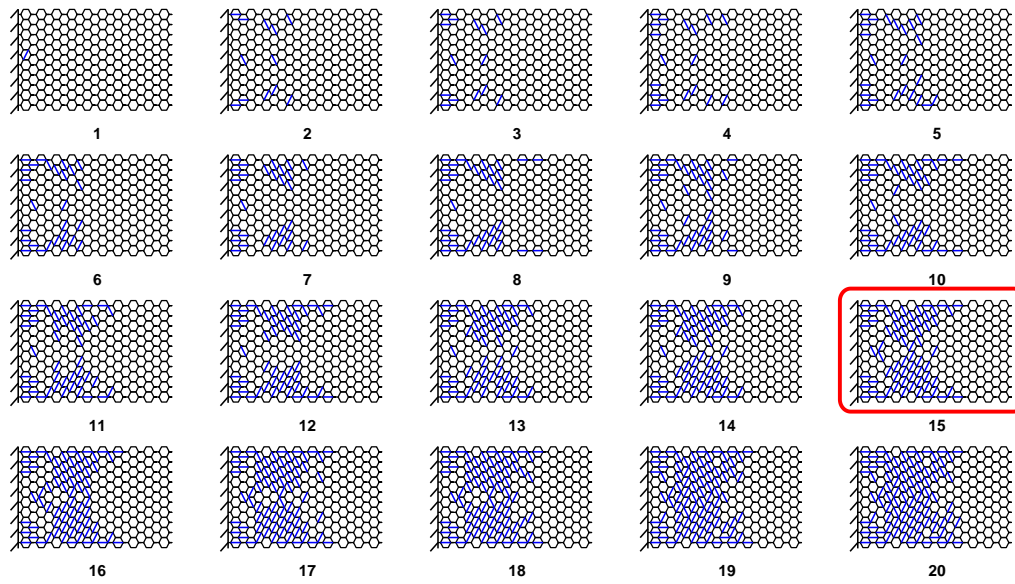


Figure 6.11: Optimal designs identified by Adaptive IBEA for the cantilever sandwich plate when targeting the second mode (torsion). The configuration in the red box is identified by a green point in Figure 6.7.

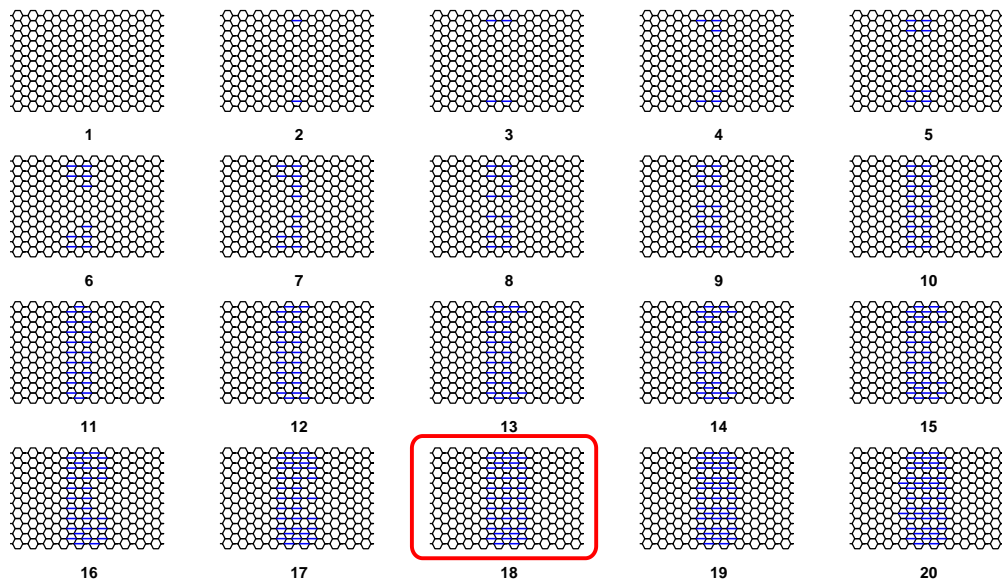


Figure 6.12: Optimal designs identified by Adaptive IBEA for the free sandwich plate when targeting the first mode (bending). The configuration in the red box is identified by a green point in Figure 6.8.

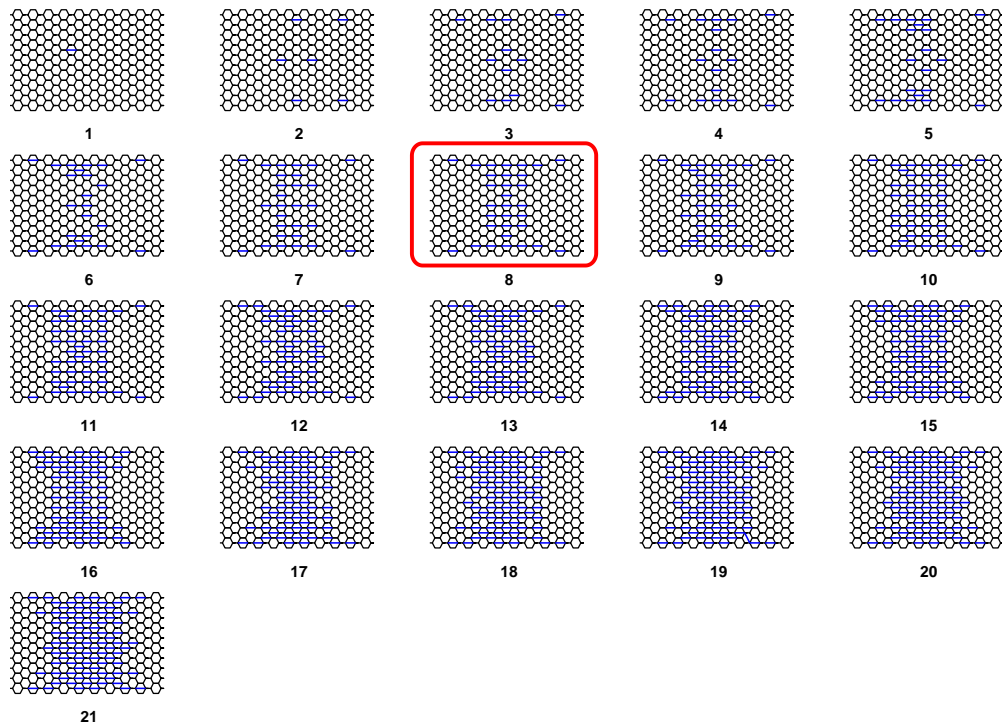


Figure 6.13: Optimal designs identified by Adaptive IBEA for the free sandwich plate when targeting the second mode (torsion). The configuration in the red box is identified by a green point in Figure 6.9.

6.3.3 3-objective optimisation

It is possible to optimise for more than one mode at a time. Here Adaptive IBEA was used as 3-objective optimiser that maximises simultaneously the first two modal loss factors while minimising the added mass in a 3-objective optimisation. When modes are considered individually for the cantilever or free plates, the 3-objective optimised solutions perform less well (i.e. they are heavier and less damped) than the 2-objective optimised solutions, see Figures 6.14 and 6.15. However, the 2-objective solutions that were determined by maximising the first modal loss factor exhibit very poor ability at damping the second mode, and vice versa. The 3-objective solution has identified compromise solutions that are capable of damping efficiently and simultaneously modes 1 and 2. For clarity and because the search population was initialised to 100, only 20 of the non-dominated configurations are represented for the 3-objective optimisation. The distributions of DSLJ inserts in the 3-objective optimised configurations appear to be combinations of the 2-objective configurations where the modal loss factors are maximised individually, see Figures 6.16 and 6.17.

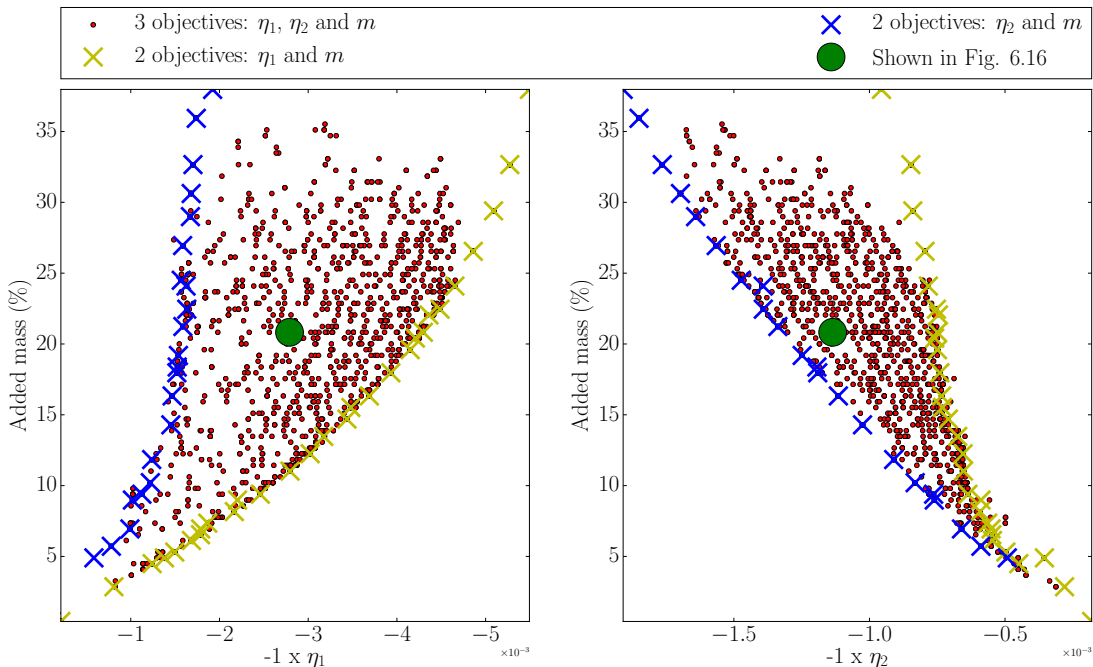


Figure 6.14: The non-dominated solutions identified by the 3-objective (red points) and 2-objective optimisations targeting the first mode (yellow crosses) or second mode (blue crosses) are shown for the cantilever sandwich plate.

6.3. RESULTS

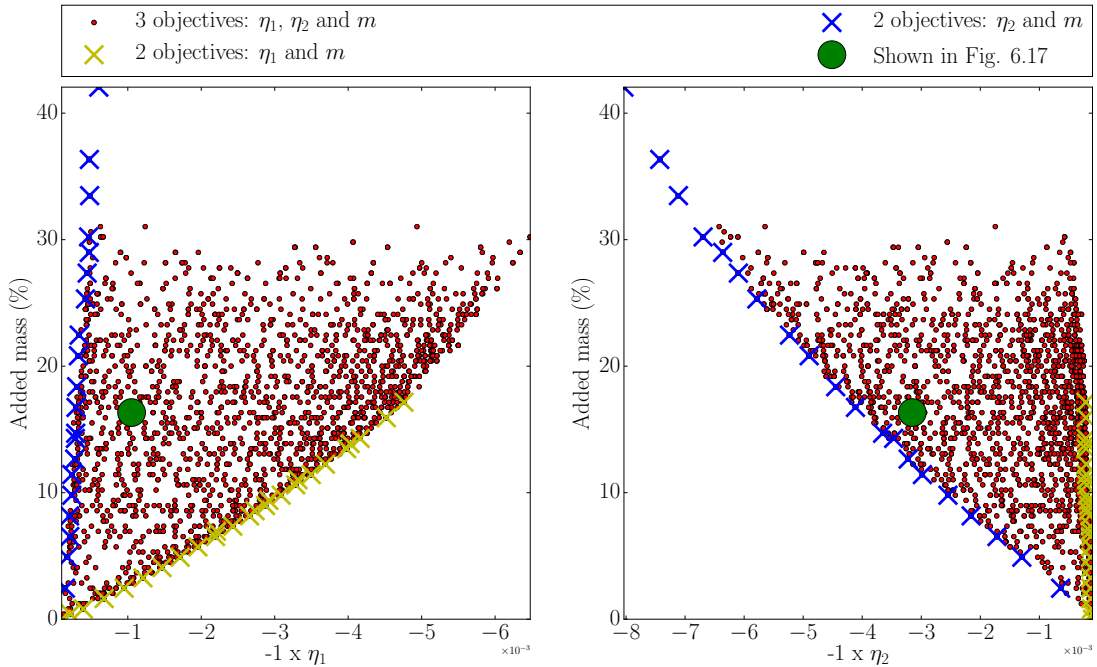


Figure 6.15: The non-dominated solutions identified by the 3-objective (red points) and 2-objective optimisations targeting the first mode (yellow crosses) or second mode (blue crosses) are shown for the sandwich plate in free boundary conditions.

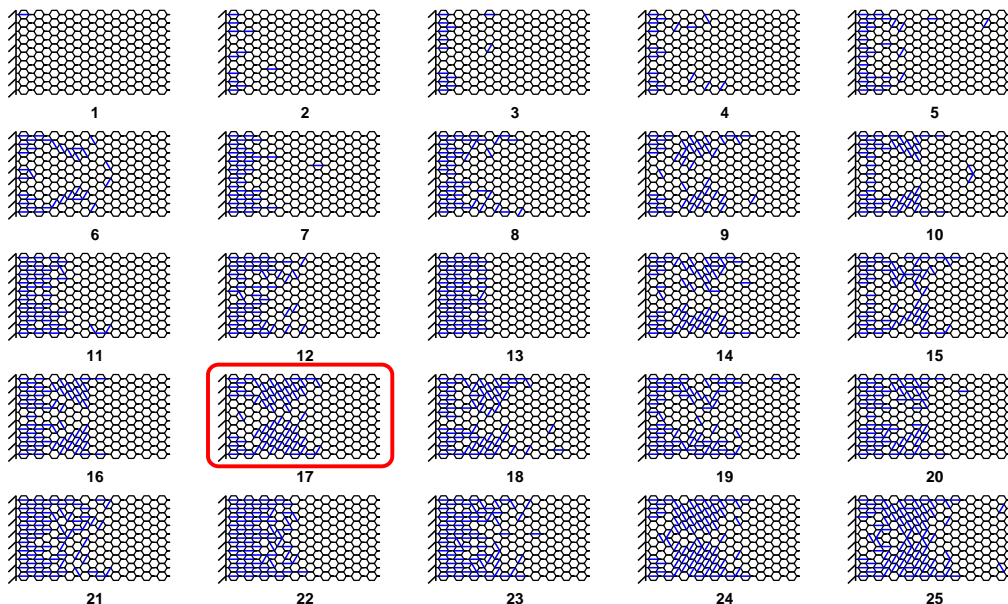


Figure 6.16: Optimal designs identified by Adaptive IBEA for the cantilever sandwich plate when targeting the first and second mode simultaneously. The configuration in the red box is identified by a green point in Figure 6.14.

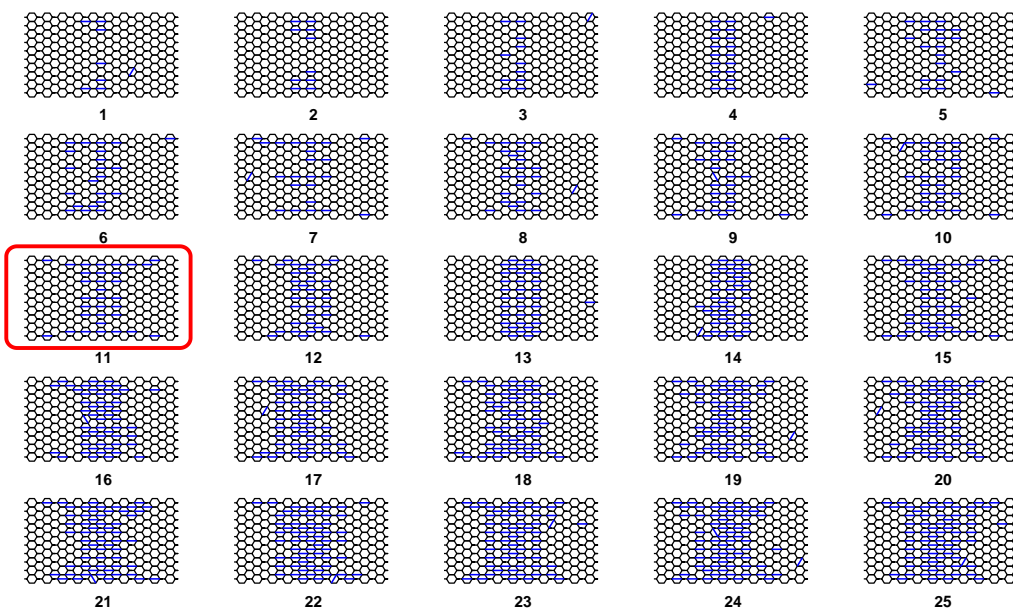


Figure 6.17: Optimal designs identified by Adaptive IBEA for the free sandwich plate when targeting the first and second mode simultaneously. The configuration in the red box is identified by a green point in Figure 6.15.

6.3.4 Parametric vs Adaptive IBEA optimisation

For comparison purposes, a configuration characterised by an increase in mass of about 20% is picked among the Pareto-optimal solutions in all the cases considered here. This configuration is identified by a green point in the Pareto graphs and by a red box in the configuration figures. The modal loss factor, mass and damping efficiencies of these configurations are shown in Table 6.2. The modal loss factors and added mass are normalised to those of the empty structure. As would be expected, all optimised configurations exhibit higher modal loss factors than the empty structure; reaching up to 43 times for the first modal loss factor in the Adaptive IBEA optimised cantilever case. These increases in loss factors come at the cost of moderate increases in mass, for example 21% additional mass for the Adaptive IBEA optimised cantilever case in mode 1. In the cantilever sandwich case optimised for mode 1, the damping efficiency is similar for both the parametric and Adaptive IBEA solution. However for all other cases, Adaptive IBEA outstrips the parametric approach, in particular for the free boundary condition cases where the damping efficiency after the Adaptive IBEA optimisation is about five and seven times higher than that of the parametric optimisation for mode 1 and 2, respectively.

The amplitude response of each of the selected designs is shown in Figures 6.18 and 6.19 for the cantilever and free plate, respectively. It is clear that both optimisation methods have identified better solutions for the mode they were targeting, which confirms the data shown in Table 6.2. In the case of the cantilever plate (Figure 6.18), Adaptive IBEA identified designs that produced a smaller amplitude response than those determined parametrically. The Adaptive IBEA design targeting mode 2 does not perform well for mode 1. However, the 3-objective optimisation has identified a compromise configuration which damps both modes 1 and 2 substantially. Similar conclusions can be drawn for the free plate even though the graph is more difficult to interpret due to the modes being close in frequency, see Figure 6.19. Most damped configurations tend to shift the natural frequency either upwards or downwards, which is expected since the ratio of the modal stiffness to the modal mass is altered after the addition of the dampers.

Optimisation approach	Boundary conditions	η_1	η_2	Mass	Damping efficiency
Parametric	Cantilever	42.0	-	1.20	34.9
		-	12.5	1.29	9.74
	Free	8.55	-	1.16	7.35
		-	4.16	1.12	3.71
Adaptive IBEA	Cantilever	43.0	-	1.21	35.6
		-	15.6	1.27	12.3
		27.9	11.4	1.21	-
	Free	41.6	-	1.14	36.4
		-	32.2	1.13	28.6
		13.4	29.4	1.16	-

Table 6.2: Performance comparison between the parametric and Adaptive IBEA optimisation for the cantilever and free boundary condition cases. The configurations compared are identified by a magenta and a green point in Figures 6.6 to 6.15 for the parametric and the Adaptive IBEA optimisation, respectively. The mass, the first η_1 and second η_2 loss factors are presented as a ratio of the empty structure value. The damping efficiencies are also indicated.

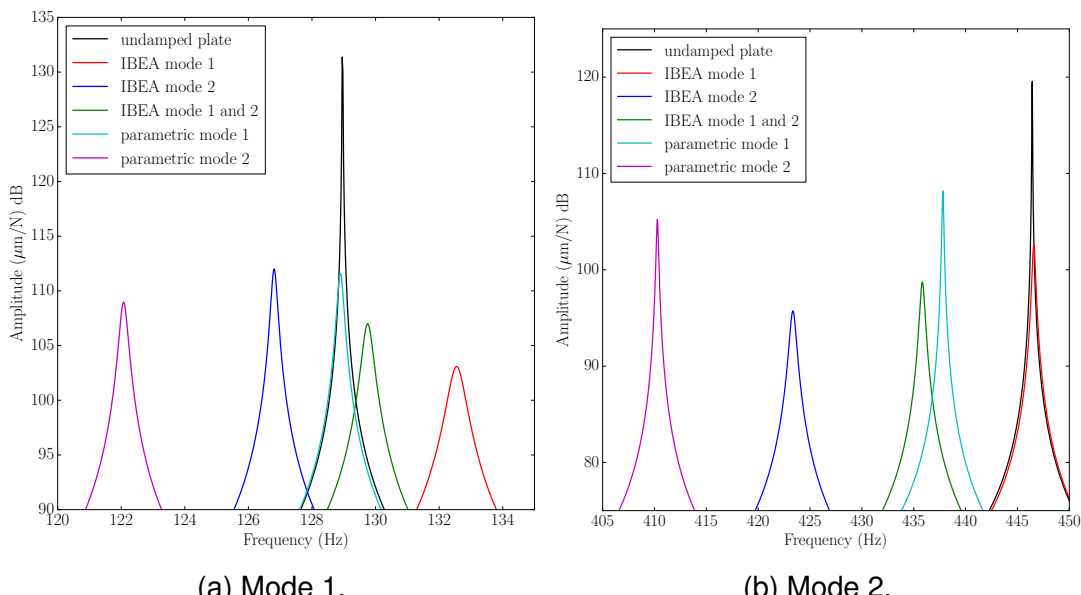


Figure 6.18: Amplitude of the frequency response function of the selected configurations optimised for the cantilever plate with the parametric approach, Adaptive IBEA when targeting mode 1, mode 2 and mode 1 and 2 simultaneously. The amplitude response of the undamped plate is also shown.

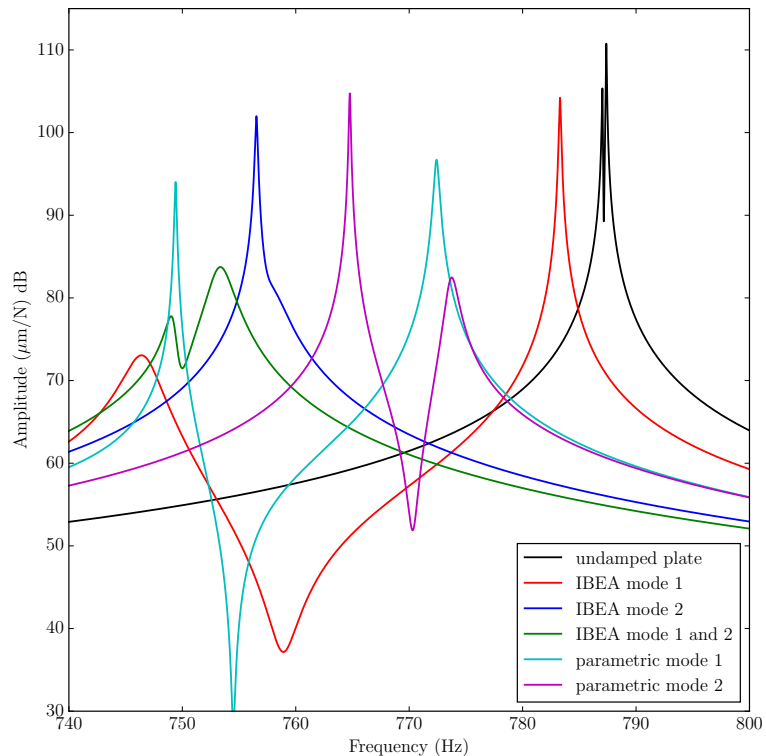


Figure 6.19: Amplitude of the frequency response function of the selected configurations optimised for the free plate with the parametric approach, Adaptive IBEA when targeting mode 1, mode 2 and mode 1 and 2 simultaneously. The amplitude response of the undamped plate is also shown.

6.4 Discussion

6.4.1 Optimisation convergence

The 20 consecutive and independent optimisation runs produced similar hypervolume values, noticeable by the relatively small errors bars in Figures 6.4 and 6.5. This demonstrates that Adaptive IBEA is a robust optimisation process for this type of problem, capable of producing repeatable results. In all cases, the hypervolume increased as the optimisation progressed which was expected since the objective space increases as the optimiser identifies better solutions. This suggests that Adaptive IBEA is a functional multi-objective evolutionary optimiser and it was correctly implemented in this study.

In Figure 6.4, it was shown that initialising the search population with the designs identified by the parametric approach yields an appreciably higher hypervolume than when the initial population is assigned randomly. A high probability of symmetry reflection also improves the performance of the optimiser, though to a lesser extent. Indeed, it may be necessary to wait up to the 19th generation to discern significant differences when considering different probabilities of symmetry (see Table 6.1). It could have been interesting to explore the effect of other alterations to Adaptive IBEA, such as the influence of the probability of mutation, the probability of crossover or the type of crossover (uniform or single point). However, these types of alteration are not specific to this particular optimisation problem. The investigation of their effects on the convergence rate relates more to the field of computer science which falls out of the scope of this study. Further modifications to Adaptive IBEA specific to this problem could also have been implemented in order to improve the convergence rate. For instance, this problem can be scaled down by optimising widely disparate regions of the sandwich plate in parallel, and subsequently exploring smaller child regions within a broadly optimised parent region. The optimisation of regions can be run on multiple cores in parallel which would also accelerate the convergence.

6.4.2 Adaptive IBEA optimisation

In this study, a multi-objective evolutionary optimiser was successfully implemented with the objective to optimise the location and orientation of DSLJ dampers deployed in a honeycomb-core sandwich plate under cantilever and free boundary conditions. Both the parametric and Adaptive IBEA optimised configurations showed better performance than the empty native structure, both in terms of absolute modal loss factors and damping efficiency, see Table 6.2, Figure 6.18 and 6.19. Therefore, these two approaches are both relevant for this type of problem.

In the cantilever sandwich plate in its first mode, Adaptive IBEA and the parametric optimisation converged towards similar optimal solutions. Indeed, the Pareto-optimal solutions share the same location on the search space for both optimisation techniques, see Figure 6.6. The configurations identified by the two techniques also feature a similar distribution of DSLJ dampers, see Figures 6.10 and 5.3. The fact that both optimisation approaches have identified similar sets of solutions, suggests that they may be optimal for this particular case, i.e. there is no other better solution. In general, a heuristic optimiser such as adaptive IBEA cannot explain why the solutions identified are optimal nor it can guarantee that the optimised solutions are the best for a particular problem.

Nevertheless, there were differences in all other cases, sometimes only subtle and sometimes more marked. The differences in performance of these configurations however can be very large, e.g. the Adaptive IBEA configuration for the free plate which had a second modal loss factor up to an order of magnitude greater for a similar additional mass, see Figure 6.9. Thus, the parametric optimisation is less effective than the Adaptive IBEA optimisation in some if not all cases.

The reason for this is that the parametric optimisation cannot cope with mode veering caused by the additional mass and stiffness occurring as dampers are inserted, whereas the evolutionary optimisation implicitly does. Indeed, Adaptive IBEA is systematically attempting to maximise the modal loss factor of the first or second mode extracted by the finite element eigensolver, whether it be a torsional or a bending mode. Since the design variables (i.e. the distribution of the DSLJ dampers here) affects directly the quality measures used to store and select designs, the problem of mode veering is circumscribed by evolutionary optimisers such as Adaptive IBEA. Hence structures prone to veering may benefit more from evolutionary optimisers which take veering into account, than from approaches such as this parametric method which do not. The detrimental consequences of mode veering can also be seen in the poor damping efficiency predicted for the free plate optimised parametrically for mode 2, see Table 6.2. When mode veering occurred, the parametric method identified designs with a damping efficiency of up to an order of magnitude lower than those identified by Adaptive IBEA. It is well known that adding damping treatments onto a lightweight structure may shift its natural frequencies upwards or downwards [265]. These frequency shifts may also be minimised –thus mitigating the consequences of veering– by regarding them as a penalty parameter in the evolutionary optimisation algorithms [195, 196, 208].

Unlike the parametric approach, Adaptive IBEA is capable of minimising more than two objectives simultaneously. Here, the 3-objective configurations presented an evident trade-off between the two 2-objective solutions, see Fig-

ures 6.14 and 6.15. Indeed the 2-objective solutions exhibited poor performance in damping for the mode that was not targeted. In contrast, the 3-objective compromise solutions retained substantial damping for both mode 1 and 2, with a relative penalty compared to the 2-objective optimisation, see Figures 6.18 and 6.19. This may be particularly useful for structures subjected to excitations covering a wide range of frequencies, such as the compressor blades of a gas turbine subjected to an unsteady airflow [311]. It can be noted that the 3-objective designs share the location and orientation features of the two 2-objective designs targeting individual modes, see Figures 6.16 and 6.17.

Adaptive IBEA is an effective –though computationally expensive and time consuming– approach to this problem. It necessitated running at least 40 generations (or 800 finite element simulations, corresponding to around 400 minutes, see Figure 6.5) to converge whereas the parametric method only required one initial finite element evaluation. However, using such heuristic methods guarantees equivalent –and in most cases substantially better– optimisation performance. This is especially true when the quality measures used to select the designs may be affected by the alteration of the design itself during the optimisation process, as it was the case here with mode veering.

6.5 Conclusion

Optimal weight-efficient configurations of DSLJ damper for honeycomb-cored sandwich plates with various boundary conditions were identified here using a multi-objective evolutionary optimisation algorithm. For example, the free sandwich plate was only made 13% heavier and produced a 32 times higher second modal loss factor than the empty structure after the Adaptive IBEA optimisation. It was shown that this optimisation technique is as, if not more, effective than the parametric approach for all the cases considered here. Although computationally demanding and complex to implement, evolutionary optimisation techniques are capable of dealing with the coupling between quality measures and the updating of the designs in the search population. In the present problem, the placement of damping inserts had a direct influence on the mode shapes and the order of extraction of the natural frequencies, which in turn determined the value of the modal loss factor to be minimised. Adaptive IBEA is thus a more sophisticated and a cleverer optimisation method than the parametric approach since it can account for any potential mode veering by dynamically updating its quality measures instead of targeting a pre-determined mode shape. Two alterations to the initial Adaptive IBEA algorithm were also implemented, i.e. the initialisation of the search population with parametrically optimised configurations and the use of symmetry reflection. It was shown that such modifications

substantially improved the convergence rate of the optimisation process. Finally, Adaptive IBEA is a multi-objective optimisation algorithm capable of minimising the modal loss factors of a large number of modes simultaneously, which can be an interesting property for structures subjected to a wide range of excitation frequencies.

CHAPTER 6. EVOLUTIONARY OPTIMISATION OF DSLJ DAMPING INSERTS

Chapter 7

Experimental modal testing of optimally damped honeycomb sandwich panels

7.1 Introduction

The main purpose of the work described in this thesis was to investigate the performance of a novel and weight-efficient damping treatment for lightweight sandwich structures. Using numerical methods, it was shown in the previous chapters that the DSLJ insert is a highly efficient damping treatment when deployed in honeycomb sandwich structures and it can yield similar or even superior performance to the CLD. The location and orientation of these DSLJ inserts were then optimised for standard sandwich panels and a high increase in modal loss factor was reported for a minimal increase in added mass. However, the numerical model used to evaluate the eigenfrequencies and eigenvectors of the structures does not account for the various imperfections introduced by the manufacture of physical samples, especially for complex structures such as honeycomb-cored sandwich panels and DSLJ inserts. It is important to note that the numerical model described in the previous chapters was not intended to provide an accurate description of the behaviour of experimental samples, but only to compare damping in structures with different damping treatments. However, it is necessary to appraise the fidelity of the numerical model at capturing the differences in damping between two structures. In this chapter, honeycomb-cored sandwich structures under various damping configurations are manufactured and tested experimentally. Although absolute values of modal loss factors are not expected to match the numerical predictions, attention is focused on the evolution of modal loss factor between undamped and damped samples.

7.2 Method

The structures considered here are honeycomb-cored sandwich plates under free boundary conditions. The modal testing of these structures is carried out in order to evaluate their Frequency Response Function (FRF), from which the modal loss factors and natural frequencies can be extracted. Three different damping configurations will be applied to this plate: (i) a CLD patch positioned so as to damp the first mode of the sandwich plate considered under free boundary conditions (ii) the DSLJ configuration that targets the first mode of the free sandwich plate, as determined in Chapter 6 (iii) an undamped honeycomb sandwich plate.

7.2.1 Manufacturing of the samples

A total of six samples were manufactured, including two identical pairs of sandwich plates with a CLD, DSLJ inserts and no dampers. These structures will subsequently be referred to as *CLD*, *DSLJ* and *undamped*, respectively. The design of these sandwich structures matched as closely as possible the finite element model described in Chapter 3. The honeycomb plates were made of 10×10 regular hexagonal cells, plus 9×9 interleaving cells. The honeycomb core, supplied by Goodfellow, was 20 mm thick and had a density of 0.062 g.cm^{-3} . It was formed by expansion from stacked aluminium foil (alloy 5052). The cell walls were 0.1 mm thick and the cell rib was 7.5 mm long. The skins consisted of a rectangular aluminium sheet cut to dimension with a guillotine. The hard tempered aluminium sheets (AL1013) manufactured by Advent Research Materials were made of 0.2 mm thick 99.5% pure aluminium. The skins were bonded to the core using the high performance epoxy laminating resin EL2 cured with the epoxy hardener AT30 - FAST (supplied by Easy Composites). The external surface of the skins was protected with a sticky tape to avoid its contamination with cured epoxy, which would impede the modal testing. The inner surface of the skins was cleaned with acetone and keyed with an abrasive sand paper in order to enhance its bonding to the core. The epoxy was applied with a brush and left to cure overnight. Once the first skin was bonded, the same process was repeated for the second skin in order to prevent the leakage of liquid epoxy inside the honeycomb core. The undamped samples are shown in Figure 7.1.

The CLD dampers were supplied by Heathcote Industrial Plastics Ltd. (product 2002) and were made of a 0.5 mm thick constraining layer and a 0.05 mm thick viscoelastic layer. The viscoelastic layer consisted of the HIP2 damping polymer whose material loss factor and shear modulus at 20°C and 1,000 Hz are approximately 1.2 and 2.5 GPa, respectively. The CLD patch of dimensions

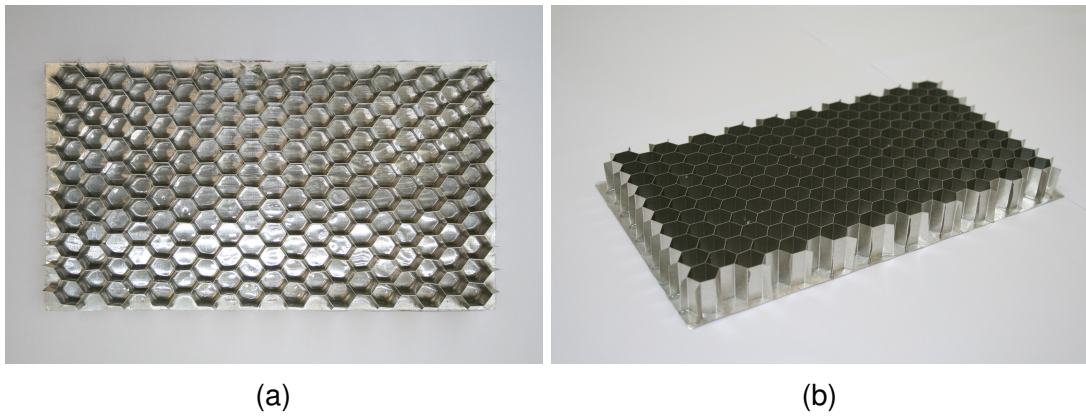


Figure 7.1: Undamped samples without upper skin shown in top (a) and isometric views (b).

125×117 mm covered about half of the surface of the plate and was bonded in the middle. This design maximises the shear strain in the CLD's viscoelastic layer for the geometry and boundary condition considered, as suggested by Chia et al. [13]. The CLD samples are shown in Figure 7.2.

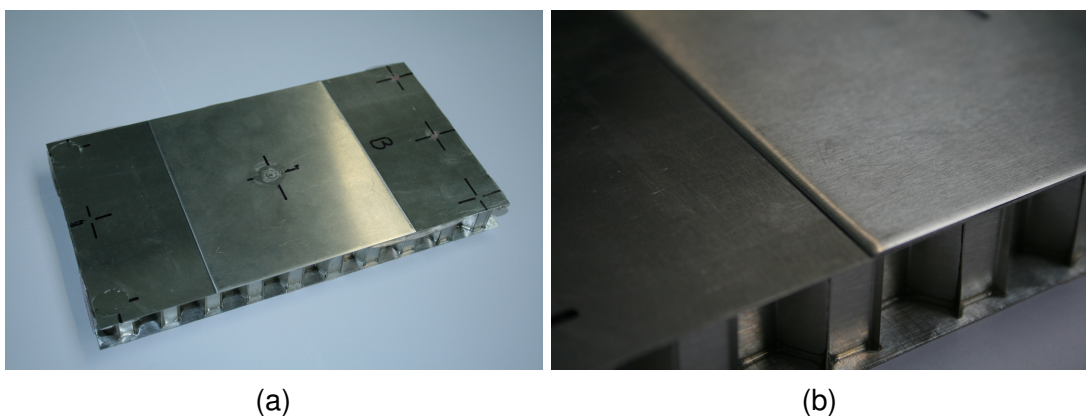


Figure 7.2: Honeycomb sandwich panel with a CLD damper (a). A close-up view of the bonding of the CLD onto the sandwich skin is shown in (b).

The DSLJ inserts were manufactured in-house by folding two 0.2mm-thick aluminium sheets into a double shear lap-joint construct, as shown in Figure 7.3. Such construct was then filled with the Dow Corning viscoelastic polymer 3-6512, which cures into a translucent gel. This 2-part silicone gel was degassed under vacuum and cured at 70 °C for two hours. The material loss factor of this polymer measured by dynamic mechanical analysis at 25 °C and 1,000 Hz is approximately 0.03. The DSLJ inserts were cut to a length of 18 mm so that contact with the skins would be prohibited once inserted in the 20mm-thick honeycomb core. These inserts were made as thin as the manufacturing constraints allow (i.e. approximately 3.5 mm thick) in order to obtain a high shear strain in the viscoelastic material. The inserts were designed to fit between two opposite vertices of a hexagonal cell, see Figure 7.4(c). The inserts were then permanently bonded to the cell vertices with cyanoacrylate glue, facilitating

CHAPTER 7. EXPERIMENTAL MODAL TESTING OF OPTIMALLY DAMPED HONEYCOMB SANDWICH PANELS

the transfer of rotation from the deformed cell rib to the DSLJ's rigid elements. The DSLJ dampers were positioned and oriented following the configuration determined in Chapter 6, which was optimised to damp the first mode of the sandwich plate under free boundary conditions, see Figure 7.4(a). The different samples manufactured are shown in Figure 7.5. The dimensions of the samples are relatively similar and can be found in Table 7.1.

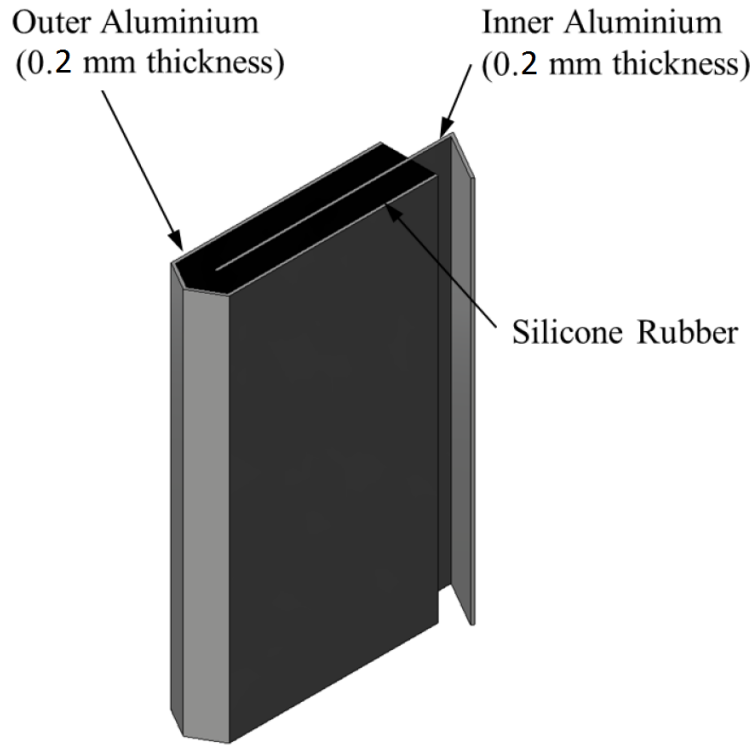


Figure 7.3: Sketch of a DSLJ damping insert for hexagonal honeycomb cells.

Structure	Length (mm)	Width (mm)	Depth (mm)
Sample a	238	131	20.3
Sample b	238	131	20.4
Sample c	237	130	20.4
Sample d	240	130	20.4
Sample e	237	131	20.5
Sample f	237	130	20.3
FE model	220	127	20.0

Table 7.1: Dimensions of the samples shown in Figure 7.5. The dimensions of the finite element model is also indicated.

7.2.2 Experimental setup

The FRF of the samples were measured by Single-Input Single-Output (SISO) modal testing, following the setup shown in Figures 7.6 and 7.7. The samples

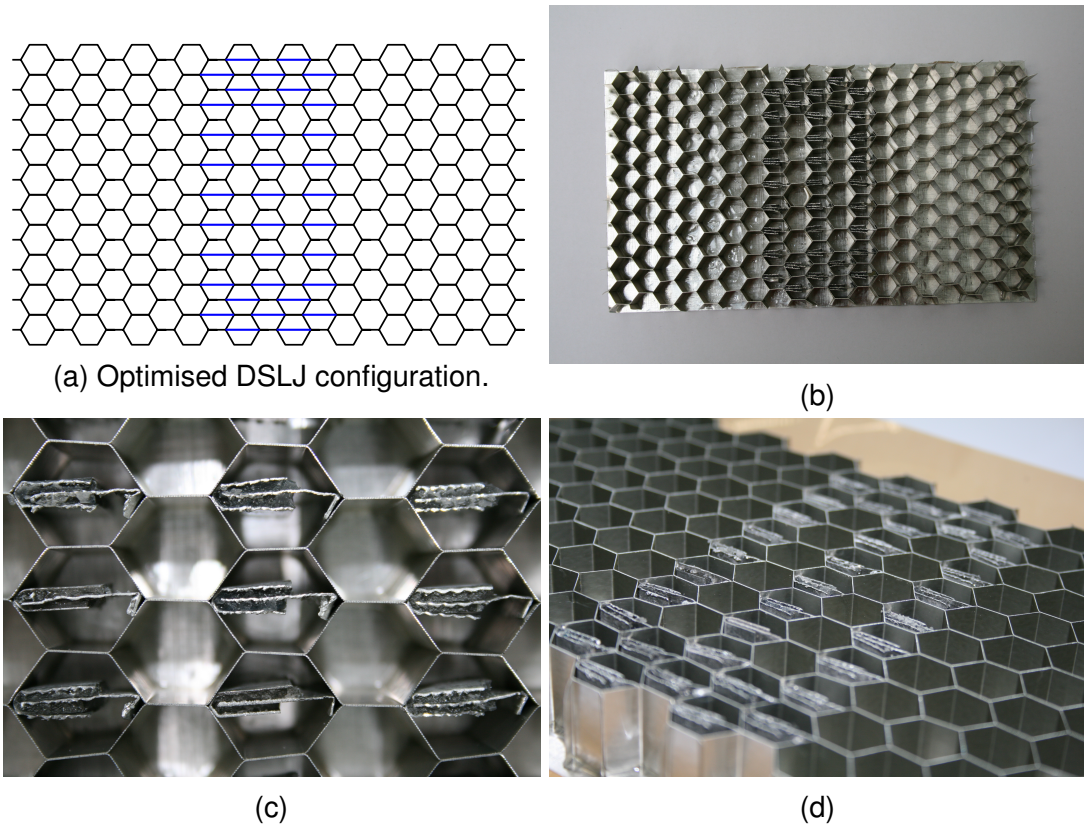


Figure 7.4: A sketch of an optimised DSLJ configuration (a) and photographs of manufactured samples (b-d) including detail of DSLJ in place (c).

were hung vertically with elastic cords to simulate free boundary conditions and isolate them from external excitations. The elastic cords were attached to a retort stand and wrapped around the samples at a distance of 4 cm from the top and bottom edges. The samples were excited with the modal electrodynamic exciter K2004E01 (The Modal Shop, Inc), which has a very light armature mass, making it ideal for exciting lightweight structures. A flexible nylon stinger was connected to the shaker and the low impedance load cell 9712B50 (Kistler) was mounted at the other end. This integrated electronic piezoelectric load cell was chosen for its high sensitivity and low mass. A mounting stud was screwed onto the load cell and stuck to the samples with cyanoacrylate glue (see Figure 7.8 (a)). The mounting stud was cleaned with acetone between each measurement in order to remove the cured adhesive and mitigate its damping effect. The out-of-plane acceleration was measured with the lightweight integrated electronic piezoelectric accelerometer 8640A50 from Kistler which was stuck onto the surface of the structure using beeswax (see Figure 7.8 (b)). Its frequency range (25 kHz) was high enough to measure the first 10 natural frequencies of the samples. The dynamic signal analyser SignalCalc ACE Quattro (Data Physics) generated a random signal to the modal exciter and it was also used as a data acquisition system and spectrum analyser for the signals generated by the load cell and accelerometer.

CHAPTER 7. EXPERIMENTAL MODAL TESTING OF OPTIMALLY DAMPED HONEYCOMB SANDWICH PANELS

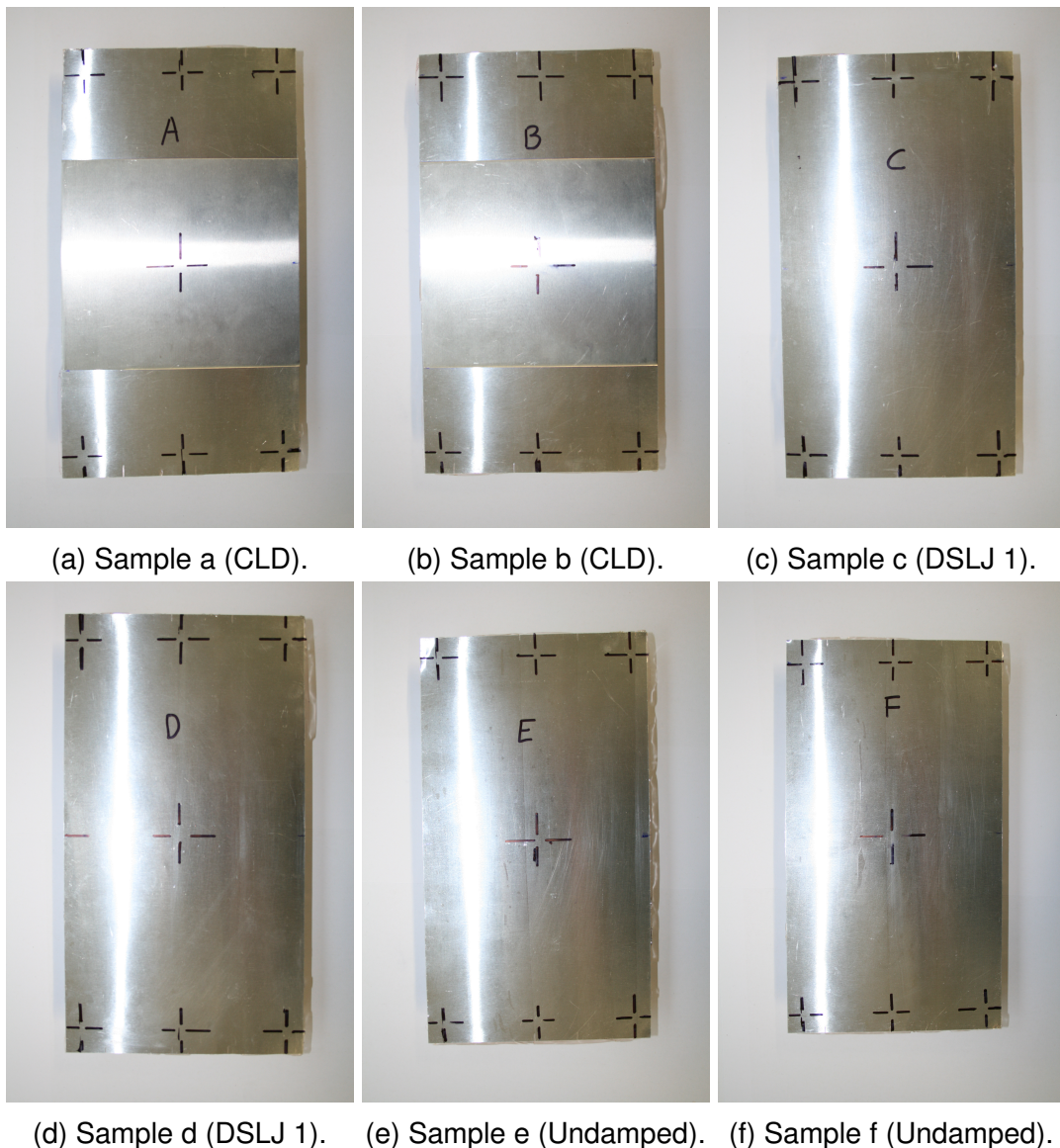


Figure 7.5: All of six of the sandwich panel samples used in testing.

It is assumed here that the first mode shape was the same as that predicted by the finite element analysis for the undamped sandwich plate under free boundary conditions, i.e. a torsional mode (see Figure 7.9). Therefore, the forcing input and acceleration output were respectively applied and measured at two opposite corners on the plate in order to capture the frequency response of the first mode. A random waveform signal of 100 mV Root Mean Square (RMS) was used to excite the structure under a frequency range of 0 to 4,000 Hz, which encompasses the first eigenfrequency. The analogue output signals of the accelerometer and load cell were respectively converted to an acceleration $x(t)$ and a force $f(t)$ using the sensitivity values provided by the manufacturer. Given that the mass of the shaker's moving armature, the load cell, the stinger and the mounting stud is 54 g, a RMS voltage of 100 mV applied to the modal exciter's amplifier generates a force of about 13 N peak-peak for a random excitation with a maximum frequency of 4,000 Hz. In the case of random

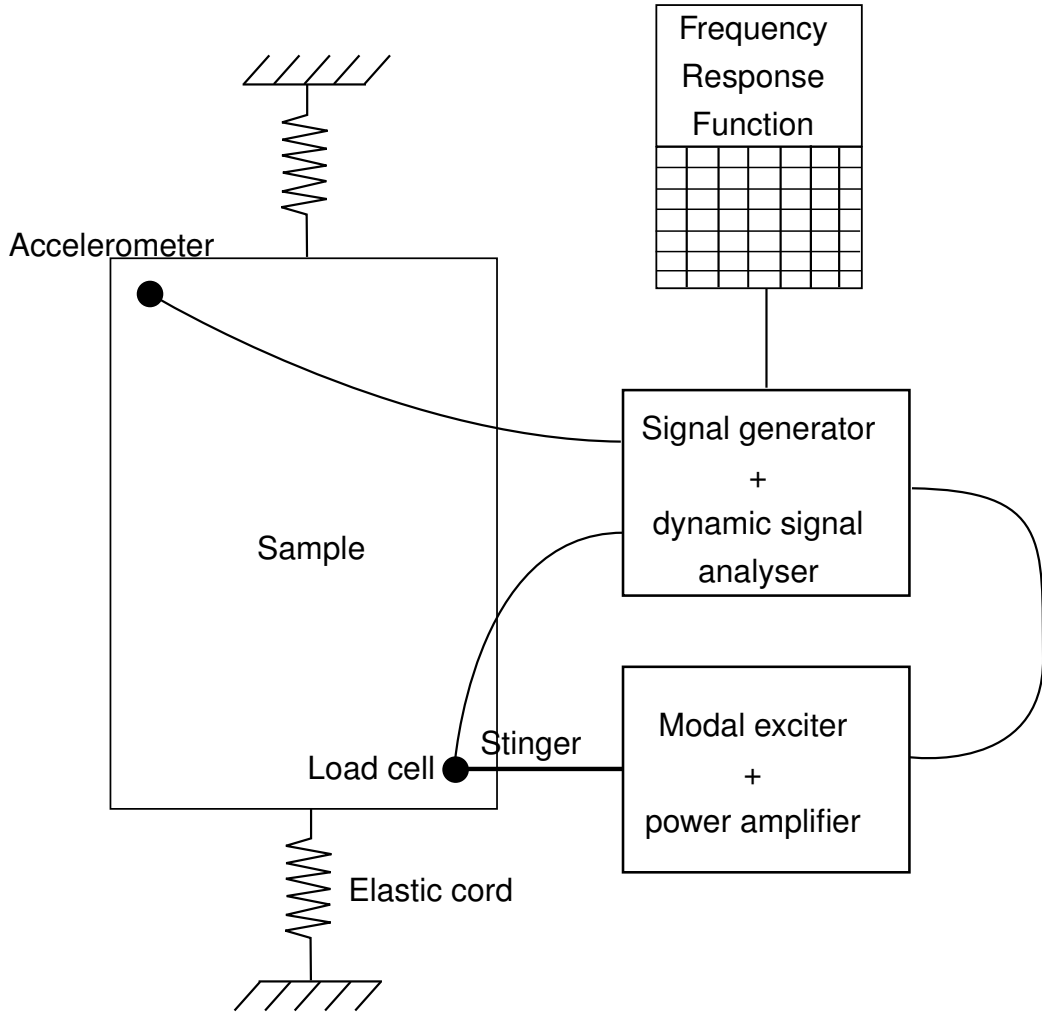


Figure 7.6: Sketch of the modal testing setup. The sample is excited with a random waveform excitation and the FRF is computed from the input force and output acceleration signals.

excitation, the autocorrelation and cross correlation functions give a measure of the similarity between two signals in the time domain. They can be calculated as follows,

$$R_{ff}(\tau) = \lim_{T \rightarrow +\infty} \frac{1}{T} \int_{-T/2}^{T/2} f(t)f(t+\tau) d\tau$$

$$R_{xf}(\tau) = \lim_{T \rightarrow +\infty} \frac{1}{T} \int_{-T/2}^{T/2} x(t)f(t+\tau) d\tau \quad (7.1)$$

The power spectral densities and cross spectral densities are the Fourier transforms of the autocorrelation and cross correlation functions, respectively:

$$S_{ff}(\omega) = \frac{1}{2\pi} \int_{-\infty}^{+\infty} R_{ff}(\tau) e^{-i\omega\tau} d\tau$$

$$S_{xf}(\omega) = \frac{1}{2\pi} \int_{-\infty}^{+\infty} R_{xf}(\tau) e^{-i\omega\tau} d\tau \quad (7.2)$$

CHAPTER 7. EXPERIMENTAL MODAL TESTING OF OPTIMALLY DAMPED HONEYCOMB SANDWICH PANELS

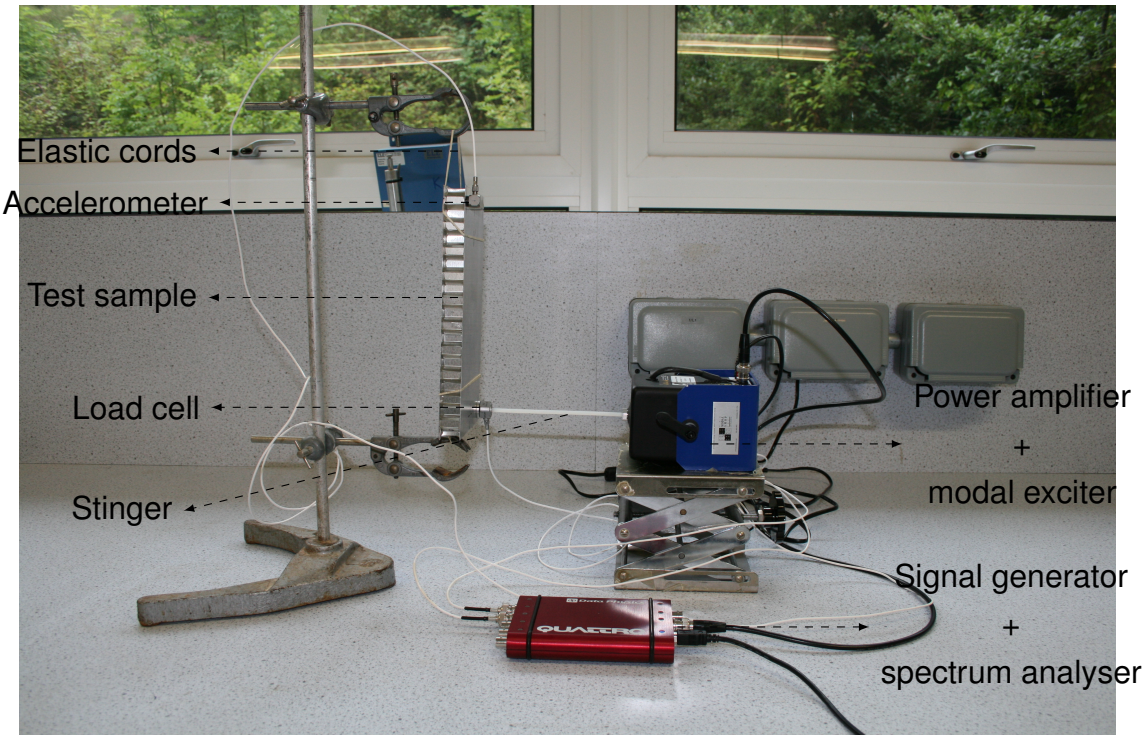


Figure 7.7: Modal testing setup of a honeycomb sandwich panel.



Figure 7.8: Sample free supports using elastic cords and transducers attachments. The load cell is connected to the exciter via a nylon stinger and attached to the sample with a mounting stud (a). The accelerometer is stuck onto the sandwich skin with beeswax (b).

Two accelerances (FRF computed from an acceleration input) can be estimated from the power and cross spectral densities as follows,

$$A_1(\omega) = \frac{S_{fx}(\omega)}{S_{ff}(\omega)}$$

$$A_2(\omega) = \frac{S_{xx}(\omega)}{S_{xf}(\omega)} \quad (7.3)$$

These FRFs are two estimates of the same quantity. It is possible to define a

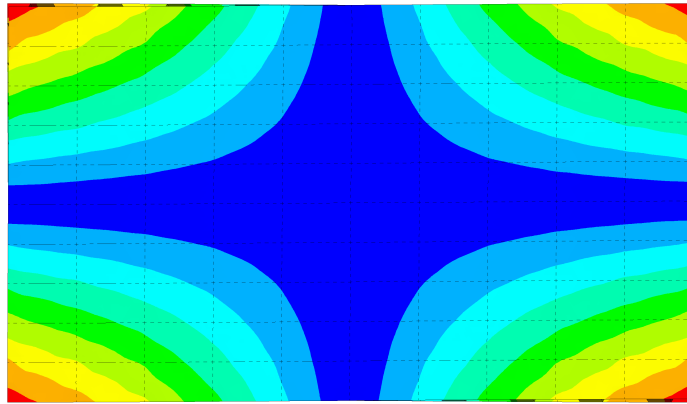


Figure 7.9: First mode shape (at 1346 Hz) of the undamped sandwich plate with honeycomb core under free boundary conditions predicted by the finite element model. The colours indicate the displacement, with blue being the lowest and red the highest.

coherence function as the ratio of these FRFs:

$$\Gamma^2 = \frac{A_1(\omega)}{A_2(\omega)} \quad (7.4)$$

The coherence function gives a measure of the noise present in the signals and should ideally be equal to unity. The *receptance* (ratio of the output displacement to the input force signals in the frequency domain) can be calculated by integrating the accelerance twice in the frequency domain:

$$H(\omega) = \frac{A(\omega)}{-\omega^2} \quad (7.5)$$

The modulus and argument of the complex receptance correspond to the amplitude response and phase angle of the FRF. The amplitude response, phase angle and coherence function were calculated in the frequency domain with 25,600 data points. In order to reduce the noise and obtain a better quality data, 30 stable measurements were taken successively and averaged. An overlap of 50% was applied between each frame. A Hanning window was imposed on the time signal prior to applying the Fourier transform in order to minimise the effect of leakage, as advised by Ewins [24] for continuous random excitation. The free run trigger was used to acquire data continuously. The first modal loss factor was computed from the first peak using the half-power bandwidth method, as described in Chapter 2 Equation 2.36. The damping

CHAPTER 7. EXPERIMENTAL MODAL TESTING OF OPTIMALLY DAMPED HONEYCOMB SANDWICH PANELS

efficiencies Ef_1 was computed as follows,

$$Ef_1 = \frac{\eta_1^2}{m} \quad (7.6)$$

where η_1 and m are the first modal loss factor and the mass of the sample, respectively.

7.2.3 Finite element model

The finite element model of the honeycomb sandwich plate damped with CLDs or DSLJ dampers was described in Chapter 3. The model parameters were adapted here to match the material properties and dimensions of the samples manufactured. Specifically,

- The thickness of the plate was increased from 10 mm to 20 mm.
- The honeycomb wall thickness was changed from 0.2 mm to 0.1 mm.
- The cell ribs length was reduced from 10 mm to 7.5 mm.
- The CLD viscoelastic layer and constrained layer thicknesses were set to 0.05 mm and 0.5 mm, respectively.
- The DSLJ insert thickness was increased from 0.25 mm to 3.5 mm, which was the thinnest design possible given the manufacturing constraints.
- The input force was set to 13 N.

7.3 Results

The receptances of the damped and undamped samples are compared in this section. A typical receptance measurement comprising the amplitude, phase angle and coherence function is illustrated in Figure 7.10. A mode can be identified by a peak in amplitude or a change in phase angle from 0 to -180°. The coherence function is close to unity across the frequency range of interest, showing that a reliable estimate of the receptance has been measured.

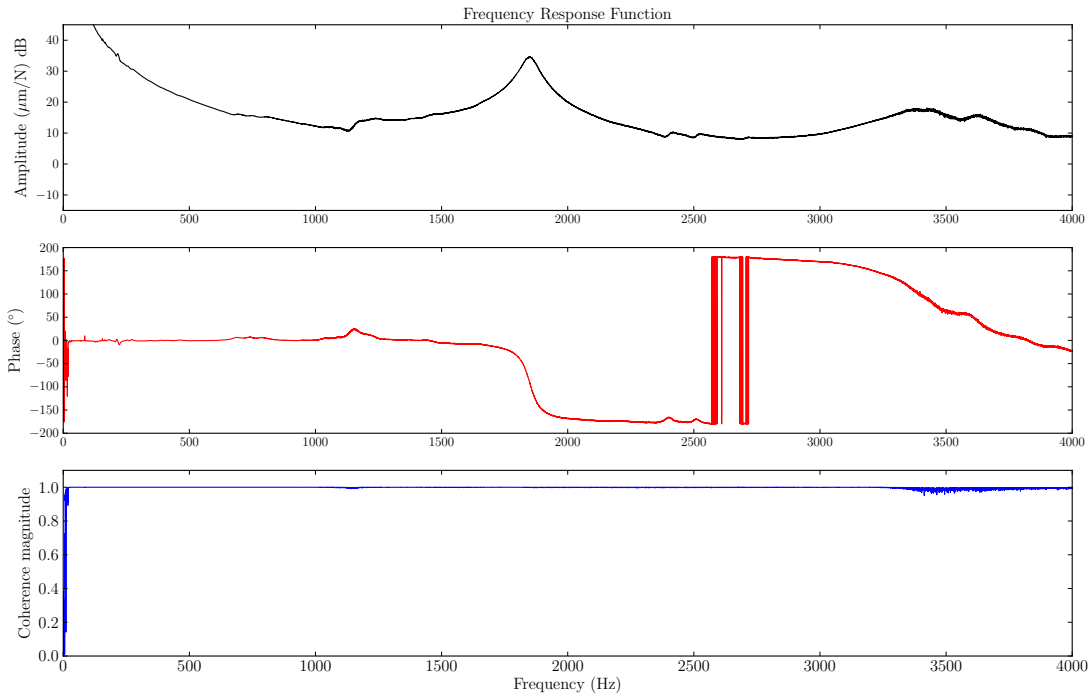


Figure 7.10: Amplitude, phase and coherence function of a modal test.

7.3.1 Repeatability of the tests

Inaccuracies in measurement can arise from two sources, either from the testing itself or from the manufacture of the samples. For instance, inaccuracies in testing can arise if the transducers are positioned at a slightly different location between two measures. A faulty manufacturing procedure can also alter the intrinsic mass, stiffness and damping of the structure upon which its dynamic properties heavily depend. In order to quantify the inaccuracies caused by the testing, 20 consecutive FRF measures of the same sample were taken and the transducers were detached then reconnected to the structure at the same location between the measures. The resulting FRF values were then averaged and the standard deviation was calculated, see Figure 7.11. The similar amplitude responses obtained after the 20 tests suggests that the testing procedure is reliable and repeatable.

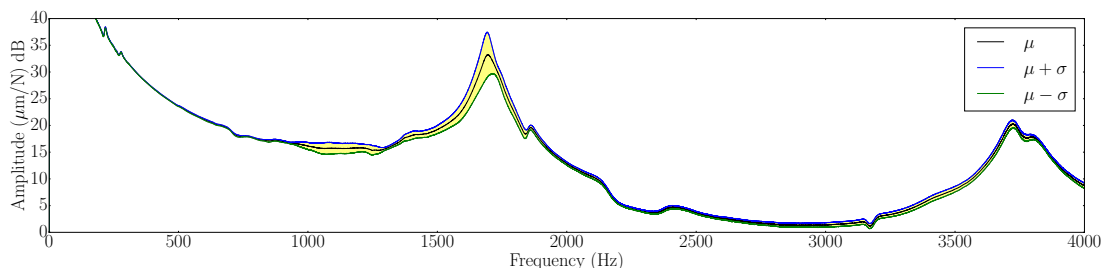


Figure 7.11: Average and standard deviation of the amplitude response obtained after 20 successive modal tests.

7.3.2 Repeatability of the samples

In an effort to quantify the structural imperfection of the samples, two identical samples – one pair for each damping treatment (DSLJ, CLD and undamped) – were manufactured and tested. As the samples are symmetrical with respect to the median plane, the FRFs were measured by sticking the transducers on both faces of each sample, which allowed two measures to be obtained for a single structure. The samples tested on the rear face are denoted with an apostrophe. The amplitude response is shown in Figures 7.12 to 7.14. Although there is some variability in amplitude response between each manufactured sample, it is possible to identify clearly the peak corresponding to the first mode at around 1700 Hz.

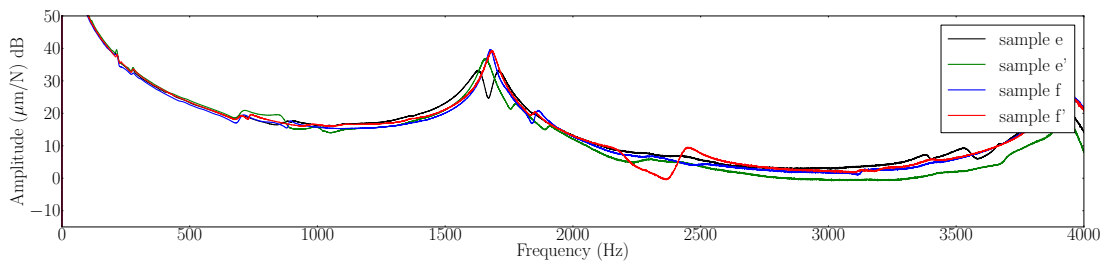


Figure 7.12: Amplitude response of the four undamped samples.

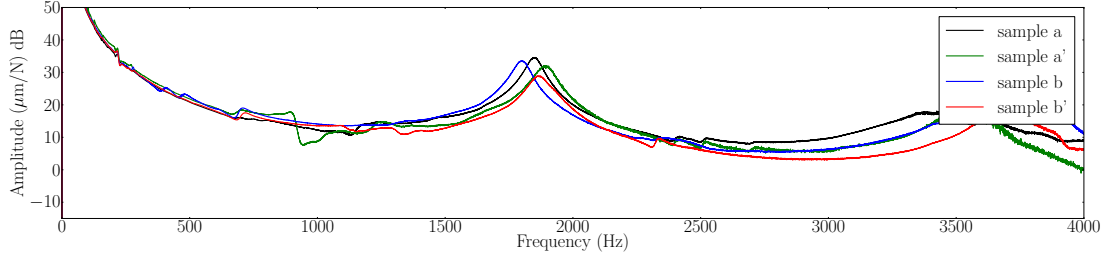


Figure 7.13: Amplitude response of the four CLD samples.

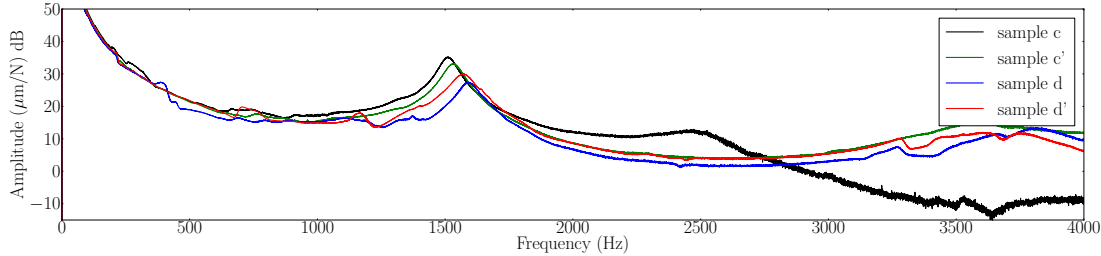


Figure 7.14: Amplitude response of the four DSLJ samples.

7.3.3 Amplitude response comparison

The amplitude response of all the samples focused around the first natural frequency is shown in Figure 7.15(a). As expected, the peak amplitude of

the undamped samples is higher than that of the damped samples. A similar behaviour can be noticed from the finite element predictions, although the difference between damped and undamped are much more marked. The finite element model also overestimates the amplitude response and underestimates the natural frequency.

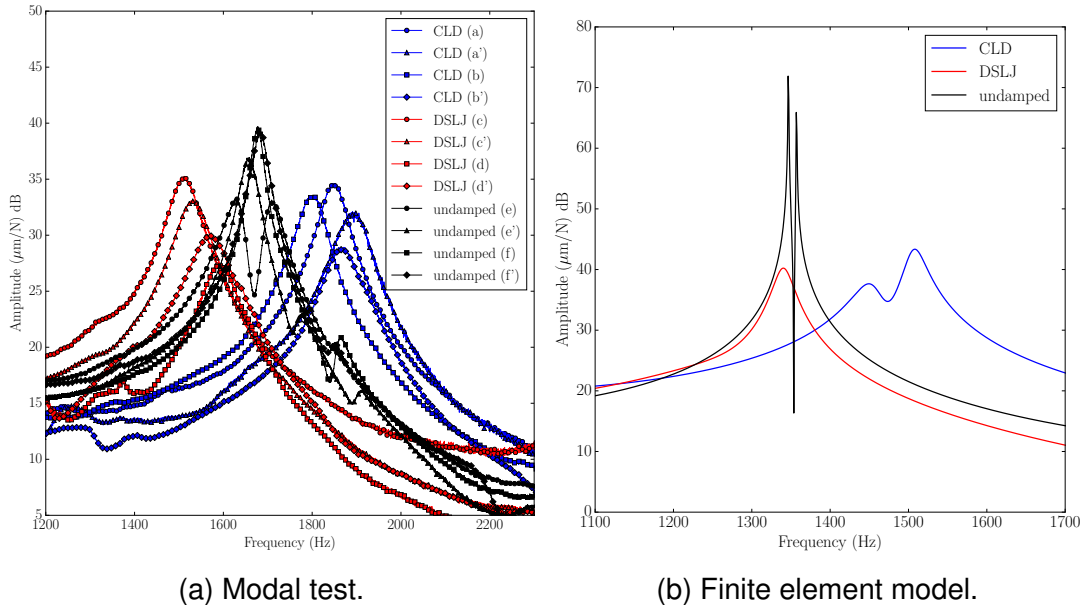


Figure 7.15: Amplitude response of the samples with CLD (blue), DSLJ (red) and undamped (black) treatments measured experimentally (a) and predicted numerically by finite element analysis (b).

7.3.4 Damping efficiency comparison

The mass, natural frequencies, modal loss factors and damping efficiencies of all the samples are given in Table 7.2. For ease of interpretation, their average values – along with the numerical predictions from the finite element model – are given in Table 7.3. These average values are normalised to that of the undamped structures and shown in Table 7.4. The modal loss factor increases substantially with the addition of either the CLD or the DSLJ inserts, see Table 7.4. It is higher for the samples damped with the DSLJ dampers, reaching a 111% increase from the undamped samples on average. Similar trends were predicted by the finite element model, although the absolute modal loss factor values were much higher than those measured experimentally. Both the CLD and DSLJ dampers show appreciable performance in terms of damping efficiency, both experimentally and numerically. Both damping solutions add approximately 27% mass to the structure, the CLD being slightly heavier than the DSLJ damping treatment. The CLD tends to shift the natural frequency upwards – the stiffening effect of the damper having more influence on the mode

CHAPTER 7. EXPERIMENTAL MODAL TESTING OF OPTIMALLY DAMPED HONEYCOMB SANDWICH PANELS

frequency than the increase in mass. On the contrary, the DSLJ treatment tends to lower the natural frequency.

sample	damping	mass (g)	f_1 (Hz)	$\eta_1 (\times 10^{-3})$	Ef_1 (g^{-1})
a	CLD	105.8	1852.0	33.1	10.3
a'	CLD	105.8	1890.9	39.6	14.8
b	CLD	107.8	1801.0	36.8	12.5
b'	CLD	107.8	1871.3	42.8	17.0
c	DSLJ	106.3	1511.6	43.4	17.7
c'	DSLJ	106.3	1529.2	49.0	22.6
d	DSLJ	104.9	1586.2	49.5	23.4
d'	DSLJ	104.9	1570.5	58.2	32.3
e	undamped	83.6	1629.5	31.3	11.7
e'	undamped	83.6	1657.8	25.3	7.7
f	undamped	83.4	1677.9	16.6	3.3
f'	undamped	83.4	1687.1	21.4	5.5

Table 7.2: Mass, natural frequencies, modal loss factors and damping efficiencies of the samples.

method	damping	mass (g)	f_1 (Hz)	$\eta_1 (\times 10^{-3})$	Ef_1 (g^{-1})
experiment	undamped	83.5	1663.1	23.7	7.05
experiment	CLD	106.8	1853.8	38.1	13.7
experiment	DSLJ	105.6	1549.4	50.1	24.0
Finite element	undamped	58.1	1346.4	1.19	0.02
Finite element	CLD	73.5	1508.0	18.6	4.69
Finite element	DSLJ	66.1	1340.0	19.7	5.87

Table 7.3: The mass, natural frequencies, modal loss factors and damping efficiencies of the samples measured experimentally and averaged are compared to the values predicted by finite element analysis.

method	damping	mass	f_1	η_1	Eff_1
experiment	undamped	1.00	1.00	1.00	1.00
experiment	CLD	1.28	1.11	1.61	1.94
experiment	DSLJ	1.26	0.93	2.11	3.40
Finite element	undamped	1.00	1.00	1.00	1.00
Finite element	CLD	1.27	1.12	15.6	234
Finite element	DSLJ	1.14	0.99	16.5	293

Table 7.4: The average values of the mass, natural frequencies, modal loss factors and damping efficiencies of the samples are shown normalised to that of the undamped configuration.

7.4 Discussion

In this chapter, it is shown experimentally that the CLD and DSLJ dampers are both weight-efficient damping solutions for the particular honeycomb-cored sandwich plate considered. Indeed, the damping efficiency measured in the damped structures is marginally higher than that of the undamped structures, see Table 7.4. This confirms the predictions computed from the numerical finite element model. However, discrepancy in damping between the damped and undamped structures is higher in the finite element model than in the experiments, see Figure 7.15. This is likely due to manufacturing imperfections in the physical samples that were not accounted for in the finite element model. These manufacturing imperfections introduce additional structural damping, notably in the undamped samples. In particular, structural damping may arise at unadhered metal-metal contacts between the sandwich skins and the core and between the corrugated strips forming the honeycomb cell [8]. The relative displacements in the various joints of the samples dissipate vibrational energy by friction whereas the finite element model assumed perfect bonding in the structure. Additional energy dissipation may also be introduced from the inherent material damping in the epoxy adhesive used to bond the skin to the core.

The finite element model also underestimates the natural frequency, see Table 7.3. The reason for this is that the sample's modal mass and modal stiffness are influenced by physical details that were ignored in the numerical model. For instance, the honeycomb core was made by expansion process from stacked aluminium sheets, resulting in doubling the thickness of 1 out of 6 walls of each hexagonal cell, thus stiffening the structure. The epoxy layer also accounts for extra mass (15.3 g) and stiffness in each manufactured samples. However, similar trends in the evolution of the natural frequency can be noticed between the experimental measurements and the numerical predictions, i.e. the

CHAPTER 7. EXPERIMENTAL MODAL TESTING OF OPTIMALLY DAMPED HONEYCOMB SANDWICH PANELS

DSLJ dampers tend to shift the first modal frequency downwards whereas the CLD pushes it upwards, see Table 7.4. This may be problematical for systems subjected to external excitations at a specific forcing frequency, for example in transport. If a damping treatment alters the modal frequency of a structure such that it coincides with the forcing frequency, the system may enter into resonance, which may cause severe structural damage.

It should be pointed out that the finite element model used in this thesis was not aimed at describing the frequency response of the systems considered here with accuracy, nor to provide a precise and absolute estimate of the modal loss factors, but only to compare damping values between two structures in different damping configurations. Therefore, it was not deemed worthwhile adding complexity to the model, for instance by modelling the structural damping arising from manufacturing defects.

Experimental errors can arise either from the testing procedure or from the manufacture of the samples and both of these sources of errors were quantified here by carrying out repeatability tests. As can be seen in Figure 7.11, 20 consecutive tests yielded a very similar amplitude response, showing that the bonding of the accelerometer and the force transducer onto the sample can be repeated accurately. The testing accuracy may have been improved further by using non-contact measurement techniques. This would have avoided mass loading caused by the bonding of the load cell and accelerometer to the samples, thus preventing the structure's intrinsic dynamic properties from being altered. An example of non-contact measurement techniques consists in using a laser Doppler vibrometer to measure the velocity at the surface of the vibrating structure, replacing the role of the accelerometer [312]. The modal exciter may also be replaced by an impact hammer or even a non-contact magnetic exciter such as an Eddy current actuator in order to mitigate the effect of the mass added by the load cell and the shaker's armature. Finally, a Hanning window was applied to the transducer's signal to attenuate the influence of leakage. It should be noted that, although sometimes necessary, the use of windows distorts the amplitude measured and tends to attenuate the peak amplitude, thereby giving an impression of higher damping than is actually present in the structure [24].

The greatest variabilities in the measurements are mainly due to the variation introduced by the manufacturing process. Indeed, two supposedly identical samples presented a moderately different amplitude response, see Figure 7.12 to 7.14. For future experiments, the author recommends automatising the manufacturing process – in particular that of the DSLJ inserts – in order to minimise such variations. For example, the structure could have been made by additive layer manufacturing, which would have greatly improved the design

and therefore the reliability of the tests. This would also have eliminated the relative displacements between the various assembled parts of the samples, thereby diminishing the additional structural damping introduced artificially in the structures. Besides, measuring the vibration response of small and lightweight samples is delicate, thus designing larger samples would allow greater out-of-plane displacements, which would improve the quality of the measurements. Finally, it is also possible that the DSLJ inserts introduced nonlinearities in the structure, noticeable from the noisier signal in the DSLJ sample's FRF. The nonlinear vibration response of the DSLJ dampers could be an interesting phenomenon to research further.

7.5 Conclusion

In this chapter the modal testing of honeycomb-cored sandwich plates with CLD, DSLJ inserts or no damper was carried out. It was established that the DSLJ damper is capable of providing high passive damping to a structure for a minimal increase in mass. The DSLJ dampers were shown to be a competitive passive damping solution to the CLD in terms of damping per unit mass. This confirms the global trends predicted by the numerical finite element model.

The present finite element model was not intended to describe the dynamical properties of experimental samples with accuracy, but rather to compare damping performance between damped and undamped structures. Here, the numerical model and the modal tests showed a satisfactory correlation in the evolution of the modal loss factor and the natural frequency between the different damping configurations considered.

CHAPTER 7. EXPERIMENTAL MODAL TESTING OF OPTIMALLY DAMPED
HONEYCOMB SANDWICH PANELS

Chapter 8

Conclusion

8.1 General discussion

The work undertaken in this thesis investigated the performance of a novel passive damping treatment, namely the Double Shear Lap-Joint damper (DSLJ), when deployed in structures such as lightweight honeycomb-cored sandwich panels. Attention was focused on methods for identification of configurations which produce the highest achievable damping for the least addition of mass into the structure.

The advantage of the DSLJ damper lies in its high weight efficiency, utilising a minimal amount of material while producing significant passive damping, see Chapter 4 Table 4.3. This advantage arises from the innovative damping mechanism introduced by its double lap-joint design which is used to amplify the shear strain in a lossy polymer. Similarly to traditional dampers such as the Constrained Layer Damper (CLD), the DSLJ damper converts deformation in the host structure into relative displacement of the stiff elements of the damper, which in turn generates shear strain in a damping polymer connecting those stiff elements. Vibrational motion of the host structure is used to drive relative rotation of the stiff elements, as opposed to relative translations as is the case for CLDs, see Figures 3.10 and 3.8.

Another benefit of the DSLJ over traditional damping device such as the CLD is that it may be inserted inside internal holes of the host structure, resulting in being more space efficient than external dampers. Deploying dampers externally may also not always be possible, for instance in parts that require accurate control of a fluid flow such as a fan blade or a helicopter blade. Additionally, the DSLJ insert has a discrete direction and distribution set at manufacture, which both allows and requires that it be finely tuned to target specific vibration modes by orienting it in different directions. On the contrary, CLDs produce identical damping responses in all directions of the surface onto which it is bonded.

The modelling approach used herein has been shown to be sufficiently

accurate. Evidence presented in Chapter 3 shows that the models were derived correctly, for instance similar modal loss factors, mode shapes and natural frequencies were obtained both numerically and analytically. Similar verification tests have been carried out by other researchers on their models, see for example [83]. The amplitude responses of sandwich panels damped with DSLJ dampers and CLDs were also compared against experimental data, see Chapter 7. Satisfactory agreement in the evolution of modal loss factors before and adding the dampers was observed between the experimental measurements and the numerical predictions, showing the pertinence of the finite element model. The apparent differences in absolute modal loss factor between simulations and experiments are likely due to manufacturing imperfections which introduced additional structural damping and to the epoxy layer, which was not modelled numerically. It is also commonly accepted that numerical models tend to underestimate the modal loss factors in damped structures, especially when using the modal strain energy method [173, 286]. Commercially available honeycomb sandwich panel systems manufactured for use in aerospace applications are made to much higher specifications than those in this work. CLDs are used in such commercial systems because they provide significant damping enhancement. The DSLJ if similarly deployed in commercial systems would likely demonstrate significant benefits, much more so than is apparent in the experimental data which is dominated by the structural damping of the imperfect honeycomb panels.

The premise of the work in this thesis was that the DSLJ damper could be made more weight-efficient than existing alternatives such as the CLD. Optimised DSLJ configurations were shown to be competitive and very often better than published optimised CLD configurations in terms of additional weight required to achieving a given damping effect, see Chapter 4 Table 4.3. The higher efficiency of the DSLJ damper vs the CLD was also shown experimentally, see Chapter 7 Table 7.4. The reason for this is that the DSLJ exploits the damping material more effectively than the CLD does, constraining the viscoelastic material to higher shear strains for a given thickness of the viscoelastic layer, see Chapter 3 Figures 3.15 and 3.16. In essence the DSLJ, or indeed a single lap joint version of this, has both rigid elements at the boundary of the damping material to displace under global vibration, whereas the CLD configuration has only one rigid element displacing.

One of the main characteristics of the DSLJ damper is that it is a discrete damper whose damping response changes depending on its orientation in the host structure. Consequently, an evident question to investigate was to identify the optimal location and orientation of such dampers in the host structure which produces the highest damping-to-mass ratio. In this problem the decision

parameters (i.e. the location and orientation of the dampers) are coupled with the quality measures of the optimiser (i.e. mass and modal loss factor). If not accounted for, such coupling may have detrimental effects on the performance of the optimisation technique adopted. Therefore, a decision must be made whether to use a simple and quick approach but one prone to errors arising from veering or a more sophisticated and robust but computationally demanding evolutionary optimiser (see Chapters 5 and 6). Other works in the literature have optimised the design of passive damper using parametric methods but have also neglected the effects of mode veering [89, 179]. Optimisation problems where decision parameters are coupled with the objective functions to be minimised include any topological optimisation problems where the structural properties of the system – especially its strength, stiffness and mass – are directly dependant on the decision to remove or not a given part of material in the structure. These structural properties must be dynamically updated during the optimisation process. The particular damping device used here is quite new, but the distributions of dampers identified and the suitability of the optimisation approaches (i.e parametric studies and evolutionary algorithms) may well be generic to any passive or even active discrete damper, such as pairs of piezoelectric actuators and sensors.

There is a move across the entire transport sector towards lightweighting, driven mainly by customer and legislative pressure for fuel efficiency. A solution put forward by the transport sector – and especially the aerospace industry – has been to use composites and in some cases honeycomb cored composite skinned sandwich panels. However, these industrial sectors are expected to face increasing problems associated with structural vibrations in such lightweight slender and stiff structures. Optimisation methods such as the ones used herein may find use in identifying compromise solutions for such problems.

8.2 Recommendations for future work

Although the finite element model in Chapter 3 and onwards did not aim at providing precise estimate of the dynamic properties of the structures considered, it could be refined in order to represent the damping behaviour of the structures with more fidelity. Such refinements would include modelling epoxy layers, delaminations during manufacture, metal-metal frictional contacts, and the double thickness of the honeycomb walls. More sophisticated techniques to estimate the modal loss factor could also be employed, such as the anelastic displacement fields, the iterative modal strain energy method or the Golla-Hugues-McTavish model [313]. The modal strain energy method used here is computationally simple but may be inaccurate, especially for highly damped

structures. It also does not include the temperature and frequency dependence of viscoelastic materials. However for comparative purposes, such as those in this work, this method yields satisfactory results.

Enhancements for CLD dampers have been suggested (see literature review in Chapter 2). Similarly, the design of the DSLJ could be modified to magnify shear in the viscoelastic material. For instance, the damping performance of triple or quadruple lap joint constructs could be investigated. The DSLJ concept could also be adapted to other structures where relative motion of two or more parts occurs, for instance by constraining viscoelastic material between two concentric cylinders rotating in out-of-phase fashion. A combined DSLJ-CLD – consisting of a cellular solid filled with DSLJ damper that can be bonded on the surface of a vibrating host structure – could be considered but it would face severe cost penalty compared to a traditional CLD. Additionally, it could be interesting to use active elements such as piezoceramics or electro or magnetostrictive materials in order to magnify the shear strain in the viscoelastic material i.e. a hybrid DSLJ damper.

The performance of other heuristic set-based optimisation algorithms for tackling this problem could also be investigated further. Examples of such algorithms include the Strength Pareto Evolutionary Algorithm-II (SPEA-II), the Pareto Archived Evolutionary Strategy (PAES), Non-dominated Sorting Genetic Algorithm-II (NSGA-II) and cellular automaton. The manufacturing process of the sandwich panels and the DSLJ damper should be automated in order to limit the imperfections in the structures, thereby diminishing the effect of the structural damping introduced by such imperfections. Using additive layer manufacturing could help mitigating the relative motion at the interface of loosely assembled parts, generating artificial extra structural damping. Non-contact measurement techniques such as using a scanning laser vibrometer or other full-field measurement techniques could also enhance the quality of the measurements. Finally, alternative excitation methods could attenuate the effect of mass loading caused by the bonding of a load cell onto the structure, for instance using an impulse hammer or non-contact magnetic exciters such as Eddy current actuators.

Appendix A

Modal Strain Energy method

The Modal Strain Energy (MSE) method described by Johnson and Kienholtz [28] is used to estimate the modal loss factor of a viscoelastically damped system. This method assumes that the energy dissipated in a damped system depends only on the strain energy of the undamped system. Such system is characterised by a complex stiffness matrix, eigenvalues and eigenvectors and the Rayleigh quotient 2.12 can be generalised in complex:

$$\lambda_k^* = \frac{\{\Phi_k^*\}^T [\mathbf{K}^*] \{\Phi_k^*\}}{\{\Phi_k^*\}^T [\mathbf{M}] \{\Phi_k^*\}} \quad (\text{A.1})$$

where

$$\begin{aligned} [\mathbf{K}^*] &= [\mathbf{K}^R] + j[\mathbf{K}^I] \\ \{\Phi_k^*\} &= \{\Phi_k^R\} + j\{\Phi_k^I\} \\ \lambda_k^* &= \lambda_k^R + j\lambda_k^I \end{aligned} \quad (\text{A.2})$$

The MSE method assumes that the eigenvector is approximately represented by its real part, i.e. $\{\Phi_k^*\} \simeq \{\Phi_k^R\}$. The modal loss factor of mode k is defined as $\eta_k = \frac{\lambda_k^I}{\lambda_k^R}$. Substituting Equation A.1 into A.2 yields:

$$\lambda_k^R(1 + j\eta_k) \simeq \frac{\{\Phi_k^R\}^T [\mathbf{K}^R] \{\Phi_k^R\}}{\{\Phi_k^R\}^T [\mathbf{M}] \{\Phi_k^R\}} + j \frac{\{\Phi_k^R\}^T [\mathbf{K}^I] \{\Phi_k^R\}}{\{\Phi_k^R\}^T [\mathbf{M}] \{\Phi_k^R\}} \quad (\text{A.3})$$

Equating the real and imaginary parts of both sides of this equations gives:

$$\begin{aligned} \lambda_k^R &= \frac{\{\Phi_k^R\}^T [\mathbf{K}^R] \{\Phi_k^R\}}{\{\Phi_k^R\}^T [\mathbf{M}] \{\Phi_k^R\}} \\ \lambda_k^R \eta_k &= \frac{\{\Phi_k^R\}^T [\mathbf{K}^I] \{\Phi_k^R\}}{\{\Phi_k^R\}^T [\mathbf{M}] \{\Phi_k^R\}} \end{aligned} \quad (\text{A.4})$$

APPENDIX A. MODAL STRAIN ENERGY METHOD

This can be expressed as:

$$\eta_k = \frac{\{\Phi_k^R\}^T [\mathbf{K}^I] \{\Phi_k^R\}}{\{\Phi_k^R\}^T [\mathbf{K}^R] \{\Phi_k^R\}} \quad (\text{A.5})$$

The damped systems considered in this thesis are constituted of elastic and viscoelastic materials characterised by different material loss factors. The contribution of each material can be isolated by separating the stiffness matrix in terms its real elastic and complex viscoelastic part: $[\mathbf{K}] = [\mathbf{K}_e] + [\mathbf{K}_v^*]$. The complex viscoelastic stiffness matrix can be expressed as: $[\mathbf{K}_v^*] = [\mathbf{K}_v^R] + j[\mathbf{K}_v^I]$. Since only the imaginary part of $[\mathbf{K}_v^*]$ contributes to the imaginary part of the global stiffness matrix, $[\mathbf{K}_v^I] = [\mathbf{K}_v^I]$. If m is the number of different materials in the structure, $[\mathbf{K}_v^I]$ and $[\mathbf{K}_v^R]$ can be expressed as follows:

$$[\mathbf{K}_v^I] = \sum_{i=1}^m \eta_{i,k} [\mathbf{K}_{v,i}^R] \quad (\text{A.6})$$

$$[\mathbf{K}_v^R] = \sum_{i=1}^m [\mathbf{K}_i^R] \quad (\text{A.7})$$

where $\eta_{i,k}$ is the material loss factor of material i in mode k . Substituting this expression in equation A.5 gives,

$$\eta_k = \frac{\sum_{i=1}^m \eta_{i,k} \{\Phi_k^R\}^T [\mathbf{K}_{v,i}^R] \{\Phi_k^R\}}{\sum_{i=1}^m \{\Phi_k^R\}^T [\mathbf{K}_i^R] \{\Phi_k^R\}} \quad (\text{A.8})$$

The modal strain energy of material i in mode k is defined as $U_{i,k} = \frac{1}{2} \{\Phi_k^R\}^T [\mathbf{K}_{i,k}] \{\Phi_k^R\}$. Substituting this expression in the previous equation yields:

$$\eta_k = \frac{\sum_{i=1}^m \eta_{i,k} U_{i,k}}{U_{tot}} \quad (\text{A.9})$$

where U_{tot} is the strain energy in the whole structure.

Appendix B

Finite element model

The finite element model of the honeycomb-cored sandwich structure with DSLJ inserts described in Chapter 3 was implemented using ANSYS Parametric Design Language (APDL):

```
*****  
! Ansys APDL macro "honeycomb_sandwich.mac": free and forced vibration response  
! of a honeycomb-cored sandwich structure damped with optimised configurations  
! DSLJ dampers  
! arg1 = string describing the boundary condition ('FREE', 'CFFF', 'SSSS')  
! arg2 = string describing the damping configuration ('dslj1', 'dslj2',  
! 'cld', 'none')  
! arg3 = string describing the orientation ('orient1', 'orient2')  
! arg4 = string describing the location of the forced excitation ('middle',  
! 'corner')  
! arg5 = string describing the location of the output displacement ('tip',  
! 'corner', 'corner2')  
! This macro may be called using the following command:  
! *use,ansys_macro.mac,arg1,arg2,arg3,arg4,arg5  
*****  
  
FINISH  
/CLEAR,start  
/NERR,,1000000  
  
! File parameters  
*****  
  
BC = arg1  
damping = arg2  
orientation = arg3  
excite = arg4  
measure = arg5  
name = '%BC%_%damping%_%excite%_%measure%'  
/FILENAME, name  
  
! Honeycomb cell geometry parameters  
*****  
  
PI = acos(-1)  
l = 0.01  
h = 0.01  
t = 0.0002  
theta = 30  
  
x1al = h/2+l*sin(theta*PI/180)
```

APPENDIX B. FINITE ELEMENT MODEL

```

x2al = h/2
y2al = l*cos(theta*PI/180)
x15al = h+l*sin(theta*PI/180)

d_y = 2*l*cos(theta*PI/180)
d_x = 2*l*sin(theta*PI/180)+2*h

! DSLJ insert geometry parameters
!*****



avisco_tot = 0.00001
avisco = avisco_tot/2
a1 = tan(theta*PI/180)/2
b1 = -x1al
c1 = avisco/4
del1 = sqrt(b1*b1-4*a1*c1)
tlig = (-b1-del1)/(2*a1)
alpha = atan(y2al/x2al)*180/PI

! Sandwich panel geometry parameters
!*****



*IF,orientation,eq,'orient1',then
    nb_cell_X = 10
    nb_cell_Y = 10
*ELSEIF,orientation,eq,'orient2',then
    nb_cell_X = 6
    nb_cell_Y = 18
*ENDIF

nb_cells = nb_cell_Y*nb_cell_X+(nb_cell_Y-1)*(nb_cell_X-1)
depth = 0.01
l_panel = (nb_cell_X-1)*d_x+2*x15al
w_panel = (nb_cell_Y-1)*d_y+2*y2al

tablig =
*DIM, tablig, array, nb_cells,1

! Materials parameters
!*****



! Viscoelastic material
n_vem = 0.3
E_vem = 8.7e6
nu_vem = 0.45
vem_dens = 1100

! Aluminium
n_alu = 0.0001
E_al = 7e10
nu_al = 0.3
al_dens = 2700

! Modal analysis parameters
!*****



! nb_modes must be >6 in the case of free boundary condition (rigid body modes)
nb_modes = 10

! Skip the rigid body modes (first 6 modes) under free boundary conditions
*IF,BC,eq,'FREE',then
    start_mode = 7
*ELSE
    start_mode = 1

```

```

*ENDIF

! Harmonic analysis parameters
!*****



f_min = 0
f_max = 4000
nstep = 12800
P = 13

!*****
! PRE PROCESSING
!*****



/PREP7

! Element and material properties
!*****



ET,1,SHELL181
R,1,t

MP,EX,1,E_al
MP,EY,1,E_al
MP,EZ,1,E_al
MP,NUXY,1,nu_al
MP,NUYZ,1,nu_al
MP,NUXZ,1,nu_al
MP,dens,1,al_dens
MP,DMPR,1,n_alu/2

ET,2,SOLID185
! Enhanced strain formulation
KEYOPT,2,2,2

MP,EX,2,E_vem
MP,EY,2,E_vem
MP,EZ,2,E_vem
MP,NUXY,2,nu_vem
MP,NUYZ,2,nu_vem
MP,NUXZ,2,nu_vem
MP,dens,2,vem_dens
MP,DMPR,2,n_vem/2

! Honeycomb cell modelling
!*****



K,1,x1al,0,0
K,2,x2al,y2al,0
K,3,-x2al,y2al,0
K,4,-x1al,0,0
K,5,-x2al,-y2al,0
K,6,x2al,-y2al,0
K,7,x15al,,0
K,8,-x15al,,0

K,10,0,0,0
K,11,0,0,depth

K,12,0,0,depth/10+2*depth
K,13,0,0,9*depth/10+2*depth
K,14,x1al,0,depth/10
K,15,-x1al,0,depth/10

```

APPENDIX B. FINITE ELEMENT MODEL

```

L,10,11
L,1,2
,2,3
,3,4
,4,5
,5,6
,6,1
,7,1
,4,8
L,12,13

ADRAG,2,3,4,5,6,7,1
ADRAG,8,,,,1
ADRAG,9,,,,1

! Modelling of DSLJ attachments at cell corner
!*****



K,1000,x1al-tlig*tan(theta*PI/180),tlig,depth/10
K,1001,x1al-tlig*tan(theta*PI/180),-tlig,depth/10
K,1002,x1al+tlig/cos(theta*PI/180),0,depth/10
K,1003,x1al,0,depth/10

K,1004,-(x1al-tlig*tan(theta*PI/180)),tlig,depth/10
K,1005,-(x1al-tlig*tan(theta*PI/180)), -tlig,depth/10
K,1006,-(x1al+tlig/cos(theta*PI/180)),0,depth/10
K,1007,-x1al,0,depth/10

K,1008,x2al+tlig*tan(theta*PI/180),y2al-tlig,depth/10
K,1009,x2al-tlig/cos(theta*PI/180),y2al,depth/10
K,1010,x2al,y2al,depth/10

K,1011,x2al+tlig*tan(theta*PI/180),-(y2al-tlig),depth/10
K,1012,x2al-tlig/cos(theta*PI/180),-y2al,depth/10
K,1013,x2al,-y2al,depth/10

K,1014,-(x2al+tlig*tan(theta*PI/180)),y2al-tlig,depth/10
K,1015,-(x2al-tlig/cos(theta*PI/180)),y2al,depth/10
K,1016,-x2al,y2al,depth/10

K,1017,-(x2al+tlig*tan(theta*PI/180)),-(y2al-tlig),depth/10
K,1018,-(x2al-tlig/cos(theta*PI/180)), -y2al,depth/10
K,1019,-x2al,-y2al,depth/10

L,1003,1000
L,1003,1001
L,1003,1002

L,1007,1004
L,1007,1005
L,1007,1006

L,1010,1008
L,1010,1009

L,1013,1011
L,1013,1012

L,1016,1014
L,1016,1015

L,1019,1017
L,1019,1018

```

```

*DO,i,29,42
ADRAG,i,,,,,,10
*ENDDO

! Skins modelling
*****



*GET,kp_xmin,kp,0,mnloc,x
*GET,kp_xmax,kp,0,rxloc,x
*GET,kp_ymin,kp,0,mnloc,y
*GET,kp_ymax,kp,0,rxloc,y
*GET,kp_zmin,kp,0,mnloc,z
*GET,kp_zmax,kp,0,rxloc,z

K,1050,kp_xmin,kp_ymin
K,1051,kp_xmax,kp_ymin
K,1052,kp_xmax,kp_ymax
K,1053,kp_xmin,kp_ymax

A,1050,1051,1052,1053
ASEL,s,loc,z,0
AGEN,2,all,,,,depth
ALLSEL,all

! Unit cell meshing
*****



AOVLAP,all
ESIZE,1/3
TYPE,1
MAT,1
AMESH,all

ASEL,s,,,all
CM, honey, area
ALLSEL,all

! Create group sup_lig
*****



K,1020,x1al-3*tlig*tan(theta*PI/180),-tlig,depth/10+depth
K,1021,x1al-3*tlig*tan(theta*PI/180),tlig,depth/10+depth
K,1022,x1al-3*tlig*tan(theta*PI/180),0,depth/10+depth
K,1023,-(x1al-3*tlig*tan(theta*PI/180)),0,depth/10+depth

K,1024,x1al,0,depth/10+depth
K,1025,-(x1al-tlig*tan(theta*PI/180)),tlig,depth/10+depth
K,1026,-(x1al-tlig*tan(theta*PI/180)), -tlig,depth/10+depth

K,1027,-(x1al-3*tlig*tan(theta*PI/180)),tlig,depth/10+depth
K,1028,-(x1al-3*tlig*tan(theta*PI/180)), -tlig,depth/10+depth
K,1029,-(x1al-3*tlig*tan(theta*PI/180)),tlig,9*depth/10+depth
K,1030,-(x1al-3*tlig*tan(theta*PI/180)), -tlig,9*depth/10+depth

L,1024,1022
L,1022,1023
L,1025,1021
L,1026,1020

ADRAG,12,,,,,,10
ADRAG,13,,,,,,10
ADRAG,15,,,,,,10
ADRAG,17,,,,,,10

```

APPENDIX B. FINITE ELEMENT MODEL

```

ASEL,s,loc,z,depth+depth/10,depth*2
CM, sup_lig, area
AMESH,all
ALLSEL,all

CSYS, 1
AGEN,2,sup_lig,,,alpha,depth
CSYS, 0

ASEL,s,loc,z,depth*2,depth*3
CM, sup_lig2, area
ALLSEL,all

CSYS, 1
AGEN,2,sup_lig2,,, -2*alpha,depth
CSYS, 0

ASEL,s,loc,z,depth*3,depth*4
CM, sup_lig3, area
ALLSEL,all

! Create group visco_i
!*****
```

V,1027,1029,29,1023,1021,35,27,1022
V,1023,29,1030,1028,1022,27,43,1020

```

! DSLJ meshing
!*****
```

TYPE,2
MAT,2

VSEL,s,,,**all**
CM, visco_i, volu
VMESH,**all**
ALLSEL,**all**

CSYS, 1
VGEN,2,visco_i,,,alpha,depth
CSYS, 0

VSEL,s,**loc**,z,depth*2,depth*3
CM, visco_i2, volu
ALLSEL,**all**

CSYS, 1
VGEN,2,visco_i2,,, -2*alpha,depth
CSYS, 0

VSEL,s,**loc**,z,depth*3,depth*4
CM, visco_i3, volu
ALLSEL,**all**

/UIS, MSGPOP, 3

```

! Cell + support ligament generation
!*****
```

*IF,damping,eq,'**dslj1**',then
*VREAD,tablig(1),lig_f1,txt
(e2.0)
*ELSEIF,damping,eq,'**dslj2**',then
*VREAD,tablig(1),lig_f2,txt

```

(e2.0)
*ELSE
  *VREAD,tablig(1),lig_none,txt
  (e2.0)
*ENDIF

row_x = 1
row_y = 1
sum_lig = 0

*DO,i,1,nb_cells

  ! "even" cells
  *IF,i,le,nb_cell_X*nb_cell_Y,then

    *IF, row_y,gt,nb_cell_Y,then
      row_x = row_x+1
      row_y = 1
    *ENDIF

    lig_value = tablig(i)
    sum_lig = sum_lig+lig_value

    *IF,lig_value,eq,1,then
      AGEN,2,sup_lig,,, (row_x-1)*d_x,(row_y-1)*d_y,-depth,,,0
      VGEN,2,visco_i,,, (row_x-1)*d_x,(row_y-1)*d_y,-depth,,,0
    *ENDIF

    *IF,lig_value,eq,2,then
      AGEN,2,sup_lig2,,, (row_x-1)*d_x,(row_y-1)*d_y,-2*depth,,,0
      VGEN,2,visco_i2,,, (row_x-1)*d_x,(row_y-1)*d_y,-2*depth,,,0
    *ENDIF

    *IF,lig_value,eq,3,then
      AGEN,2,sup_lig3,,, (row_x-1)*d_x,(row_y-1)*d_y,-3*depth,,,0
      VGEN,2,visco_i3,,, (row_x-1)*d_x,(row_y-1)*d_y,-3*depth,,,0
    *ENDIF

    AGEN,2,honey,,, (row_x-1)*d_x,(row_y-1)*d_y,,,0

  ! "odd" cells
  *ELSE

    *IF,i,eq,nb_cell_X*nb_cell_Y+1,then
      row_x = 1
      row_y = 1
    *ENDIF

    *IF, row_y,gt,nb_cell_Y-1,then
      row_x = row_x+1
      row_y = 1
    *ENDIF

    lig_value = tablig(i)
    sum_lig = sum_lig+lig_value

    *IF,lig_value,eq,1,then
      AGEN,2,sup_lig,,, (row_x-1)*d_x+x1al+x2al,(row_y-1)*d_y+y2al,-depth,,,0
      VGEN,2,visco_i,,, (row_x-1)*d_x+x1al+x2al,(row_y-1)*d_y+y2al,-depth,,,0
    *ENDIF

    *IF,lig_value,eq,2,then
      AGEN,2,sup_lig2,,, (row_x-1)*d_x+x1al+x2al,(row_y-1)*d_y+y2al,-2*depth,,,0
      VGEN,2,visco_i2,,, (row_x-1)*d_x+x1al+x2al,(row_y-1)*d_y+y2al,-2*depth,,,0
    *ENDIF

```

APPENDIX B. FINITE ELEMENT MODEL

```

*ENDIF

*IF,lig_value,eq,3,then
    AGEN,2,sup_lig3,,, (row_x-1)*d_x+x1al+x2al,(row_y-1)*d_y+y2al,-3*depth,,,0
    VGEN,2,visco_i3,,, (row_x-1)*d_x+x1al+x2al,(row_y-1)*d_y+y2al,-3*depth,,,0
*ENDIF

*ENDIF
row_y = row_y+1

*ENDDO

! Clear and delete original unit cell and DSLJ
! ****
ACLEAR,honey
ACLEAR,honey,,,1

VCLEAR,visco_i,,,1
VCLEAR,visco_i2,,,1
VCLEAR,visco_i3,,,1
VDELE,visco_i,,,1
VDELE,visco_i2,,,1
VDELE,visco_i3,,,1

ACLEAR,sup_lig
ACLEAR,sup_lig2
ACLEAR,sup_lig3
ADELE,sup_lig,,,1
ADELE,sup_lig2,,,1
ADELE,sup_lig3,,,1

ACLEAR,58
ACLEAR,69
ADELE,58
ADELE,69

ALLSEL,all
CPINTF,ALL,0.0001
/UIS, MSGPOP, 2

*get,n_xmin,node,0,mnloc,x
*get,n_xmax,node,0, mxloc,x
*get,n_ymin,node,0,mnloc,y
*get,n_ymax,node,0, mxloc,y
*get,n_zmin,node,0,mnloc,z
*get,n_zmax,node,0, mxloc,z

xmid = (n_xmax+n_xmin)/2
ymid = (n_ymax+n_ymin)/2
length = n_xmax-n_xmin
width = n_ymax-n_ymin
depth = n_zmax-n_zmin

! ****
! SOLVER
! ****

FINISH
/SOLU

! Modal analysis
! ****

```

```

ANTYPE,2
MODOPT,LANPCG,nb_modes,,,1
MXPAND,nb_modes,,yes
MSAVE,ON
EQSLV,PCG

*IF,BC,eq,'CFFF',and,orientation,eq,'orient1',then
  NSEL,s,loc,x,n_xmin
  D,all,all,0
*ELSEIF,BC,eq,'CFFF',and,orientation,eq,'orient2',then
  NSEL,s,loc,y,n_ymin
  D,all,all,0
*ELSEIF,BC,eq,'SS',OR,BC,eq,'SSSS',then
  nsel,s,loc,x,n_xmin
  nsel,a,loc,x,n_xmax
  nsel,u,loc,z,0.00001,depth*10
  d,all,uz,0
  d,all,ux,0
  d,all,uy,0
*ENDIF

ALLSEL,all
SOLVE
FINISH

! Harmonic analysis
*****



/SOLU
ANTYPE,3
HROPT,msup,nb_modes,,yes
MSAVE,ON
KBC,1
HARFRQ,f_min,f_max
NSUBST,nstep

SELTOL,5e-4

*IF,excite,eq,'middle',then
  NSEL,s,loc,z,n_zmin
  NSEL,r,loc,x,xmid
  NSEL,r,loc,y,ymid
*ELSEIF,orientation,eq,'orient1',and,excite,eq,'tip',then
  NSEL,s,loc,z,n_zmin
  NSEL,r,loc,x,n_xmax
  NSEL,r,loc,y,ymid
*ELSEIF,orientation,eq,'orient2',and,excite,eq,'tip',then
  NSEL,s,loc,z,n_zmin
  NSEL,r,loc,x,xmid
  NSEL,r,loc,y,n_ymin+y2al
*ELSEIF,excite,eq,'corner',then
  NSEL,s,loc,z,n_zmin
  NSEL,r,loc,x,n_xmin
  NSEL,r,loc,y,n_ymin
*ELSEIF,excite,eq,'corner2',then
  NSEL,s,loc,z,n_zmin
  NSEL,r,loc,x,n_xmax
  NSEL,r,loc,y,n_ymin
*ENDIF

SELTOL
F,all,fz,P
ALLSEL,all
SOLVE

```

APPENDIX B. FINITE ELEMENT MODEL

```

FINISH

! *****
! POST PROCESSING
! *****

/POST1

*CFOpen,name,CSV
*VWRITE,'mode number','frequency','loss Ansys','loss MSE','damping efficiency'
%C ,%C ,%C ,%C ,%C
*CFCLOS

! Natural frequency
! *****

SET,,,,,,start_mode
*DO,j,start_mode,nb_modes

*GET,freq%j%,mode,j,freq

! Participation factor and effective mass
! *****

*GET,PF_x,MODE,j,PFACT,,DIREC,X
*GET,PF_y,MODE,j,PFACT,,DIREC,Y
*GET,PF_z,MODE,j,PFACT,,DIREC,Z
*GET,PF_rotX,MODE,j,PFACT,,DIREC,ROTX
*GET,PF_rotY,MODE,j,PFACT,,DIREC,ROTY
*GET,PF_rotZ,MODE,j,PFACT,,DIREC,ROTZ

effm_x = PF_x**2
effm_y = PF_y**2
effm_z = PF_z**2
effm_rotX = PF_rotX**2
effm_rotY = PF_rotY**2
effm_rotZ = PF_rotZ**2

! Modal mass and modal stiffness
! *****

ETABLE,kene_,kene
SSUM
*GET,ke,ssum,,item,kene_
OMEGA = 2*PI*freq%j%
MODEMASS = 2*ke/omega**2
MODESTIFF = omega**2*modemass

! Modal loss factor (Modal Strain Energy method)
! *****

*IF,sum_lig,ne,0,then

ESEL,s,mat,,2
ETABLE,VOLU,VOLU
SSUM
*GET,vol_vem,SSUM,0,ITEM,VOLU
ETABLE,ERAS
mass_vem = vol_vem*vem_dens

ETABLE,SENE,SENE
SSUM
*GET,se_vem,SSUM,0,ITEM,SENE
ETABLE,ERAS
*ELSE

```

```

    vol_vem = 0
    mass_vem = 0
    se_vem = 0
*ENDIF

ESEL,s,mat,,1
ETABLE,VOLU,VOLU
SSUM
*GET,vol_al,SSUM,0,ITEM,VOLU
ETABLE,ERAS
mass_al = vol_al*al_dens

ETABLE,SENE,SENE
SSUM
*GET,se_al,SSUM,0,ITEM,SENE
ETABLE,ERAS

allsel,all
vol_tot = vol_vem+vol_al
mass_tot = mass_vem+mass_al
se_tot = se_vem+se_al
loss_MSE = (n_alu*se_al+n_vem*se_vem)/se_tot
effi = loss_MSE/mass_tot

*GET,damp_ratio,MODE,j,damp
loss_ANSYS = damp_ratio*2

*CFOOPEN,name,csv,,append
*VWRITE,j,freq%j%,loss_ANSYS,loss_MSE,effi
%G, %G, %G, %G, %G
*CFCLOS

! Mode shapes
*****
PLNSOL, U, Sum
/show,png,,,8

/PLOPTS,INFO,0
/PLOPTS,LEG1,0
/PLOPTS,LEG2,0
/PLOPTS,LEG3,0
/PLOPTS,FRAME,0
/PLOPTS,TITLE,0
/PLOPTS,MINM,0
/PLOPTS,FILE,0
/PLOPTS,WINS,0
/PLOPTS,WP,0
/PLOPTS,DATE,0

/RGB,INDEX,100,100,100, 0
/RGB,INDEX, 80, 80, 80,13
/RGB,INDEX, 60, 60, 60,14
/RGB,INDEX, 0, 0, 0,15

/TRIAD,off
/VIEW, 1, 1, 1, 1
/WINDOW,, -1,1.67,-1,1
/TYPE,,6
/EFACET,4
/COLOR,OUTL,15
/COLOR,wbak,0,1
/GRAPHICS,power
/GFILE,2400

```

APPENDIX B. FINITE ELEMENT MODEL

```

/REPLOT
/SHOW,CLOSE

SET,NEXT
*ENDDO

*CFOpen,name,csv,,append
*VWRITE,'mass','length','width','depth','excitation','measure'
%C ,%C ,%C ,%C ,%C
*VWRITE,mass_tot,length,width,depth,excite,measure
%G ,%G ,%G, %G, %C, %C
*CFCLOS

FINISH

! Frequency response function
! ****
! ****
! *****

/POST26
FILE,,rfreq
NUMVAR,200

*IF,orientation,eq,'orient1',and,measure,eq,'tip',then
  n1 = node(n_xmax,ymid,n_zmin)
*ELSEIF,orientation,eq,'orient2',and,measure,eq,'tip',then
  n1 = node(xmid,n_ymax,n_zmin)
*ELSEIF,measure,eq,'corner',then
  n1 = node(n_xmax,n_ymax,n_zmin)
*ENDIF

NSOL,2,n1,U,z,UZ_-2
STORE,MERGE
par =
*DIM,par,array,nstep,2
VGET,par(1,1),1

REALVAR,3,2,,,REAL2
IMAGIN,4,2,,,IMAG2
PROD,5,3,3
PROD,6,4,4
ADD,5,5,6
SQRT,6,5,,,AMPL2

VGET,par(1,2),6

*cfopen,name,csv,,append
*vwrite,'freq','amplitude'
%C ,%C
*vwrite,par(1,1),par(1,2)
%G ,%G
*CFCLOS

PLVAR,2
/GROPT,LOGY,ON
/REPLOT

FINISH

```

Appendix C

Parametric optimiser

The parametric optimisation procedure described in Chapter 5 was implemented using ANSYS Parametric Design Language (APDL):

```
*****  
! Ansys APDL macro "parametric_optimisation.mac"  
! returns the strain deformation in percent between all opposite vertices of  
! all the honeycomb cells in the sandwich panel deformed under a specific  
! mode shape  
! This macro may be called as follows:  
! *use,parametric_optimisation.mac,arg1  
! arg1 = integer indicating the mode number  
*****  
  
/POST1  
SET,,,,,,arg1  
  
*CFOOPEN,name,CSV  
*VWRITE,'node 1','node 2','initial dist','final dist','percent change','lig type','cell nb'  
%C, %C, %C, %C, %C, %C, %C  
*CFCLOS  
  
row_x = 1  
row_y = 1  
cell_number = 1  
  
*DO,i,1,nb_cells  
  
    ! "even" cells  
    *IF,i,le,nb_cell_X*nb_cell_Y,then  
  
        *IF,row_y,gt,nb_cell_Y,then  
            row_x = row_x+1  
            row_y = 1  
        *ENDIF  
  
        ! horizontal dslj  
        type_lig = 1  
  
        nd1 = node(x1al+2*x15al*(row_x-1),y2al*2*(row_y-1),depth)  
        nd1_loc_x = NX(nd1)  
        nd1_loc_y = NY(nd1)  
        nd1_loc_z = NZ(nd1)  
        d1_x = ux(nd1)  
        d1_y = uy(nd1)  
        d1_z = uz(nd1)  
        np1_x = d1_x+nd1_loc_x
```

APPENDIX C. PARAMETRIC OPTIMISER

```

np1_y = d1_y+nd1_loc_y
np1_z = d1_z+nd1_loc_z

nd2 = node(-x1al+2*x15al*(row_x-1),y2al*2*(row_y-1),depth)
nd2_loc_x = NX(nd2)
nd2_loc_y = NY(nd2)
nd2_loc_z = NZ(nd2)
d2_x = ux(nd2)
d2_y = uy(nd2)
d2_z = uz(nd2)
np2_x = d2_x+nd2_loc_x
np2_y = d2_y+nd2_loc_y
np2_z = d2_z+nd2_loc_z

l_init = sqrt((nd2_loc_x-nd1_loc_x)**2+(nd2_loc_y-nd1_loc_y)**2+(nd2_loc_z-nd1_loc_z)**2)
l_fin = sqrt((np2_x-np1_x)**2+(np2_y-np1_y)**2+(np2_z-np1_z)**2)
percent_change = abs(l_init-l_fin)/l_init*100

*CFOPEN,name,csv,,append
*VWRITE,nd1,nd2,l_init,l_fin,percent_change,type_lig,cell_number
%G, %G, %G, %G, %G, %G, %G
*CFCLOS

! 60 degrees dslj
type_lig = 2

nd1 = node(x2al+2*x15al*(row_x-1),y2al*(2*row_y-1),depth)
nd1_loc_x = NX(nd1)
nd1_loc_y = NY(nd1)
nd1_loc_z = NZ(nd1)
d1_x = ux(nd1)
d1_y = uy(nd1)
d1_z = uz(nd1)
np1_x = d1_x+nd1_loc_x
np1_y = d1_y+nd1_loc_y
np1_z = d1_z+nd1_loc_z

nd2 = node(-x2al+2*x15al*(row_x-1),y2al*(2*row_y-3),depth)
nd2_loc_x = NX(nd2)
nd2_loc_y = NY(nd2)
nd2_loc_z = NZ(nd2)
d2_x = ux(nd2)
d2_y = uy(nd2)
d2_z = uz(nd2)
np2_x = d2_x+nd2_loc_x
np2_y = d2_y+nd2_loc_y
np2_z = d2_z+nd2_loc_z

l_init = sqrt((nd2_loc_x-nd1_loc_x)**2+(nd2_loc_y-nd1_loc_y)**2+(nd2_loc_z-nd1_loc_z)**2)
l_fin = sqrt((np2_x-np1_x)**2+(np2_y-np1_y)**2+(np2_z-np1_z)**2)
percent_change = abs(l_init-l_fin)/l_init*100

*CFOPEN,name,csv,,append
*VWRITE,nd1,nd2,l_init,l_fin,percent_change,type_lig,cell_number
%G, %G, %G, %G, %G, %G, %G
*CFCLOS

! -60 degrees dslj
type_lig = 3

nd1 = node(-x2al+2*x15al*(row_x-1),y2al*(2*row_y-1),depth)
nd1_loc_x = NX(nd1)
nd1_loc_y = NY(nd1)
nd1_loc_z = NZ(nd1)

```

```

d1_x = ux(nd1)
d1_y = uy(nd1)
d1_z = uz(nd1)
np1_x = d1_x+nd1_loc_x
np1_y = d1_y+nd1_loc_y
np1_z = d1_z+nd1_loc_z

nd2 = node(x2al+2*x15al*(row_x-1),y2al*(2*row_y-3),depth)
nd2_loc_x = NX(nd2)
nd2_loc_y = NY(nd2)
nd2_loc_z = NZ(nd2)
d2_x = ux(nd2)
d2_y = uy(nd2)
d2_z = uz(nd2)
np2_x = d2_x+nd2_loc_x
np2_y = d2_y+nd2_loc_y
np2_z = d2_z+nd2_loc_z

l_init = sqrt((nd2_loc_x-nd1_loc_x)**2+(nd2_loc_y-nd1_loc_y)**2+(nd2_loc_z-nd1_loc_z)**2)
l_fin = sqrt((np2_x-np1_x)**2+(np2_y-np1_y)**2+(np2_z-np1_z)**2)
percent_change = abs(l_init-l_fin)/l_init*100

*CFOPEN,name,csv,,append
*VWRITE,nd1,nd2,l_init,l_fin,percent_change,type_lig,cell_number
%G, %G, %G, %G, %G, %G, %G
*CFCLOS

*ELSE

! odd cells
*IF,i,eq,nb_cell_X*nb_cell_Y+1,then
    row_x=1
    row_y=1
*ENDIF

*IF, row_y,gt,nb_cell_Y-1,then
    row_x=row_x+1
    row_y=1
*ENDIF

! horizontal dslj
type_lig = 1

nd1 = node(x1al+(2*row_x-1)*x15al,y2al*(2*row_y-1),depth)
nd1_loc_x = NX(nd1)
nd1_loc_y = NY(nd1)
nd1_loc_z = NZ(nd1)
d1_x = ux(nd1)
d1_y = uy(nd1)
d1_z = uz(nd1)
np1_x = d1_x+nd1_loc_x
np1_y = d1_y+nd1_loc_y
np1_z = d1_z+nd1_loc_z

nd2 = node(-x1al+(2*row_x-1)*x15al,y2al*(2*row_y-1),depth)
nd2_loc_x = NX(nd2)
nd2_loc_y = NY(nd2)
nd2_loc_z = NZ(nd2)
d2_x = ux(nd2)
d2_y = uy(nd2)
d2_z = uz(nd2)
np2_x = d2_x+nd2_loc_x
np2_y = d2_y+nd2_loc_y
np2_z = d2_z+nd2_loc_z

```

APPENDIX C. PARAMETRIC OPTIMISER

```

l_init = sqrt((nd2_loc_x-nd1_loc_x)**2+(nd2_loc_y-nd1_loc_y)**2+(nd2_loc_z-nd1_loc_z)**2)
l_fin = sqrt((np2_x-np1_x)**2+(np2_y-np1_y)**2+(np2_z-np1_z)**2)
percent_change = abs(l_init-l_fin)/l_init*100

*CFOPEN,name,csv,,append
*VWRITE,nd1,nd2,l_init,l_fin,percent_change,type_lig,cell_number
%G, %G, %G, %G, %G, %G, %G
*CFCLOS

! 60 degrees dslj
type_lig = 2

nd1 = node(x2al+(2*row_x-1)*x15al,y2al*2*row_y,depth)
nd1_loc_x = NX(nd1)
nd1_loc_y = NY(nd1)
nd1_loc_z = NZ(nd1)
d1_x = ux(nd1)
d1_y = uy(nd1)
d1_z = uz(nd1)
np1_x = d1_x+nd1_loc_x
np1_y = d1_y+nd1_loc_y
np1_z = d1_z+nd1_loc_z

nd2 = node(x1al+2*x15al*(row_x-1),y2al*2*(row_y-1),depth)
nd2_loc_x = NX(nd2)
nd2_loc_y = NY(nd2)
nd2_loc_z = NZ(nd2)
d2_x = ux(nd2)
d2_y = uy(nd2)
d2_z = uz(nd2)
np2_x = d2_x+nd2_loc_x
np2_y = d2_y+nd2_loc_y
np2_z = d2_z+nd2_loc_z

l_init = sqrt((nd2_loc_x-nd1_loc_x)**2+(nd2_loc_y-nd1_loc_y)**2+(nd2_loc_z-nd1_loc_z)**2)
l_fin = sqrt((np2_x-np1_x)**2+(np2_y-np1_y)**2+(np2_z-np1_z)**2)
percent_change = abs(l_init-l_fin)/l_init*100

*CFOPEN,name,csv,,append
*VWRITE,nd1,nd2,l_init,l_fin,percent_change,type_lig,cell_number
%G, %G, %G, %G, %G, %G, %G
*CFCLOS

! -60 degrees dslj
type_lig = 3

nd1 = node(x1al+2*x15al*(row_x-1),y2al*2*row_y,depth)
nd1_loc_x = NX(nd1)
nd1_loc_y = NY(nd1)
nd1_loc_z = NZ(nd1)
d1_x = ux(nd1)
d1_y = uy(nd1)
d1_z = uz(nd1)
np1_x = d1_x+nd1_loc_x
np1_y = d1_y+nd1_loc_y
np1_z = d1_z+nd1_loc_z

nd2 = node(x2al+(2*row_x-1)*x15al,y2al*2*(row_y-1),depth)
nd2_loc_x = NX(nd2)
nd2_loc_y = NY(nd2)
nd2_loc_z = NZ(nd2)
d2_x = ux(nd2)
d2_y = uy(nd2)

```

```

d2_z = uz(nd2)
np2_x = d2_x+nd2_loc_x
np2_y = d2_y+nd2_loc_y
np2_z = d2_z+nd2_loc_z

l_init = sqrt((nd2_loc_x-nd1_loc_x)**2+(nd2_loc_y-nd1_loc_y)**2+(nd2_loc_z-nd1_loc_z)**2)
l_fin = sqrt((np2_x-np1_x)**2+(np2_y-np1_y)**2+(np2_z-np1_z)**2)
percent_change = abs(l_init-l_fin)/l_init*100

*CFOPEN,name,csv,,append
*VWRITE,nd1,nd2,l_init,l_fin,percent_change,type_lig, cell_number
%G, %G, %G, %G, %G, %G, %G
*CFCLOS

*ENDIF

row_y = row_y+1
cell_number = cell_number+1

*ENDDO
FINISH

```

APPENDIX C. PARAMETRIC OPTIMISER

Appendix D

Evolutionary optimiser

The adaptive IBEA introduced by Zitzler and Künzli [304] and modified to manipulate binary string representation, was implemented in the numerical environment MATLAB. The initialisation of the search population and a reflection symmetry operator was included to the original algorithm in an effort to increase the convergence rate.

```
function [Archive,Archive_objectives, X, Xo, samples, samples_objectives,...  
time_count] = IBEA_binary(pop_size, generations, type, cost_function, l, ...  
num_obj, x_over_type, key, p_cross, p_reflect, p_mut, kappa, old_X, old_Xo, old_samples, old_samples_o)  
  
% Implements the adaptive IBEA_epsilon+ algorithm described in 2004 PPSN paper by  
% Zitzler and Kunzli, modified to manipulate binary string representation  
%  
% inputs:  
% pop_size = number of members in search population  
% generations = number of iterations of algorithm  
% cost_function = string containing the name of the objective  
%   function to optimise, must take as arguments the decision vector  
%   followed by the number of objectives, and return an array (1 by  
%   D) of the D objectives evaluated  
% type = 'CFFF2' or 'FFFF2' or 'CFFF1' or 'FFFF1' or 'CFFF3' or 'FFFF3'  
% l = number of decision parameters  
% num_obj = number of objectives  
% x_over_type = crossover type, 1 indicates single point, uniform otherwise  
% key: if key = 1, no initial population, if key = 2, initial population is  
% generated from the parametric optimisation, else, the initial  
% population is generated from previous run with a 'samples' history  
% p_reflect = probability of reflected symmetry mutation (typically 0.1)  
% p_mut (optional) = probability of bit flip mutation, will default to 1/l  
% p_cross = probability of crossovers (typically 0.9)  
% kappa (optional) = discount factor for indicator, will default to 0.05  
% old_X = archive output of previous run -- set as empty set [] if you do  
%       not wish to restart from previous run  
% old_Xo = archive objectives output of previous run -- set as empty set []  
%       if you do not wish to restart from previous run  
% old_samples = samples output of previous run -- set as empty set [] if you do  
%       not wish to restart from previous run  
% old_samples_o = samples objectives output of previous run -- set as empty set []  
%       if you do not wish to restart from previous run  
%  
% returns:  
%  
% Archive = matrix of archive decision vectors  
% Archive_objectives = matrix of archive member evaluations
```

APPENDIX D. EVOLUTIONARY OPTIMISER

```
% samples = history of algorithm state in terms of its locations evaluated
% samples_objectives = corresponding objectives
% time_count = time elapsed (the index correspond to the samples index)
%
% (c) Jonathan Fieldsend, University of Exeter, 2014

p_mut_backup = p_mut;
if ~exist('p_mut','var')
    p_mut = 1;
else
    p_mut = ceil(p_mut*1);
end
% p_mut now holds the number of elements of a vector to flip each time
if ~exist('kappa','var')
    kappa = 0.05;
end

% INITIALISATION
% generates an initial population of size pop_size

if ~exist('old_X','var')
    old_X = [];
end
if ~exist('old_Xo','var')
    old_Xo = [];
end
if ~exist('old_samples','var')
    old_samples = [];
end
if ~exist('old_samples_o','var')
    old_samples_o = [];
end

mating_pool = rand(pop_size,1);
offspring = rand(pop_size,1);
off_o = rand(pop_size,num_obj);

time_count = zeros((generations+1)*pop_size,1);
tic; % start elapsing time

[samples, samples_objectives, sample_index, X, Xo, time_count] = initialise(pop_size, ...
key, generations, l, num_obj, type, cost_function, time_count, old_X, old_Xo, ...
old_samples, old_samples_o);

for kk=1:generations % loop for generations

    % FITNESS ASSIGNMENT: scale objective and indicator values and use them
    % to assign fitness value to the individual in the initial population
    Xo_scaled = rescale_objectives(Xo);
    [fitness,c] = fitness_assignment(Xo_scaled,kappa);

    % ENVIRONMENTAL SELECTION
    while size(X,1)>pop_size
        % select the individual with the smallest fitness value = best
        % individual !
        [~,j] = min(fitness);
        % remove it from the population and store its objectives in ty
        X(j,:) = [];
        ty = Xo_scaled(j,:);
        Xo(j,:) = [];
        Xo_scaled(j,:)=[];
        fitness(j) = [];
        % update fitness value of the remaining individuals
        fitness = update_fitness(fitness,Xo_scaled,kappa,ty,c);
    end
end
```

```

end

% MATING SELECTION
for j=1:pop_size;
    I=randperm(pop_size);
    % binary tournament selection on fitness value with replacement
    % in order to fill the temporary mating pool
    if fitness(I(1))<fitness(I(2))
        mating_pool(j,:)=X(I(1),:);
    else
        mating_pool(j,:)=X(I(2),:);
    end
end

% VARIATION: apply crossover, mutation and symmetry reflection to the
% mating pool and add the resulting offspring to the main population
offspring = mating_pool;
% Crossover
for j=1:2:pop_size-1;
    c1 = mating_pool(j,:);
    c2 = mating_pool(j+1,:);
    if rand()<p_cross % crossover with p_cross probability
        if x_over_type==1 % single point
            k = randperm(l-1);
            ks = k(1);
            c1 (ks+1:end) = mating_pool(j+1,ks+1:end);
            c2 (ks+1:end) = mating_pool(j,ks+1:end);
        else % uniform
            k = randperm(l);
            % uniformly random selected elements, crossover 50%
            uni_I = k(1:ceil(length(k)/2));
            c1 (uni_I) = mating_pool(j+1,uni_I);
            c2 (uni_I) = mating_pool(j,uni_I);
        end
    end % otherwise children are direct copies of parents
    offspring(j,:) = c1;
    offspring(j+1,:) = c2;
end

% BIT FLIP MUTATION
for j=1:pop_size;
    k=randperm(l);
    % randomly bitflip p_mut elements
    offspring(j,k(1:p_mut))=abs(offspring(j,k(1:p_mut))-1);
end

% SYMMETRY REFLECTION
rows = 10;
cols = 19;
I = randperm(pop_size);

if p_reflect ~= 0

    for i=1:floor(pop_size*p_reflect)
        sym_index = I(i);
        sym_vector_int = bin2int(offspring(sym_index,:));

        % if CFFF2, perform a horizontal reflection
        if strcmp(type,'CFFF1') || strcmp(type,'CFFF2') || strcmp(type,'CFFF3')
            sym_vector_int = reflect_solution(sym_vector_int, rows, cols, 1);
        % if FFFF2, alternate between vertical and horizontal reflection
        elseif strcmp(type,'FFFF1') || strcmp(type,'FFFF2') || strcmp(type,'FFFF3')
            sym_vector_int = reflect_solution(sym_vector_int, rows, cols, floor(rand(1)*2));
        end
    end
end

```

APPENDIX D. EVOLUTIONARY OPTIMISER

```

        offspring(sym_index,: ) = int2bin(sym_vector_int);
    end

end

% add offspring to population
for i=1:pop_size
    % evaluate offspring objectives
    off_o(i,:) = feval(cost_function,offspring(i,:),num_obj,type);
    % add offspring to population
    samples(sample_index,: ) = offspring(i,:);
    samples_objectives(sample_index,: ) = off_o(i,:);
    time_count(sample_index) = toc;
    sample_index = sample_index+1;
end
if rem(kk,10)==0
    fprintf('Iteration %d, Evaluation %d\n',kk, kk*pop_size+pop_size);
end
Xo = [Xo; off_o];
X = [X; offspring];

end

% TERMINATION
I = pareto_front_with_duplicates(samples_objectives);
Archive = samples(I,:);
Archive_objectives = samples_objectives(I,:);

%-----
function [samples, samples_objectives, sample_index, X, Xo, time_count] = initialise(pop_size, ...
key, generations, l, num_obj, type, cost_function, time_count, old_X, old_Xo, old_samples, old_samples_o)

% no initial population
if key == 1

    samples = zeros((generations+1)*pop_size,l);
    samples_objectives = zeros((generations+1)*pop_size,num_obj);
    % declare archive and associated objective evaluations as empty
    % Create random individual (Uniform) bits and evaluate
    X = floor(rand(pop_size,l)*2);
    Xo = zeros(pop_size,num_obj);

    for i=1:pop_size
        Xo(i,:) = feval(cost_function,X(i,:),num_obj,type);
        time_count(i) = toc;
    end

    samples(1:pop_size,: ) = X;
    samples_objectives(1:pop_size,: ) = Xo;
    sample_index = pop_size+1;

    % if the initial population is created from the parametric optimisation
elseif key == 2
    X = old_X;
    Xo = old_Xo;
    if size(X,1) < pop_size
        temp_length = size(X,1);

        % if fewer than pop_size from parametric optimisation, then fill
        % out rest of the search population with random solutions
        X = [X; floor(rand(pop_size-temp_length,l)*2)];
        Xo = [Xo; zeros(pop_size-temp_length,num_obj)];

        for i=temp_length:pop_size

```

```

Xo(i,:) = feval(cost_function,X(i,:),num_obj,type);
time_count(i) = toc;
end
end

samples = zeros(generations*pop_size+size(X,1),1);
samples_objectives = zeros(generations*pop_size+size(Xo,1),num_obj);

samples(1:size(X,1),:) = X;
samples_objectives(1:size(Xo,1),:) = Xo;
sample_index = size(X,1)+1;

% if initial population is created from previous run with a 'sample' history
else
    if size(old_X,1) ~= 2*pop_size
        error('old population size does not match the population size now being used...
               -- the old population should be twice the pop_size argument');
    end

    X = old_X;
    Xo = old_Xo;
    samples = [old_samples; zeros(generations*pop_size+size(X,1),1)];
    samples_objectives = [old_samples_o; zeros(generations*pop_size+size(Xo,1),num_obj)];
    sample_index = size(old_samples,1);

    samples(sample_index+1:sample_index+size(X,1),:) = X;
    samples_objectives(sample_index+1:sample_index+size(Xo,1),:) = Xo;
    sample_index = sample_index+size(Xo,1)+1;
end

%-----
function Xo_scaled = rescale_objectives(Xo)
% rescale each objectives to the interval [0,1]

n = size(Xo,1);
upb = max(Xo);
lwb = min(Xo);

Xo_scaled = (Xo-repmat(lwb,n,1))./repmat(upb-lwb,n,1);

%-----
function [fitness,c] = fitness_assignment(Xo,kappa)

[n,m] = size(Xo);
fitness = zeros(n,1);
indicator = zeros(n,n);

for i=1:n
    for j=1:n
        if i~=j
            indicator(i,j) = max(Xo(i,:)-Xo(j,:)); % get shift value
            %fitness(i) = fitness(i) -exp(-indicator/kappa);
        end
    end
end

c =max(max(indicator));

for j=1:n
    fitness(j) = sum(-exp(-indicator(:,j)/(c*kappa)));
end

%-----

```

APPENDIX D. EVOLUTIONARY OPTIMISER

```

function fitness = update_fitness(fitness,Xo,kappa,old_val,c)

[n,m] = size(Xo);
for i=1:n
    indicator = max(old_val-Xo(i,:)); % get shift value
    fitness(i) = fitness(i) + exp(-indicator/(c*kappa));
end

%-----
function new_solution_vector = reflect_solution(solution_vector, rows, cols, orientation)
% new_solution_vector = reflect_solution(solution_vector, rows, columns, orientation)
%
% function reflects the solution vector either reflecting through the
% vertical or horizontal axis once the solution_vector is converted back to
% its underlying 2D form (comprising hexagonal cells)
%
% solution_vector = vector representing solution, contents of each element
% either 0, 1, 2 or 3 indicating if element unused, or if used the
% orientation of the insert. Total number of elements should be rows * cols
% - floor(cols/2), and error check will assert this.
%
% rows, columns = number of rows and columns the solution represents
% 10 rows and 19 columns for orientation 1 and 18 rows by 11 columns for
% orientation 2. The 'rows' term is the maximum (as alternate
% columns of cells will have rows and row-1 elements).
%
% In mapping the first part of the vector is mapping 'even solutions' --
% i.e. those in columns with an even number of rows and the second part
% 'odd solutions', those in columns with an odd number of rows
%
% orientation = reflection through vertical line (0) or horizontal line
% (argument not 0)

if min(size(solution_vector)) ~= 1
    error('solution_vector argument must be a vector!')
end
if length(solution_vector) ~= (rows*cols) - floor(cols/2)
    error('solution_vector is wrong length, cannot be mapped to a 2D plane of hexagonal cells');
end
if (rem(cols/2,2)==0) && (orientation ==0)
    error('There must be an odd number of columns when reflecting through the vertical line');
end

if orientation == 0
    % reflect through vertical line
    new_solution_vector = vertical_reflection(solution_vector, rows, cols);
else
    % reflect through horizontal line
    new_solution_vector = horizontal_reflection(solution_vector, rows, cols);
end

%-----
function new_solution_vector = vertical_reflection(solution_vector, rows, cols)

r = rand()>0.5; % random draw, do we reflect left to right, or right to left?

new_solution_vector = solution_vector;
% process the 'even' chunk
num_even_cols = floor((cols+1)/2);
to_swap = floor(num_even_cols)/2;
for i = 1:to_swap
    if (r == 0)
        I = (i-1)*rows+(1:rows);
        II = (num_even_cols-1)*rows+(1:rows);

```

```

    else
        II = (i-1)*rows+(1:rows);
        I = (num_even_cols-1)*rows+(1:rows);
    end
    new_solution_vector(I) = solution_vector(II);
    I2 = find(new_solution_vector(I)==2);
    I3 = find(new_solution_vector(I)==3);
    new_solution_vector(I(I2)) = 3;
    new_solution_vector(I(I3)) = 2;
    num_even_cols = num_even_cols - 1;
end
offset = floor((cols+1)/2)*rows;
% process the 'odd chunk'
num_odd_cols = floor((cols-1)/2);
to_swap = floor(num_odd_cols)/2;
srows = rows-1;

for i = 1:to_swap
    if (r == 0)
        I = (i-1)*srows+offset+(1:srows);
        II = (num_odd_cols-1)*srows+offset+(1:srows);
    else
        II = (i-1)*srows+offset+(1:srows);
        I = (num_odd_cols-1)*srows+offset+(1:srows);
    end
    new_solution_vector(I) = solution_vector(II);
    I2 = find(new_solution_vector(I)==2);
    I3 = find(new_solution_vector(I)==3);
    new_solution_vector(I(I2)) = 3;
    new_solution_vector(I(I3)) = 2;
    num_odd_cols = num_odd_cols - 1;
end

%-----
function new_solution_vector = horizontal_reflection(solution_vector, rows, cols)

r = rand()>0.5; % random draw, do we reflect top to bottom, or bottom to top?

new_solution_vector = solution_vector;
% process the 'even' chunk
num_even_cols = floor((cols+1)/2);
to_swap = floor(rows/2);

for i = 1:num_even_cols
    if (r == 0)
        I = rows*(i-1) + (1:to_swap);
        II = rows*(i-1) + (rows:-1:rows-(to_swap-1));
    else
        II = rows*(i-1) + (1:to_swap);
        I = rows*(i-1) + (rows:-1:rows-(to_swap-1));
    end
    new_solution_vector(I) = solution_vector(II);
    I2 = find(new_solution_vector(I)==2);
    I3 = find(new_solution_vector(I)==3);
    new_solution_vector(I(I2)) = 3;
    new_solution_vector(I(I3)) = 2;
end
offset = floor((cols+1)/2)*rows;
% process the 'odd chunk'
num_odd_cols = floor((cols-1)/2);
to_swap = floor(rows-1)/2;
srows = rows - 1;
for i = 1:num_odd_cols
    if (r == 0)

```

APPENDIX D. EVOLUTIONARY OPTIMISER

```

I = offset + srows*(i-1) + (1:to_swap);
II = offset + srows*(i-1) + (srows:-1:srows-(to_swap-1));
else
    II = offset + srows*(i-1) + (1:to_swap);
    I = offset + srows*(i-1) + (srows:-1:srows-(to_swap-1));
end
new_solution_vector(I) = solution_vector(II);
I2 = find(new_solution_vector(I)==2);
I3 = find(new_solution_vector(I)==3);
new_solution_vector(I(I2)) = 3;
new_solution_vector(I(I3)) = 2;
end

%-----
function [indices] = pareto_front_with_duplicates(Y)
% Y = A n by m matrix of objectives, where m is the number of objectives
% and n is the number of points
%
% copes with duplicates
% assumes minimisation
% returns indices (array which contains the indices of the dominating
% individuals

[n,m] = size(Y);
S = zeros(n,1);

% S is an n-long list of 0 and 1
% if S(i)=1: the ith item dominate the population ie both of its objectives
% are >= than the rest of the population AND at least 1 of its objective is
% > than the rest of the population
for i=1:n
    % get number of points that dominate Y
    S(i) = sum((sum(Y<=repmat(Y(i,:),n,1),2) == m) & (sum(Y<repmat(Y(i,:),n,1),2) > 0));
end
indices = find(S==0);

%-----
function x = int2bin(y)
% convert an array of integers (less or equal than 3) to the corresponding
% array of binary numbers
% y is an array of integers

x = zeros(1,length(y)*2);

j = 1;
for i = 1:length(y)
    if y(i) == 1
        j = j+1;
        x(j) = 1;
        j = j+1;
    elseif y(i) == 2
        x(j) = 1;
        j = j+2;
    elseif y(i) == 3;
        x(j) = 1;
        j = j+1;
        x(j) = 1;
        j = j+1;
    else
        j = j+2;
    end
end

```

```

function x = bin2int(y)
% convert an array of binary number to the corresponding array of integers
% (less or equal to 3)
% y is an array of binary

if rem(length(y),2)~=0
    error('The array of binary number must have an even number of elements')
end

n = length(y);
x = zeros(1,n/2);
j=1;

for i=1:2:n-1
    x(j) = y(i)*2+y(i+1);
    j=j+1;
end

%-----
function [a,ao]=create_initial_archive(n, type)
% create initial archive based on the parametric optimisation
% n = population size of the initial population (typically: 20)
% type = 'CFFF2' or 'FREE2' or 'CFFF1' or 'FREE1'

for i=1:n
    b = load(strcat(type,'/init_pop/mlig_',int2str(i),'.txt'));
    a(i,:)= int2bin(b');
    b = load(strcat(type,'/init_pop/obj1_loss_',int2str(i),'.txt'));
    c = load(strcat(type,'/init_pop/obj2_mass_',int2str(i),'.txt'));
    ao(i,:)= [-b, c];
end

end

%-----
function [a,ao]=create_initial_archive(n, type)
% create initial archive based on the parametric optimisation
% n = population size of the initial population (typically: 20)
% type = 'CFFF3' or 'FREE3'

for i=1:n
    b = load(strcat(type,'/init_pop3/mlig_',int2str(i),'.txt'));
    a(i,:)= int2bin(b');
    b = load(strcat(type,'/init_pop3/obj1_loss_',int2str(i),'.txt'));
    c = load(strcat(type,'/init_pop3/obj2_loss_',int2str(i),'.txt'));
    d = load(strcat(type,'/init_pop3/obj3_mass_',int2str(i),'.txt'));
    ao(i,:)= [-b, -c, d];
end

end

%-----
function y = ansys_fit2(x,m,type)
% x = decision vector (X(i,:) in IBEA)
% m = number of objectives (must be = 2 here)
% type = string defining the cost function ('CFFF2' or 'FREE2' or 'CFFF1' or 'FREE1')

if m~=2
    error('Function only works with two objectives');
end

y = zeros(1,2);
x = bin2int(x);

```

APPENDIX D. EVOLUTIONARY OPTIMISER

```

fid=fopen(strcat(type,'_lig.txt'),'w');
fprintf(fid,'%d\n',x);
fclose(fid);

% open Ansys with input file
system(strcat('/usr/local/ansys_inc/v160/ansys/bin/ansys160" -p aa_r -np 16 -dir...
"/scratch/pa269/new_IBEA" -j ",type,'" -s read -l en-us -b nolist...
< "/scratch/pa269/new_IBEA/",type,'.inp" '))

fid=fopen(strcat(type,'_loss1.txt'),'r');
y(1)= -(fscanf(fid,'%f'));
fclose(fid);

fid=fopen(strcat(type,'_mass2.txt'),'r');
y(2) = fscanf(fid,'%f');
fclose(fid);

%-----
function y = ansys_fit3(x,m,type)
% x = decision vector (X(i,:) in IBEA)
% m = number of objectives (must be = 2 here)
% type = string defining the cost function ('CFFF3' or 'FREE3')

if m~=3
    error('Function only works with three objectives');
end

y = zeros(1,3);
x = bin2int(x);

fid=fopen(strcat(type,'_lig.txt'),'w');
fprintf(fid,'%d\n',x);
fclose(fid);

% open Ansys with input file
system(strcat('/usr/local/ansys_inc/v160/ansys/bin/ansys160" -p aa_r -np 16 -dir...
"/scratch/pa269/new_IBEA" -j ",type,'" -s read -l en-us -b nolist...
< "/scratch/pa269/new_IBEA/",type,'.inp" '))

fid=fopen(strcat(type,'_loss1.txt'),'r');
y(1)= -(fscanf(fid,'%f'));
fclose(fid);

fid=fopen(strcat(type,'_loss2.txt'),'r');
y(2)= -(fscanf(fid,'%f'));
fclose(fid);

fid=fopen(strcat(type,'_mass3.txt'),'r');
y(3) = fscanf(fid,'%f');
fclose(fid);

```

Bibliography

- [1] S. Batchu. Solid Metal Versus Sandwich Panels, 2015.
- [2] W. D. Callister and D. G. Rethwisch. *Materials Science and Engineering: An Introduction*. John Wiley & Sons, 7th edition, 2009.
- [3] P. Wennhage. *Structural Acoustic Optimization of Sandwich Panels*. PhD thesis, Department of aeronautics, division of lightweight structures, Royal Institute of Technology, Stockholm, 2001.
- [4] S. M. Jeong. *Analysis of vibration of two-dimensional periodic cellular structures*. PhD thesis, Georgia Institute of Technology, 2005.
- [5] H. N. G. Wadley. Multifunctional periodic cellular metals. *Philosophical Transactions of the Royal Society A*, 364(1838):31–68, 2006.
- [6] R. D. Cook, D. S. Malkus, M. E. Plesha, and R. J. Witt. *Concepts and Applications of Finite Element Analysis*. Wiley, New York, 4th edition, 2001.
- [7] R. Lakes. *Viscoelastic Materials*. Cambridge University Press, Cambridge, 2009.
- [8] S. S. Rao. *Mechanical vibrations*. Prentice Hall, 5th editio edition, 2011.
- [9] J. E. Ruzicka. Damping Structural Resonances Using Viscoelastic Shear-Damping Mechanisms: Part I - Design Configurations. *Journal of Engineering for Industry*, 83(4):403, nov 1961.
- [10] J. A. Staley. Light viscoelastic damping structure, patent US 4778028 A, 1988.
- [11] J. Park and D. L. Palumbo. Damping of Structural Vibration Using Lightweight Granular Materials. *Experimental Mechanics*, 49(5):697–705, 2008.
- [12] M. A. Boucher, C. W. Smith, F. Scarpa, W. Miller, and M. R. Hassan. Damping capacity in shape memory alloy honeycomb structures. In *SPIE Proceedings*, volume 7643, 2010.

BIBLIOGRAPHY

- [13] C. M. Chia, J. A. Rongong, and K. Worden. Strategies for using cellular automata to locate constrained layer damping on vibrating structures. *Journal of Sound and Vibration*, 319(1-2):119–139, jan 2009.
- [14] IATA. International Air Transport Association - facts sheet. Technical report, 2015.
- [15] D. Zenkert. *Handbook of Sandwich Construction*. EMAS, 1997.
- [16] R. Rajasekaran, M. A. Boucher, C. W. Smith, F. Scarpa, and K. E. Evans. Vibration damping, Patent US20130264757 A1, 2013.
- [17] L. J. Gibson and M. F. Ashby. *Cellular Solids: Structure and Properties*. Cambridge University Press, jul 1999.
- [18] A. G. Evans, J. W. Hutchinson, N. A. Fleck, M. F. Ashby, and H. N. G. Wadley. The topological design of multifunctional cellular metals. *Progress in Materials Science*, 46(3–4):309–327, 2001.
- [19] T. N. Bitzer. *Honeycomb Technology: Materials, Design, Manufacturing, Applications and Testing*. Springer, 1997.
- [20] L. Meirovitch. *Fundamentals of Vibrations*. Waveland Pr Inc., 1st edition, 2010.
- [21] W. Thomson. *Theory of Vibration with Applications*. CRC Press, 1996.
- [22] M. Petyt. *Introduction to Finite Element Vibration Analysis*. Cambridge University Press, 1998.
- [23] Olek C Zienkiewicz, Robert L Taylor, and J Z Zhu. *The Finite Element Method: Its Basis and Fundamentals, Seventh Edition*. Butterworth-Heinemann, Amsterdam; Boston, 7 edition edition, sep 2013.
- [24] D. J. Ewins. *Modal Testing: Theory, Practice and Application*. Wiley, 2nd edition, 2003.
- [25] D. I. G. Jones. *Handbook of viscoelastic vibration damping*. J. Wiley, New York, 2001.
- [26] M. D. Rao. Recent applications of viscoelastic damping for noise control in automobiles and commercial airplanes. *Journal of Sound and Vibration*, 262(3):457–474, 2003.
- [27] B. Azvine, G. R. Tomlinson, and R. J. Wynne. Use of active constrained-layer damping for controlling resonant vibration. *Smart Materials and Structures*, 4(1):1–6, mar 1995.

- [28] C. D. Johnson and D. A. Kienholz. Finite Element Prediction of Damping in Structures with Constrained Viscoelastic Layers. *AIAA Journal*, 20(9):1284–1290, 1982.
- [29] C. M. A. Vasques, R. A. S. Moreira, and J. Dias. Viscoelastic Damping Technologies - Part I: Modeling and Finite Element Implementation. *Journal of Advanced Research in Mechanical Engineering*, 1(2):76–95, 2010.
- [30] F. P. Landi, F. Scarpa, J. A. Rongong, and G. Tomlinson. Improving the modal strain energy method for damped structures using a dyadic matrix perturbation approach. *J. Eng. Mech. Eng. Sci.*, 216(12):1207–1216, 2002.
- [31] M. A. Trindade, A. Benjeddou, and R. Ohayon. Modeling of Frequency-Dependent Viscoelastic Materials for Active-Passive Vibration Damping. *Journal of Vibration and Acoustics*, 122(2):169, apr 2000.
- [32] M. H. Tsai and K. C. Chang. A study of the modal strain energy method for viscoelastically damped structures. *J. Chin. Inst. Eng.*, 24(3):311–320, may 2001.
- [33] F. P. Landi, F. Scarpa, J. A. Rongong, and G. R. Tomlinson. Improving the MSE method for damped structures. In P Sas and D Moens, editors, *SPIE Proceedings*, Heverlee, 2002.
- [34] Y. Xu, Y. Liu, and B. S. Wang. Revised modal strain energy method for finite element analysis of viscoelastic damping treated structures. In *SPIE's 9th Annual International Symposium on Smart Structures and Materials*, pages 35–42. International Society for Optics and Photonics, jun 2002.
- [35] P. J Torvik and B. Runyon. Modifications to the method of modal strain energy for improved estimates of loss factors for damped structures. *Shock and vibration*, 14(5):339–353, 2007.
- [36] D. J. McTavish. *The mini-oscillator technique : a finite element method for the modeling of linear viscoelastic structures*. PhD thesis, Toronto University, 1988.
- [37] D. F. Golla and P. C. Hughes. Dynamics of Viscoelastic Structures - A Time-Domain, Finite Element Formulation. *Journal of Applied Mechanics*, 52(4):897, dec 1985.
- [38] M. Enelund and G. A. Lesieutre. Time domain modeling of damping using anelastic displacement fields and fractional calculus. *International Journal of Solids and Structures*, 36(29):4447–4472, oct 1999.

BIBLIOGRAPHY

- [39] B. E. Douglas and J. C. S. Yang. Transverse compressional damping in the vibratory response of elastic-viscoelastic-elastic beams. *AIAA Journal*, 16(9):925–930, sep 1978.
- [40] A. Nashif, D. I. G. Jones, and J. Henderson. *Vibration Damping*. Wiley, 1985.
- [41] Z. Li and M. J. Crocker. A Review on Vibration Damping in Sandwich Composite Structures. *International Journal of Acoustics and Vibration*, 10(4):159–169, 2005.
- [42] E. M. Kerwin. Damping of Flexural Waves by a Constrained Viscoelastic Layer. *Journal of the Acoustical Society of America*, 31(7):952–962, 1959.
- [43] D. Ross, E. E. Ungar, and E. M. Kerwin. Damping of plate flexural vibrations by means of viscoelastic laminae. *Structural Damping*, pages 49 – 87, 1960.
- [44] E. E. Ungar and E. M. Kerwin. Loss Factors of Viscoelastic Systems in Terms of Energy Concepts. *Journal of the Acoustical Society of America*, 34(7):954–957, 1962.
- [45] E. E. Ungar. Loss Factors of Viscoelastically Damped Beam Structures. *Journal of the Acoustical Society of America*, 34(8):1082, jul 1962.
- [46] R. A. DiTaranto. Theory of Vibratory Bending for Elastic and Viscoelastic Layered Finite-Length Beams. *Journal of Applied Mechanics*, 32(4):881, dec 1965.
- [47] R. A. DiTaranto and W. Blasingame. Composite Damping of Vibrating Sandwich Beams. *Journal of Engineering for Industry*, 89(4):633, nov 1967.
- [48] D. Mead. The Effect of Certain Damping Treatments on the Response of Idealized Aeroplane Structures Excited by Noise. Technical report, Ft. Belvoir, 1965.
- [49] D. J. Mead and S. Markus. The forced vibration of a three-layer, damped sandwich beam with arbitrary boundary conditions. *Journal of Sound and Vibration*, 10(2):163–175, sep 1969.
- [50] D. J. Mead and S. Markus. Loss factors and resonant frequencies of encastré damped sandwich beams. *Journal of Sound and Vibration*, 12(1):99–112, may 1970.

- [51] D.J. Mead. A comparison of some equations for the flexural vibration of damped sandwich beams. *Journal of Sound and Vibration*, 83(3):363–377, aug 1982.
- [52] E. D. Shoua. The Composite Damping Capacity of Sandwich Cantilever Beams. *Experimental Mechanics*, 8(7):300–308, 1968.
- [53] D. K. Rao. Forced vibration of a damped sandwich beam subjected to moving forces. *Journal of Sound and Vibration*, 54(2):215–227, sep 1977.
- [54] R.C. Das Vikal, K.N. Gupta, and B.C. Nakra. Vibration of an excitation system supported flexibly on a viscoelastic sandwich beam at its mid-point. *Journal of Sound and Vibration*, 75(1):87–99, mar 1981.
- [55] J. M. Bai and C. T. Sun. The Effect of Viscoelastic Adhesive Layers on Structural Damping of Sandwich Beams. *Mechanics of Structures and Machines*, 23(1):1–16, jan 1995.
- [56] M.-J. Yan and E. H. Dowell. Governing Equations for Vibrating Constrained-Layer Damping Sandwich Plates and Beams. *Journal of Applied Mechanics*, 39(4):1041, dec 1972.
- [57] Š. Markuš. Shear-damping reduction effects in sandwich beams. *Journal of Sound and Vibration*, 55(4):591–593, dec 1977.
- [58] D. K. Rao. Vibration of Short Sandwich Beams. *Journal of Sound and Vibration*, 52(2):253–263, 1977.
- [59] D K Rao. Frequency and Loss Factors of Sandwich Beams under Various Boundary Conditions. *Journal of Mechanical Engineering Science*, 20(5):271–282, oct 1978.
- [60] B. E. Douglas. Compressional damping in three-layer beams incorporating nearly incompressible viscoelastic cores. *Journal of Sound and Vibration*, 104(2):343–347, jan 1986.
- [61] S. He and M. D. Rao. Vibration and Damping Analysis of Multi-Span Sandwich Beams with Arbitrary Boundary Conditions. *Journal of Sound and Vibration*, 164(1):125–142, jun 1993.
- [62] A. Bhimaraddi. Sandwich beam theory and the analysis of constrained layer damping. *Journal of Sound and Vibration*, 179(4):591–602, jan 1995.
- [63] T. Sakiyama, H. Matsuda, and C. Morita. Free vibration analysis of continuous sandwich beams with elastic or viscoelastic cores by applying

BIBLIOGRAPHY

- the discrete Green function. *Journal of Sound and Vibration*, 198(4):439–454, dec 1996.
- [64] T. Sakiyama, H. Matsuda, and C. Morita. Free vibration analysis of sandwich beam with elastic or viscoelastic core by applying the discrete Green function. *Journal of Sound and Vibration*, 191(2):189–206, mar 1996.
- [65] J. Vaswani, N. T. Asnani, and B. C. Nakra. Vibration and damping analysis of curved sandwich beams with a viscoelastic core. *Composite Structures*, 10(3):231–245, jan 1988.
- [66] T. L. Teng and N. K. Hu. Analysis of damping characteristics for viscoelastic laminated beams. *Computer Methods in Applied Mechanics and Engineering*, 190(29-30):3881–3892, apr 2001.
- [67] C. L. Sisemore and C. M. Darvennes. Transverse Vibration of Elastic-Viscoelastic-Elastic Sandwich Beams: Compression-Experimental and Analytical Study. *Journal of Sound and Vibration*, 252(1):155–167, apr 2002.
- [68] M. Hao and M. D. Rao. Vibration and Damping Analysis of a Sandwich Beam Containing a Viscoelastic Constraining Layer. *Journal of Composite Materials*, 39(18):1621–1643, jan 2005.
- [69] Z. Xie and W. S. Shepard. An enhanced beam model for constrained layer damping and a parameter study of damping contribution. *Journal of Sound and Vibration*, 319(3-5):1271–1284, jan 2009.
- [70] I. Elkhaldi, I. Charpentier, and E. M. Daya. A gradient method for viscoelastic behaviour identification of damped sandwich structures. *C. R. Mec.*, 340(8):619–623, aug 2012.
- [71] O. Sylwan. Shear and compressional damping effects of constrained layered beams. *Journal of Sound and Vibration*, 118(1):35–45, oct 1987.
- [72] Y. Y. Yu. Damping of Flexural Vibrations of Sandwich Plates. *Journal of the Aerospace Sciences*, 29(7):790–803, aug 1962.
- [73] Y. Y. Yu. Viscoelastic Damping of Vibrations of Sandwich Plates and Shells. *IASS Symposium*, pages 551–571, 1963.
- [74] D. J. Mead. The damping properties of elastically supported sandwich plates. *Journal of Sound and Vibration*, 24(3):275–295, oct 1972.

- [75] Y. V. K. S. Rao. Vibrations of unsymmetrical sandwich beams and plates with viscoelastic cores. *Journal of Sound and Vibration*, 34(3):309–326, 1974.
- [76] J. F. He and B. A. Ma. Analysis of Flexural Vibration of Viscoelastically Damped Sandwich Plates. *Journal of Sound and Vibration*, 126(1):37–47, oct 1988.
- [77] S. Mahmoudkhani, H. Haddadpour, and H. M. Navazi. Free and forced random vibration analysis of sandwich plates with thick viscoelastic cores. *Journal of Vibration and Control*, 19(14):2223–2240, sep 2012.
- [78] J. F. He and B. A. Ma. Vibration analysis of viscoelastically damped sandwich shells. *Shock and Vibration*, 3(6):403–417, 1996.
- [79] W. J. Anderson, E. J. Kovac, and R. A. Scott. Forced Non-Linear Vibrations of a Damped Sandwich Beam. *Journal of Sound and Vibration*, 17(1):25–39, 1971.
- [80] M. W. Hyer, W. J. Anderson, and R. A. Scott. Non-linear vibrations of three-layer beams with viscoelastic cores - part I Theory. *Journal of Sound and Vibration*, 46(1):121–136, may 1976.
- [81] M. W. Hyer, W. J. Anderson, and R. A. Scott. Non-linear vibrations of three-layer beams with viscoelastic cores - part II: Experiment. *Journal of Sound and Vibration*, 61(1):25–30, nov 1978.
- [82] E. M. Daya, L. Azrar, and M. Potier-Ferry. An amplitude equation for the non-linear vibration of viscoelastically damped sandwich beams. *Journal of Sound and Vibration*, 271(3-5):789–813, apr 2004.
- [83] M. Bilasse, E. M. Daya, and L. Azrar. Linear and nonlinear vibrations analysis of viscoelastic sandwich beams. *Journal of Sound and Vibration*, 329(23):4950–4969, nov 2010.
- [84] Z. Q. Xia and S. Lukasiewicz. Non-linear, Free, Damped Vibrations Of Sandwich Plates. *Journal of Sound and Vibration*, 175(2):219–232, aug 1994.
- [85] Z. Q. Xia and S. Lukasiewicz. Nonlinear damped vibrations of simply-supported rectangular sandwich plates. *Nonlinear Dynamics*, 8(4):417–433, 1995.
- [86] D. I. G. Jones and M. L. Parin. Technique for measuring damping properties of thin viscoelastic layers. *Journal of Sound and Vibration*, 24(2):201–210, sep 1972.

BIBLIOGRAPHY

- [87] G. R. Tomlinson. The use of constrained layer damping in vibration control. *International Journal of Mechanical Sciences*, 32(3):233–242, 1990.
- [88] D. I. G. Jones, A. D. Nashif, and M. L. Parin. Parametric study of multiple-layer damping treatments on beams. *Journal of Sound and Vibration*, 29(4):423–434, aug 1973.
- [89] P. Grootenhuis. The control of vibrations with viscoelastic materials. *Journal of Sound and Vibration*, 11(4):421–433, apr 1970.
- [90] S. A. Nayfeh. Damping of flexural vibration in the plane of lamination of elastic-viscoelastic sandwich beams. *Journal of Sound and Vibration*, 276(3-5):689–711, sep 2004.
- [91] B. P. Yadav. Vibration damping using four-layer sandwich. *Journal of Sound and Vibration*, 317(3-5):576–590, nov 2008.
- [92] F. Lin. *Vibro-acoustical Analysis and Design of a Multiple-layer Constrained Viscoelastic Damping Structure*. Michigan Technological University, 2010.
- [93] F. Lin and M. D. Rao. Vibration Analysis of a Multiple-Layered Viscoelastic Structure Using the Blot Damping Model. *AIAA Journal*, 48(3):624–634, mar 2010.
- [94] F. Lin and M. D. Rao. Vibroacoustical Analysis of Multiple-Layered Structures with Viscoelastic Damping Cores. *ISRN Mechanical Engineering*, 2013, 2013.
- [95] R. A. S. Moreira, J. D. Rodrigues, and A. J. M. Ferreira. A generalized layerwise finite element for multi-layer damping treatments. *Computational Mechanics*, 37(5):426–444, apr 2006.
- [96] R. A. S. Moreira and J. D. Rodrigues. A layerwise model for thin soft core sandwich plates. *Computers & Structures*, 84(19-20):1256–1263, jul 2006.
- [97] Q. Qiu, Z. P. Fang, H. C. Wan, and L. Zheng. Transfer function method for frequency response and damping effect of multilayer PCLD on cylindrical shell. *Journal of Physics: Conference Series*, 448(1):012006, jul 2013.
- [98] J. E. Ruzicka. Damping Structural Resonances Using Viscoelastic Shear-Damping Mechanisms: Part II - Experimental Results. *Journal of Engineering for Industry*, 83(4):414, 1961.
- [99] E. R. Marsh and A. H. Slocum. An integrated approach to structural damping. *Precision Engineering*, 18(2-3):103–109, may 1996.

- [100] E. R. Marsh and L. C. Hale. Damping of flexural waves with imbedded viscoelastic materials. *Journal of Vibration and Acoustics*, 120(1):188–193, jan 1998.
- [101] J. H. Yim, S. Y. Cho, Y. J. Seo, and B. Z. Jang. A study on material damping of 0 degrees laminated composite sandwich cantilever beams with a viscoelastic layer. *Composite Structures*, 60(4):367–374, jun 2003.
- [102] A. K. Mukhopadhyay and H. B. Kingsbury. On the dynamic response of a rectangular sandwich plate with viscoelastic core and generally orthotropic facings. *Journal of Sound and Vibration*, 47(3):347–358, aug 1976.
- [103] P. Cupial and J. Nizioł. Vibration and Damping Analysis of a 3-Layered Composite Plate with a Viscoelastic Mid-Layer. *Journal of Sound and Vibration*, 183(1):99–114, may 1995.
- [104] A. Muc and P. Zuchara. Sandwich plates - Free vibrations and damping analysis. *Mechanics of Composite Materials*, 34(2):203–211, apr 1998.
- [105] M. Afshin, M. Sadighi, and M. Shakeri. Vibration and damping analysis of cylindrical sandwich panels containing a viscoelastic flexible core. *Journal of Sandwich Structures and Materials*, 13(3):331–356, may 2010.
- [106] C. Yang, G. Jin, Z. Liu, X. Wang, and X. Miao. Vibration and damping analysis of thick sandwich cylindrical shells with a viscoelastic core under arbitrary boundary conditions. *International Journal of Mechanical Sciences*, 92:162–177, mar 2015.
- [107] P. Trompette, D. Boillot, and M.-A. Ravanel. The effect of boundary conditions on the vibration of a viscoelastically damped cantilever beam. *Journal of Sound and Vibration*, 60(3):345–350, oct 1978.
- [108] C.T. Sun, B.V. Sankar, and V.S. Rao. Damping and vibration control of unidirectional composite laminates using add-on viscoelastic materials. *Journal of Sound and Vibration*, 139(2):277–287, jun 1990.
- [109] S. He and M. D. Rao. Prediction of loss factors of curved sandwich beams. *Journal of Sound and Vibration*, 159(1):101–113, nov 1992.
- [110] M. G. Sainsbury and Q. J. Zhang. The Galerkin element method applied to the vibration of damped sandwich beams. *Computers & Structures*, 71(3):239–256, may 1999.

BIBLIOGRAPHY

- [111] X. Chen, H. L. Chen, and X. L. Hu. Damping Prediction of Sandwich Structures by Order-Reduction-Iteration Approach. *Journal of Sound and Vibration*, 222(5):803–812, may 1999.
- [112] F. S. Barbosa and M. C. R. Farage. A finite element model for sandwich viscoelastic beams: Experimental and numerical assessment. *Journal of Sound and Vibration*, 317(1-2):91–111, oct 2008.
- [113] S. G. Won, S. H. Bae, J. R. Cho, S. R. Bae, and W. B. Jeong. Three-layered damped beam element for forced vibration analysis of symmetric sandwich structures with a viscoelastic core. *Finite Elements in Analysis and Design*, 68:39–51, jun 2013.
- [114] Y. Wang and D. J. Inman. Finite element analysis and experimental study on dynamic properties of a composite beam with viscoelastic damping. *Journal of Sound and Vibration*, 332(23):6177–6191, nov 2013.
- [115] F. Cortes and I. Sarria. Dynamic Analysis of Three-Layer Sandwich Beams with Thick Viscoelastic Damping Core for Finite Element Applications. *Shock and Vibration*, 2015, 2015.
- [116] B.-A. Ma and J.-F. He. A finite element analysis of viscoelastically damped sandwich plates. *Journal of Sound and Vibration*, 152(1):107–123, jan 1992.
- [117] R. Rikards. Finite element analysis of vibration and damping of laminated composites. *Composite Structures*, 24(3):193–204, 1993.
- [118] Q. J. Zhang and M. G. Sainsbury. The Galerkin element method applied to the vibration of rectangular damped sandwich plates. *Computers & Structures*, 74(6):717–730, feb 2000.
- [119] Q. Chen and Y. W. Chan. Integral finite element method for dynamical analysis of elastic - viscoelastic composite structures. *Computers & Structures*, 74(1):51–64, jan 2000.
- [120] M. Bilasse and D. C. D. Oguamanam. Forced harmonic response of sandwich plates with viscoelastic core using reduced-order model. *Composite Structures*, 105:311–318, nov 2013.
- [121] Z. Huang, Z. Qin, and F. Chu. Vibration and damping characteristics of sandwich plates with viscoelastic core. *Journal of Vibration and Control*, aug 2014.

- [122] A. Korjakin, R. Rikards, A. Chate, and H. Altenbach. Free Damped Vibrations of Sandwich Shells of Revolution. *Journal of Sandwich Structures and Materials*, 3(3):171–196, jul 2001.
- [123] C. Saravanan, N. Ganesan, and V. Ramamurti. Vibration and damping analysis of multilayered fluid filled cylindrical shells with constrained viscoelastic damping using modal strain energy method. *Computers & Structures*, 75(4):395–417, apr 2000.
- [124] K. Amichi and N. Atalla. A new 3D finite element for sandwich structures with a viscoelastic core. *Canadian Acoustics*, 35(3):198–199, sep 2007.
- [125] L. Rouleau, J.-F. Deü, A. Legay, and J.-F. Sigrist. Vibro-acoustic study of a viscoelastic sandwich ring immersed in water. *Journal of Sound and Vibration*, 331(3):522–539, jan 2012.
- [126] M. D. Rao, R. Echempati, and S. Nadella. Dynamic analysis and damping of composite structures embedded with viscoelastic layers. *Composites Part B: Engineering*, 28(5-6):547–554, jan 1997.
- [127] J. A. Zapfe and G. A. Lesieutre. A discrete layer beam finite element for the dynamic analysis of composite sandwich beams with integral damping layers. *Computers & Structures*, 70(6):647–666, mar 1999.
- [128] M. Ganapathi, B. P. Patel, P. Boisse, and O. Polit. Flexural loss factors of sandwich and laminated composite beams using linear and nonlinear dynamic analysis. *Composites Part B: Engineering*, 30(3):245–256, apr 1999.
- [129] S. H. Zhang and H. L. Chen. A study on the damping characteristics of laminated composites with integral viscoelastic layers. *Composite Structures*, 74(1):63–69, jul 2006.
- [130] V. Pradeep, N. Ganesan, and K. Bhaskar. Vibration and thermal buckling of composite sandwich beams with viscoelastic core. *Composite Structures*, 81(1):60–69, nov 2007.
- [131] H. Arvin, M. Sadighi, and A. R. Ohadi. A numerical study of free and forced vibration of composite sandwich beam with viscoelastic core. *Composite Structures*, 92(4):996–1008, mar 2010.
- [132] S. Assaf. Finite Element Vibration Analysis of Damped Composite Sandwich Beams. *International Journal of Acoustics and Vibration*, 16(4):163–172, 2011.

BIBLIOGRAPHY

- [133] S. Ghinet and N. Atalla. Modeling thick composite laminate and sandwich structures with linear viscoelastic damping. *Computers & Structures*, 89(15–16):1547–1561, aug 2011.
- [134] A. Fereidoon, A. Ghoddosian, and A. A. Niyari. Non-Linear Damping Analysis of Sandwich Composite Structures. *Contemporary Engineering Sciences*, 4(1):37–42, 2011.
- [135] A. Fereidoon and A. H. Niyari. Investigation of the nonlinear behaviour of damping of aluminum foam core sandwich composite beams. *Journal of Reinforced Plastics and Composites*, 31(9):639–653, may 2012.
- [136] H. Arvin. Frequency response analysis of higher order composite sandwich beams with viscoelastic core. *IJST, Transactions of Mechanical Engineering*, 38:143–155, 2014.
- [137] B. Hu. *Finite element analysis of damped vibrations of laminated composite plates*. PhD thesis, nov 1992.
- [138] D. P. Makhecha, M. Ganapathi, and B. P. Patel. Vibration and damping analysis of laminated/sandwich composite plates using higher-order theory. *Journal of Reinforced Plastics and Composites*, 21(6):559–575, 2002.
- [139] E. Manconi and B. R. Mace. Estimation of the loss factor of viscoelastic laminated panels from finite element analysis. *Journal of Sound and Vibration*, 329(19):3928–3939, sep 2010.
- [140] R. A. S. Moreira and J. D. Rodrigues. Static and dynamic analysis of soft core sandwich panels with through-thickness deformation. *Composite Structures*, 92(2):201–215, jan 2010.
- [141] A. L. Araujo, C. M. Mota Soares, and C. A. Mota Soares. A viscoelastic finite element model for the analysis of passive damping in anisotropic laminated sandwich structures. In *8th International Conference on Sandwich Structures*, pages 865–876, 2008.
- [142] A. L. Araujo, C. M. Mota Soares, and C. A. Mota Soares. A Viscoelastic Sandwich Finite Element Model for the Analysis of Passive, Active and Hybrid Structures. *Applied Composite Materials*, 17(5):529–542, oct 2010.
- [143] A. L. Araujo, C. M. Mota Soares, C. A. Mota Soares, and J. Herskovits. Material identification of viscoelastic core materials in sandwich structures. In *International Conference on Engineering Optimization*, 2012.

- [144] A. Chate, R. Rikards, and A. Korjakin. Analysis of free damped vibrations of laminated composite cylindrical shells. *Mechanics of Composite Materials*, 31(5):474–484, 1996.
- [145] M. L. Soni and F. K. Bogner. Finite Element Vibration Analysis of Damped Structures. *AIAA Journal*, 20(5):700–707, may 1982.
- [146] M. Macé. Damping of Beam Vibrations By Means of a Thin Constrained Viscoelastic Layer: Evaluation of a New Theory. *Journal of Sound and Vibration*, 172(5):577–591, may 1994.
- [147] T. T. Baber, R. A. Maddox, and C. E. Orozco. A finite element model for harmonically excited viscoelastic sandwich beams. *Computers & Structures*, 66(1):105–113, jan 1998.
- [148] L. H. Silva, F. Santade, P. J. P. Goncalves, and E. A. C. Sousa. Dynamic analysis for different finite element models of beams with viscoelastic damping layer. In *9th International Conference on Structural Dynamics*, pages 1769–1773, 2014.
- [149] E. Ioannides and P. Grootenhuis. A finite element analysis of the harmonic response of damped three-layer plates. *Journal of Sound and Vibration*, 67(2):203–218, nov 1979.
- [150] Y. P. Lu, J. W. Killian, and G. C. Everstine. Vibrations of three layered damped sandwich plate composites. *Journal of Sound and Vibration*, 64(1):63–71, may 1979.
- [151] Y. P. Lu and G. C. Everstine. More on finite element modeling of damped composite systems. *Journal of Sound and Vibration*, 69(2):199–205, mar 1980.
- [152] Y. P. Lu, J. C. Clemens, and A. J. Roscoe. Vibrations of composite plate structures consisting of a constrained-layer damping sandwich with viscoelastic core. *Journal of Sound and Vibration*, 158(3):552–558, nov 1992.
- [153] M. Bilasse, L. Azrar, and E. M. Daya. Complex modes based numerical analysis of viscoelastic sandwich plates vibrations. *Computers & Structures*, 89(7-8):539–555, apr 2011.
- [154] D. S. Nokes and F. C. Nelson. Constrained layer damping with partial coverage. *The shock and vibration bulletin*, 68(3):5 – 12, 1968.

BIBLIOGRAPHY

- [155] A. K. Lall, N. T. Asnani, and B. C. Nakra. Damping analysis of partially covered sandwich beams. *Journal of Sound and Vibration*, 123(2):247–259, jun 1988.
- [156] H. Dewa, Y. Okada, and B. Nagai. Damping Characteristics of Flexural Vibration for Partially Covered Beams with Constrained Viscoelastic layers. *JSME international journal*, 34(2):210–217, jun 1991.
- [157] T. H. Park. Vibration and Damping Characteristics of a Beam with a Partially Sandwiched Viscoelastic Layer. *The Journal of Adhesion*, 61(1-4):97–122, feb 1997.
- [158] B. C. Nakra. Vibration control in machines and structures using viscoelastic damping. *Journal of Sound and Vibration*, 211(3):449–465, apr 1998.
- [159] C. Cai, H. Zheng, and G. R. Liu. Vibration analysis of a beam with PCLD Patch. *Applied Acoustics*, 65(11):1057–1076, nov 2004.
- [160] M. Yaman. Finite element vibration analysis of a partially covered cantilever beam with concentrated tip mass. *Materials & Design*, 27(3):243–250, 2006.
- [161] A. K. Lall, N. T. Asnani, and B. C. Nakra. Vibration and Damping Analysis of Rectangular Plate With Partially Covered Constrained Viscoelastic Layer. *Journal of Vibration Acoustics Stress and Reliability in Design*, 109(3):241, jul 1987.
- [162] K. D. D. Cho, J. H. H. Han, and I. Lee. Vibration and damping analysis of laminated plates with fully and partially covered damping layers. *Journal of Reinforced Plastics and Composites*, 19(15):1176–1200, jan 2000.
- [163] H. J. Wang and L. W. Chen. Vibration and damping analysis of a three-layered composite annular plate with a viscoelastic mid-layer. *Composite Structures*, 58(4):563–570, dec 2002.
- [164] H. J. Wang and L. W. Chen. Vibration and damping analysis of annular plates with constrained damping layer treatments. *Journal of Sound and Vibration*, 264(4):893–910, jul 2003.
- [165] H. J. Wang and L. W. Chen. Axisymmetric vibration and damping analysis of rotating annular plates with constrained damping layer treatments. *Journal of Sound and Vibration*, 271(1-2):25–45, mar 2004.

- [166] R. A. S. Moreira and J. D. Rodrigues. Partial constrained viscoelastic damping treatment of structures: A modal strain energy approach. *International journal of structural stability and dynamics*, 6(3):397–411, sep 2006.
- [167] A. Castel, A. Loredo, A. El Hafidi, and B. Martin. Complex power distribution analysis in plates covered with passive constrained layer damping patches. *Journal of Sound and Vibration*, 331(11):2485–2498, may 2012.
- [168] R. S. Masti and M. G. Sainsbury. Vibration damping of cylindrical shells partially coated with a constrained viscoelastic treatment having a standoff layer. *Thin-Walled Structures*, 43(9):1355–1379, sep 2005.
- [169] M. G. Sainsbury and R. S. Masti. Vibration damping of cylindrical shells using strain-energy-based distribution of an add-on viscoelastic treatment. *Finite Elements in Analysis and Design*, 43(3):175–192, jan 2007.
- [170] D. Granger and A. Ross. Effects of partial constrained viscoelastic layer damping parameters on the initial transient response of impacted cantilever beams: Experimental and numerical results. *Journal of Sound and Vibration*, 321(1-2):45–64, mar 2009.
- [171] C. Levy and Q. Chen. Vibration Analysis Of A Partially Covered, Double Sandwich-Type, Cantilever Beam. *Journal of Sound and Vibration*, 177(1):15–29, oct 1994.
- [172] Q. Chen and C. Levy. Vibration analysis of a partially covered double sandwich cantilever beam with concentrated mass at the free end. *International Journal of Solids and Structures*, 31(17):2377–2391, sep 1994.
- [173] Q. Chen and C. Levy. Comparison of theory with experimental data for a partially covered double-sandwich cantilever beam. *International Journal of Mechanical Sciences*, 40(4):399–403, apr 1998.
- [174] H. Zheng, X. M. Tan, and C. Cai. Damping analysis of beams covered with multiple PCLD patches. *International Journal of Material Sciences*, 48(12):1371–1383, dec 2006.
- [175] S.-W. Kung and R. Singh. Complex eigensolutions of rectangular plates with damping patches. *Journal of Sound and Vibration*, 216(1):1–28, sep 1998.
- [176] S.-W. Kung and R. Singh. Vibration analysis of beams with multiple constrained layer damping patches. *Journal of Sound and Vibration*, 212(5):781–805, may 1998.

BIBLIOGRAPHY

- [177] P. J. Torvik. Damping Additions for Plates Using Constrained Viscoelastic Layers. *The Journal of the Acoustical Society of America*, 51(3B):985, aug 1972.
- [178] A. B. Spalding. Placing small constrained layer damping patches on a plate to attain global or local velocity changes. *The Journal of the Acoustical Society of America*, 97(6):3617, jun 1995.
- [179] M. N. Darrouj and R. G. Faulkner. Optimum design of constrained layer damping panels. *Materials & Design*, 10(4):202–208, jul 1989.
- [180] R. S. Masti and M. G. Sainsbury. A study on the partial coating of a shell with an add-on viscoelastic layer for optimal damping design. In *Proceedings of ISMA2004*, pages 611–618, 2004.
- [181] D. Sun, X. Zhang, Y. Song, and B. Yan. Optimization for sandwich damping composite structure: Used in sprockets of crawler vehicles. *Journal of Sandwich Structures and Materials*, 14(1):95–110, dec 2011.
- [182] B. R. Sher and R. A. S. Moreira. Dimensionless analysis of constrained damping treatments. *Composite Structures*, 99:241–254, may 2013.
- [183] K. Deb. *Multi-Objective Optimization Using Evolutionary Algorithms*. John Wiley & Sons, 2001.
- [184] P. R. Mantena, R. F. Gibson, and S. J. Hwang. Optimal constrained viscoelastic tape lengths for maximizing damping in laminated composites. *AIAA Journal*, 29(10):1678–1685, oct 1991.
- [185] J. M. Lifshitz and M. Leibowitz. Optimal sandwich beam design for maximum viscoelastic damping. *International Journal of Solids and Structures*, 23(7):1027–1034, 1987.
- [186] S. Kodiyalam and J. Molnar. Optimization of constrained viscoelastic damping treatments for passive vibration control. In *33rd structures, structural dynamics and materials conference*, 1992.
- [187] A. L. Araujo, P. Martins, C. M. Mota Soares, C. A. Mota Soares, and J. Herskovits. Damping optimization of viscoelastic laminated sandwich composite structures. *Structural and Multidisciplinary Optimization*, 39(6):569–579, dec 2009.
- [188] Z. Xie, W. S. Shepard, and K. A. Woodbury. Design optimization for vibration reduction of viscoelastic damped structures using genetic algorithms. *Shock and Vibration*, 16(2009):455–466, 2009.

- [189] A.L. Araújo, C.M. Mota Soares, C.A. Mota Soares, and J. Herskovits. Optimal design and parameter estimation of frequency dependent viscoelastic laminated sandwich composite plates. *Composite Structures*, 92(9):2321–2327, aug 2010.
- [190] M. Hamdaoui, G. Robin, M. Jrad, and E. M. Daya. Optimal design of frequency dependent three-layered rectangular composite beams for low mass and high damping. *Composite Structures*, 120:174–182, feb 2015.
- [191] S. W. Hou, Y. H. Jiao, and Z. B. Chen. Optimum Layout of Passive Constrained Layer Damping Treatment Using Genetic Algorithms. In *Volume 13: Sound, Vibration and Design*, pages 371–376. ASME, jan 2010.
- [192] R. Plunkett and C. T. Lee. Length Optimization for Constrained Viscoelastic Layer Damping. *The Journal of the Acoustical Society of America*, 48(1B):150–161, 1970.
- [193] P. Trompette and J. Fatemi. Damping of beams. Optimal distribution of cuts in the viscoelastic constrained layer. *Structural Optimization*, 13(2-3):167–171, apr 1997.
- [194] G. Lepoittevin and G. Kress. Optimization of segmented constrained layer damping with mathematical programming using strain energy analysis and modal data. *Mater. Des.*, 31(1):14–24, jan 2010.
- [195] M. A. Trindade. Optimization of sandwich/multilayer viscoelastic composite structure for vibration damping. In M Salama, editor, *Proceedings of OMAE'01*, volume 3, pages 257–264, 2001.
- [196] M. A. Trindade. Optimization of passive constrained layer damping treatments applied to composite beams. *Latin American Journal of Solids and Structures*, 4(1):19–38, mar 2007.
- [197] M. Montemurro, Y. Koutsawa, S. Belouettar, A. Vincenti, and P. Vannucci. Design of damping properties of hybrid laminates through a global optimisation strategy. *Composite Structures*, 94(11):3309–3320, nov 2012.
- [198] J. F. A. Madeira, A. L. Araújo, C. M. Mota Soares, C. A. Mota Soares, and A. J. M. Ferreira. Multiobjective design of viscoelastic laminated composite sandwich panels. *Composites Part B: Engineering*, 77:391–401, aug 2015.
- [199] J. F. A. Madeira, A. L. Araújo, C. M. Mota Soares, and C. A. Mota Soares. Multiobjective optimization of viscoelastic laminated sandwich structures

BIBLIOGRAPHY

- using the Direct MultiSearch method. *Computers & Structures*, 147:229–235, jan 2015.
- [200] W. Chen and S. Liu. Topology optimization of microstructures of viscoelastic damping materials for a prescribed shear modulus. *Structural and Multidisciplinary Optimization*, 50(2):287–296, feb 2014.
- [201] R. Lundén. Optimum distribution of additive damping for vibrating beams. *Journal of Sound and Vibration*, 66(1):25–37, sep 1979.
- [202] R. Lundén. Optimum distribution of additive damping for vibrating frames. *Journal of Sound and Vibration*, 72(3):391–402, oct 1980.
- [203] P. Hajela and C.-Y. Lin. Optimal Design of Viscoelastically Damped Beam Structures. *Applied Mechanics Reviews*, 44(11S):S96, 1991.
- [204] J.-L. Marcelin, P. Trompette, and A. Smati. Optimal constrained layer damping with partial coverage. *Finite Elements in Analysis and Design*, 12(3-4):273–280, dec 1992.
- [205] J. L. Marcelin and P. Trompette. Optimal Location of Plate Damped Parts by Use of a Genetic Algorithm. *Shock and Vibration*, 1(6):541–547, 1994.
- [206] J. L. Marcelin, S. Shakeshi, and F. Pourroy. Optimal Constrained Layer Damping of Beams: Experimental and Numerical Studies. *Shock and Vibration*, 2(6):445–450, 1995.
- [207] J L Marcelin, P Trompette, and R Dornberger. Optimization of composite beam structures using a genetic algorithm. *Structural Optimization*, 9(3-4):236–244, jul 1995.
- [208] Y.-C. Chen and S.-C. Huang. An optimal placement of CLD treatment for vibration suppression of plates. *International Journal of Mechanical Sciences*, 44(8):1801–1821, aug 2002.
- [209] M. Al-Ajmi. *Homogenization and Topology Optimization of Constrained Layer Damping Treatments*. PhD thesis, University of Maryland, apr 2004.
- [210] H. Zheng, C. Cai, and X. M. Tan. Optimization of partial constrained layer damping treatment for vibrational energy minimization of vibrating beams. *Computers & Structures*, 82(29–30):2493–2507, nov 2004.
- [211] H. Zheng and C. Cai. Minimization of sound radiation from baffled beams through optimization of partial constrained layer damping treatment. *Appl. Acoust.*, 65(5):501–520, may 2004.

- [212] H. Zheng, C. Cai, G. S. H. Pau, and G. R. Liu. Minimizing vibration response of cylindrical shells through layout optimization of passive constrained layer damping treatments. *Journal of Sound and Vibration*, 279(3-5):739–756, jan 2005.
- [213] H. Zheng, G. S. H. Pau, and Y. Y. Wang. A comparative study on optimization of constrained layer damping treatment for structural vibration control. *Thin-Walled Struct.*, 44(8):886–896, aug 2006.
- [214] M. Alvelid. Optimal position and shape of applied damping material. *Journal of Sound and Vibration*, 310(4–5):947–965, mar 2008.
- [215] C. M. Chia, J. A. Rongong, and K. Worden. Evolution of constrained layer damping using a cellular automaton algorithm. *Proceedings of the Institution of Mechanical Engineers, Part C: Journal of Mechanical Engineering Science*, 222(4):585–597, apr 2008.
- [216] S. W. Hou, Y. H. Jiao, and Z. B. Chen. Optimum Layout of Partially Covered Sandwich Beam with Constrained Layer Damping. *Applied Mechanics and Materials*, 66-68:588–593, jul 2011.
- [217] N. Le Maoût, E. Verron, and J. Bégué. On the use of discontinuous elastomer patches to optimize the damping properties of composite sandwich plates. *Composite Structures*, 93(11):3057–3062, oct 2011.
- [218] S. Y. Kim. *Topology design optimization for vibration reduction: reducible design variable method*. PhD thesis, Queen’s University, 2011.
- [219] Z. Ling, X. Ronglu, W. Yi, and A. El-sabbagh. Topology optimization of constrained layer damping on plates using Method of Moving Asymptote (MMA) approach. *Shock and Vibration*, 18(1):211–244, 2011.
- [220] S. W. Hou, Y. H. Jiao, X. Wang, Z. B. Chen, and Y. B. Fan. Optimization of Plate with Partial Constrained Layer Damping Treatment for Vibration and Noise Reduction. *Applied Mechanics and Materials*, 138-139:20–26, nov 2011.
- [221] X. B. Li, G. Wang, J. H. Wen, and X. S. Wen. Evolution of Constrained Layer Damping Using a Modified Cellular Automata Algorithm. *Applied Mechanics and Materials*, 226-228:129–132, nov 2012.
- [222] Z. Kang, X. Zhang, S. Jiang, and G. Cheng. On topology optimization of damping layer in shell structures under harmonic excitations. *Structural and Multidisciplinary Optimization*, 46(1):51–67, jul 2012.

BIBLIOGRAPHY

- [223] M. Ansari, A. Khajepour, and E. Esmailzadeh. Application of level set method to optimal vibration control of plate structures. *Journal of Sound and Vibration*, 332(4):687–700, feb 2013.
- [224] J. S. Grewal, R. Sedaghati, and E. Esmailzadeh. Vibration analysis and design optimization of sandwich beams with constrained viscoelastic core layer. *Journal of Sandwich Structures and Materials*, 15(2):203–228, feb 2013.
- [225] M. Montemurro, A. Vincenti, Y. Koutsawa, and P. Vannucci. A two-level procedure for the global optimization of the damping behavior of composite laminated plates with elastomer patches. *Journal of Vibration and Control*, 21(9):1778–1800, sep 2013.
- [226] S. Y. Kim, C. K. Meechefske, and I. Y. Kim. Optimal damping layout in a shell structure using topology optimization. *Journal of Sound and Vibration*, 332(12):2873–2883, jun 2013.
- [227] W. Zheng, Y. Lei, S. Li, and Q. Huang. Topology optimization of passive constrained layer damping with partial coverage on plate. *Shock and vibration*, 20(2):199–211, 2013.
- [228] L. Zoghaib and P.-O. Mattei. Modeling and optimization of local constraint elastomer treatments for vibration and noise reduction. *Journal of Sound and Vibration*, 333(26):7109–7124, dec 2014.
- [229] Z. Fang and L. Zheng. Topology optimization approach of constrained layer damping layout using level-set method. In *The 21st International Congress on Sound and Vibration*, 2014.
- [230] Z. Fang and L. Zheng. Topology Optimization for Minimizing the Resonant Response of Plates with Constrained Layer Damping Treatment. *Shock and Vibration*, 2015, 2015.
- [231] C. Xu, S. Lin, and Y. Yang. Optimal design of viscoelastic damping structures using layerwise finite element analysis and multi-objective genetic algorithm. *Computers & Structures*, 157:1–8, sep 2015.
- [232] M. Meunier and R. A. Shenoi. Dynamic analysis of composite sandwich plates with damping modelled using high-order shear deformation theory. *Composite Structures*, 54(2-3):243–254, nov 2001.
- [233] A. K. Nayak, R. A. Shenoi, and S. S. J. Moy. Damping prediction of composite sandwich plates using assumed strain plate bending elements based on Reddy’s higher order theory. In *Structural Dynamics and*

- Materials Conference*, Denver, USA, apr 2002. American Institute of Aeronautics and Astronautics.
- [234] M. Meunier and R. A. Shenoi. Forced response of FRP sandwich panels with viscoelastic materials. *Journal of Sound and Vibration*, 263(1):131–151, may 2003.
 - [235] M. Assarar, A. El Mahi, and J.-M. Berthelot. Damping Analysis of Sandwich Composite Materials. *Journal of Composite Materials*, 43(13):1461–1485, jun 2009.
 - [236] M. Assarar, A. El Mahi, and J.-M. Berthelot. Analysis of the Damping of Sandwich Materials and Effect of the Characteristics of the Constituents. *International Journal of Material Science*, 3(2), jun 2013.
 - [237] H. Teodorescu-draghicescu, S. Vlase, D. Rosu, R. Purcarea, and V. Munteanu. Damping Analysis of a New Sandwich Structure. In *World Congress on Engineering 2009*, volume II, pages 3–8, 2009.
 - [238] M. Matter, T. Gmür, J. Cugnoni, and A. Schorderet. Identification of the elastic and damping properties in sandwich structures with a low core-to-skin stiffness ratio. *Composite Structures*, 93(2):331–341, jan 2011.
 - [239] J. Sargianis and J. Suhr. Core material effect on wave number and vibrational damping characteristics in carbon fiber sandwich composites. *Composites Science and Technology*, 72(13):1493–1499, aug 2012.
 - [240] J. Sargianis and J. Suhr. Effect of core thickness on wave number and damping properties in sandwich composites. *Compos. Sci. Technol.*, 72(6):724–730, mar 2012.
 - [241] J. J. Sargianis, H.-I. Kim, E. Andres, and J. Suhr. Sound and vibration damping characteristics in natural material based sandwich composites. *Composite Structures*, 96:538–544, feb 2013.
 - [242] T. S. Plagianakos and D. A. Saravacos. High-order layerwise mechanics and finite element for the damped dynamic characteristics of sandwich composite beams. *International Journal of Solids and Structures*, 41(24–25):6853–6871, dec 2004.
 - [243] J. Santos Silva, J. Dias Rodrigues, and R. A. S. Moreira. Application of Cork Compounds in Sandwich Structures for Vibration Damping. *Journal of Sandwich Structures and Materials*, 12(4):495–515, jun 2009.

BIBLIOGRAPHY

- [244] P. Jorge, P. Hugo, and M. M. Neves. Cork composition damping layer to reduce vibrations. In *15th International Conference on Experimental Mechanics*, 2012.
- [245] J. C. Sun and E. J. Richards. Prediction of total loss factors of structures, part I: Theory and experiments. *Journal of Sound and Vibration*, 103(1):109–117, nov 1985.
- [246] J. C. Sun, H. B. Sun, L. C. Chow, and E. J. Richards. Predictions of total loss factors of structures, part II: Loss factors of sand-filled structure. *Journal of Sound and Vibration*, 104(2):243–257, jan 1986.
- [247] H. B. Sun, J. C. Sun, and E. J. Richards. Prediction of total loss factors of structures, Part III: Effective loss factors in quasi-transient conditions. *Journal of Sound and Vibration*, 106(3):465–479, may 1986.
- [248] J.-L. Tsai and N.-R. Chang. Investigating damping properties of nanocomposites and sandwich structures with nanocomposites as core materials. *Journal of Composite Materials*, 45(21):2157–2164, apr 2011.
- [249] X. Q. Zhou, D. Y. Yu, X. Y. Shao, S. Wang, and Y. H. Tian. Asymptotic analysis on flexural dynamic characteristics for a sandwich plate with periodically perforated viscoelastic damping material core. *Composite Structures*, 119:487–504, jan 2015.
- [250] S. C. C. Conlon and S. A. A. Hambric. Damping and induced damping of a lightweight sandwich panel with simple and complex attachments. *J. Sound Vibr.*, 322(4-5):901–925, may 2009.
- [251] M. Rébillat and X. Boutillon. Identification of elastic and damping properties of sandwich structures based on high resolution modal analysis of point measurements. In *ISMA2010 including USD2010*, oct 2010.
- [252] M. Rebillat and X. Boutillon. Measurement of relevant elastic and damping material properties in sandwich thick plates. *Journal of Sound and Vibration*, 330(25):6098–6121, dec 2011.
- [253] N. Seera. *Viscoelastic Damping of Hexagonal Honeycomb Sandwich Panels*. PhD thesis, Clemson university, 2011.
- [254] M. R. Maher. *Vibration damping in composite/honeycomb sandwich beams*. Ph.d., University of Bristol, 1991.
- [255] R. D. Adams and M. R. Maher. The dynamic shear properties of structural honeycomb materials. *Composites Science and Technology*, 47(1):15–23, jan 1993.

- [256] M. R. Maher and R. D. Adams. Steady-state flexural vibration damping of honeycomb sandwich beams. *Composites Science and Technology*, 52(3):333–347, 1994.
- [257] J. Hugon, G. Laduree, M. R. Maher, and R. D. Adams. Finite element prediction of vibration damping in honeycomb sandwich panels. In *European Conference on Spacecraft Structures, Materials and Mechanical Testing 2005*, volume 581, page 48, 2005.
- [258] M. R. Maher, R. D. Adams, and J. Hugon. Vibration damping in sandwich panels. *Journal of Material Science*, 43(20):6604–6618, oct 2008.
- [259] R. D. Adams, M. R. Maher, and J. Hugon. The vibration properties of sandwich panels: eigenfrequencies and damping. In *8th International conference on sandwich structures*, 2008.
- [260] K. Renji and S. Shankar Narayan. Loss Factors of Composite Honeycomb Sandwich Panels. *Journal of Sound and Vibration*, 250(4):745–761, feb 2002.
- [261] P. Nagasankar, S. Balasivanandha Prabu, and R. Velmurugan. Role of temperatures and fiber orientations on transverse shear damping of polypropylene honeycomb sandwich structures. *Journal of Reinforced Plastics and Composites*, 34(9):696–707, apr 2015.
- [262] G. Michon, A. Almajid, J.-F. Ferrero, G. Aridon, V. Fascio, and J.-P. Heurteau. Dissipation mechanisms identification of soft hollow particle-dampers in honeycomb structures for micro-vibrations environment. In *11th European Conference on Spacecraft Structures, Materials & Mechanical Testing (ECSSMMT)*, sep 2009.
- [263] G. Michon, A. Almajid, and G. Aridon. Soft hollow particle damping identification in honeycomb structures. *Journal of Sound and Vibration*, 332(3):536–544, feb 2013.
- [264] B. Wang and M. Yang. Damping of honeycomb sandwich beams. *Journal of Materials Processing Technology*, 105(1-2):67–72, sep 2000.
- [265] H. Panossian. Optimized Non-Obstructive Particle Damping (NOPD) Treatment for Composite Honeycomb Structures. In *47th AIAA/ASME/ASCE/AHS/ASC Structures, Structural dynamics and material conference*, 2006.
- [266] S. Maley. *Particulate enhanced damping of sandwich structures*. PhD thesis, Purdue University, 2001.

BIBLIOGRAPHY

- [267] Y. Ma, F. Scarpa, D. Zhang, B. Zhu, L. Chen, and J. Hong. A nonlinear auxetic structural vibration damper with metal rubber particles. *Smart Materials and Structures*, 22(8):084012, aug 2013.
- [268] Z. Xu, M. Y. Wang, and T. Chen. Particle damping for passive vibration suppression: numerical modelling and experimental investigation. *Journal of Sound and Vibration*, 279(3–5):1097–1120, jan 2005.
- [269] S. C. Woody and S. T. Smith. Damping of a thin-walled honeycomb structure using energy absorbing foam. *Journal of Sound and Vibration*, 291(1–2):491–502, mar 2006.
- [270] Z. Li and M. J. Crocker. Effects of thickness and delamination on the damping in honeycomb–foam sandwich beams. *Journal of Sound and Vibration*, 294(3):473–485, jun 2006.
- [271] Z. Li. Vibration and acoustical properties of sandwich composite materials, may 2006.
- [272] R. Zhou and M. J. Crocker. Sound transmission loss of foam-filled honeycomb sandwich panels using statistical energy analysis and theoretical and measured dynamic properties. *Journal of Sound and Vibration*, 329(6):673–686, mar 2010.
- [273] V. N. Burlayenko and T. Sadowski. Analysis of structural performance of sandwich plates with foam-filled aluminum hexagonal honeycomb core. *Computational Materials Science*, 45(3):658–662, may 2009.
- [274] T. Sadowski and J. Bec. Effective properties for sandwich plates with aluminium foil honeycomb core and polymer foam filling – Static and dynamic response. *Computational Materials Science*, 50(4):1269–1275, feb 2011.
- [275] O. Romberg, M. Tausche, C. Pereira, L. Panning, D. Zentrum, R. Dlr, and A. Fallturm. Passive Damping of Spacecraft Sandwich Panels. *1st European Air and Space Conference 2007*, (September):10–13, sep 2007.
- [276] O. Romberg. Passive Damping Device for Sandwich Structures. *Recent Patents on Mechanical Engineering*, 3(3):183–190, oct 2010.
- [277] R.-X. Zhang, Q.-Q. Ni, A. Masuda, T. Yamamura, and M. Iwamoto. Vibration characteristics of laminated composite plates with embedded shape memory alloys. *Composite Structures*, 74(4):389–398, aug 2006.

- [278] P. Butaud, M. Ouisse, E. Foltete, and C. Rogueda-Berriet. SMP-Based solution for structural damping. In *Noise and Vibration - Emerging technologies*, 2015.
- [279] H. Hao, C.-R. Joe, and D-U. Kim. Mechanical Behavior of Rubberfilled Multifunctional Honeycomb Sandwich Composite. In *Sandwich Structures 7: Advancing with Sandwich Structures and Materials*, pages 671–680. 2005.
- [280] G. Murray. *Two novel uses of cellular structures*. PhD thesis, 2009.
- [281] G. Murray, F. Gandhi, and E. Hayden. Polymer-filled honeycombs to achieve a structural material with appreciable damping. *J. Intell. Mater. Syst. Struct.*, 23(6):703–718, apr 2012.
- [282] G. J. Murray and F. Gandhi. Auxetic honeycombs with lossy polymeric infills for high damping structural materials. *Journal of Intelligent Material Systems and Structures*, 24(9):1090–1104, jun 2013.
- [283] W.-Y. Jung and A. J. Aref. A combined honeycomb and solid viscoelastic material for structural damping applications. *Mechanics of Materials*, 35(8):831–844, aug 2003.
- [284] M. Sola, M.-A. Jetté, E. R. Fotsing, and M. Cimmino. Analytical and experimental study of embedded damping elements in composites. In *16th International congress on sound and vibration*, 2009.
- [285] E. R. Fotsing, M. Sola, A. Ross, and E. Ruiz. Lightweight damping of composite sandwich beams: Experimental analysis. *Journal of Composite Materials*, 47(12):1501–1511, jun 2012.
- [286] J. Yang, J. Xiong, L. Ma, B. Wang, G. Zhang, and L. Wu. Vibration and damping characteristics of hybrid carbon fiber composite pyramidal truss sandwich panels with viscoelastic layers. *Composite Structures*, 106:570–580, dec 2013.
- [287] G. Xu and J. Jun. Passive vibration control of truss-cored sandwich plate with planar Kagome truss as one face plane. *Science China Technological Sciences*, 54(5):1113–1120, may 2011.
- [288] M.-A. Boucher, C. W. Smith, F. Scarpa, R. Rajasekaran, and K. E. Evans. Effective topologies for vibration damping inserts in honeycomb structures. *Composite Structures*, 106:1–14, dec 2013.
- [289] R. Rajasekaran, F. Scarpa, C. W. Smith, W. Miller, and K. Evans. Vibration Damping Structures, sep 2011.

BIBLIOGRAPHY

- [290] L. J. Gibson, M. F. Ashby, G. S. Schajer, and C. I. Robertson. The Mechanics of Two-Dimensional Cellular Materials. *Proceedings of the Royal Society of London. Series A, Mathematical and Physical Sciences*, 382(1782):25–42, jul 1982.
- [291] I. G. Masters and K. E. Evans. Models for the elastic deformation of honeycombs. *Composite Structures*, 35(4):403–422, aug 1996.
- [292] W. Young and R. Budynas. *Roark's Formulas for Stress and Strain*. McGraw-Hill, 7th edition, 2002.
- [293] Ansys Mechanical APDL release 14.0, Theory Reference Manual, ANSYS, Inc.
- [294] M. E. Raville and C. E. S. Ueng. Determination of natural frequencies of vibration of a sandwich plate. *Experimental Mechanics*, 7(11):490–493, nov 1967.
- [295] S. Srinivas, C. V. Joga Rao, and A. K. Rao. An exact analysis for vibration of simply-supported homogeneous and laminated thick rectangular plates. *Journal of Sound and Vibration*, 12(2):187–199, jun 1970.
- [296] B. Marvalova and I. Petrikova. *Constitutive Models for Rubber IX*. CRC Press, 2015.
- [297] P. Aumjaud, C. W. Smith, and K. E. Evans. A novel viscoelastic damping treatment for honeycomb sandwich structures. *Composite Structures*, 119:322–332, jan 2015.
- [298] M. Palermo, S. Silvestri, G. Gasparini, and T. Trombetti. Seismic Modal Contribution Factors. *Bulletin of Earthquake Engineering*, apr 2015.
- [299] L. C. Hau and E. H. K. Fung. Multi-objective optimization of an active constrained layer damping treatment for shape control of flexible beams. *Smart Materials and Structures*, 13(4):896, aug 2004.
- [300] P. Aumjaud, J.E. Fieldsend, M.-A. Boucher, K.E. Evans, and C.W. Smith. Multi-objective optimisation of viscoelastic damping inserts in honeycomb sandwich structures. *Composite Structures*, 132:451–463, nov 2015.
- [301] P.S. Nair and S. Durvasula. On quasi-degeneracies in plate vibration problems. *International Journal of Mechanical Sciences*, 15(12):975–986, dec 1973.
- [302] A. W. Leissa. On a curve veering aberration. *Journal of Applied Mathematics and Physics*, 25(1):99–111, jan 1974.

- [303] J. L. Dubois, S. Adhikari, and N. A. J. Lieven. On the Quantification of Eigenvalue Curve Veering: A Veering Index. *Journal of Applied Mechanics*, 78(4):041007, jul 2011.
- [304] E. Zitzler and S. Kunzli. Indicator-based selection in multiobjective search. In *Parallel Problem Solving from Nature (PPSN VIII)*, volume 3242, pages 832–842. Springer, Berlin, 2004.
- [305] S. S. Rao. *Engineering Optimization: Theory and Practice*. John Wiley & Sons, 1996.
- [306] K. I. Smith, R. M. Everson, J. E. Fieldsend, C. Murphy, and R. Misra. Dominance-Based Multi-Objective Simulated Annealing. *IEEE Transactions on Evolutionary Computation*, 12(3):323–342, 2008.
- [307] E. Zitzler, L. Thiele, M. Laumanns, C.M. Fonseca, and V.G. Da Fonseca. Performance assessment of multiobjective optimizers: an analysis and review. *IEEE Transactions on Evolutionary Computation*, 7(2):117–132, apr 2003.
- [308] J. Knowles, L. Thiele, and E Zitzler. A Tutorial on the Performance Assessment of Stochastic Multiobjective Optimizers. Technical report, Computer Engineering and Networks Laboratory (TIK), ETH Zurich, Switzerland, 2006.
- [309] E. Zitzler. *Evolutionary Algorithms for Multiobjective Optimization: Methods and Applications*. PhD thesis, ETH Zurich, 1999.
- [310] J. M. Bader. *Hypervolume-Based Search for Multiobjective Optimization: Theory and Methods*. PhD thesis, feb 2010.
- [311] Rolls-Royce Ltd. *The Jet Engine*. Rolls-Royce, Derby, England, 1986.
- [312] A. B. Stanbridge and D. J. Ewins. Modal testing using a scanning laser doppler vibrometer. *Mechanical Systems and Signal Processing*, 13(2):255–270, mar 1999.
- [313] S. Adhikari. *Damping models for structural vibration*. PhD thesis, Cambridge University, 2000.